The use of periodic *ab initio* methods in the determination of NMR quadrupole parameters

Thesis

UNRESTRICTED

The use of periodic *ab initio* methods in the determinatlon of NMR quadrupoie parameters

A Thesis Presented to The Open University

for the Degree of Doctor of Philosophy

Clive Johnson, B.Sc.

Department of Chemistry

The Open University

December, 2002

Submission date: 23 December 2002

Award date: 7 May 2003

Abstract

Although significant progress has been made in recent years in the development of new experimental techniques for the measurement of high-resolution nuclear magnetic resonance spectra for half-integer quadrupolar nuclei in solids, a particular problem still arises in the assignment of these resonances for materials in which there are several distinct crystallographic sites.

This thesis demonstrates that a periodic Hartree-Fock *ab initio* method, based on modified 3-21G and 6-21G elemental basis sets used in a consistent manner, enables linear correlations between calculated and experimental NMR quadrupole parameters to be obtained. Comparable calculations using density functional theory did not significantly improve the correlations. In the case of ^{23}Na NMR experiments, the correlations are of sufficient accuracy to confirm and provide new assignments for a range of crystalline sodium compounds, including Na_2SO_3, Na_2HPO_4, $Na_4P_2O_7$ and $Na_5P_3O_{10}\cdot 6H_2O$. Furthermore, it is demonstrated that the calculations are sufficiently sensitive to the local electronic environment such that (i) anomalies in crystal structure determinations for $Na_4P_2O_7$ and the phase I polymorph of anhydrous $Na_5P_3O_{10}$ can be identified and (ii) information can be gained on the position of hydrogen within the hydrogen bond in Na_2HPO_4. Specific calculations for the ionic compound sodium oxide chloride, Na_3OCl, provide insight into the origin of the Sternheimer factor and its link to the polarization of the sodium 2p orbitals.

The periodic *ab initio* correlation method is also applied to ^{17}O NMR studies and is shown to be independent of the nature of the oxygen bonding. Specific calculations, using pseudopotentials for silicon, are made for the 10 distinct oxygen sites in ferrierite, a siliceous zeolite. It is shown that the calculations are able to distinguish between two proposed crystal structures for this material. A summary of results for ^{27}Al and ^{51}V is also presented.

Acknowledgements

I owe an immense debt of gratitude for their help, encouragement and friendship during my time at The Open University to many people. There are, inevitably, too many to name individually but I am, none the less, grateful to every one of them.

I would like to thank my supervisors, Dr M. Mortimer and Dr E.A. Moore, for their good humour in the face of my ignorance, their unflagging support and guidance during the course of my PhD studies. It would not be right if I failed to acknowledge the contributions made by Gordon Oates, Fred Vetel, Neil Creamer and Charlie Harding to the many useful and wide ranging philosophical discourses that regularly took place in Lab. 6, especially Fred's contributions to the French love of irony and the never-to-be-resolved merits, or otherwise, of a left-handed golf swing.

I would like to take the opportunity to thank Professors R.C.F. Jones and F.J. Berry for the use of the facilities of the Chemistry Department and a special thank you to the technical staff of the department, especially Gordon Howell, without whose help the practical aspects of this thesis would not have been possible.

Finally I would like to thank the United Kingdom Computational Chemistry Working Party for time on the Columbus Super-Scalar Facility at Rutherford Appleton Laboratory and EPSRC for the funding of my research studentship.

Dedication

To my parents, Frank and Norma.

Contents

Chapter 7

A correlation approach for solid-state ^{17}O NMR spectroscopy

Appendices

Chapter 1

Introduction

Introduction

The recording and analysis of high-resolution nuclear magnetic resonance (NMR) spectra for half-integer quadrupolar nuclei provides a powerful means of investigating local structure in the solid state [1-3]. Although significant progress has been made in recent years in the development of new experimental techniques [1], a particular problem still arises in the assignment of resonances for materials in which there are several distinct crystallographic sites. In the absence of intensity or chemical shielding information, assignment may be made on the basis of a comparison between the experimental nuclear quadrupole parameters, namely the nuclear quadrupole coupling constant C_Q and the asymmetry parameter η, and those obtained by calculation. The development of a reliable method for the calculation of these parameters based on structural data is, therefore, of practical use as well as being of fundamental importance in its own right.

The electric field gradient (efg) tensor is a ground-state property of a system and, as such, is defined as the second derivative of the Coulomb potential with respect to a Cartesian coordinate frame centred on the nucleus of interest. For many years the calculation of this derivative, for ionic solids, the determination of C_Q and η, has relied on simple electrostatic models [4, 5] along with the use of Sternheimer antishielding factors [6, 7] to account for polarisation effects. However, such predictions necessarily rely upon empirically-derived parameters and often deviate significantly from values obtained by experiment. In a more recent study Koller and co-workers [8] have demonstrated that it is possible to find linear correlations between experimental ^{23}Na quadrupole parameters and those obtained by a simple point-charge model in which the expansion of the Coulomb potential is limited to just the monopole terms. This point-charge correlation approach is of direct use for the assignment of ^{23}Na NMR spectra and has subsequently been used to

interpret solid-state NMR spectra for other nuclei, including caesium [9] and vanadium [10]. It represents a significant step forward towards finding a simple transferable method for site assignment in solid-state NMR based on the measurement of quadrupole parameters.

An important approach to calculating efgs from first principles, based upon the linear augmented plane-wave method (LAPW), has been proposed by Blaha and co-workers [11]. This method derives a general potential, using an *ab initio* self-consistent band structure calculation, based upon the full crystal structure rather than an embedded cluster. The efg at the nucleus of interest can be derived without the need for empirical data. In general, progress in the development of computational algorithms and increasing computer power has also seen several other electronic structure methods being applied, with varying degrees of success, to the calculation of efgs in solids [12-17]. However, the main focus of such work has been to obtain accurate efg tensor information for individual compounds.

The main aim of the work in this thesis is to extend the correlation approach suggested by Koller *et al.* so that it is based on periodic *ab initio* calculation. Furthermore, the modelling procedure should be capable of calculating quadrupole parameters, on a transferable basis, with sufficient accuracy to not only be useful for assignment purposes but also to be a predictive tool for quadrupole parameters in solids which have yet to be studied experimentally.

The first part of the thesis gives an overview of a selection of key areas in solid state physics and begins in Chapter 2 with a discussion of crystal lattices (Bravais and

reciprocal) and a definition for the Brillouin zone. Features of nuclear quadrupole moments, electric field gradients and Sternheimer antishielding are also considered. By introducing these topics, the chapter functions as a preamble to the main thesis and introduces concepts on which subsequent theory is based. The more detailed theory underlying periodic *ab initio* methods is presented in Chapter 3. These methods, based on Hartree-Fock (HF) and Density Functional Theory (DFT), facilitate the detailed modelling of an efg at a nucleus of interest in a three-dimensional crystalline solid and constitute the principal *ab initio* methods used in this thesis. An outline of the theory of NMR spectroscopy, with specific reference to the nuclear quadrupole interaction in the solid-state, is also included in this chapter.

Chapter 4 begins with the calculation of the relatively complex sodium efg tensor in sodium nitrite ($NaNO_2$) using both HF and DFT levels of theory. The relative merits of embedded cluster compared to periodic *ab initio* methods of calculation are investigated. The information gained then leads to the first steps towards using a periodic *ab initio* method for the calculation of ^{23}Na quadrupole parameters using simple basis sets; primarily 3-21G and 6-21G [18-22]. In particular, a method is found which provides a transferable basis set for sodium in compounds in which sodium is exclusively coordinated to oxygen in oxyanions of the lighter p-block elements. This basis set, along with those for other atoms present in the compounds studied, is then used in a consistent manner for the calculation of ^{23}Na quadrupole parameters using both HF and DFT, approaches for a wide range of ionic compounds. Linear correlations between experimental and calculated $C_Q(^{23}Na)$ values, and to some extent $\eta(^{23}Na)$, are found. The linear correlations obtained for $C_Q(^{23}Na)$ are sufficiently good to be used for assignment purposes.

In Chapter 5, the periodic *ab initio* method established in the previous chapter is applied to the calculation of $C_Q(^{23}Na)$ for ionic compounds of sodium containing transition metal and heavy atom oxyanions. Linear correlations are obtained which are suitable for the purposes of site assignment. The same method is also shown to give good agreement between calculation and experiment for two aluminofluorides in which sodium is coordinated to fluorine rather than oxygen. Finally the method is used to predict, with reasonable accuracy, a $C_Q(^{23}Na)$ value for the sodium site in the purely ionic compound, sodium oxide chloride (Na_3OCl) which is then used as a model compound for a study of the polarisation of sodium core electrons and the Sternheimer factor.

The predictive potential of the periodic *ab initio* method is demonstrated in Chapter 6 for a range of sodium phosphates. Inconsistencies in the reported crystal structures of tetrasodium pyrophosphate ($Na_4P_2O_7$) and the phase I polymorph of anhydrous pentasodium triphosphate ($Na_5P_3O_{10}$) are resolved. The separation of strongly overlapped ^{23}Na MAS NMR spectra is always problematic in the absence of data obtained by other techniques. The periodic *ab initio* method is shown to provide good starting parameters for the complete simulation of the ^{23}Na MAS NMR spectrum of $Na_4P_2O_7$ which consists of four overlapped resonances and, even more complex, that of $Na_5P_3O_{10}\cdot 6H_2O$ which has five overlapped resonances. Finally, the sensitivity of the ^{23}Na quadrupole parameters, especially the asymmetry parameter, to local structural environment is exploited in order to investigate the position of the hydrogen atom within the hydrogen-bonded compound, disodium hydrogenphosphate (Na_2HPO_4).

In Chapter 7, which is the final chapter, the periodic *ab initio* method is applied to the calculation of ^{17}O efg tensors in a range of compounds in which oxygen bonds either

purely ionically (oxides), as part of an oxyanion or is involved in covalent bonding. The polymorphs of silica are studied in more detail with a view to finding a modified simple basis set, which can be used to model large zeolite compounds. The basis set, based on a large-core pseudopotential for silicon, was used to distinguish between the two proposed structures of siliceous ferrierite. The chapter concludes with the establishment of a three-dimensional correlation for the calculated value of $C_Q(^{17}O)$, the experimental O–Si–O bond angle and the average experimental O–Si bond length which is used to predict the ^{17}O quadrupole parameters of the four discrete oxygen sites in siliceous zeolite faujasite which contains 576 atoms per unit cell.

Three appendices are provided. Appendix A gives a 8-411G basis set for nitrogen. Appendix B shows the Rietveld refined lattice and atomic parameters for the phase I (high temperature) polymorph of $Na_5P_3O_5$. The final appendix provides a summary of further periodic HF *ab initio* calculations for the quadrupole parameters of aluminium and vanadium in a wide range of compounds.

References

1. M.E. Smith and E.R.H. van Eck, *Prog. NMR Spectrosc.*, **34**, 159, 1993.
2. D. Freude and J. Haase, in *NMR Basic Principles and Progress*, Vol 29, ed. P. Diehl, E. Fluck, H. Günther, R. Kosfeld and J. Seelig, Springer-Verlag, Berlin, 1993.
3. A.P.M. Kentgens, *Geoderma*, **80**, 271, 1997.
4. M.H. Cohen and F. Reif, *Solid State Phys.*, **5**, 321, 1957.
5. R. Bersohn, *J. Chem. Phys.*, **29**, 326, 1958.
6. R.M. Sternheimer, *Phys. Rev.*, **95**, 736, 1954.

7. P.C. Schmidt, K.D. Sen, T.P. Das and A. Weiss, *Phys. Rev. B*, **22**, 4167,1980.

8. H. Koller, G. Engelhardt, A.P.M. Kentgens and J. Sauer., *J. Phys. Chem.*, **98**, 1544, 1994.

9. J. Skibsted, T. Voosegaard. H. Bildsøe and H.J. Jakobsen, *J. Phys. Chem.*, **100**, 1472, 1996.

10. J. Skibsted, C.J.H. Jakobsen and H.J. Jakobsen, *Inorg. Chem.*, **37**, 3083, 1998.

11. P. Blaha, K. Schwarz and P. Herzig, *Phys. Rev. Lett.*, **54**, 1192, 1985.

12. M. Methfessel and S. Frota-Pessôa, *J. Phys.: Condens. Matter*, **2**, 149, 1990.

13. H.M. Petrilli and S. Frota-Pessôa, *J. Phys.: Condens. Matter*, **2**, 135, 1990.

14. H. Akai, M. Akai, S. Blügel, B. Drittler, H. Ebert K. Terakura, R. Zeller and P.H. Dederichs, *Prog. Theor. Phys. Suppl.*, **101**, 11 1990.

15. D.E. Ellis, D. Guenzburger and H.B. Jansen, *Phys. Rev. B*, **28**, 3697, 1983, and references therein.

16. V. Sliwko, P. Mohn and K. Schwarz, *J. Phys.: Condens. Matter*, **6**, 6557, 1994.

17. B. Meyer, K. Hummler, C. Elsässer and Mähnle, *J. Phys.: Condens. Matter*, **7**, 9201, 1995.

18. J.S. Binkley, J.A. Pople, W.J. Hehre, *J. Am. Chem. Soc.*, **102**, 939, 1980.

19. M.S. Gordon, J.S. Binkley, J.A. Pople, W.J. Pietro and W.J. Hehre, *J. Am. Chem. Soc.*, **104**, 2797, 1983.

20. K.D. Dobbs, W.J. Hehre, *J. Comput. Chem.*, **7**, 359, 1986.

21. K.D. Dobbs, W.J. Hehre, *J. Comput. Chem.*, **8**, 861, 1987.

22. K.D. Dobbs, W.J. Hehre, *J. Comput. Chem.*, **8**, 880, 1987.

Chapter 2

Essential aspects of crystal structure and nuclear quadrupole interactions

2.1 Introduction

On Earth, matter is found to occur in various phases but only the solid state is characterised by long-range spatial order. This three-dimensional regularity of structure is a result of the proximity of the atomic species making up the solid and the forces, attractive and repulsive, acting between them. In a crystalline solid, the constituent atomic species form a regular spatially-periodic arrangement. The materials that will be considered in this thesis are exclusively crystalline solids.

The quantum mechanical methods used to treat crystalline systems are often very different from those used to study isolated molecules. One purpose of this chapter, therefore, is to outline those basic physical concepts relating to crystalline and reciprocal lattices that are relevant to the application of *ab initio* calculations to periodic systems. This is in preparation for a fuller description of this type of calculation in the following chapter. The description is not intended to be exhaustive and further details may be found in standard textbooks of solid-state physics [1-4].

The remainder of this chapter turns to a different aspect of solid state physics. Basic ideas relating to nuclear electric quadrupole interactions in crystals are introduced. These ideas form the foundation for all further discussions of the NMR spectroscopy of half-integer quadrupolar nuclei in this thesis.

2.2 Bravais lattices

In order to calculate the physical properties of a crystal, it is necessary to be able to describe such a structure mathematically and, usually in modern research, within a

computer. In general, a perfect crystal is made up of atoms, ions or molecules closely packed together and arranged periodically in three dimensions. The structure of a crystal can be defined by the size and shape of the basic repeating unit (unit cell) and the position of the atoms within it. The unit cell of a crystal is that grouping of atoms that is repeated in three dimensions to fill the entire crystal lattice without gaps or overlap. It is a parallelepiped in shape and is characterised by three unit vectors ***a***, ***b*** and ***c***, and the angles α, β and γ, between them (Figure 2.1).

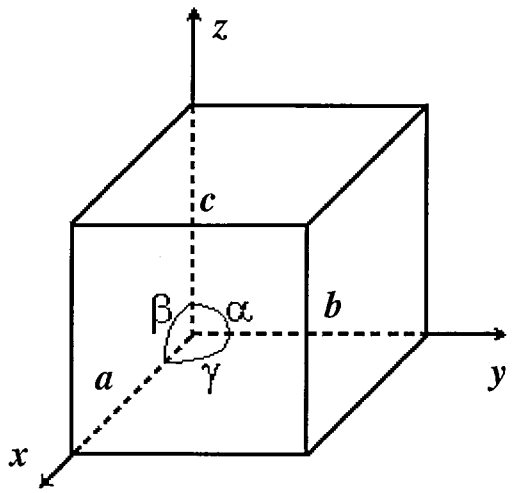

Figure 2.1 The unit cell of a lattice showing the unit vectors ***a***, ***b***, ***c***, and the angles between them α, β, γ.

The atomic positions within the unit cell are related to equivalent sites in other unit cells throughout the lattice by the lattice vector ***R***, which can be written as:

$$\boldsymbol{R} = n_1\boldsymbol{a} + n_2\boldsymbol{b} + n_3\boldsymbol{c} \qquad (2.1)$$

where n_i are integers. That is, they are translationally invariant under ***R***.

Using these ideas, it is possible to construct seven different lattice types and these are shown in Table 2.1 along with their definitions and examples of compounds that adopt them. In 1850, Bravais showed that from these seven lattice types, 14 possible unit cells could be constructed. Now called Bravais lattices, these are shown in Figure 2.2.

Table 2.1 A summary of the seven lattice types, their definitions and some examples of compounds adopting these structures.

Lattice type	Unit cell		Examples
	Lengths	Angles	
Cubic	$a = b = c$	$\alpha = \beta = \gamma = 90°$	NaCl, Cu
Tetragonal	$a = b \neq c$	$\alpha = \beta = \gamma = 90°$	TiO_2, Sn
Orthorhombic	$a \neq b \neq c$	$\alpha = \beta = \gamma = 90°$	$MgSO_4.7H_2O$, $BaSO_4$
Monoclinic	$a \neq b \neq c$	$\alpha = \gamma = 90°; \beta \neq 90°$	PbCrO4, $CaSO_4.2H_2O$
Triclinic	$a \neq b \neq c$	$\alpha \neq \beta \neq \gamma \neq 90°$	$K_2Cr_2O_7$, $CuSO_4.5H_2O$
Hexagonal	$a = b \neq c$	$\alpha = \beta = 90°; \gamma = 120°$	SiO_2, C, ZnO
Rhombohedral	$a = b = c$	$\alpha = \beta = \gamma \neq 90°$	$CaCO_3$, HgS

Along with the translational symmetry that the unit cell must possess, there can also be other symmetry elements that relate atoms to each other within the unit cell. The particular symmetry elements in the crystal define its space group and there are 230 different space groups. If a unit cell contains the symmetry elements for a particular space group, it is only necessary to specifically define those atoms that make up the unique part of the structure, the asymmetric unit. The other atoms will be generated by the application of the appropriate symmetry operations.

The conventional parallelepiped unit cells shown in Figure 2.2 are not the only way to describe the 14 Bravais lattices. A different type of construction can be used to provide a family of polyhedra that satisfy the criterion of filling all available space. Cells constucted in this way are known as Wigner-Seitz (WS) cells and are always primitive cells.

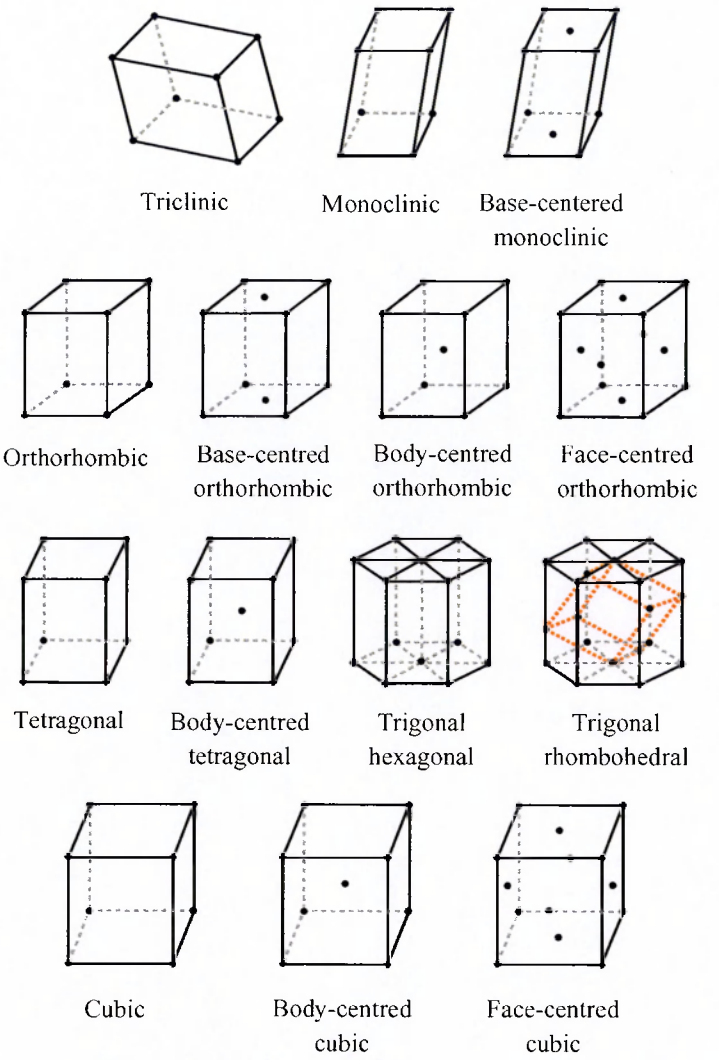

Figure 2.2 The fourteen Bravais lattices: triclinic, monoclinic, base-centred monoclinic; orthorhombic, base-centred orthorhombic, body-centred orthorhombic, face-centred orthorhombic; tetragonal, body-centred tetragonal, trigonal hexagonal, trigonal rhombohedral; cubic, body-centred cubic, face-centred cubic.

The construction and illustration of WS cells is easiest to visualise for a two-dimensional square lattice, Figure 2.3. The first step in constructing the WS for a given lattice point (black circle) is to determine its nearest neighbours, shown as red circles. Lines are then drawn (shown in black) which connect the lattice point to its nearest neighbour lattice points. Planes (shown in blue) can be constructed at the midpoint and normal to the lines connecting these lattice points. The smallest area enclosed in this way is the WS cell (shaded red) and always contains a single lattice point. This procedure can be extended to three dimensions (see Section 2.4).

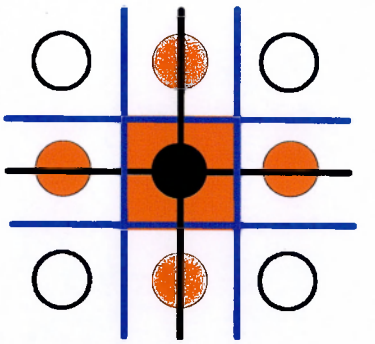

Figure 2.3 Construction of the Wigner-Seitz cell for a 2-dimensional square lattice.

2.3 The reciprocal lattice

The reciprocal lattice is defined by three unit vectors $\boldsymbol{a}^*$, $\boldsymbol{b}^*$ and $\boldsymbol{c}^*$ such that $\boldsymbol{a}^*$ is perpendicular to the real space unit vectors **b** and **c** and scaled such that the scalar product of $\boldsymbol{a}^*$ and $\boldsymbol{a}$ equals 1. The $\boldsymbol{b}^*$ and $\boldsymbol{c}^*$ vectors are defined similarly leading to the following definitions:

$$\boldsymbol{a}^* = \frac{\boldsymbol{b}\times\boldsymbol{c}}{\boldsymbol{a}\cdot\boldsymbol{b}\times\boldsymbol{c}};\quad \boldsymbol{b}^* = \frac{\boldsymbol{c}\times\boldsymbol{a}}{\boldsymbol{a}\cdot\boldsymbol{b}\times\boldsymbol{c}};\quad \boldsymbol{c}^* = \frac{\boldsymbol{a}\times\boldsymbol{b}}{\boldsymbol{a}\cdot\boldsymbol{b}\times\boldsymbol{c}} \tag{2.2}$$

Positions within the reciprocal unit cell are related to equivalent sites in other cells throughout the lattice by the reciprocal lattice vector $\boldsymbol{G}$, written as:

$$\boldsymbol{G} = n_1\boldsymbol{a}^* + n_2\boldsymbol{b}^* + n_3\boldsymbol{c}^* \tag{2.3}$$

where n_i are integers.

It turns out to be more convenient to use an expanded reciprocal space where the lattice vectors are multiplied by 2π

$$\boldsymbol{a}^{\$} = 2\pi\boldsymbol{a}^*;\quad \boldsymbol{b}^{\$} = 2\pi\boldsymbol{b}^*;\quad \boldsymbol{c}^{\$} = 2\pi\boldsymbol{c}^* \tag{2.4}$$

Simple illustrative examples of reciprocal lattices are shown in Figure 2.4. In the case of the 2D square lattice, the reciprocal lattice vectors $\boldsymbol{a}^{\$}$ and $\boldsymbol{b}^{\$}$ define a square lattice with a separation of $2\pi/a$. The 2D hexagonal lattice is a more complex example in that the

reciprocal vectors give rise to a hexagonal lattice rotated 30° with respect to the real space lattice.

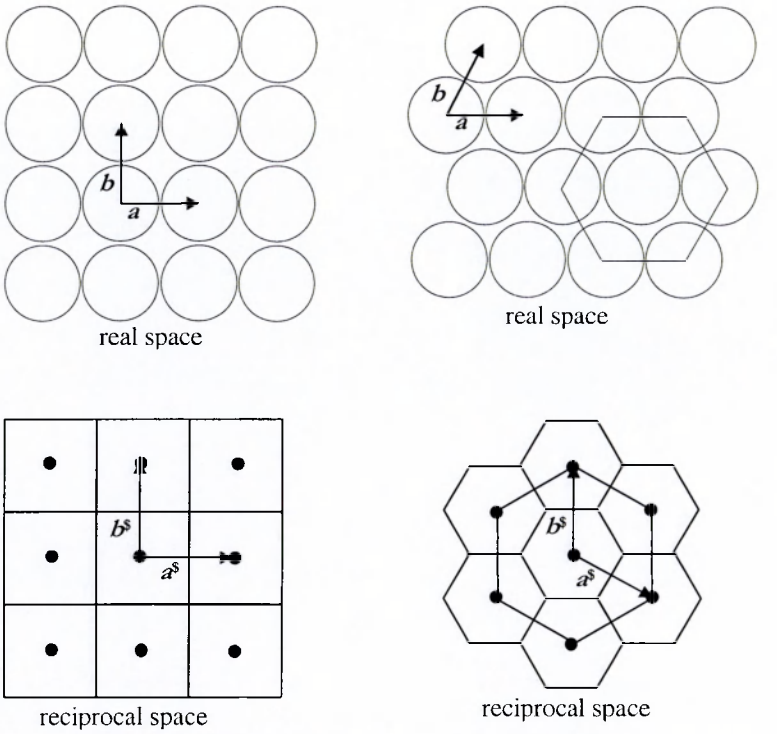

Figure 2.4 The real and reciprocal space arrangements of a 2D square lattice and a 2D hexagonal close-packed lattice.

In the same way that a crystal lattice is made up of unit cells, so the reciprocal lattice may be considered to be constructed from a series of primitive cells. An important method of constructing these primitive cells is as for a Wigner-Seitz cell. Each cell contains a single reciprocal lattice point.

2.4 The Brillouin zone

When discussing electronic structure, the Wigner-Seitz cell of the reciprocal lattice is usually referred to as the first Brillouin zone (BZ). There will be 14 first BZs corresponding to the 14 reciprocal Bravais lattices. The construction of BZs follow that for the Wigner-Seitz cell in Section 2.2. The first step in constructing the BZs for a point

is to determine its nearest neighbours, next nearest neighbours and so on. This is conveniently illustrated with reference to a square reciprocal lattice, Figure 2.5 (a), where the nearest neighbours are shown as red, the next nearest, blue, and the next as magenta, circles. Bragg planes are constructed at the midpoint, and normal to, lines connecting a given lattice point to all nearby lattice points (colour-coded lines). The smallest volume enclosed in this way is the first BZ (shaded red). The second BZ (shaded blue) is defined as the points that may be reached from the first BZ by crossing only one Bragg plane and subsequent zones in a like manner. These other zones are one-to-one mappings of the first zone, but they are cut up in pieces.

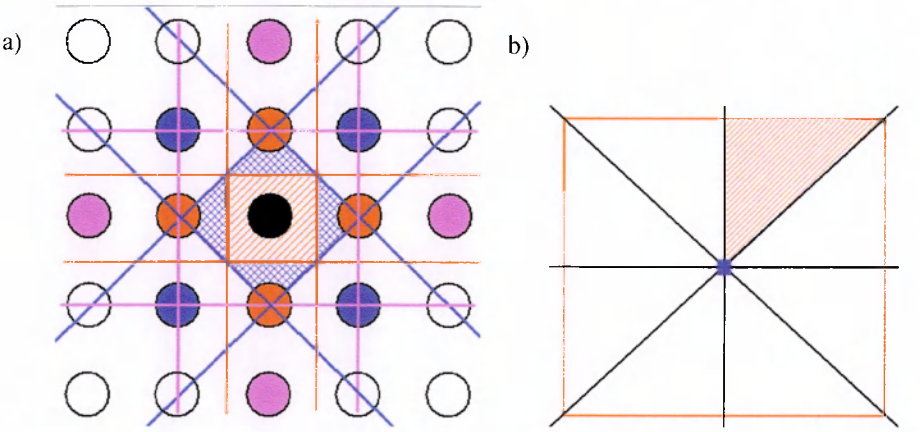

Figure 2.5 a) The first and second Brillouin zones (shaded red and blue, respectively) for a point in a square lattice. b) The first Brillouin zone for a point in a square lattice, showing the four mirror planes (black lines), the four-fold rotation axis (blue square) and the irreducible part of the Brillouin zone (shaded).

The first BZ for a point in a 2D square lattice can be further subdivided into 8 irreducible parts by the use of symmetry opertations, Figure 2.5 (b).

The first Brillouin zone for a face-centered cubic lattice, Figure 2.6, is a truncated octahedron and may be divided into 48 irreducible segments by use of the 48 symmetry operations of the O_h space group. This means that all properties will be identical for any points that may be mapped onto one another by point group operations. Consequently,

for periodic *ab initio* calculations, only the irreducible part of the first BZ need be considered.

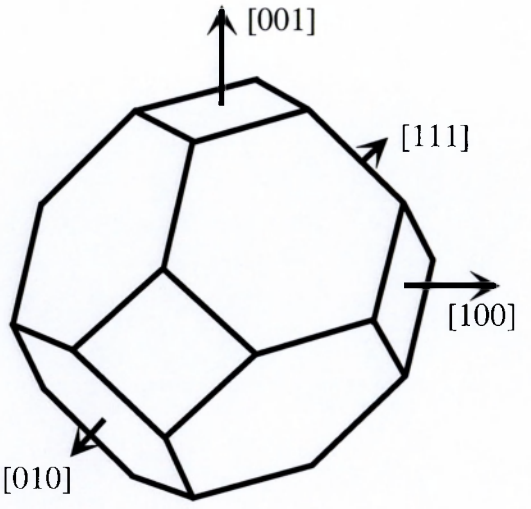

Figure 2.6 The first Brillouin zone for a crystal based on the face-centred cubic lattice showing the direction of four reciprocal lattice vectors.

2.5 Nuclear quadrupole moment

Of the approximately 110 NMR-active isotopes, 29 have spin $I = ½$. The rest of the nuclei are characterised by a nuclear quadrupole moment (Q). Quadrupolar nuclei of integer spin have an odd number of both protons and neutrons and of these only ^{2}H and ^{14}N are routinely studied by NMR experiments. The remaining quadrupolar nuclei have half-integer spins (i.e., 3/2, 5/2, 7/2 and 9/2) resulting from an odd number of total nucleons. Since the majority of the nuclei in the Periodic Table are quadrupolar nuclei, and because they occur in a vast number of ionic and covalent crystal structures, it is of great interest to better understand the nature and properties of quadrupolar nuclei.

The first evidence that many nuclei possessed a magnetic moment came from the hyperfine splitting observed in visible atomic spectra. This interaction between the nuclear magnetic moment and the electrons of the atom in question gives rise to a

relatively simple spectrum characterised by the "interval rule". However, departures from this interval rule in the spectrum of europium led to the suggestion that a nucleus could also possess a nuclear quadrupole moment [5].

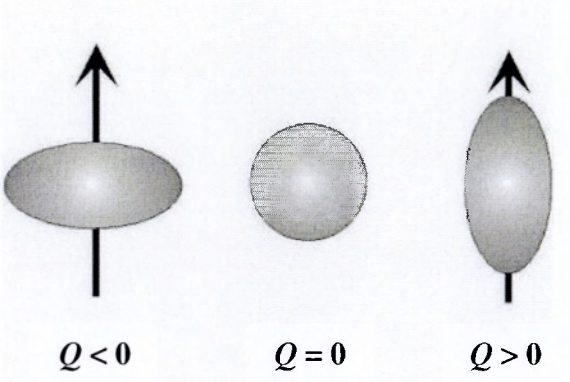

Figure 2.7 Distribution of electric charge within the nucleus for different values of the nuclear quadrupole moment

The nuclear quadrupole moment is the result of a non-spherical distribution of charge within the nucleus. This distribution can take the form of either an oblate or a prolate spheroid, Figure 2.7. If the nuclear quadrupole moment is less than zero the distribution is prolate, greater than zero it is oblate. A spherical distribution occurs when $Q = 0$ and the nucleus is not quadrupolar. Either of the non-spherical distributions will have an electrostatic interaction with an electrostatic field gradient that does not possess spherical symmetry. This is shown schematically in Figure 2.8.

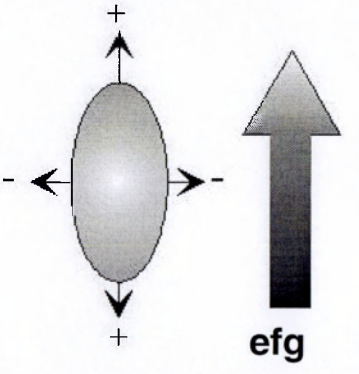

Figure 2.8 The interaction of a nuclear quadrupole moment with an electrostatic field gradient (efg).

The value of Q, in principle, can be obtained from experiments with free nuclei. However, in some cases it is not known with a high degree of precision. The present standard value for $Q(^{23}Na) = 0.1089 \times 10^{-28}$ m^2 [6]. Values for other nuclei studied in this work are shown in Table 2.2.

Table 2.2 Values of the nuclear quadrupole moment (Q) for a selected group of nuclei.

Nucleus	Q / 10^{-28} m^2
^{7}Li	-0.041
^{17}O	-0.02558
^{23}Na	+0.1089
^{27}Al	+0.1403
^{51}V	-0.052

All values taken from [7].

If the nuclear quadrupole moment is known, the electric field gradient can be deduced from experimentally determined transition frequencies between the nuclear energy levels. The efg is a ground-state property of the system and depends upon the local electronic environment and symmetry about the nucleus. Consequently, if the characteristics of the electric field gradient can be determined from experiments, much can be learnt about the chemical bonding and electronic structure of solids.

2.6 Electric field gradient

The magnitude of the electric field gradient (efg) at the nucleus is given by the tensor **V**. The traceless symmetric tensor of the efg at a nucleus in the origin of the laboratory co-ordinate system is defined as:

$$V_{ij} = \left.\frac{\partial^2 \Phi}{\partial x_i \partial x_j}\right|_0 - \frac{1}{3}\delta_{ij}\Delta\Phi|_0 , \qquad (2.5)$$

where

$$\Phi(r) = \int \frac{\rho(r')}{|r - r'|} dr' \tag{2.6}$$

is the electrostatic potential and $\rho(r)$ the ground-state charge density of the system. The subscript 0 indicates that the derivatives are taken at $r = 0$; that is at the nucleus. Inserting Equation (2.6) into Equation (2.5) gives

$$V_{ij} = \int \rho(r) \left(\frac{3x_i x_j}{r^5} - \frac{\delta_{ij}}{r^3} \right) dr \tag{2.7}$$

However, it is possible to transform this symmetric tensor by diagonalisation if a new set of orthogonal axes 1, 2, 3, called the principal axis system (PAS), is selected. In such a system, all components vanish except those associated with V_{11}, V_{22} and V_{33}. These three remaining components are not independent, as they must still satisfy the traceless condition:

$$V_{11} + V_{22} + V_{33} = 0 \tag{2.8}$$

It is conventional to express the values of the principal components of the efg in terms of the so-called quadrupole parameters. The PAS is oriented such that the relative magnitudes of the principal components satisfy the condition:

$$|V_{33}| \geq |V_{22}| \geq |V_{11}| \tag{2.9}$$

so that axis 3 corresponds to the maximum efg. The quadrupole parameters are then the electric field gradient

$$C_Q = \frac{eQV_{33}}{h} \tag{2.10}$$

and the asymmetry parameter

$$\eta = \frac{V_{11} - V_{22}}{V_{33}} \tag{2.11}$$

which lies in the range $0 \leq \eta \leq 1$. The asymmetry parameter is a measure of the deviation from axial symmetry. If the efg is spherically symmetric then $V_{33} = V_{22} = V_{11} = 0$; hence, no quadrupolar interaction occurs in sites of high symmetry such as cubic, octahedral or tetrahedral lattice sites. In the case of an axially symmetric efg we have $V_{11} = V_{22}$ and, therefore, $\eta = 0$.

For ionic crystals, the efg can be estimated by means of an electrostatic calculation in which the potential function, due to the surrounding charges, is expanded in terms of a series of multipoles summed over the whole lattice. In the case of the point-charge approximation, only the first term of this expansion is required. Here, effective charges, usually formal, are assigned to the ions in the crystal structure and the sum is then taken over all the lattice points. The matrix elements V_{ij}^{Ext} of this external efg tensor, at the nucleus of interest are calculated according to:

$$V_{ij}^{Ext} = (1/4\pi\varepsilon_0)\int_0^k \int_0^{R\max} z_k e(3x_i x_j - \delta_{ij} r^2)/r^5 d\vec{x} \qquad (2.12)$$

where $x_{i,j}$ (i,j = 1, 2, 3) are the coordinate components of $z_k e$ which is a distinct point charge of magnitude z_k, e is the charge on the electron, δ_{ij} is the Dirac delta function, r the distance between a point charge and the ion of interest, and ε_0 is the vacuum permittivity. The integration is over all point-charges within a sphere centred on the site of interest whose radius is given by R_{max}. Regarding the number of lattice points, sufficient convergence is normally achieved for a radius approximately 50 Å around the site of interest [8,9].

2.7 Sternheimer factor

A simple point-charge model can be used, as an approximation, to derive the efg due to an ionic lattice. However, for a closed-shell atom or ion it is important to consider the distortion from spherical symmetry of the core electrons very close to the nucleus. The nature of this distortion is proportional to the applied field due to the ions, electrons and nuclei external to the atom of interest and gives rise to a secondary field. This field has the same spatial symmetry as the applied field. In essence, this distortion leads to a correction of the gradient V_{33}^0 due to the applied field alone:

$$V_{33} = CV_{33}^0 \tag{2.13}$$

where V_{33} is the measured efg and C is a factor characteristic of the atom or ion.

R.M. Sternheimer was the first of various workers to consider the interaction of electric fields with nuclei of atoms possessing a nuclear quadrupole moment [10, 11]. In his treatment, the actual efg was given by:

$$V_{33} = V_{33}^0(1-\gamma(r)) \tag{2.14}$$

where the quantity V_{33}^0 is again the efg due to the external electric field alone, $\gamma(r)$ is the so-called Sternheimer antishielding factor and r is the distance from the nucleus to a given charge. If this charge is deep inside the closed shell distribution $\gamma(r) << 1$. For charges well outside the closed shell γ becomes independent of r to be replaced by the quantity γ_∞. The Sternheimer antishielding effect enhances the actual field gradient. The results of *ab initio* calculations of γ_∞ for a group of representative free ions are given in Table 2.3.

Table 2.3 Values of γ_∞ for a selected group of ions.

Ion	γ_∞ [a]
Na^+	-4.1
Cl^-	-56.6
Cu^+	-15.0
Rb^+	-70.7
Cs^+	-143.5

[a] Values taken from reference [12].

There are several theoretical approaches to the calculation of Sternheimer antishielding factors for various ions in the solid state [10, 13, 14] and their predictions concerning the same ion are not always in complete agreement. This is demonstrated, for example, by the summary of reported values of $\gamma_\infty(Na^+)$ given in Table 2.4.

Table 2.4 Values of γ_∞ (Na^+) calculated by different groups.

$\gamma_\infty(Na^+)$	Ref.
-4.1	[12]
5.03, 5.06	[15]
-5.06. –5.00	[16]
-5.45	[17]
-5.26	[18]
-5.59	[19]
-4.53	[20]
-4.56	[21]
-4.514, -4.505, -4.497	[22]

References

1. C. Kittel, *Introduction to Solid State Physics, 7th Ed.*, Wiley, New York, 1995.
2. H.P. Myers, *Introduction to Solid State Physics, 2nd Ed.*, Taylor and Francis, London, 1997.

3. M.N. Rudden, *Elements of Solid State Physics*, Wiley, Chichester, 1980.

4. H.E. Hall, *Solid State Physics*, Wiley, New York, 1974.

5. E.A.C. Lucken, *Nuclear Quadrupole Coupling Constants*, Academic Press, London and New York, 1969.

6. A. Sundholn and J. Olsen, *Phys. Lett.*, **68**, 927, 1992.

7. WebElements Periodic Table: www.webelements.com - accessed 17-12-02.

8. A.A. Gusev, I.M. Reznik and V.A. Tsitrin, *J. Phys.: Condens. Matter*, **7**, 4855, 1995.

9. A. Trokiner, P.-V. Bellot, Y. Zhdanov and A. Yakubovskii, *Solid State Nuclear Magnetic Resonance*, **16**, 171, 2000.

10. R.M. Sternheimer, *Phys. Rev.*, **80**, 102, 1950.

11. R.M. Sternheimer, *Phys. Rev.*, **84**, 244, 1951.

12. R.M. Sternheimer and H.M. Foley, *Phys. Rev.*, **102**, 731, 1956.

13. R.E. Watson and A.J. Freeman, *Phys. Rev.*, **135**, 1209, 1964.

14. P.C. Schmidt, K.D. Sen, T.P. Das and A. Weiss, *Phys. Rev. B*, **22**, 4167, 1980.

15. G.B. Bacskay and A.D. Buckingham, *Mol. Phys.*, **91**, 391, 1997.

16. Y. Michihiro and G.D. Mahan, *Phys. Rev. B*, **56**, 12151, 1997.

17. P.C. Schmidt, K.D. Sen, T.P. Das, and A. Weiss, *Phys. Rev. B*, **22**, 4167, 1980.

18. P. Tripathi and N.C. Mohapatra, *J. Phys B: At. Mol. Opt. Phys.*, **23**, 3241, 1990.

19. A.A. Gusev, I.M. Reznik and V.A. Tsitrin, *J. Phys.: Condens Matter*, **7**, 4855, 1995.

20. T.P. Das and R. Bersohn, *Phys. Rev.*, **102**, 360, 1956.

21. R.M. Sternheimer, *Phys. Rev.*, **115**, 1198, 1959.

22. P.W. Longhoff and R.P. Hurst, *Phys. Rev.*, **139**, A1415, 1965.

Chapter 3

Theory: *ab initio* calculation and magic-angle-spinning nuclear magnetic resonance

3.1 Introduction

This chapter outlines the theory underlying both the *ab initio* calculation of electric field gradient information, on which the remainder of this thesis is based, and the NMR experimental techniques used to obtain nuclear quadrupole parameters.

Section 2 looks at how the *ab initio* techniques used in this work attempt to solve the quantum mechanical equations governing the behaviour of the systems studied. The exact solution of these equations is an intractable problem requiring a number of approximations to be made, though, in contrast to semi-empirical approaches, those used in *ab initio* methods are based on general physical principles. There are also many complexities underlying the application of *ab initio* methods to different classes of system, however, this chapter will only discuss in detail those that are of direct relevance to the study of periodic ionic systems. Detailed accounts of *ab initio* methods are provided in various textbooks such as those listed in references [1] to [3].

Section 3 provides an outline description of the magic-angle-spinning nuclear magnetic resonance (MAS NMR) technique [4-7], particularly as applied to quadrupolar nuclei [8-10], and includes a technical summary of the apparatus used. Details of particular experimental procedures are given and, where relevant, these are illustrated with specific examples taken from results that are to be discussed in more detail in later chapters.

3.2.1 The Schrödinger equation

A fundamental idea of quantum mechanics is that, for any (chemical) system there exists a wavefunction, Ψ, that characterises that system. The observable properties of the

system are returned when the appropriate operator acts on the wavefunction. In mathematical notation this can be written as:

$$\vartheta\Psi = \varepsilon\Psi \tag{3.1}$$

where ϑ is an operator and ε is a scalar value for some property of the system. When this equation holds, Ψ is called an eigenfunction and ε an eigenvalue. The probability that a system, described by Ψ, will be found in a given state is proportional to the product of the wavefunction with itself, that is Ψ^2 (or $\Psi^*\Psi$ if Ψ is complex). This interpretation means that the square integral of the wavefunction must be known:

$$\int|\Psi|^2 dr < \infty \tag{3.2}$$

where the integral is over all the space accessible to the particle. For the total energy of a system, E, the quantum mechanical operator is called the "Hamiltonian" operator, $\hat{H}$, and in this case we have:

$$\hat{H}\Psi = E\Psi \tag{3.3}$$

This is the reduced form of the Schrödinger equation.

Atomic units

Quantum mechanical calculations are primarily concerned with atomic particles. When the properties of such particles are expressed in SI units, their values become cumbersome since they involve many factors of 10. In order to make these values more manageable, a system of atomic units has been devised which also incorporates such quantities as the mass of an electron and the electronic charge. The atomic units of charge, mass, length and energy are defined as follows:

1 unit of charge equals the absolute charge on the electron, $|e| = 1.60219 \times 10^{-19}$ C

1 mass unit equals the mass of the electron, $m_e = 9.10593 \times 10^{-31}$ kg

1 unit of length (1 Bohr) is given by $a_0 = h^2 / 4\pi^2 m_e e^2 = 5.29177 \times 10^{-11}$ m

1 unit of energy (1 Hartree) is given by $E_a = e^2 / 4\pi\varepsilon_0 a_0 = 4.35981 \times 10^{-18}$ J

The atomic unit of length is the radius of the first orbit in Bohr's treatment of the hydrogen atom. The atomic unit of energy corresponds to the interaction between two electronic charges separated by the Bohr radius. In atomic units, Plank's constant $h = 2\pi$ and so $\hbar \equiv 1$.

One-electron atom

In the case of an atom composed of a single electron and a nucleus with Z protons, in the absence of an external field, the total energy will be given by the sum of the kinetic energy and potential energy terms. In general, the Hamiltonian can be written:

$$\hat{H} = \hat{T} + \hat{V} \tag{3.4}$$

where $\hat{T}$ represents the kinetic energy operator and $\hat{V}$ represents the potential energy operator involving a nuclear-electron attraction term. These operators can be written as follows:

$$\hat{T} = -\frac{\hbar^2}{2m_e}\left(\frac{\partial^2}{\partial x^2} + \frac{\partial^2}{\partial y^2} + \frac{\partial^2}{\partial z^2}\right) \tag{3.5}$$

which can be abbreviated to

$$\hat{T} = -\frac{\hbar^2}{2m_e}\nabla^2 \tag{3.6}$$

and

$$\hat{V} = \frac{-Ze^2}{4\pi\varepsilon_0 r} \tag{3.7}$$

In atomic units the Hamiltonian is

$$\hat{H} = -\frac{1}{2}\nabla^2 - \frac{Z}{r} \tag{3.8}$$

where Z is the charge on the nucleus and r is the distance between the electron and the nucleus.

General poly-electronic systems

In the more general case of a chemical system composed of M nuclei and N electrons, in the absence of an external field, the total energy will be given by the sum of (i) a kinetic energy operator involving the nuclei and electrons, respectively, and (ii) a potential energy operator involving three terms: nuclear-electron attraction, electron-electron repulsion and nuclear-nuclear repulsion. These operators can be written, using atomic units, as:

$$\hat{T} = -\sum_{k}^{M} \frac{1}{2m_k} \nabla_k^2 - \frac{1}{2}\sum_{i}^{N} \nabla_i^2 \tag{3.9}$$

$$\hat{V} = -\sum_{k}^{M}\sum_{i}^{N} \frac{Z_k}{r_{ik}} + \sum_{i<j}^{N} \frac{1}{r_{ij}} + \sum_{k<l}^{M} \frac{Z_k Z_l}{r_{kl}} \tag{3.10}$$

where m_k is the mass of nucleus k; k and l denote nuclei; i and j denote electrons; Z_k is the charge of nucleus k; r_{ij} is the distance between the electrons i and j; r_{ik} is the distance between the electrons i and nuclei k and r_{kl} is the distance between the nuclei k and l.

Although the Schrödinger equation for such a system can be written in relatively simple terms, it is an example of an N-body problem and as such cannot be solved analytically. In order to overcome this difficulty, computational chemists are forced to make a variety of approximations. The first approximation generally used is the Born-Oppenheimer approximation.

The Born-Oppenheimer approximation

The kinetic energy of a chemical system can be partitioned into separate contributions from the electrons and the nuclei. However, for the potential energy it is the term:

$$\sum_{k}^{M}\sum_{i}^{N}\frac{Z_k}{r_{ik}} \tag{3.11}$$

that prevents a separation of the electronic and nuclear contributions. The Born-Oppenheimer approximation assumes that this separation is possible. The nuclei are very much more massive than the electrons and so move relatively slowly; hence, as an approximation they may be treated as stationary. On the other hand, electrons can respond almost instantaneously to any change in the position of the nuclei. Therefore, the Born-Oppenheimer approximation allows the Schrödinger equation to be simplified so that the kinetic energy of the nuclei can be neglected and the nuclear-nuclear repulsion term considered as a constant since the nuclei have a definite separation. The result is the *N*-electron Hamiltonian $\hat{H}_e$:

$$\hat{H}_e = -\frac{1}{2}\sum_{i}^{N}\nabla_i^2 - \sum_{k}^{M}\sum_{i}^{N}\frac{Z_k}{r_{ik}} + \sum_{i<j}^{N}\frac{1}{r_{ij}} \tag{3.12}$$

where the first term of Equation (3.12) represents the electron kinetic energy, the second term is the Coulomb potential generated by the nuclei and the third term is the electron-electron Coulomb interaction. The nuclei are held in fixed positions during the calculation so that r_{ij} varies only if the electrons move.

3.2.2 Hartree-Fock theory

Hartree-Fock (HF) theory was the initial approach taken in an attempt to solve the *N*-body Schrödinger equation and involved the transformation of the full *N*-body equation into *N* single-body equations. From Equation (3.12), the *N*-electron Hamiltonian can be seen to

be the sum of three terms; the first two involve the coordinates of just one electron and the third just two. These are termed one- and two-electron operators respectively. If it is assumed that the electrons are non-interacting, then, apart from the nuclear-nuclear repulsion constant, the N-electron Hamiltonian can be rewritten as the sum of N one-electron Hamiltonians:

$$\hat{h}_i = -\frac{1}{2}\nabla_i^2 - \sum_k^M \frac{Z_k}{r_{ik}} \tag{3.13}$$

$$\hat{H}_e = \sum_i^N \hat{h}_i \tag{3.14}$$

The ground state of any Hamiltonian, $\hat{H}$, can be determined by means of the variational principle for the normalised wavefunction $\Psi(1,2,\cdots,N)$:

$$\left\langle \Psi \middle| \hat{H} \middle| \Psi \right\rangle = \sum_{s_1}\sum_{s_2}\cdots\sum_{s_N}\int \Psi^*(1,2,\cdots,N)\hat{H}\Psi(1,2,\cdots,N)d\boldsymbol{r}_1 d\boldsymbol{r}_2 \cdots d\boldsymbol{r}_N$$

$$= minimum = E_0 \tag{3.15}$$

where s_i is the spin direction of the i-th electron. According to the variational principle, an approximate wavefunction, $\Psi(1,2,\cdots,N)$, can be found which minimizes the expectation value $\left\langle \Psi \middle| \hat{H} \middle| \Psi \right\rangle$, since the expectation value is always greater than the true ground state energy. If it is assumed that the electrons are independent, then $\Psi(1,2,\cdots,N)$ is a Slater determinant of single-particle wavefunctions such that:

$$\Psi(1,2,\cdots,N) = \frac{1}{\sqrt{N!}}\begin{vmatrix} \psi_1(1) & \psi_2(1) & \cdots & \psi_N(1) \\ \psi_1(2) & \psi_2(2) & \cdots & \psi_N(2) \\ \vdots & \vdots & \ddots & \vdots \\ \psi_1(N) & \psi_2(N) & \cdots & \psi_N(N) \end{vmatrix} \tag{3.16}$$

where $\psi_\lambda(i)$ is the one-electron wavefunction of the λ-th level, which depends on the position, $\boldsymbol{r}_i$, and spin direction, s_i, of the i-th electron, and forms an orthonormal set:

$$\langle \psi_\lambda | \psi_\nu \rangle = \sum_{s_i} \int \psi_\lambda^*(i) \psi_\nu(i) d\boldsymbol{r}_i = \delta_{\lambda\nu} \tag{3.17}$$

If Equation (3.16) is used as a trial solution, the expectation value can be evaluated as:

$$\langle \Psi | \hat{H} | \Psi \rangle = \sum_{\lambda=1}^{N} \langle \psi_\lambda | \hat{H}_0 | \psi_\lambda \rangle + \frac{1}{2} \sum_{\lambda,\nu} \langle \psi_\lambda \psi_\nu | U | \psi_\lambda \psi_\nu \rangle - \frac{1}{2} \sum_{\lambda,\nu} \langle \psi_\lambda \psi_\nu | U | \psi_\nu \psi_\lambda \rangle \tag{3.18}$$

where the Hamiltonian is divided into the one-electron part $\hat{H}_0$ and the electron-electron Coulomb interaction U as shown in Equation (3.12). Putting Equation (3.18) in variational form and introducing Lagrangian multipliers in order to guarantee the normalization condition, Equation (3.17), we obtain:

$$\sum_{\lambda=1}^{N} \langle \delta\psi_\lambda | \hat{H}_0 | \psi_\lambda \rangle + \sum_{\lambda,\nu} \langle \delta\psi_\lambda \psi_\nu | U | \psi_\lambda \psi_\nu \rangle - \sum_{\lambda,\nu} \langle \delta\psi_\lambda \psi_\nu | U | \psi_\nu \psi_\lambda \rangle$$

$$- \sum_{\lambda} \varepsilon_\lambda \langle \delta\psi_\lambda | \psi_\lambda \rangle = 0 \tag{3.19}$$

where $\varepsilon_\lambda (\lambda = 1,2,\cdots,N)$ denotes the Lagrangian multiplier. In order that Equation (3.19) is satisfied for an arbitrary variation $\langle \delta\psi_\lambda |$, the one-electron wavefunction ψ_λ should satisfy:

$$\hat{H}_0 \psi_\lambda(i) + \left[\sum_{\nu=1}^{N} \sum_{s_j} \int \psi_\nu^*(j) U(i,j) \psi_\nu(j) d\boldsymbol{r}_j \right] \psi_\lambda(i)$$

$$- \left[\sum_{\nu=1}^{N} \sum_{s_j} \int \psi_\nu^*(j) U(i,j) \psi_\nu(j) d\boldsymbol{r}_i \right] \psi_\nu(i) = \varepsilon_\lambda \psi_\lambda(i) \tag{3.20}$$

Equation (3.20) is known as the Hartree-Fock equation and represents the one-electron approximation for interacting fermions that includes the anti-symmetry of the wavefunction. The use of the single Slater determinant, Equation (3.16), to express the many-electron wavefunction is known as the Hartree-Fock approximation. This approximation affects the accuracy with which the 'exchange-correlation' contribution to

the total energy is calculated. The exchange contribution comes about as a direct consequence of Pauli's exclusion principle, which prohibits two fermions from occupying the same quantum state. This reduces the probability of one electron being near another electron of the same spin. The correlation contribution is due to the reduction in probability of an electron being near another electron due to strong electron-electron Coulomb repulsion. The most significant drawback of HF theory is that it fails to adequately represent electron correlation with the effect that the correlation energy can be defined as the difference between the exact energy and the HF energy for the system.

3.2.3 Density functional theory

In contrast to HF theory, which tries to determine approximations to the *N*-electron wavefunction, Density Functional Theory (DFT) is a formally exact theory based on the electron density, $\rho(\mathbf{r})$, of a system. In 1964, Hohenberg and Kohn [11] considered the ground state of an electron-gas system in an external potential $v(\mathbf{r})$, and proved that the following density functional theorem holds exactly: there is a universal functional $F[\rho(\boldsymbol{r})]$ of the electron charge density $\rho(\boldsymbol{r})$ that defines the total energy of the electronic system as:

$$E = \int v(\boldsymbol{r})\rho(\boldsymbol{r})d\boldsymbol{r} + F[\rho(\boldsymbol{r})] \tag{3.21}$$

There is a constraint on the electron density since the total number of electrons (N) is fixed:

$$N = \int \rho(\boldsymbol{r})d\boldsymbol{r} \tag{3.22}$$

The energy of the system can be minimised, in order to find the true electron charge density in the external potential, by introducing this constraint as a Lagrange multiplier ($-\mu$). This theory is exact for a non-degenerate ground state, however, no exact general form of the functional, $F[\rho(\boldsymbol{r})]$, has yet been found, so approximations must be used.

Local density approximation

The local density approximation (LDA), first formulated by Kohn and Sham [12], assumes that the exchange-correlation functional can be defined as a simple function of the density at any position, $\boldsymbol{r}$. If the electron kinetic energy is written as $T[\rho(\boldsymbol{r})]$ then in the LDA the universal functional is given by:

$$F[\rho(\boldsymbol{r})]=T[\rho(\boldsymbol{r})]+\frac{1}{2}\int\frac{\rho(\boldsymbol{r})\rho(\boldsymbol{r}')}{|\boldsymbol{r}-\boldsymbol{r}'|}d\boldsymbol{r}d\boldsymbol{r}'+E_{xc}[\rho(\boldsymbol{r})]-\mu\int\rho(\boldsymbol{r})d\boldsymbol{r} \tag{3.23}$$

where $E_{xc}[\rho(\boldsymbol{r})]$ is the exchange-correlation energy functional and is given as:

$$E_{xc}[\rho(\boldsymbol{r})]=\int\rho(\boldsymbol{r})\varepsilon_{xc}(\rho(\boldsymbol{r}))d\boldsymbol{r} \tag{3.24}$$

The LDA uses the exchange-correlation energy of the homogeneous electron gas, $\varepsilon_{xc}(\rho(\boldsymbol{r}))$, evaluated from the charge density at the point $\boldsymbol{r}$ under consideration. Effectively at $\boldsymbol{r}$, $\rho = \rho(\boldsymbol{r})$ and E_{xc} is equal to the exchange-correlation energy for the electron-gas system which has a homogeneous charge density ρ. Such a situation is valid if the inhomogeneity of $\rho(\boldsymbol{r})$ is small, however, the main approximation of LDA is that this is applied even if the inhomogeneity is large. Application of the variational principle to Equation (3.21), with the constraint that for an N-electron system $\int\rho(\boldsymbol{r})d\boldsymbol{r} = N$, gives:

$$\int\delta\rho(\boldsymbol{r})\left\{\frac{\delta T[\rho]}{\delta\rho(\boldsymbol{r})}+v(\boldsymbol{r})+\int\frac{\rho(\boldsymbol{r}')}{|\boldsymbol{r}-\boldsymbol{r}'|}d\boldsymbol{r}'+\frac{\delta E_{xc}}{\delta\rho(\boldsymbol{r})}-\mu\right\}d\boldsymbol{r}=0 \tag{3.25}$$

Kohn and Sham proposed using a set of N single-electron wavefunctions. The charge density is then defined as:

$$\rho(\boldsymbol{r})=\sum_{\lambda=1}^{N}|\psi_\lambda(\boldsymbol{r})|^2 \tag{3.26}$$

where $\psi_\lambda(\boldsymbol{r})$ is the wavefunction of the λth level allowing the kinetic energy to be defined as:

$$T[\rho(r)] = -\frac{1}{2}\sum_{\lambda=1}^{N}\int \psi_\lambda^*(r)\nabla^2\psi_\lambda(r)dr \tag{3.27}$$

The solution of Equation (3.25) is then given by solving the following effective one-electron Schrödinger equation for ψ_λ:

$$\left\{-\frac{1}{2}\nabla^2 + v(r) + \int\frac{\rho(r')}{|r-r'|}dr' + \frac{\delta E_{xc}}{\delta\rho(r)}\right\}\psi_\lambda(r) = \varepsilon_\lambda\psi_\lambda(r) \tag{3.28}$$

where ε_λ is the orbital energy.

Equation (3.28) is called the Kohn-Sham equation and its eigenvalues are usually identified as the one-electron energy levels although, due to the electron-correlation effects for the states far below the Fermi level, this is not generally correct [1]. If Equation (3.28) is solved self-consistently then the solutions, ψ_λ, will be related to the electron charge density and kinetic energy density via Equations (3.26) and (3.27). However, the Slater determinant, constructed from ψ_λ, is not the true *N*-electron Hartree-Fock wavefunction and ψ_λ are not the same as the one-electron wavefunctions in the Hartree-Fock approximation. They are more directly related to the true electronic charge density.

Generalised gradient approximation

The local density approximation, although remarkably accurate, often fails when the electrons are strongly correlated, as in systems containing d and f orbital electrons. Many modern codes implementing DFT now use more advanced approximations such as the generalised gradient approximation (GGA) [13-16] in order to improve accuracy. Gradient-corrected functionals have been found to be of particular benefit in the

calculation of relative conformational energies and the study of intermolecular systems, particularly involving hydrogen bonding [17].

As stated above, the LDA uses the exchange-correlation energy for the uniform electron gas at every point in the system regardless of the homogeneity of the real charge density. However, in the case of non-uniform charge densities, the exchange-correlation energy can deviate significantly from that derived for the uniform state and such a deviation can be expressed in terms of the gradient and higher spatial derivatives of the total charge density. The GGA uses the gradient of the charge density to correct for this deviation. For systems where the charge density is slowly varying, the GGA has proved to be an improvement over LDA.

Hybrid HF / DFT Method

A key feature of DFT is the incorporation of correlation effects from the outset, unlike HF theory. However, it is important to note that HF theory does provide an essentially exact treatment for the exchange contribution. The hybrid method seeks to combine the correlation energy derived from DFT (using the LDA) with the HF energy. Becke [18, 19] proposed that the exchange-correlation energy E_{xc} be written as:

$$E_{xc} = \int_0^1 U_{xc}^{\lambda} d\lambda \tag{3.29}$$

where λ is a coupling parameter, which takes values from 0 to 1. When $\lambda = 0$, there is no Coulomb repulsion between the electrons, as λ increases the inter-electronic Coulomb repulsion is introduced until the full interaction of the 'real' system is establised for $\lambda = 1$. It is not practical to perform this integration analytically and so it must be approximated. In Becke's original paper, his own gradient correction for exchange (B88) [20] was used

along with a gradient correction for correlation suggested by Perdew and Wang [21]. However, an alternative scheme, and the one used in this work, is to employ the correlation functional (with gradient term) of Lee-Yang-Parr (LYP) [22] and the standard local correlation functional due to Vosko, Wilk and Nusair (VWN) [23]. This is the 'B3LYP' density functional and can be written:

$$E_{xc}^{B3LYP} = (1-a_0)E_x^{LSDA} + a_0E_x^{HF} + a_x\Delta E_x^{B88} + a_cE_c^{LYP} + (1-a_c)E_c^{VWN} \tag{3.30}$$

with values of the empirical coefficients $a_0 = 0.20$, $a_x = 0.72$ and $a_c = 0.81$.

3.2.4 Periodic systems

Ab initio calculations for the properties of real crystals need to take into account that these are periodically repeating systems. This section outlines the methods used to represent the interactions of an infinite repeating system with an *ab initio* treatment.

From Chapter 2, the atomic positions of a pure bulk crystal are invariant when they are translated by the lattice vector, $\boldsymbol{R}$. This means that the potential of an infinite crystal system $V(\boldsymbol{r})$ has translational invariance and perfect periodicity such that $V(\boldsymbol{r} + \boldsymbol{R}) = V(\boldsymbol{r})$. Since the one-electron Hamiltonian is translationally invariant, the effective one-electron wavefunctions can be written as the product of an exponential and a periodic function, $u_{k\lambda}(\boldsymbol{r} + \boldsymbol{R}) = u_{k\lambda}(\boldsymbol{r})$ for the λ-th level, such that:

$$\psi_{k\lambda}(\boldsymbol{r}) = e^{i\boldsymbol{k}.\boldsymbol{r}}u_{k\lambda}(\boldsymbol{r}) \tag{3.31}$$

where $\boldsymbol{k}$ is the wavevector. This is an example of the Bloch Theorem and

$$\psi_{k\lambda}(\boldsymbol{r} + \boldsymbol{R}) = e^{i\boldsymbol{k}.\boldsymbol{R}}\psi_{k\lambda}(\boldsymbol{r}) \tag{3.32}$$

where $\psi_{k\lambda}(\boldsymbol{r})$ is a Bloch function. The orthonormality condition is

$$\int \psi_{k\lambda}^{*}(\boldsymbol{r})\psi_{k'\lambda'}(\boldsymbol{r})d\boldsymbol{r} = \delta_{kk'}\delta_{\lambda\lambda'} \tag{3.33}$$

where δ_{ij} is the Kronecker delta and the integral is over the whole system. It can be verified that $\psi_{k\lambda}(\boldsymbol{r})$ and $u_{k\lambda}(\boldsymbol{r})$ satisfy the eigenvalue equation for the effective one-electron problem:

$$\hat{H}\psi_{k\lambda}(\boldsymbol{r}) = \left[-\frac{1}{2}\nabla^2 + V(\boldsymbol{r})\right]\psi_{k\lambda}(\boldsymbol{r}) = \varepsilon_{k\lambda}\psi_{k\lambda}(\boldsymbol{r}) \tag{3.34}$$

and

$$\hat{H}_k u_{k\lambda}(\boldsymbol{r}) = \left[\frac{1}{2}(\boldsymbol{k} - i\nabla)^2 + V(\boldsymbol{r})\right]u_{k\lambda}(\boldsymbol{r}) = \varepsilon_{k\lambda}u_{k\lambda}(\boldsymbol{r}) \tag{3.35}$$

for the wavevector $\boldsymbol{k}$, where $V(\boldsymbol{r}) = v(\boldsymbol{r}) + \int \frac{\rho(\boldsymbol{r}')}{|\boldsymbol{r} - \boldsymbol{r}'|}d\boldsymbol{r}' + \frac{\delta E_{xc}}{\delta\rho(\boldsymbol{r})}$. The energy eigenvalue $\varepsilon_{k\lambda}$ of each level, λ, changes smoothly as a function of $\boldsymbol{k}$ and forms a curve along one direction of $\boldsymbol{k}$ in $\varepsilon - k$ space. Plots of these curves in different $\boldsymbol{k}$ directions are called the band structure of the crystal.

By using reciprocal lattice vectors and $\boldsymbol{G}$, the reciprocal space equivalent of $\boldsymbol{R}$, the periodic function can be expanded as a Fourier series:

$$u_{k\lambda}(\boldsymbol{r}) = \frac{1}{\sqrt{\Omega}}\sum_{G}\tilde{u}_{k\lambda}(\boldsymbol{G})e^{i\boldsymbol{G}.\boldsymbol{r}} \tag{3.36}$$

$$\tilde{u}_{k\lambda}(\boldsymbol{G}) = \frac{1}{\sqrt{\Omega}}\int_{cell} u_{k\lambda}(\boldsymbol{r})e^{-i\boldsymbol{G}.\boldsymbol{r}}d\boldsymbol{r} \tag{3.37}$$

where Ω is the volume of the unit cell. Substitution of Equation (3.36) into the Bloch theorem, Equation (3.31), gives:

$$\psi_{k\lambda} = \frac{1}{\sqrt{\Omega}}\sum_{G}\tilde{u}_{k\lambda}(\boldsymbol{G})e^{i(\boldsymbol{k}+\boldsymbol{G}).\boldsymbol{r}} \tag{3.38}$$

If N is the total number of unit cells in the system, then the basis function

$$|k+G\rangle = \frac{1}{\sqrt{N\Omega}} e^{i(k+G).r} \tag{3.39}$$

is called a 'plane wave' and the representation of the one-electron wavefunction in a periodic potential by Equation (3.38) is called a 'plane wave expansion'. For real calculations, the maximum value of the kinetic energy, $\frac{1}{2}G^2$, of the plane waves is limited to the 'cut-off energy'. The larger this value, the more accurate will be the result.

It is also possible to represent the effective one-electron wavefunction in the periodic potential as a superposition of 'localised orbitals', $\phi_\lambda(r)$, centred at each unit cell:

$$\psi_{k\lambda}(r) = \frac{1}{\sqrt{N}} \sum_R e^{ik.R} \phi_\lambda(r-R) \tag{3.40}$$

Again, Equation (3.40) satisfies the Bloch theorem.

Using the fact that the wavefunction does not change if an arbitrary value of G is added to the wavevector, that is $\psi_{k\lambda}(r) = \psi_{(k+G)\lambda}(r)$, the wavevector can be confined within the first Brillouin zone (1st BZ). The ground-state charge density becomes the sum over the occupied levels of Bloch functions within the 1st BZ:

$$\rho(r) = \sum_{\lambda_{occ}} \sum_{k \in 1stBZ} |\psi_{k\lambda}(r)|^2 \tag{3.41}$$

where $\psi_{k\lambda}(\mathbf{r})$ is an eigenstate of Equation (3.34). Following on from this, translational symmetry dictates that

$$\langle \psi_{k\lambda} | H | \psi_{k'\lambda'} \rangle = \varepsilon_{k\lambda} \delta_{kk'} \delta_{\lambda\lambda'} \tag{3.42}$$

if k and k' belong to the 1st BZ. For calculations involving insulators and semiconductors, where there is an energy gap between valence and conduction bands, the density can be accurately defined using the special k-point method of Monkhorst and

Pack [24] for k-point sampling of the 1st BZ. If full advantage is taken of the space group, then sampling is only required for the irreducible part of the 1st BZ.

3.2.5 Mulliken population analysis

Although the concept of an atomic point charge is widely used in computational quantum mechanics, there is no unique definition of atomic charge in a molecule or periodic system. The first and most widely used definition of atomic charge, based on the wave function, was suggested by Mulliken [25] and is a scheme for assigning charges by dividing orbital overlap evenly between the atoms involved. This method is somewhat arbitrary because atomic charges are not quantum mechanical observables and, therefore, the charge distribution is not explicitly predictable from first principles.

In the Mulliken method, all the electron density, $P_{\mu\mu}$, in an orbital, ϕ_μ, is allocated to the atom on which that orbital resides. The remaining electron density, $P_{\mu\nu}$, is associated with the overlap, $S_{\mu\nu}$, between the two orbitals, ϕ_μ and ϕ_ν. For each element, $\phi_\mu\phi_\nu$, in the density matrix, half of the density is allocated to the atom that has ϕ_μ as an orbital and the other half to the atom on which ϕ_ν is located. The total charge on an atom A is given by subtracting the total number of electrons from the nuclear charge Z_A

$$q_A = Z_A - \sum_{\mu=1;\mu \text{ on A}}^{N} P_{\mu\mu} - \sum_{\mu=1;\mu \text{ on A}}^{N} \sum_{\nu=1:\nu\neq\mu}^{N} P_{\mu\nu}S_{\mu\nu} \tag{3.43}$$

A significant disadvantage of a Mulliken population analysis is the need for a balanced basis set, such that the number of basis functions present on each atom in the system is the same. When using extended basis sets, unphysical results may occur (orbital charges of

more than 2e) if the basis orbitals centred at one atom are responsible for the description of electron density close to another nucleus.

3.2.6 Basis sets

The most commonly used basis sets in quantum mechanical calculations are composed of atomic functions. An obvious choice would be the Slater-type orbitals (STOs) [26] because of their similarity to the atomic orbitals of the hydrogen atom. However, evaluation of some of the integrals required by *ab initio* calculations is difficult particularly when orbitals are on different atoms. It is now common to replace the Slater orbitals with those based upon gaussians.

Gaussian-type orbitals

Unlike Slater functions, gaussians do not have a cusp at the origin and decay towards zero more quickly, Figure 3.1. This problem was solved in 1950 when S.F. Boys [27] developed a method of using a linear combination of gaussian functions to form gaussian Type Orbitals (GTOs). The summing of a number of GTOs with different exponents and coefficients can form the approximate shape of the STO function, Figure 3.1. The more gaussian primitives that are used the more accurate will be the approximation to the STO.

The exponents and contraction coefficients for these gaussians can be determined in several different ways, for example by fitting to an STO or by optimising the energy in *ab initio* calculations on atoms and small molecules. Once the exponents and contraction coefficients have been determined, they define a standard basis set and are not changed in calculations on other systems.

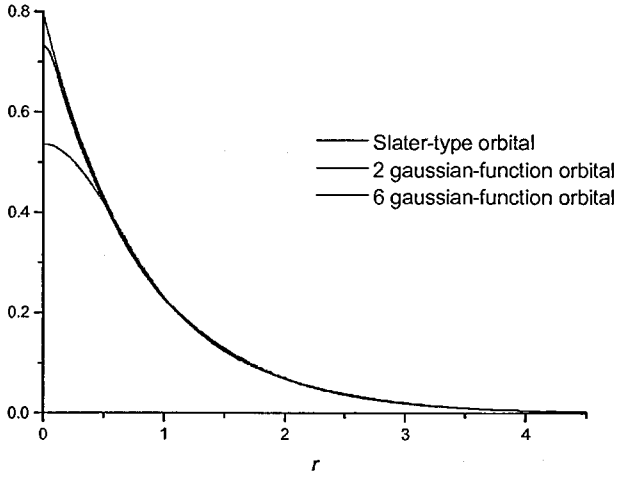

Figure 3.1 Comparison of 1s Slater-type orbital and gaussian expansions with two and six terms.

Pople basis sets

The *ab initio* calculations involving gaussian type orbitals in this work use those of Pople and co-workers. Two sets, 3-21G covering the atoms H to Cd [28–32] and 6-21G covering the atoms H – Ar [28, 29] have been used extensively. The notation used to describe these basis sets emphasises their split valence nature. Generally, for basis sets derived by Pople's group, the s and p contractions belonging to the same 'electron shell' are folded into a sp-shell. In this way, the number of s-type and p-type primitives is the same, and they have identical exponents. However, the coefficients for s- and p-type contractions are different.

In the 3-21G basis the 1s atomic orbital of a second-row element is represented by a fixed combination of 3 GTOs. The 2s ($2p_x$ etc.) are approximated by a fixed combination of 2 GTOs and the extra valence orbitals 2s' ($2p_x'$ etc.) have just one GTO. The 3-21G basis set offers a reasonable compromise between computational burden and quality of results. A larger basis set such as 6-21G gives a much lower energy but at the expense of having

more integrals over GTOs to be calculated, while for chemical phenomena (energy differences) the advantage is only small. Basis sets with two sets of gaussians describing the valence electrons are often referred to as sets of double zeta quality.

Polarisation and diffuse functions

The original contractions derived from atomic HF calculations are frequently augmented with other functions. The most popular are the polarisation and diffuse functions. The polarisation functions have higher values of the principal quantum number than those of the occupied atomic orbitals for the same atom and their use is denoted by a star after the basis set description e.g. 3-21G*. The exponents for polarisation functions cannot be derived from HF calculations for the atom, since they are not populated.

The polarisation effect is the result of bringing two atoms close together and therefore polarisation functions are important for modelling chemical bonding. Taking into account this effect means accounting for the d and f-shells, which are usually added as uncontracted gaussians. It is important to remember that adding them is costly since including a d shell adds 5 (or 6) basis functions and adding an f shell adds 7 (or 10). Pople's 6-31G* basis set adds 6 d-type functions: d_{z2}, d_{x2} and d_{y2} all being included rather than reduced to the two functions d_{z2} and d_{x2-y2}. This is equivalent to adding 5 d functions and an s function.

The basis sets may also be augmented with diffuse functions whose gaussians have very small exponents and decay only slowly with distance from the nucleus. Diffuse gaussians are usually of s- and p-type, although sometimes, diffuse polarisation functions are also used. Diffuse functions are sometimes necessary for the correct description of anions and

weak bonds (e.g. hydrogen bonds) and are most often used for calculations of properties such as dipole moments or polarisabilities. In the case of Pople's basis sets, the addition of a plus sign after the basis set description is used to denote the use of augmented functions e.g. 3-21+G.

It is important to note that the HF method scales as N^4, where N is the number of basis functions, and a careful check must be made of the number of functions that will be used in a calculation. This is especially important in circumstances involving a unit cell of low symmetry containing a large number of formula units.

Planewaves

The use of a plane wave (PW) basis set has a number of advantages, including the simplicity of the basis functions, and their ability to calculate efficiently the forces on atoms, the latter being particularly important if structure optimisation is required. In general, the representation of an arbitrary orbital in terms of a PW basis set would require a continuous, and hence infinite, basis set. However, for studies of the solid state, the imposition of periodic boundary conditions allows the use of Bloch's Theorem. The principle disadvantage of the use of a PW basis set is the number of basis functions required to accurately represent the Kohn-Sham orbitals. This problem may be reduced by the use of pseudopotentials as described in the next section, but several hundred basis functions per atom must still be used, compared with a few tens of basis functions when using atom-centred basis sets.

Pseudopotentials

In contrast to all-electron methods, the pseudopotential approach implies the frozen core approximation and allows computational effort to concentrate solely on valence states, which are the only ones responsible for chemical bonding. Moreover, the use of pseudopotentials leads to pseudo-wavefunctions, which vary smoothly in the core region [33, 34], and are amenable to a plane-wave expansion.

The approach taken in planewave DFT calculations is to use norm-conserving pseudopotentials where the pseudo-wavefunction matches the all-electron wavefunction beyond a cut-off radius that defines the core region. Within this region, the pseudo-wavefunction has no nodes and is related to the all-electron wave function by the norm-conservation condition; that is both wavefunctions carry the same charge. Such potentials can be constructed to give very accurate results at the price of having to use very high cut-off energies. Pseudopotential construction has itself been the subject of a great deal of study in the past [35-43] and for the work in this thesis the pseudopotentials generated by the method of Troullier and Martins [44] have been used.

3.2.7 Programs used for *ab initio* calculation

GAUSSIAN

One of the most popular computer programs for carrying out *ab initio* quantum chemical calculations is the 'Gaussian' series developed by J.A. Pople *et al.* [45]. It uses both HF and DFT to model a broad range of molecular systems under a variety of conditions. Although the code is molecular in nature, periodic systems have been studied [46] by the careful selection of clusters [47] to represent the site of interest. The embedded cluster

calculation reported in this work were carried out using 'Gaussian 94' on the DEC alpha 600 cluster of the Science and Technology Faculties at The Open University

CRYSTAL

In this study, the CRYSTAL95 [48], running on the DEC alpha 600 cluster of the Science and Technology Faculties at The Open University, and CRYSTAL98 codes, on both the DEC alpha 600 cluster and the EPSRC DEC 8400 facility, Columbus, at the Rutherford Appleton Laboratory, were used to perform periodic HF and DFT calculations (LDA and GGA). Hybrid density functional calculations were performed using the CRYSTAL98 [49] version of the code. Both software packages approximate the one-electron wavefunctions by a linear combination of gaussian localized atomic orbitals. CRYSTAL is a periodic code and generates an infinite 3D system from a specified unit cell and lattice vectors. All calculations were performed using restricted Hartree-Fock where the overall spin of the electrons on each atom is restricted to zero. There is no geometry optimisation available in CRYSTAL so all calculations were performed using experimentally-determined crystal structures obtained from the United Kingdom Chemical Database Service (CDS) at the University of Cambridge [50].

ABINIT

The ABINIT code [51] calculates the total energy, charge density and electronic structure of periodic systems within DFT, using pseudopotentials and a planewave basis set. The pseudopotentials are generated using the FHI98PP code [52]. ABINIT also allows for geometry optimisation according to the DFT forces and stresses. The code takes the description of the unit cell and atomic positions and assembles a crystal potential from the input atomic pseudopotentials. It then uses either an input wavefunction or simple

gaussians to generate the initial charge density and screening potential. Finally, a self-consistent algorithm is used to iteratively adjust the planewave coefficients until a sufficient convergence is reached in the energy. Atomic forces and the stress tensor are found from analytic derivatives of the energy with respect to atomic positions and unit cell primitive translations respectively. In this work, the ABINIT code, running under LINUX on a 550 MHz Pentium III desktop computer, was used to compute the total energy (DFT) for different hydrogen positions within the unit cell of anhydrous disodium hydrogenphosphate and to optimise its structure constrained by space group and unit cell parameters.

3.3 NMR spectroscopy in solids

The NMR spectra obtained from samples in the solid state are generally more complex than those in the liquid state since isotropic averaging of the various NMR interactions does not generally occur. The motion of atoms, ions or molecules in solids is relatively restricted giving rise to the appearance of orientation-dependent, anisotropic characteristics in the spectra. It is not always possible to record spectra for single crystals and solid-state NMR spectra of polycrystalline powders, which have crystallites in all possible orientations, are generally quite broad, and often ill defined. However, if it were possible to determine the magnitudes, as well as the orientations, of the chemical shielding, dipolar coupling and quadrupolar interactions this would provide valuable chemical information about the solid material. Unfortunately, the difficulty lies in the acquisition and interpretation of solid-state NMR spectra, and the extraction of the required information. Over the past thirty years, experimental techniques have become available that enable solid-state NMR spectra of polycrystalline samples to be obtained while selectively retaining those features that provide the desired chemical information.

MAS NMR spectroscopy, in particular, has proved a valuable means of obtaining high-resolution spectra from solids and, consequently, has established itself as a major technique in solid-state studies for a wide range of materials.

3.3.1 Basic NMR concepts

All nuclei with an odd number of either protons, neutrons, or both, possess a nuclear or intrinsic angular momentum ('spin') $\boldsymbol{I}$ and consequently a magnetic moment $\boldsymbol{\mu}$:

$$\boldsymbol{\mu} = \gamma \boldsymbol{I} \tag{3.44}$$

The quantity γ is called the magnetogyric ratio of the nucleus.

In an external magnetic field $\boldsymbol{B}_0$, along the z-direction, the energy of an isolated nucleus is not independent of its orientation; the nuclear spin angular momentum can take up only certain orientations with respect to the direction of this field. These orientations are such that the component along the z-direction is quantized,

$$I_z = m_I \hbar \tag{3.45}$$

where m_I is the magnetic quantum number and can take $2I + 1$ values, $m = I, I\text{-}1, \ldots -I$. In a magnetic field of magnitude B_0, the allowed energy states which are referred to as the nuclear Zeeman levels, are given by:

$$E = -\gamma \hbar m_I B_0 \tag{3.46}$$

Figure 3.2 illustrates the nuclear spin energy level diagram for an $I = 3/2$ nucleus and adjacent energy levels are separated by $|\gamma \hbar B_0|$.

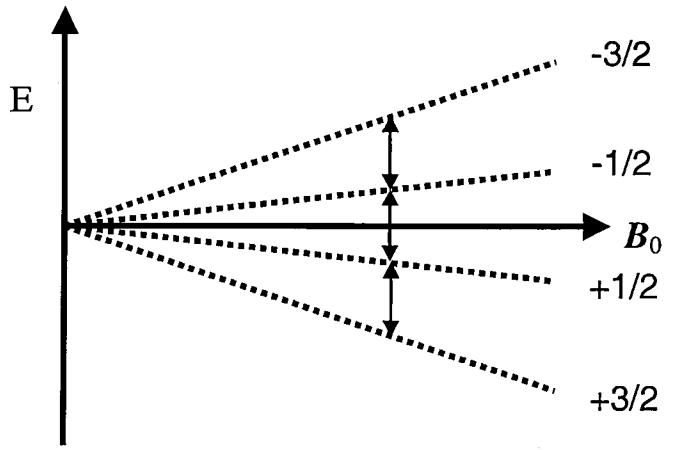

Figure 3.2 The nuclear spin energy level diagram for an $I = 3/2$ nucleus in a magnetic field B_0.

A NMR experiment involves the application of a time-varying magnetic field, usually in the form of a pulse, at right angles to B_0 in order to induce transitions between the various magnetic energy levels. Transitions between magnetic energy levels requires electromagnetic radiation of frequency:

$$\nu = \left| \left(\frac{\gamma}{2\pi} \right) B_1 \Delta m_I \right| \tag{3.47}$$

Since NMR transitions are governed by the selection rule, $\Delta m_I = \pm 1$ this equation simplifies to give the basic NMR resonance condition:

$$\nu = \left| \frac{\gamma}{2\pi} \right| B_0 \tag{3.48}$$

The nuclear spin quantum numbers and NMR properties of a few selected nuclei, including those involved in this work, are given in Table 3.1.

Table 3.1 Some common magnetic nuclei.

Nuclei	Natural abundance / %	I	ν^a / MHz	γ/ 10^7 rad $T^{-1}s^{-1}$
^1H	99.985	1/2	399.985	26.7520
^{13}C	1.108	1/2	100.533	6.7282
^{17}O	0.037	5/2	54.210	-3.6279
^{23}Na	100.000	5/2	105.750	7.0808
^{27}Al	100.000	5/2	104.169	6.9760
^{31}P	100.000	1/2	161.858	10.8410
^{51}V	99.760	7/2	105.075	7.0453

[a] The values shown are for nuclei in a magnetic field of 9.4 T.

3.3.2 Nuclear spin interactions and MAS

In general, the total NMR interaction in the absence of electromagnetic radiation can be represented by a spin Hamiltonian with parts corresponding to the Zeeman (*Z*), magnetic dipole-dipole (*D*), chemical shielding (*CS*) and, for nuclei with spin $I > ½$, nuclear quadrupole interaction (*Q*).

$$\hat{H} = \hat{H}_Z + \hat{H}_D + \hat{H}_{CS} + \hat{H}_Q \tag{3.49}$$

($\hat{H}_Q = 0$ for spin $I = ½$)

The Zeeman interaction is, in many cases, so large that all the other contributions can be taken as perturbations such that application of first-order perturbation theory (assuming without loss of generality an axially symmetric environment) leads to:

$$\omega^{(1)} = \sum_{\lambda} \omega^{(1)}_{\lambda,iso} + \omega^{(1)}_{\lambda,2} P_2(\cos\theta) \tag{3.50}$$

The angular frequency of the interaction, $\omega^{(1)}$, consists of an isotropic component $\omega^{(1)}_{\lambda,iso}$ ($\lambda = D$, *CS* or *Q*) and an anisotropic terms where $P_2(\cos\theta)$ is the second-order Legendre polynomial of $\cos\theta$ and θ is a characteristic angle defined for each interaction with respect to the applied magnetic field. In the case of λ = *CS*, the chemical shift derives from a

linear combination of an isotropic component and an anisotropic one scaled by $P_2(\cos\theta)$. For $\lambda = D$ or Q, only the anisotropic components need be considered $(\omega^{(1)}_{D,iso} = \omega^{(1)}_{Q,iso} = 0)$.

In a static polycrystalline sample, the tensorial nature of the NMR interactions results in spectra that are broadened as a consequence of the random distribution of crystallite orientations relative to the magnetic field. Magic-angle-spinning shown diagrammatically in Figure 3.3, is the single most used technique in solid state NMR and its popularity is due to its ability to remove the anisotropic broadening of a powder spectrum. Rapid spinning of a sample at a frequency ν_r, and an angle ϕ to $\boldsymbol{B}_0$, imparts an external time dependence on the internal spin interactions resulting in time averages depending on a common modulation factor of the form $(3\cos^2\phi - 1)$. By selecting $\phi = 54.74°$, the 'magic angle', the Hamiltonian is reduced to the isotropic parts just as in a liquid. However, quadrupolar nuclei present a particular challenge for study by MAS since in many cases the quadrupole interaction has to be treated to second order.

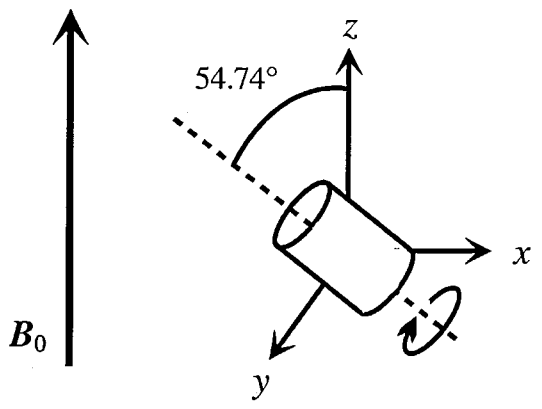

Figure 3.3 Schematic representation of magic-angle spinning.

3.3.3 Solid-state NMR of quadrupolar nuclei with half-integer spin

The nuclear quadrupole interaction Hamiltonian is given by:

$$H_Q = \frac{e^2qQ}{4I(2I-1)}\left\{3I_{33}^2 - I(I+1) + \frac{1}{2}\eta(I_+^2 + I_-^2)\right\} \tag{3.51}$$

and for a quadrupolar nucleus with half-integer spin in a strong magnetic field, the Zeeman interaction usually predominates over the internal spin interactions (*D*, *CS* and *Q*)

$$\|H_Z\| >> \|H_D\|, \|H_{CS}\|, \|H_Q\| \tag{3.52}$$

Furthermore, in many samples the magnetic dipole-dipole interaction between quadrupolar nuclei will be weak and any heteronuclear dipolar couplings, if present, can be removed by decoupling schemes. In effect, the contribution of magnetic dipole-dipole couplings can be neglected and it is only necessary to consider the single-spin chemical shielding and quadrupolar interactions. The isotropic chemical shift of the quadrupolar nucleus can be included in the Zeeman interaction and the assumption

$$\|H_Q\| >> \|H_{CSA}\| \tag{3.53}$$

where *CSA* is the anisotropic chemical shift contribution, is often valid. Thus, overall, the NMR behaviour of a quadrupolar nucleus with half-integer spin can be taken, to a good approximation, to be that of this nucleus experiencing just a single-spin quadrupole interaction.

If the strength of the quadrupole interaction is such that $C_Q > 0.05\nu_0$ (ν_0 is the resonant frequency), then first-order perturbation theory is insufficient to describe the NMR behaviour as second-order terms contribute significantly.

$$H_Q = H_Q^{(1)} + H_Q^{(2)} \tag{3.54}$$

The influences of first- and second-order quadrupole interactions on the magnetic energy levels of a spin $I = 3/2$ quadrupolar nucleus shown in Figure 3.4. To first-order, there is no effect of the quadrupole interaction on the central (+½, -½) transition; the second-order contribution is dominant in this case.

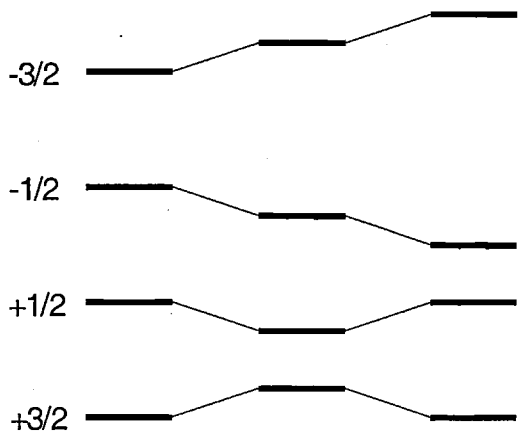

Figure 3.4 The effect of first- and second-order quadrupole interactions on the nuclear spin energy level diagram for an $I = 3/2$ nucleus in a magnetic field, B_0.

Focussing on the central transition, it can be shown [53] (again assuming axial symmetry for simplicity) that:

$$\omega_Q^{(2)} = \omega_{Q,iso}^{(2)} + \omega_{Q,2}^{(2)} P_2(\cos\theta) + \omega_{Q,4}^{(2)} P_4(\cos\theta) \tag{3.55}$$

The interaction now consists of an isotropic component and two anisotropic terms, the latter being proportional to the second- and fourth-order Legendre polynomials of $\cos\theta$, respectively. There is no spinning axis direction that will allow both the $P_2(\cos\theta)$ and $P_4(\cos\theta)$ terms to be completely time-averaged simultaneously. MAS averages the $P_2(\cos\theta)$ term to zero and partially averages the $P_4(\cos\theta)$ term producing spectra which have a characteristic line shapes. Computer simulations of these lineshapes provide not only values of the quadrupole parameters C_Q and η but also the isotropic chemical shift,

$\delta_{iso,cs}$. Figure 3.5 shows the effect on the MAS second-order central transition lineshape as η varies between 0 and 1.

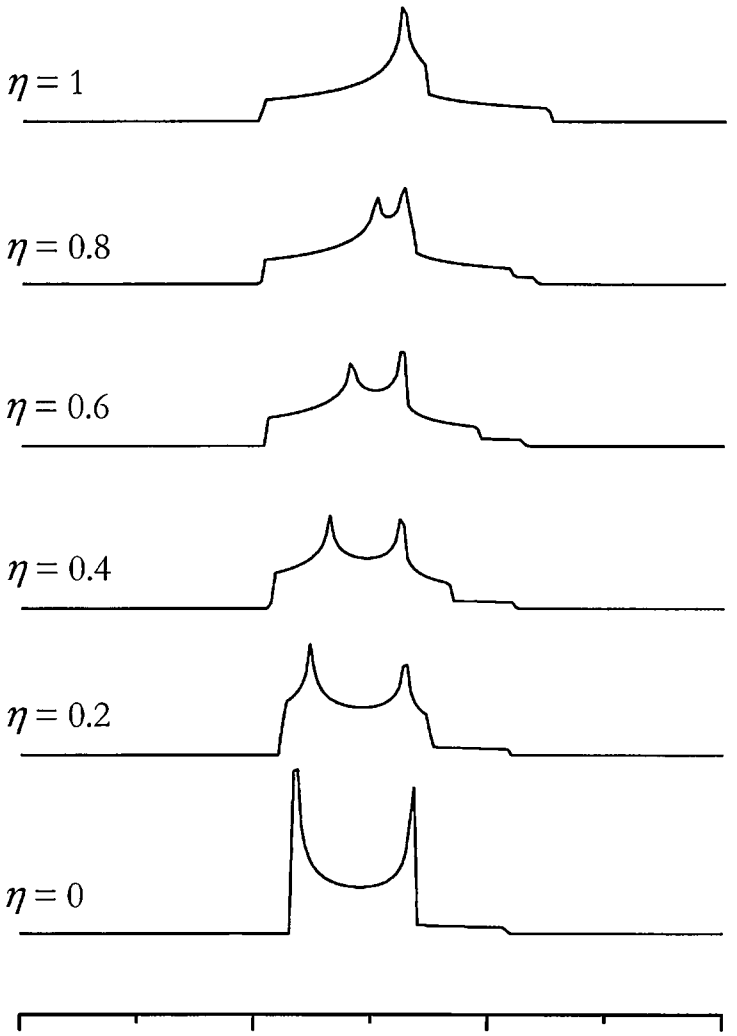

Figure 3.5 The effect of the asymmetry parameter (η) on the MAS second-order central transition lineshape.

Quantitative analysis

When dealing with a non-integer quadrupolar nucleus such as ^{23}Na (I = 3/2), it is important to consider, for a multi-site compound, that the different sites may have different responses to the irradiation pulse. The observed central transition lineshape

depends upon the amplitude, duration and offset of the radiofrequency pulse, ν_{rf}, because the quadrupole coupling is so strong that its effect during the pulse cannot be ignored. Two extreme cases can be considered. Firstly, 'selective' excitation of the central transition only occurs when the quadrupole frequency, $\nu_Q = 3C_Q / [2I(2I\text{-}1)]$, greatly exceeds the rf-field strength, $\nu_{rf} << \nu_Q$. Secondly, 'non-selective' excitation of all transitions when $\nu_{rf} >> \nu_Q$. In both these extremes the observed magnetisation as a function of pulse duration shows a simple sinusoidal oscillation at ν_{rf} and $(I + ½)\nu_{rf}$. However, in the intermediate regime when $\nu_Q \sim \nu_{rf}$ the excitation behaviour becomes complex and the response to the pulse duration becomes non sinusoidal. In these circumstances, the signal intensities from different sites in a solid will be affected to different extents. In order to ensure equal excitation of sites with widely differing values of C_Q it is necessary to satisfy the condition,

$$(I+1/2)2\pi\nu_{rf}T_p \leq \pi/6 \qquad (3.56)$$

where T_p is the pulse duration. If this condition is satisfied experimentally the error in intensity due to this 'pulse duration' effect will be less than ~5% [54].

However, the pulse length is not the only parameter that is important for quantitative intensity measurements. Although the prominent central transition is often the only one that can be recorded accurately, the act of spinning a sample also produces sidebands with the result that the total intensity of the resonance is distributed between them. A full simulation of the spectrum is possible but problematic, requiring high signal-to-noise for the spinning sidebands. A more pragmatic approach is to measure the intensity of the central transition and make corrections depending upon the fraction of magnetisation that appears in the isotropic line which Massiot and co-workers [55] defined as:

$$I^{Iso} = I_{1/2}^{Iso} + \sum_{m \neq 1/2} I_m^{Iso} \tag{3.57}$$

I_m^{Iso} depends only on $|1-2m|\nu_Q/\nu_r$ and η_Q, and $I_{1/2}^{Iso}$ depends on $\nu_Q^2/\nu_r\nu_0$ and η_Q. In this way I^{Iso} can be calculated and the experimental intensity corrected by the factor $1/I^{Iso}$.

3.3.4 Instrumentation

All the ^{23}Na MAS NMR data were recorded on a JEOL JNM-EX400 FT NMR instrument equipped with a JEOL EX Solid NMR facility coupled with a Doty Scientific Inc. MAS NMR probe (5 mm, high speed (14 kHz), double-tuned, multinuclear, CP/MAS). The probe had a maximum ^{1}H decoupling field strength of 60 kHz ($1.4\text{x}10^{-3}$ T) at 400 MHz. The 5mm rotors were made of silicon nitride and were fitted with Vespel caps. A compressed air system was used for sample spinning. The probe had two air inlets, one for bearing gas, which prevents the rotor colliding with the walls of the stator, and the other as a drive to spin the rotor. Rotor speeds of 14 kHz were attainable with this system although typically samples were spun in the range of 7 to 10 kHz. NMR signal data was transferred to a PC for processing using the Bruker WIN-NMR and WIN-FIT software [56]. The results of fitting simulated second-order quadrupole ^{23}Na MAS NMR lineshapes to experimental spectra are shown for the compounds, sodium dihydrogenphosphate (NaH_2PO_4), sodium pyrophosphate decahydrate ($Na_4P_2O_7{\cdot}10H_2O$) and sodium sulphite (Na_2SO_3), in Figure 3.7. The quadrupole parameters extracted from these fits are given in Chapter 4.

In order to gain a measure of the uncertainties associated with the fitting procedure used to simulate the quadrupole lineshapes, the ^{23}Na MAS NMR spectrum of $NaNO_2$ was

analysed in detail. The ^{23}Na NMR parameters have been well characterised for this compound ($C_Q(^{23}Na) = 1100.3 \pm 0.8$ kHz, $\eta(^{23}Na) = 0.1092 \pm 0.0009$ [57] and $\delta_{iso,cs}(^{23}Na)$ = -8.1 ± 0.2 ppm [58]) and by simply varying the parameters in the direct fitting procedure, a measure of their limits was obtained. If these uncertainties are taken to be fairly general for the compounds studied in this work then reliability in $C_Q(^{23}Na)$ is of the order of ± 5%, that for $\eta(^{23}Na)$ is ± 0.05 and $\delta_{iso,cs}(^{23}Na)$ is ± 0.5 ppm.

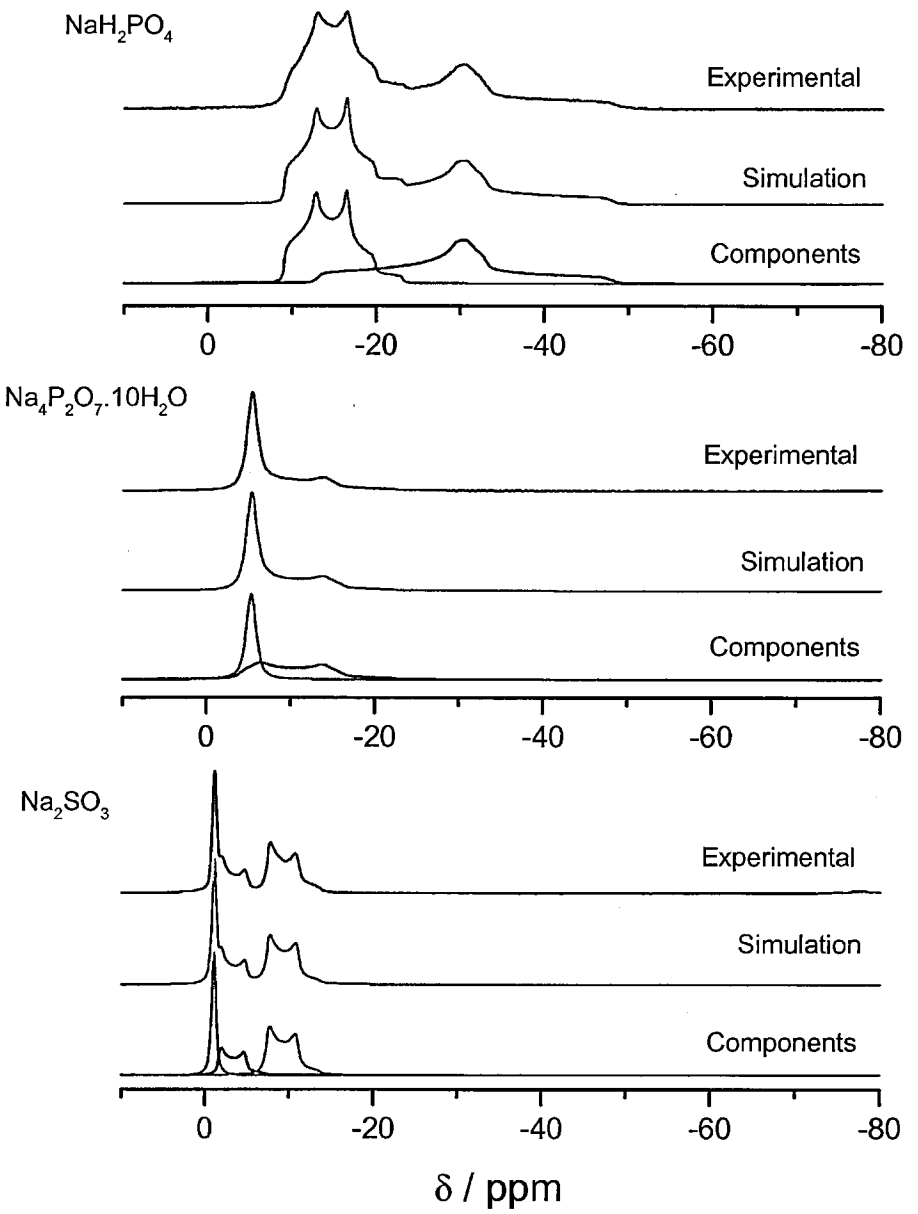

Figure 3.5 Experimental and simulated ^{23}Na MAS NMR spectra for NaH_2PO_4, $Na_4P_2O_7 \cdot 10H_2O$ and Na_2SO_3.

3.3.5 Experimental procedure

All samples were prepared for MAS NMR experiments using the same procedure but acquisition parameters used for the collection of data varied depending upon sample type.

Sample preparation

Before any sample was loaded into a NMR rotor, it was ground into a fine powder. It was found that careful packing of the finely-powdered sample was required to ensure even spinning of the rotor, particularly at high frequencies. Consistency in sample packing was achieved using a methodical approach and accurately-machined plastic tools. The first step was to take a small amount of sample and carefully place it into the rotor followed by gentle tapping to remove air and compaction using a plastic ram. This procedure was repeated until the rotor was full whereupon, using another plastic tool, a portion of the sample was removed to the depth of the Vespel cap and the cap fitted.

^{23}Na MAS NMR methods

^{23}Na is a quadrupolar nucleus with nuclear spin I = 3/2 and natural abundance of 100%. Potentially it is a good nucleus for NMR study since it has a sensitivity, relative to that of ^{13}C, of 530. All ^{23}Na MAS NMR spectra were recorded at 105.8 MHz with reference to an external sample of solid NaCl; $\delta(^{23}\text{Na}) = 0 \pm 1$ ppm.

All ^{23}Na MAS NMR data presented in this work were recorded with pulse widths of 1 μs in order to avoid, as much as possible, distortion of the second-order quadrupole NMR lineshapes.

References

1. K. Ohno, K. Esfarjani, and Y. Kawazoe, *Computational Materials Science,* Springer, Berlin, 1999.
2. M. Springborg, *Methods of Electronic-Structure Calculations, From Molecules to Solids*, Wiley, Chichester, 2000.
3. A.R. Leach, *Molecular Modelling, Principles and Applications*, Prentice Hall, Harlow, 2001.
4. R.K. Harris, *NMR Spectroscopy*, Pitman, London, 1984.
5. M. Mehring, *High Resolution NMR in Solids*, Springer, Berlin, 1982.
6. B.C. Gerstein and C. Dybowski, *Transient Techniques in the NMR of Solids*, Academic Press, New York, 1985.
7. E.O. Stejskal and J.D. Memory, *High Resolution in the Solid State, Fundamentals of CP/MAS*, Oxford University Press, Oxford, 1994.
8. D. Freude and J. Haase, in *NMR Basic Principles and Progress*, Vol 29, ed. P. Diehl, E. Fluck, H. Günther, R. Kosfeld and J. Seelig, Springer-Verlag, Berlin, 1993.
9. A.P.M. Kentgens, *Geoderma*, **80**, 271, 1997.
10. M.E. Smith and E.R.H. van Eck, *Prog.NMR Spectrosc.*, **34**, 159, 1999.
11. P. Hohenberg and W. Kohn, *Phys. Rev.*, **136**, 864, 1964.
12. W. Kohn and L.J. Sham, *Phys. Rev.*, **140**, 1133, 1965.
13. D.C. Langreth and J.P. Perdew, *Phys. Rev. B*, **21**, 5469, 1980.
14. D.C. Langreth and M.J. Mehl, *Phys. Rev. B*, **28**, 1809, 1983.
15. J.P. Perdew and Y. Wang, *Phys. Rev. B*, **33**, 8800, 1986.
16. J.P. Perdew, *Phys. Rev. B*, **33**, 8822, 1986.

17. F. Sim, A. St-Amant, I. Papai and D.R. Salahub, *J. Am. Chem. Soc.*, **114**, 4391, 1992.

18. A.D. Becke, *J. Chem. Phys.*, **98**, 1372, 1993.

19. A.D. Becke, *J. Chem. Phys.*, **98**, 5648, 1993.

20. A.D. Becke, *Phys. Rev. A*, **38**, 3098, 1988.

21. J.P. Perdew in P. Ziesche and H. Eschrig, editors, *Electronic Structure of Solids*, Akademie Verlag, Berlin, 1991.

22. C. Lee, W. Yang and R.G. Parr, *Phys. Rev. B*, **37**, 785, 1988.

23. S.H. Vosko, L. Wilk and M. Nusair, *Can. J. Phys.*, **58**, 1200, 1980.

24. H.J. Monkhorst and J.D. Pack, *Phys. Rev. B*, **13**, 5188, 1976.

25. R. S. Mulliken, *J. Chem. Phys.*, **23**, 1833, 1955.

26. J.C. Slater, *Phys. Rev.*, **36**, 57, 1930.

27. S.F. Boys, *Proc. Roy. Soc. London A*, **200**, 542, 1950.

28. J.S. Binkley, J.A. Pople, W.J. Hehre, *J. Am. Chem. Soc.*, **102**, 939, 1980.

29. M.S. Gordon, J.S. Binkley, J.A. Pople, W.J. Pietro and W.J. Hehre, *J. Am. Chem. Soc.*, **104**, 2797, 1983.

30. K.D. Dobbs, W.J. Hehre, *J. Comput. Chem.*, **7**, 359, 1986.

31. K.D. Dobbs, W.J. Hehre, *J. Comput. Chem.*, **8**, 861, 1987.

32. K.D. Dobbs, W.J. Hehre, *J. Comput. Chem.*, **8**, 880, 1987.

33. J.C. Phillips, *Phys. Rev.*, **112**, 685, 1958.

34. J.C. Phillips and L. Kleinman, *Phys. Rev.*, **116**, 287, 1959.

35. A. Redondo, W.A. Goddard III and T.C. McGill, *Phys. Rev. B*, **15**, 5038, 1977.

36. D.R. Hamann, M. Schlüter and C. Chiang, *Phys. Rev. Lett.*, **43**, 1494, 1979.

37. A. Zunger and M.L. Cohen, *Phys. Rev. B*, **20**, 4082, 1979.

38. G. P. Kerker, *J. Phys. C*, **13**, L189 1980.

39. G. B. Bachelet, D. R. Hamann and M. Schlüter, *Phys. Rev. B*, **26**, 4199, 1982.

40. D. R. Hamann, *Phys. Rev. B*, **40**, 2980, 1989.

41. A.M. Rappe, K.M. Rabe, E. Kaxiras and J.D. Joannopoulos, *Phys. Rev. B*, **41**, 1227, 1990.

42. J.S. Lin, A. Qteish, M.C. Payne and V. Heine, *Phys. Rev. B*, **47**, 4174, 1993.

43. M.-H. Lee, Ph.D. thesis, University of Cambridge, Cavendish Laboratory, 1994.

44. N. Troullier and J.L. Martins, *Phys. Rev. B*, **43**, 1993, 1991.

45. GAUSSIAN 94, Revision E.3, M.J. Frisch, G.W. Trucks, H.B. Schlegel, P.M.W. Gill, B.G. Johnson, M.A. Robb, J.R. Cheeseman, T. Keith, G.A. Petersson, J.A. Montgomery, K. Raghavachari, M.A. Al-Laham, V.G. Zakrzewski, J.V. Ortiz, J.B. Foresman, J. Cioslowski, B.B. Stefanov, A. Nanayakkara, M. Challacombe, C.Y. Peng, P.Y. Ayala, W. Chen, M.W. Wong, J.L. Andres, E.S. Replogle, R. Gomperts, R.L. Martin, D.J. Fox, J.S. Binkley, D.J. Defrees, J. Baker, J.P. Stewart, M. Head-Gordon, C. Gonzalez and J.A. Pople, Gaussian Inc., Pittsburgh PA, 1995.

46. H. Koller, G. Engelhardt, A.P.M. Kentgens and J. Sauer, *J. Phys. Chem.*, **98**, 1544, 1994.

47. J. Sauer, *Chem Rev.*, **89**, 199, 1989.

48. R. Dovesi, V.R. Saunders, C. Roetti, M. Causà, N.M. Harrison, R. Orlando and E. Aprà, *CRYSTAL95 User's Manual*, University of Torino, Torino, 1996.

49. V.R. Saunders, R. Dovesi, C. Roetti, M. Causà, N.M. Harrison, R. Orlando, and C.M. Zicovich-Wilson, *CRYSTAL98 User's Manual*, University of Torino, Torino, 1998.

50. D.A. Fletcher, R.F. McMeeking and D. Parkin, *J. Chem. Inf. Comp. Sci.*, **36**, 746, 1996.

51. The ABINIT code is a common project of the Université Catholique de Louvain, Corning Incorporated, and other contributors (http://www.abinit.org, accessed 17-12-02).

52. M. Fuchs and M. Scheffler, *Comput. Phys. Commun.*, **119**, 67, 1999.

53. A. Medek, J.R. Sachleben, P. Beverwyk and L. Frydman, *J. Chem. Phys.*, 104, 14, 1996.

54. E. Lipmaa, A. Samoson and M. Magi, *J. Am. Chem. Soc.*, **108**, 1730, 1986.

55. D. Massiot, C. Bessada, J.P. Coutures and F. Taulelle, *J. Magn. Reson.*, **90**, 231, 1990.

56. D. Massiot, H. Thiele and A. Germanus, *Bruker Rep.*, **140**, 43, 1994.

57. A. Weiss, *Z. Naturforsch.*, **15a**, 536, 1960.

58. J. Skibsted, N.C. Nielsen, H. Bildsøe and H.J. Jakobsen, *J. Magn. Reson.*, **95**, 88, 1991.

Chapter 4

Calculation of the electric field gradient tensor for sodium in a series of ionic sodium compounds: a correlation approach

4.1 Introduction

One of the first attempts to calculate electric field gradient tensors at sodium nuclei in ionic sodium compounds ($NaNO_3$, $NaClO_3$ and $NaBrO_3$) was made by Bersohn in 1958 [1]. The small range of sodium compounds was selected on the basis that they all had both the sodium and XO_3^- ions lying on three-fold axes. This crystallographic arrangement then required that only one component of the electric field gradient tensor had to be computed, namely V_{33}, with the principal axis lying along the three-fold axis for sodium. The calculation was based upon a point-charge model along with the use of a Sternheimer factor ($\gamma_\infty(Na^+)$ = -4.53) [2], the sodium nuclear quadrupole moment (Q = 0.100) and the assumption that the charge on the X atom in XO_3^- was zero [3]. The magnitudes of $C_Q(^{23}Na)$ obtained by this method are in reasonable agreement with modern experiment for $NaNO_3$: +0.384 MHz / -0.334 MHz [4-6] and $NaClO_3$: -0.849 MHz / 0.801 MHz [7] where the first value is the calculated value of $C_Q(^{23}Na)$ and the second that determined by experiment. Unfortunately, a large discrepancy is seen for $NaBrO_3$: -0.388 MHz / 0.864 MHz [7]. However, this relatively simple model is only expected to give good results in the case of ionic compounds containing monatomic anions (halides, oxides). In the case of sodium, these have point symmetries at the cation sites leading to zero efgs at the nucleus. Nonetheless, since that time, the point-charge model has become a standard for site assignments of sodium MAS NMR spectra in all types of compound. As recently as 1995, Power [8] used a point-charge model, using formal charges, to aid in the assignment of the three ^{23}Na resonances in anhydrous sodium sulphite (Na_2SO_3). Although the absolute values of the three sodium efg tensors were not predicted, there was a significant difference between the calculated values for the Na(*1*) and Na(*2*) sites and this allowed an assignment to be made. However, it should be noted

that an unambiguous assignment would not have been possible if the Na(*3*) site had not already been assigned on the basis of experimental intensity information.

In 1994, Koller and co-workers [9] recognised that the experimental investigation of quadrupole parameters in various systems was outpacing the theory required for the purposes of assignment. In order to address this problem, they looked for a simple modelling tool that would allow them to "interpret experimentally-determined quadrupole parameters in terms of the local symmetry of the charge distribution surrounding the nucleus". In the case of solid-state ^{23}Na NMR, they suggested the use of a specific cluster, based on the first coordination sphere of the sodium nucleus, as the basis of a point-charge model where the charges were not the formal ones. This approach was effective because, in addition, they used a correlation approach with an emphasis on consistent calculation rather than the need to calculate absolute values. Such a correlation also has the advantage that it is independent of the value used for the Sternheimer factor, but it is important to note that it is necessary to assume a constant value independent of structure. Furthermore, the calculations scale according to the value that is used for the ^{23}Na nuclear quadrupole moment. Despite the simplicity of the model, it was shown to work well for compounds in which the sodium atom occupied a single site and was exclusively coordinated to oxygen. However, the assignment of sodium resonances in multi-site compounds was more testing. For example, in the case of sodium triphosphate ($Na_3P_3O_9$), the experimentally determined values of $C_Q(^{23}Na)$ for the two sodium resonances are 2.20 MHz and 1.57 MHz [9] yet calculation gave 1.94 MHz and 1.90 MHz, respectively, from the best model for the oxygen charges. Assignment, even using a correlation approach, is not possible in this case.

The general aim of this Chapter is to build on the work of Koller and co-workers [9] but instead of using a simple point-charge model, this work uses quantum mechanical *ab initio* methods. A number of *ab initio* methods, which are all suitable for the determination of the electric field gradient tensor for sodium from structural information, are explored. An important objective is to find an approach that is both accurate and easily transferable across a wide range of ionic sodium compounds.

Initial investigations focus on the calculation of the sodium efg tensor in sodium nitrite ($NaNO_2$) using a cluster model. $NaNO_2$ is a useful model system since the sodium efg tensor has been determined from single crystal studies [10] and the sign of $C_Q(^{23}Na)$ is known experimentally [11-13]; furthermore, the coordination around the single type of sodium in the crystal structure is relatively complex. However, no reliable guidelines for selecting the optimum cluster size, basis set or charge distribution could be found. A more attractive alternative is to use a periodic approach based on the CRYSTAL code [14, 15]. This package performs *ab initio* calculations of the properties of periodic systems taking into account the symmetry of the crystal lattice to form crystalline orbitals from a linear sum of atomic orbitals. As a means of testing the periodic *ab initio* approach, detailed calculations, using relatively large basis sets, were carried out on both sodium nitrite and sodium nitrate ($NaNO_3$). Given the success of these calculations, more extensive investigations were then carried out using smaller, standard basis sets and this led to the development of a surprisingly robust correlation approach. Such an approach is transferable and offers real opportunities to solve difficult assignment problems.

4.2 Cluster calculations for $NaNO_2$

4.2.1 Background

Sodium nitrite is, in many ways, an ideal model compound for testing the calculation of a sodium efg tensor using *ab initio* calculations based on a cluster model:

- the crystal structure has been accurately determined [16]. The local environment around the single sodium site, including the labelling of the orthorhombic unit cell, is shown in Figure 4.1.
- the sodium efg tensor has been completely characterised using a combination of experimental techniques [10-13]. Details are summarised in Table 4.1. The sign of $C_Q(^{23}Na)$ is known for this compound.
- the local environment of the crystallographically unique sodium cation is relatively complex.

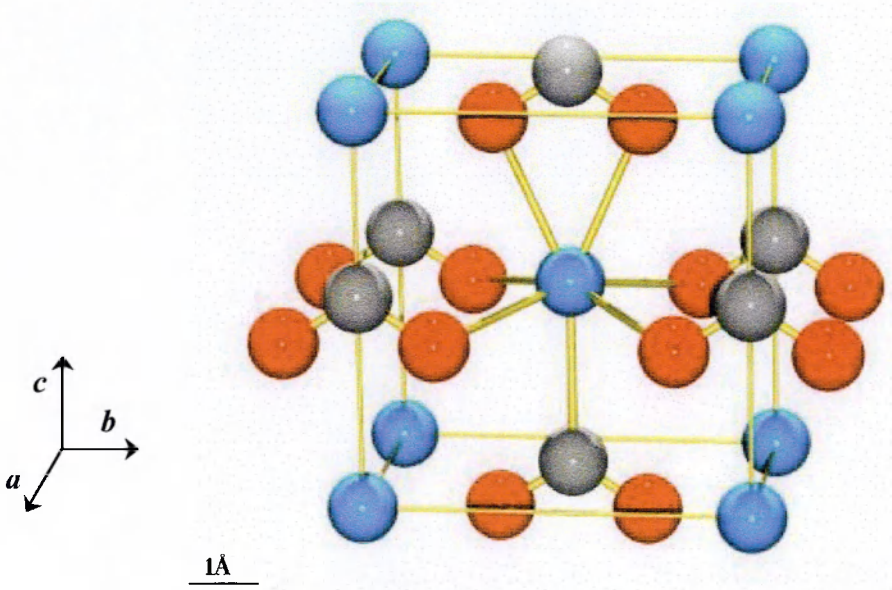

Figure 4.1 Part of the crystal structure of the room-temperature phase of $NaNO_2$. The seven tie lines around the central sodium cation indicate those atoms within the first coordination sphere, (sodium (blue), oxygen (red) and nitrogen (grey)).

Two types of model cluster were selected for this investigation. The first model was based on the immediate coordination environment of a reference sodium cation. The

second increased the size of the cluster to include the next-nearest shell of nitrite anions. In addition, both models included point charges in order to reduce the overall charge on a given cluster. In the construction of both clusters, due consideration was given to the guidelines suggested by Sauer [17] for the design of finite structure models.

In all the cluster calculations (as well as later periodic calculations in this chapter) the influence of vibrational and librational averaging effects on the comparison between experimental and calculated sodium efg tensors is assumed to be small. In the case of $NaNO_2$, it should be noted that there is strong evidence [18] that the information regarding the sodium efg tensor, shown in Table 4.1, is appropriate to the rigid-lattice regime. This is because any reorientation of the nitrite anion, which takes place at room temperature, is too slow on the NMR timescale to cause dynamic averaging.

Table 4.1 Experimental ^{23}Na efg tensor information for $NaNO_2$

$C_Q(^{23}Na)$ [a]	1100.3 ± 0.8 kHz
$\eta(^{23}Na)$ [a]	0.1092 ± 0.0009
Orientation of the principal axis frame [a]	$V_{11} \parallel \boldsymbol{b}$, $V_{22} \parallel \boldsymbol{a}$, $V_{33} \parallel \boldsymbol{c}$
Sign of $C_Q(^{23}Na)$ [b]	Negative

[a] The quadrupole parameters and the orientation of the principal axis frame were determined by NMR in a single crystal study at 20°C [10]. [b] The sign of $C_Q(^{23}Na)$ corresponds to that determined by several groups in studies of the asymmetry of ^{23}Na NMR satellites [11-13].

Cluster details

In the room-temperature phase of $NaNO_2$, as shown in Figure 4.1, the sodium cation occupies a single crystallographic site and all the V-shaped nitrite anions point along the ***c***-axis of the orthorhombic unit cell. Each sodium cation is surrounded by six nitrite anions in a roughly octahedral arrangement with the four equatorial groups co-ordinating

through one of their oxygen atoms, r(N–O) = 2.474 Å. In the case of the two axial groups, the upper nitrite anion co-ordinates via both oxygen atoms, r(Na–O) = 2.533 Å, and the lower via the nitrogen atom, r(Na–N) = 2.587 Å. Surrounding this arrangement are ten further sodium cations arranged in two shells. The first of these (Na′), shown in green in Figure 4.2(a), is at a distance r(Na– Na′) = 3.569 Å while the other shell (Na″), shown in purple, has r(Na– Na″) = 4.262 Å. The next nearest shell of nitrite anions (shown in Figure 4.2(b)) contains four such species, the lower two at a distance r(Na–N) = 4.409 Å and the upper two at a distance r(Na–N) = 4.647 Å.

The two clusters shown in Figure 4.2(a) and (b), respectively, are those selected for the *ab initio* calculations. All-electron basis sets were applied to the central sodium atom and all atoms making up the nitrite anions. Point charges were placed at the sites of the cations designated Na′ and Na″ in order to reduce the overall charge on a given cluster. In the discussion below, *pc* represents a set of point charges and the sum of these charges is the quantity n.

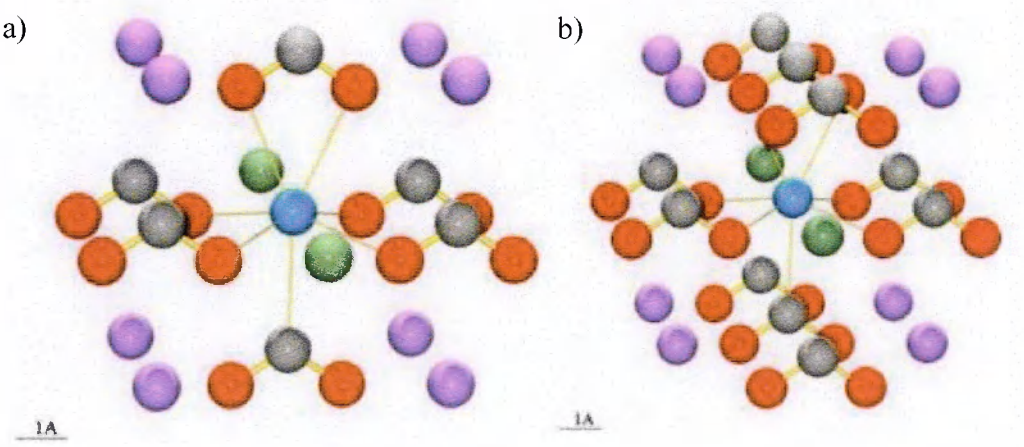

Figure 4.2 The structure of the two clusters used in the *ab initio* determination of the sodium efg tensor in $NaNO_2$. The seven tie lines around the sodium cation indicate those atoms within the first coordination sphere, (sodium (blue), oxygen (red), nitrogen (grey), Na′ (green) and Na″ (purple)).

4.2.2 Cluster of the type $\{Na(NO_2)_6 \cdot pc\}^{n-5}$

In the *ab initio* calculations, the 6-31G [19, 20] and 3-21G [21, 22] basis sets for sodium, nitrogen and oxygen were taken from the work of Pople and co-workers. The 6-311G basis sets for oxygen and nitrogen were the standard Pople sets [23], while the 6-311G basis set for sodium was taken from the work of Maclean and Chandler [24].

Table 4.2 shows a selection of results for calculations based upon this particular cluster.

Table 4.2 Calculated efg tensors at sodium in clusters of the form $\{Na(NO_2)_6 \cdot pc\}^{n-5}$

Point charges [a]		Basis set [b]	C_Q / MHz	η	Or. [c]
No.	Charge				
-	-	6-31G* [d]	-1.32	0.66	✓
10	+0.5	6-31G* [e]	-1.21	0.80	✓
10	+0.5	6-31G* B3LYP [e]	-1.60	0.15	✓
10	+0.5	6-311G* [e]	-1.54	0.93	✓
10	+0.5	6-311G* B3LYP [e]	-2.33	0.51	✓
10	+0.5	6-31G* / 6-31G* / 6-31+G / 3-21G [e]	-1.24	0.90	✓
10	+0.5	6-31G* / 6-31G* / 6-31+G / 3-21G B3LYP [e]	-1.54	0.10	✓
-	-	6-311G / 6-31G* / 6-31+G / 3-21G [d]	-1.94	0.56	✓
10	+0.5	6-311G / 6-31G* / 6-31+G / 3-21G [d]	-1.89	0.86	✓
-	-	6-311G / 6-31+G / 6-31+G / 3-21G [d]	-1.49	0.41	✓
10	+0.5	6-311G / 6-31+G / 6-31+G / 3-21G [d]	-1.36	0.75	✓
10	+0.5	6-311G / 6-31+G / 6-31+G / 3-21G B3LYP [e]	-2.26	0.31	✓
-	-	6-311G(d) / 6-31G* / 6-31+G / 3-21G [e]	-2.17	0.49	✓
10	+0.5	6-311G(d) / 6-31G* / 6-31+G / 3-21G [e]	-1.95	0.77	✓
10	+0.5	6-311G(d) / 6-31G* / 6-31+G / 3-21G B3LYP [e]	-2.42	0.43	✓

[a] The charges are located at sites corresponding to the atomic positions of Na′ and Na″. [b] A single entry indicates that all the cluster atoms were represented by this basis set. Otherwise, the basis sets are written in the order: central sodium cation / directly-coordinated oxygen atoms / nitrogens of the six nitrite anions/remaining atoms of the cluster. [c] This column refers to the calculated orientation of the principal axis frame of the sodium efg tensor. In all cases, as indicated by ✓, there is agreement with experiment. [d] GAMESS [26]. [e] GAUSSIAN 94 [27].

In general, the HF calculations correctly predict both the sign of $C_Q(^{23}Na)$ and the orientation of the sodium efg tensor. This is true for both charged and neutral clusters, and is independent of the basis sets used. These results are consistent with the cluster being a reasonable model, despite its limited size, for the immediate local environment of the sodium cation. However, the agreement between the experimentally derived ^{23}Na quadrupole parameters and those found for the HF calculations is not particularly good; both $C_Q(^{23}Na)$ and $\eta(^{23}Na)$ tend to be overestimated. On closer inspection no trends could be found in the selection of the basis sets, with or without the addition of diffuse anion functions, which could be used to suggest guidelines for the accurate calculation of the quadrupole parameters. It was also the case that the introduction of more locally-dense basis sets [25] did not significantly improve the situation. Overall, it appears that although the efg tensor is a local property of the system, a larger cluster is required to improve the accuracy of the calculations at the HF level of theory.

In comparison to the HF calculations, the hybrid DFT method B3LYP has a marked tendency to reduce the calculated value of $\eta(^{23}Na)$ and so give better agreement with experiment. However, the same improvement is not observed for the values of $C_Q(^{23}Na)$, which tend to be markedly more negative than those derived from the HF calculations using the same basis sets. The reason for this behaviour is not clear, although it may be a reflection of the artificial transfer of electron density from oxygen to sodium.

4.2.3 Cluster of the type $\{Na(NO_2)_{10} \cdot pc\}^{n-9}$

Increasing the size of the cluster to include an additional shell of four nitrite anions gives $\{Na(NO_2)_{10} \cdot pc\}^{n-9}$. A selection of the results for this cluster, using similar basis sets to those used with the smaller cluster, is shown in Table 4.3.

As was the case for the smaller cluster, the sign of C_Q and the tensor orientation are in agreement with experiment. The application of the same basis set to all the atoms of the cluster leads to reasonably good agreement with experiment for $C_Q(^{23}Na)$. However, agreement with $\eta(^{23}Na)$ is poor, the values being considerably larger than expected. This situation is improved by the introduction of diffuse anion functions on oxygen giving calculated values of the quadrupole parameters in reasonable agreement with experiment.

Table 4.3 Calculated efg tensors at sodium in clusters of the form $\{Na(NO_2)_{10} \cdot pc\}^{n-9}$

Point charges [a]		Basis set [b]	C_Q / MHz	η	Or.[c]
No.	Charge				
10	+0.9	6-21G*	-0.83	0.73	✓
10	+0.9	6-31G*	-1.10	0.65	✓
10	+0.9	6-311G*	-1.36	0.53	✓
-	-	6-311G / 6-31+G / 3-21G	-1.65	0.17	✓
10	+0.9	6-311G / 6-31+G / 6-31G / 3-21G	-1.28	0.15	✓
10	+1.0	6-311G / 6-31+G / 6-31G / 3-21G	-1.22	0.19	✓
10	+0.9	6-311G(d) / 6-31+G / 6-31G / 3-21G	-1.24	0.17	✓
10	+0.9	6-311G(d) / 6-31G(d) / 6-31G / 3-21G	-1.46	0.60	✓

[a] The charges are located at sites corresponding to the atomic positions of Na′ and Na″. [b] All calculations were carried out using GAUSSIAN 94. A single entry indicates that all the cluster atoms were represented by this basis set. Otherwise, the basis sets are written in the order: central sodium cation/directly-coordinated oxygen atoms/remaining atoms of the cluster. [c] See footnote *c* for Table 4.2.

4.2.4 Summary

Hartree-Fock calculations for clusters that were selected to reflect the local coordination environment of the sodium cation consistently predicted both the correct sign of $C_Q(^{23}Na)$ and the correct orientation of the sodium efg tensor in $NaNO_2$. However, the accuracy of the calculation of the ^{23}Na quadrupole parameters, in particular $\eta(^{23}Na)$, was far more variable; this situation was not significantly improved by the use of hybrid DFT methods. The best results were obtained for a relatively large cluster of the form $\{Na(NO_2)_{10}\}$ with

suitable point charges at the positions of the ten surrounding sodium cations. However, the agreement between the calculated and experimental values of the quadrupole parameters remained highly dependent upon basis set selection. Given these results, no clear guidelines arise as to the selection of optimum cluster size, basis set representation or, to some extent, nature of point charge distribution, that will ensure good agreement between calculation and experiment. In this sense, the routine use of cluster modelling is limited. For example, it would not be straightforward to use this approach to correlate calculated and experimental efg tensor information over a range of compounds. If an *ab initio* method is to be generally applicable for NMR assignment problems, a different modelling strategy is required.

4.3 Periodic calculations for $NaNO_2$ and $NaNO_3$

A periodic approach to the *ab initio* calculation of the sodium efg tensor is attractive because once the unit cell has been defined it is no longer necessary to specify the size of a cluster or a point charge distribution. However, the problem of basis set choice still remains.

As an initial strategy to test a periodic *ab initio* approach, calculations were carried out on $NaNO_2$ based on a reasonably large, optimised, ionic basis set. Such an approach would be expected to yield good results for the calculated sodium quadrupole parameters and this is shown to be the case. Given this result, attention was then focused on the use of smaller standard basis sets.

The results of the cluster calculations for $NaNO_2$ in Section 4.2 have shown that the relatively small 6-21G* and 6-31G* basis sets give reasonable agreement with

experiment for C_Q. It is of particular interest, therefore, given the potential usefulness of the *periodic ab initio* approach, to investigate whether these basis sets can be used in a general way for the calculation of sodium efg tensors in ionic materials. However, it is important to recognise that the use of standard molecular basis sets for *ab initio* calculations in ionic compounds can lead to non-convergence problems [28-30] and, consequently, some optimisation of the sodium basis set is required. To carry out this optimisation the calculation of the sodium efg tensor for $NaNO_2$ was compared with that for $NaNO_3$. The latter compound was chosen because it contains the same elements as $NaNO_2$ but has a markedly different coordination environment around the sodium cation (see Figure 4.3). The $NaNO_3$ sodium efg tensor has also been completely characterised.

4.3.1 [8-511 / 8-41 / 8-411] basis set calculations

The basis set description is expressed in the order [Na / N / O]. An optimised ionic 8-511G basis set for sodium, which has been used to model the structural properties of sodium fluoride and sodium chloride, was taken directly from the literature [31]. For oxygen and nitrogen, 8-411G basis sets were used with adjustments to ensure convergence in the periodic calculations. The oxygen basis set was taken from the work of Dovesi *et al.* [29, 30] although it should be noted that this basis set was optimised for the oxide anion in magnesium oxide (MgO); further optimisation was required in this work. The nitrogen basis set was optimised using the basis set optimisation function available within the GAMESS program [26]. The starting point for this was the oxygen 8-411G basis set of Dovesi *et al.* but with each gaussian exponent scaled by a factor of 0.7. (This value was obtained by comparing the exponents of oxygen and nitrogen in a range of standard basis sets.) Each of the scaled exponents, along with their associated coefficients, was then optimised by minimising the HF energy of the nitrite anion (NO_2^-)

in a molecular calculation in which oxygen was represented by the 8-411G basis set. In order to achieve convergence within CRYSTAL the diffuse outermost valence gaussian was removed giving an 8-41G representation and the 3sp shell exponent reduced to 0.27. (The full basis set is given in Appendix A.) In the case of oxygen, for the present calculations, an increase in the 4sp shell exponent, from 0.19 to 0.31, was needed to give convergence. For the calculations involving d-polarisation functions, d-exponents of 0.8 were applied to nitrogen and oxygen [32]. A value of 0.175 was used for sodium [21].

Table 4.4 Periodic *ab initio* calculation for the ^{23}Na efg tensor in $NaNO_2$ with the [Na / N / O] basis [8-511 / 8-41 / 8-411]

d-polarisation [a]	C_Q / MHz	η	Orientation [b]
-	-0.97	0.08	×
O	-1.31	0.25	✓
N	-1.10	0.01	×
Na	-0.87	0.15	×
N, O	-1.12	0.17	✓
Na, O	-1.01	0.19	✓
Na, N	-0.88	0.08	×
Na, N, O	-0.99	0.11	✓

[a] Details of the d-polarisation functions are given in the text. [b] This column refers to the orientation calculated for the principal axis frame of the efg tensor at sodium: ✓ symbol indicates agreement with experiment and × indicates that the tensor is incorrectly orientated with V_{11} || ***a*** and V_{22} || ***b***.

The results of the calculations are shown in Table 4.4. In general, these periodic HF calculations correctly predict the sign of $C_Q(^{23}Na)$ and show reasonable agreement with experiment for the ^{23}Na quadrupole parameters. However, the orientation of the sodium efg tensor is incorrectly determined, relative to experiment, in a number of cases. The correct orientation is only determined in those models where the co-ordinating oxygen atoms bear a d-polarisation function. The best fit to the experimentally determined

quadrupole parameters, including the sign of $C_Q(^{23}Na)$, is obtained with all three types of atom bearing d-polarisation functions.

As a test for transferability, the same basis sets were used to model sodium nitrate, $NaNO_3$. However, the *ab initio* calculation failed to converge in this instance. The most probable reason for this behaviour was that the nitrogen basis set had been tailored specifically for the nitrite anion and was not flexible enough to account for the bonding in the nitrate anion. This is a particular problem in the case that relatively large basis sets are optimised for particular compounds. In fact, this provides a further reason for focussing on smaller basis sets, which once optimised, may not be as sensitive to convergence problems over a diverse range of compounds.

4.3.2 6-21G basis set calculations

There is a wide range of molecular basis sets available but none specifically designed for ionic systems. For this investigation, the standard 6-21G basis set of Pople and co-workers [21, 22] as provided in the CRYSTAL code was chosen. As has already been discussed, this type of basis set gives reasonable results for the sign and value of $C_Q(^{23}Na)$ in cluster calculations.

The important aim was to keep the strategy for the periodic *ab initio* calculations as simple as possible and to this end unmodified 6-21G basis sets were applied to the nitrogen and oxygen atoms. This is undoubtedly a simplification since polyatomic anions have both molecular and ionic character. For sodium, the outer valence exponent of the standard set is very diffuse and this is known [14, 15] to lead to convergence problems in periodic calculations. In ionic systems, the sodium cation valence shell will be essentially

empty and so it was decided to modify the basis set to just core functions plus a single sp shell of relatively high exponent.

Preliminary calculations for $NaNO_2$, showed that variations in the exponent of the sodium outermost sp shell gave rise to a roughly linear response in the total HF crystalline energy. This behaviour is commonly found for nearly empty shells [14, 15] and rules out an optimisation procedure based on energy minimisation, the approach taken, therefore, was to find a sodium exponent that could be used to model as accurately as possible the sodium efg tensor in both $NaNO_2$ and $NaNO_3$. The rationale being that only a "good" description could model the experimentally observed electric field gradient in two crystallographically different environments. The quadrupole parameters were sufficiently sensitive to changes in the sodium outermost sp shell exponent so that a viable optimisation process could be developed on an essentially trial-and-error basis. A reasonable estimate of the single valence exponent on sodium was found to be in the region of 0.3 and so this value was used as a starting point in the calculations. It is useful to note that an exponent value of 0.3 is similar to that (0.27) for the 8-511G basis set for sodium used in Section 4.3.1.

The comparison with sodium nitrate

In the room-temperature phase of $NaNO_3$ [33], the sodium cation occupies a single crystallographic site with all the trigonal-planar nitrate anions lying in the ***a-b*** plane of the orthorhombic unit cell. Each sodium cation is surrounded by six nitrate anions. One oxygen atom from each of the six nitrate anions is used for co-ordination in an almost regular octahedral arrangement as shown in Figure 4.3. Both the sodium and the nitrate anions lie on threefold axes and, therefore, the principal component of the ^{23}Na efg tensor

also lies along the threefold axis. The ^{23}Na quadrupole parameters for the room-temperature phase of $NaNO_3$ are given in Table 4.5.

Table 4.5 Experimental ^{23}Na efg tensor information for $NaNO_3$

$C_Q(^{23}Na)$ [a]	337 ± 2 kHz
$\eta(^{23}Na)$ [a]	0.00 ± 0.03
Orientation of the principal axis frame [b]	V_{33} || ***c***
Sign of $C_Q(^{23}Na)$ [c]	Negative

[a] Early work found the efg tensor to be axially symmetric [4]. The quoted quadrupole parameters are taken from a recent MAS NMR study at 25°C [5]. [b] The orientation of the principal axis frame is determined by site symmetry. [c] The sign of $C_Q(^{23}Na)$ corresponds to that determined in a study of the asymmetry of ^{23}Na NMR satellites [6].

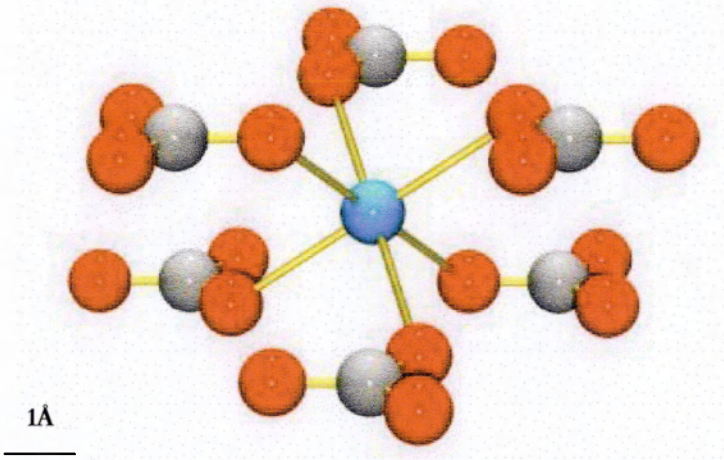

Figure 4.3 Part of the crystal structure of the room-temperature phase of sodium nitrate. The tie lines indicate the nearest neighbour oxygen atoms to the central sodium cation, (sodium (blue), oxygen (red) and nitrogen (grey)).

The results of the periodic *ab initio* calculations for $NaNO_2$ and $NaNO_3$ are given in Tables 4.6 and 4.7 respectively. The calculations, as already indicated, are based on standard 6-21G basis sets for O, N and Na but with a single valence exponent for sodium set to 0.3.

Table 4.6 Periodic *ab initio* calculations of the sodium efg tensor in $NaNO_2$ based on the 6-21G basis set

d-polarisation [a]	C_Q / MHz	η	Orientation [b]
-	-1.01	0.18	×
O	-1.32	0.27	✓
N	-1.13	0.03	×
Na	-0.91	0.44	×
N, O	-1.30	0.25	✓
Na, O	-1.17	0.09	✓
Na, N	-0.96	0.23	×
Na, N, O	-1.14	0.06	✓

[a] Details of the d-polarisation functions are: d-exponents of 0.8 on both N and O, and 0.175 on Na. [b] See footnote *b* for Table 4.4.

Overall, the results for sodium nitrite mirror those found using a larger basis set as described in Section 4.3.1: the sign of $C_Q(^{23}Na)$ is correctly predicted in all cases and the application of d-polarisation functions affects the orientation of the ^{23}Na efg tensor. In particular, there is good agreement with experiment as follows:

- with d-polarisation functions on the nitrogen atom only, $C_Q(^{23}Na)$ is well modelled but the orientation is incorrect and η is too small.
- with d-polarisation functions on just the sodium and oxygen atoms, all aspects of the tensor are well modelled.
- with d-polarisation functions on all three types of atoms, again all aspects are well modelled, although, $\eta(^{23}Na)$ is smaller than expected.

Table 4.7 Periodic *ab initio* calculations of the sodium efg tensor in $NaNO_3$ based on the 6-21G basis set [a]

d-polarisation [b]	C_Q / MHz
-	-0.57
O	-0.30
N	-0.57
Na	-0.61
N, O	-0.39
Na, O	-0.34
Na, N	-0.61
Na, N, O	-0.43

[a] By symmetry, the calculated efg tensor must be axially symmetric. [b] See footnote *a* for Table 4.6.

The results obtained for sodium nitrate show that the sign of $C_Q(^{23}Na)$ is correctly determined in all cases. This strongly suggests that the opposite result found in earlier point-charge model investigations [1] is incorrect. Good agreement with experiment, for all aspects of the efg tensor, is found in two cases:

- d-polarisation functions on the oxygen atoms only.
- d-polarisation functions on the sodium as well as on the oxygen atoms.

Taken together, the results in Table 4.6 and 4.7 are consistent with the fact that the sodium ion coordinates to both the nearest-neighbour oxygen and nitrogen atoms in the case of $NaNO_2$, but only to oxygen atoms in the case of the $NaNO_3$. This would indicate that it is the coordinating atoms that are important in determining the electric field gradient at sodium and that these are best modelled by incorporating d-polarisation functions.

The results for $NaNO_2$ and $NaNO_3$ demonstrate that it is possible, using d-polarisation functions on Na, N and O, to use common basis sets for the periodic *ab initio* calculation of quadrupole parameters in compounds with markedly different structures. The idea of using common basis sets in periodic *ab initio* calculations is an important one and is expanded upon in Section 4.4, although from a different perspective than that developed here.

As a final point, it can be noted that it is possible to refine the results for $NaNO_2$ and $NaNO_3$ even further; although still using trial-and-error procedures. It was found that with (i) d-polarisation functions on the coordinating atoms, (ii) the outermost valence exponents of oxygen and nitrogen set to 0.374 and 0.273, respectively, and (iii) the single valence gaussian exponent on sodium set to 0.314, then:

$$NaNO_2: \; C_Q(^{23}Na) = -1.112 \text{ MHz} \quad \eta(^{23}Na) = 0.087$$

$$NaNO_3: \; C_Q(^{23}Na) = -0.334 \text{ MHz} \quad \eta(^{23}Na) = 0.000$$

These results are in very good agreement with experiment.

For the purpose of later discussions, it is important to note that the calculated sign of $C_Q(^{23}Na)$ for both $NaNO_2$ and $NaNO_3$ is consistent with experiment and this suggests that this parameter can be correctly determined by the periodic *ab initio* method. However, in the case where $\eta(^{23}Na)$ is close to unity, the sign becomes much less certain. This is because, in such circumstances, the magnitude of V_{22} will be almost equal to that of V_{33} but of opposite sign resulting in an incorrect sign assignment should any slight relocation of electron density, due to an inappropriate crystal structure or basis set, occur.

4.3.3 Density functional theory calculations

The DFT approach was also applied to the periodic *ab initio* calculation of the sodium efg tensor in $NaNO_2$; polarisation functions were used on all of the atoms with, as used previously, d-exponents of 0.8 on both oxygen and nitrogen, and 0.175 on sodium. The exchange correlation potentials appropriate for both the local density approximation (LDA) and non-local (generalised gradient approximation, GGA) approaches to the correction of electron density were used along with the hybrid DFT method B3LYP [34]. In the local approach, the VWN [35] and LDA [36] parameterisations were selected for the correlation and exchange functionals, respectively. In the non-local approach, Perdew-Wang (PWGGA) [37-39] and Becke [40] parameterisations replaced these functionals, respectively. Two sets of calculations were carried out using different basis sets. The first set of calculations used the modified [8-511 / 8-41 / 8-411] basis set described in section 4.3.1. The second set used the 6-21G basis set described in the previous section, but did not incorporate the final small refinements. The hybrid DFT method B3LYP could not be used with the large basis set due to insufficient computer resources being available. The results for all the calculations are given in Table 4.8.

Overall, the results shown in Table 4.8 indicate that the basis sets which gave results in good agreement with experiment for HF calculations (see Tables 4.4 and 4.6) did not perform particularly well at the DFT level. The best agreement with experiment was obtained when the large basis set was used. VWN / LDA caused a change in the orientation of the calculated sodium efg tensor whilst PWGGA / BECKE retained the orientation but caused changes in the quadrupole parameters without significantly improving the agreement with experiment, particularly for the calculation of $\eta(^{23}Na)$. In

the case of the small basis set, B3LYP correctly determined the orientation of the efg tensor but gave poor agreement with the experimental quadrupole parameters.

Table 4.8 Results of the periodic *ab initio* calculation of the ^{23}Na NMR quadrupole parameters and efg tensor orientation, along with the charge distribution, in $NaNO_2$ for different DFT approaches and basis sets

Correlate	Exchange	8-511* [a]		Charge Distribution [b]			Orientation [c]
		C_Q / MHz	η	Na / |e|	N / |e|	O / |e|	
VWN	LDA	-1.42	0.13	10.479	7.467	8.027	×
PWGGA	BECKE	-1.24	0.23	10.440	7.464	8.048	✓
B3LYP		-	-	-	-	-	-

Correlate	Exchange	6-1G* [a]		Charge Distribution [b]			Orientation [c]
		C_Q / MHz	η	Na / |e|	N / |e|	O / |e|	
VWN	LDA	-2.08	0.03	10.380	6.643	8.489	×
PWGGA	BECKE	-1.77	0.23	10.328	6.617	8.527	✓
B3LYP		-1.93	0.38	10.370	6.580	8.525	✓

[a] The notation indicates the basis set used on the sodium atom. [b] The charge distribution was taken from a Mulliken population analysis. [c] See footnote *b* for Table 4.4.

It is interesting to note that the distribution of electron density is radically different for the small and large basis set calculations. However, it is very similar when comparing the different DFT approaches applied to the same basis set. The large negative charge on the oxygen atoms, as calculated using the small basis set, is responsible for the increased magnitude of the quadrupole coupling constant. It may also be noted that the large basis set assigns a negative charge to the nitrogen atom, which would not be predicted from a simple electronegativity assessment of the nitrite anion.

4.3.4 Summary of the calculations for $NaNO_2$

Periodic HF calculations using the relatively large basis set, [8-511 / 8-41 / 8-411; Na / N / O], incorporating published sets for Na^+ and O^{2-} and a set for N optimised for the NO_2^-

anion along with d-polarisation functions on all atoms, gave very good agreement with experiment for the sodium efg tensor in $NaNO_2$. DFT calculations, surprisingly, offered no distinct advantages. The success of the calculations using the smaller standard 6-21G basis set with appropriate modification for sodium, is of particular interest given the aim of developing a reliable technique for the calculation of quadrupole parameters. In the calculations, the 6-21G basis set for sodium was modified in line with its cationic nature, whereas the basis sets for nitrogen and oxygen were used without modification. Again, d-polarisation functions, particularly on the sodium and oxygen atoms, were essential for good agreement between calculation and experiment. Overall, these calculations suggest that it may be possible to find a consistent periodic *ab initio* method for the prediction of the sodium efg tensor from crystallographic information. Such an approach would have distinct advantages over cluster-based calculations because the selection of the cluster size, composition and basis set would be avoided. Furthermore, it would be of particular use in NMR assignment problems; especially in cases in which sodium is present at several crystallographic sites.

4.4 Periodic calculations using the 3-21G basis set and a correlation approach

4.4.1 Background

The periodic *ab initio* calculations for $NaNO_2$ and $NaNO_3$ suggest that this approach can be extended to the calculation of the sodium efg tensor for a wide range of ionic sodium compounds. This suggestion is explored in depth in this section but with an emphasis on providing a method that is:

- readily transferable from compound to compound,

- reasonable in terms of the computer resources required,
- useful for NMR assignment problems.

These requirements are mutually demanding and for this reason attention is focused on the 3-21G basis set. This basis set is related to the 6-21G basis set since it uses the same description of the valence orbitals and is available as standard within the CRYSTAL code. It provides for the widest possible range of ionic compounds to be investigated without exceeding the maximum total number of basis functions allowed by the software. The use of polarisation functions also introduces a very large overhead in terms of basis functions and so these have not been used. Omitting these functions may seem to be in conflict with the results described in Section 4.3 but, as it turns out, the effect on the final results is not significant.

Given the restrictions, an important criterion in the work is to find a set of 3-21G basis sets for individual elements that give rise to a good linear correlation between calculated and experimental values of ^{23}Na quadrupole parameters over a wide range of compounds. It is important to recognise that this correlation approach does not involve optimising the basis sets on a compound-by-compound basis. Furthermore, it does not require exact agreement between calculation and experiment; the criterion is a linear correlation. It can also be noted that such an approach is independent of the variability in the published value [41] of the ^{23}Na nuclear quadrupole moment.

Along with appropriate basis sets for the atoms, the periodic *ab initio* method requires accurate crystallographic data. Ideally, this should be taken from single crystal studies and, if hydrogen atoms are involved, neutron diffraction data is preferable. The data used in this work was taken from the United Kingdom Chemical Database Service maintained

at Daresbury Laboratory [42]. In circumstances in which more than one crystal structure determination was available for a particular compound, the structure based on a single-crystal determination was usually selected. In a number of cases, it was necessary to use structural information from x-ray powder diffraction studies.

For convenience, the description in this section is divided into three parts. First the determination of a value for the exponent for the single valence sp shell on sodium, appropriate to the 3-21G basis set, is described. Second, compounds in which sodium occupies a single crystallographic site within the unit cell are investigated. Finally, the calculations are extended to compounds in which sodium occupies multiple crystallographic sites. The experimentally-determined values of the NMR quadrupole parameters were taken from various sources, including those measured in this work.

4.4.2 The exponent for sodium

The 3-21G basis set for sodium was modified by replacing the valence shells with a single valence sp shell. The method used to determine the optimum value for the exponent of this shell was to vary its value and monitor the calculated value of $C_Q(^{23}Na)$ for a small range of compounds. The compounds selected were identified as representing a wide range of quadrupole coupling constants, as determined experimentally (see Table 4.9), for sodium present at a single crystallographic site. These compounds were sodium sulphate (Na_2SO_4), sodium metasilicate (Na_2SiO_3), sodium nitrate ($NaNO_3$) and sodium hydroxide (NaOH). The immediate oxygen coordination environment of the sodium cation in each of these compounds is shown in Figure 4.4 (and, as can be seen, the local sodium environments differ substantially from one another). The exclusive coordination of sodium to oxygen is typical of many ionic sodium compounds.

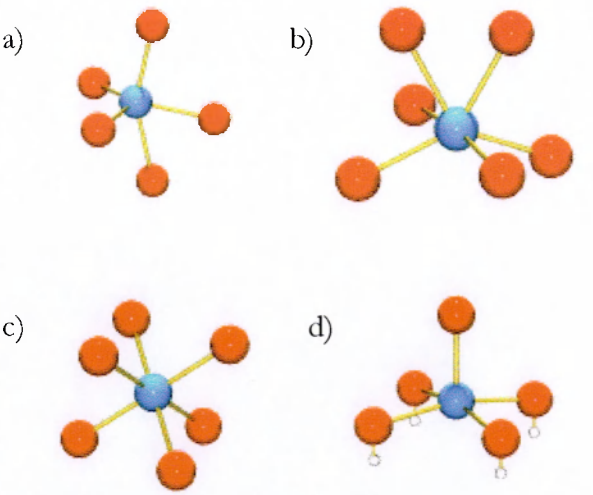

Figure 4.4 The immediate oxygen coordination environment around the sodium cation in a) Na_2SO_4 [43], b) Na_2SiO_3 [44, 45], c) $NaNO_3$ [33] and d) NaOH [46].

For the periodic *ab initio* calculations based on these four compounds, unmodified 3-21G basis sets were used for oxygen, sulphur and nitrogen atoms, whereas a small modification was made to the value of the exponent on the outermost shell of hydrogen (0.183). In the case of silicon, the outermost valence orbital is diffuse and this is known to cause convergence problems in periodic calculations. Consequently, this orbital was removed to give a 3-2G set.

The results of calculations as a function of the value of the single valence sp shell exponent for the sodium 3-1G basis set are given in Table 4.9. In general, they indicate that small values of the valence exponent are required to give better agreement with experiment.

For a transferable basis set for sodium, the same exponent value must either be able to accurately predict the experimental value of $C_Q(^{23}Na)$ for all four compounds or show a good linear correlation between calculation and experiment. Given the results in Table

4.9, an investigation of the conditions necessary to obtain the best linear correlation is the most appropriate way to proceed.

Table 4.9 Periodic *ab initio* calculations of $C_Q(^{23}Na)$ in a selected group of compounds as a function of the single valence sp shell exponent on sodium

Valence Exponent	C_Q / MHz			
	Na_2SO_4	$NaNO_3$	Na_2SiO_3	NaOH
0.15	-2.75	-0.42	+1.26	+2.92
0.17	-2.78	-0.42	+1.33	+3.32
0.18	-2.85	-0.42	+1.46	+3.56
0.19	-2.89	-0.42	+1.50	+3.62
0.20	-2.96	-0.43	+1.59	+3.73
0.25	-3.33	-0.47	+1.88	+4.02
0.30	-3.61	-0.48	+1.97	+4.06
0.35	-3.72	-0.47	+1.97	+3.98
0.40	-3.70	-0.46	+1.94	+3.86
0.45	-3.61	-0.43	+1.89	+3.73
0.50	-3.48	-0.41	+1.82	+3.59
Expt C_Q / MHz [a]	2.60 [b]	-0.34 [c]	1.46 [b]	3.50 [b]

[a] It is only in the case of $NaNO_3$ that the sign of $C_Q(^{23}Na)$ has been determined experimentally. The values of $C_Q(^{23}Na)$ for Na_2SO_4, Na_2SiO_3 and NaOH simply represent magnitudes. The periodic *ab initio* calculations determine the sign of $C_Q(^{23}Na)$ and this is shown explicitly. The NMR data were taken from the literature: [b] [9] and [c] [5, 6].

For each valence exponent in Table 4.9, the calculated values of $C_Q(^{23}Na)$ for all four compounds were plotted against their experimental counterparts and, as an approximation, each plot was fitted to a second-order polynomial. The ideal correlation will occur when all four points lie on a straight line. To test for linearity, the rate of change of the gradient, determined as a single value by taking the second-derivative of the fitted second-order polynomial, was evaluated for each plot. This second derivative is zero in the case of a straight line. Values of the second-derivatives are plotted as a function of the value of the valence exponent in Figure 4.5.

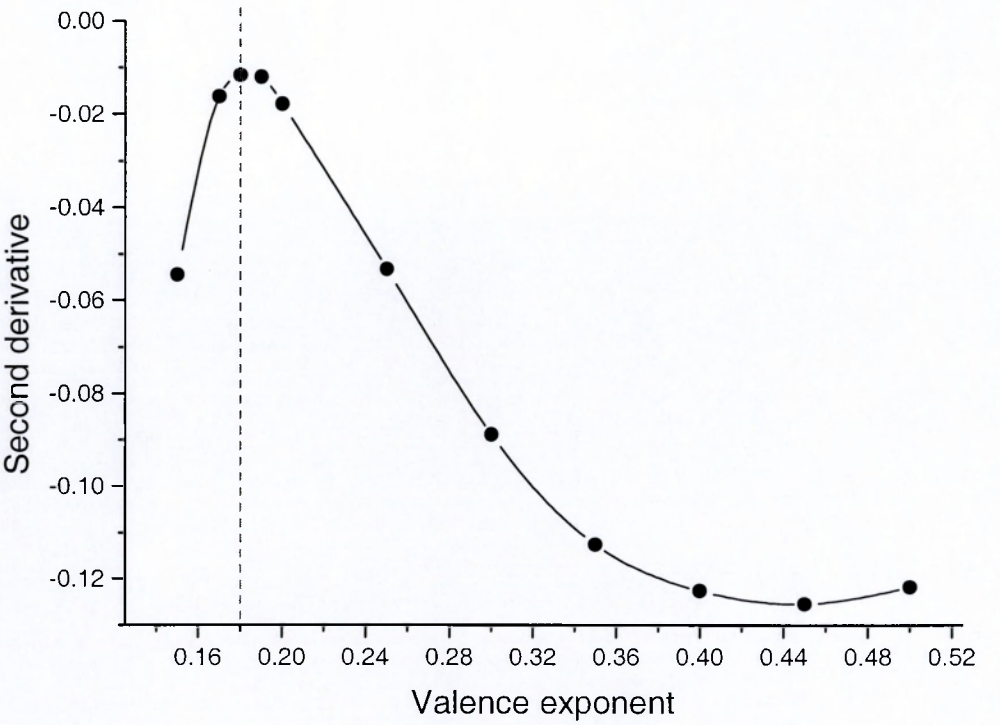

Figure 4.5 A plot of the second-derivative *versus* the valence exponent for sodium. (The line through the points is to aid the eye.)

The result in Figure 4.5 show that strictly no value of the single sp valence shell exponent will produce an exact linear correlation between calculated and experimental values of $C_Q(^{23}Na)$ for the selected compounds. However, when the exponent has a value of 0.18 there is a maximum in the plot and this maximum has a value close to zero. Overall, it seems reasonable to suggest that a single, transferable, modified 3-21G basis set for sodium may be able to provide a linear correlation between calculation and experiment for $C_Q(^{23}Na)$ over a much wider range of ionic sodium compounds.

Calculated values of $\eta(^{23}Na)$, with the sodium valence exponent set to 0.18, are shown in Table 4.10. Good agreement is obtained between calculation and experiment further supporting the more general use of the modified 3-21G basis set for sodium.

Table 4.10 Calculated values of $\eta(^{23}Na)$ using a modified 3-21G basis set for sodium with the single valence sp shell valence exponent set to 0.18

	η			
	Na_2SO_4	$NaNO_3$	Na_2SiO_3	NaOH
Calculation	0.51	0.00	0.71	0.02
Experiment	0.58[a]	0.00[b]	0.71[a]	0.00[a]

The NMR data were taken from the literature: [a] [9] and [b] [5, 6].

It should be noted that periodic *ab initio* calculations using the modified 3-21G basis set for sodium with an exponent of 0.18 and based upon the crystal structure of Na_2SiO_3 determined by McDonald and Cruickshank [45] gave values of –1.40 MHz for $C_Q(^{23}Na)$ and 0.77 for $\eta(^{23}Na)$. These results are in good agreement with those obtained using the crystal structure of Liu et al. (Tables 4.9 and 4.10), which was determined by first-principles calculations. However, the sign of $C_Q(^{23}Na)$ is reversed and this is probably a reflection of the small differences between the two crystal structures with the theoretical structure effectively being determined at 0K. Calculations of the optimised outermost shell exponent on sodium using the crystal structure of McDonald and Cruickshank, in replacement of that of Liu *et al.*, also gave the best value to be 0.18.

4.4.3 Correlations between experiment and calculation

Correlations between calculation and experiment are considered in this section for both single and multiple-site-sodium compounds. An important feature of the approach is that the same elemental basis sets are used throughout. These can be summarised as follows. For sodium, as already discussed in detail, the 3-21G basis set was modified by replacing the valence shells with a single valence sp shell with an optimised exponent of 0.18. Unmodified 3-21G basis sets were used for sulphur and chlorine. Although it will not be described in any detail, it was found useful to slightly modify the values of the exponents

of the outermost sp shell of oxygen (0.374), hydrogen (0.183), nitrogen (0.273) and carbon (0.132) to give optimum linear correlations. In the case of aluminium, the outermost valence orbital is diffuse and this is known to cause convergence problems in periodic *ab initio* calculations. Consequently, this orbital was removed to give a 3-2G set. The same type of modification was applied to silicon and phosphorous basis sets.

Single-site sodium compounds

The results of the periodic *ab initio* calculations for the ^{23}Na quadrupole parameters for a range of compounds in which sodium occupies a single type of crystallographic site are given in Table 4.11. All of these compounds, with the exception of $NaNO_2$, have sodium exclusively coordinated to oxygen and, in this respect, are similar in character to the compounds used in the optimisation of the single valence sp shell exponent for sodium.

It should be noted that the sign of an experimental quadrupole coupling constant is a difficult quantity to measure experimentally and is normally unobtainable from either single crystal, or polycrystalline NMR (or NQR) experiments. To determine the sign requires specialised experiments involving low temperatures and high magnetic fields for polycrystalline samples [58], or an investigation of the trend in the asymmetry of NMR satellites in the case of higher-temperature single crystal studies [6]. The experimental results in Table 4.11 show signs for experimental values of $C_Q(^{23}Na)$ only when these are known. Otherwise, all other values are magnitudes only. The periodic *ab initio* calculations determine the sign of $C_Q(^{23}Na)$ and these signs are shown explicitly in the Table. These comments, and the method of presentation in the table, are common to all subsequent tables.

Table 4.11 A comparison of experimental and calculated values of ^{23}Na quadrupole parameters for a range of compounds in which sodium occupies a single type of crystallographic site

Compound	Experimental[a]		Calculated		References	
	C_Q / MHz	η	C_Q / MHz	η	NMR	Struct
Na_2SiO_3	1.46	0.71	-1.40	0.77	9	46
α-$Na_2Si_2O_5$	1.82	1.00	-1.97	0.60	9	47
Na_2SO_4	2.60	0.58	-2.85	0.51	9	43
$NaH_2PO_4{\cdot}H_2O$	1.22	0.26	+1.71	0.29	9	48
$NaH_2PO_4{\cdot}2H_2O$	1.19	0.47	+1.04	0.88	9	49
Na_2O	0.00	0.00	0.00	0.00	*b*	50
NaOH	3.50	0.00	+3.56	0.02	9	45
$NaOH{\cdot}H_2O$	2.20	0.70	+2.51	0.86	9	51
$NaNO_2$	-1.10	0.11	-0.45	0.19	10	52
$NaNO_3$	-0.34	0.00	-0.42	0.00	5, 6	33
$NaHCO_3$	0.66	0.88	-0.95	0.79	*c*	53
$Na_2C_2O_4$	2.43	0.75	+2.23	0.58	*c*	54
$NaAlO_2$	2.15	0.60	-2.19	0.43	9	55
$NaClO_3$	0.80	0.00	-0.57	0.00	7	56
$NaClO_4$	0.80	0.35	-1.56	0.71	9	57

[a] See text for a discussion of the sign of C_Q. [b] Although not calculated, Na_2O provides a useful test of the linear correlation. [c] This work.

A plot of experimental versus calculated values of $C_Q(^{23}Na)$ for the compounds in Table 4.11 (with the exception of $NaNO_2$ and $NaClO_4$: see later) is shown in Figure 4.6. The calculated sign of $C_Q(^{23}Na)$ is assumed for the experimental value of this quantity: the same assumption is made throughout this chapter.

The straight line in this figure represents the line of best linear fit to the data ($R^2 = 0.99$); the slope of the line is 0.949 ± 0.031 and the intercept is 0.006 ± 0.060 MHz. Overall, there is a very good linear correlation, which is almost 1:1, with very little scatter of the data. This suggests that the small basis set has the ability to assign relative charges to the atoms in a consistent manner. It can be noted that although the hydrogen atom positions

may not be well known for some of the hydrogen-containing compounds this does not appear to influence the correlation.

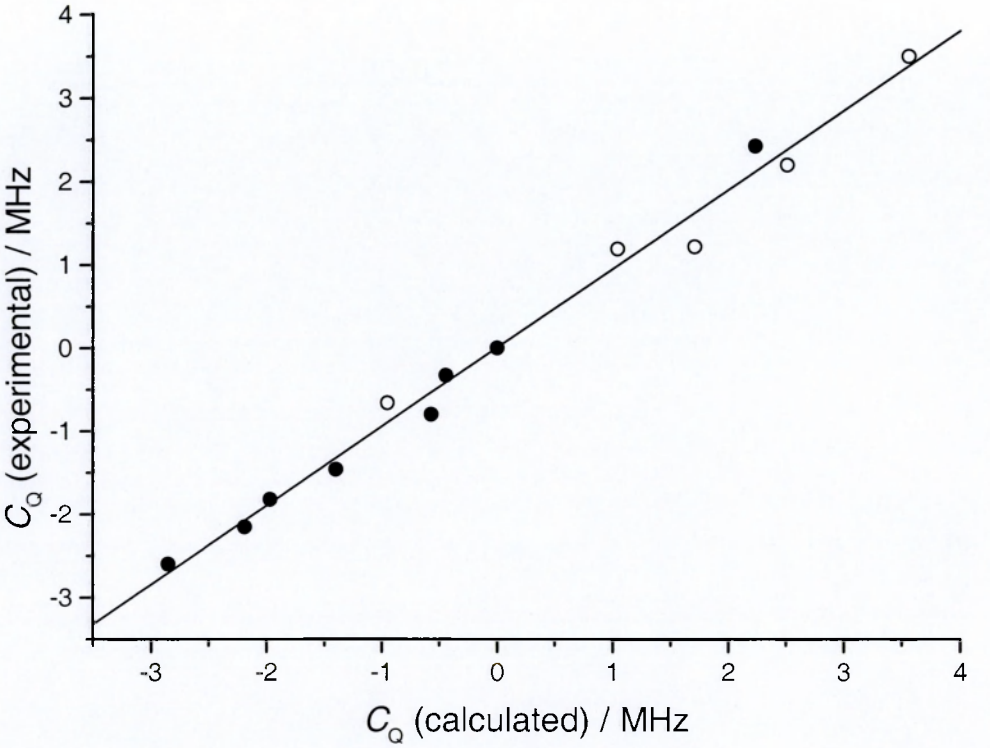

Figure 4.6 A plot of experimental versus calculated values of $C_Q(^{23}Na)$ using data (with the exception of that for $NaNO_2$ and $NaClO_4$) taken from Table 4.11. Compounds involving oxyanions with hydrogen are marked (○) and those without (●).

By contrast, the correlation between the calculated and experimental values of $\eta(^{23}Na)$, shown in Figure 4.7, shows considerable scatter. It is only for a few compounds that the calculated value of $\eta(^{23}Na)$ lies within, or close to, 10% of that determined by experiment. The overall lack of correlation is most likely due to the inflexibility of the relatively small basis set in accommodating the more subtle distributions of electron density that determine the magnitude of this particular parameter.

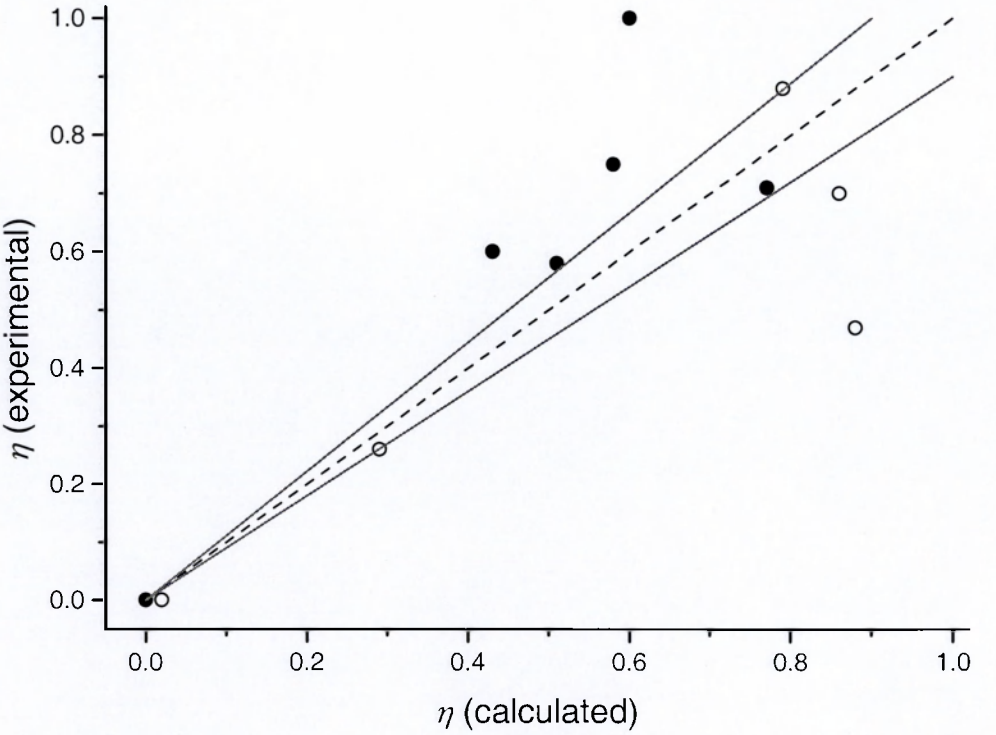

Figure 4.7 A plot of experimental versus calculated values of $\eta(^{23}Na)$ using data (with the exception of that for $NaNO_2$ and $NaClO_4$) taken from Table 4.11. Compounds involving oxyanions with hydrogen are marked (○) and those without (●). The dotted line represents a 1:1 correlation between experimental and calculated values of $\eta(^{23}Na)$. The two solid lines bound a region in which the calculated value of $\eta(^{23}Na)$ is within 10% of that determined by experiment.

Two compounds have been specifically omitted from the correlation plots for $C_Q(^{23}Na)$ and $\eta(^{23}Na)$. The calculated ^{23}Na quadrupole parameters for $NaNO_2$ (in particular, $C_Q(^{23}Na)$), as shown in Table 4.11, are in disagreement with those determined experimentally. A possible explanation for this behaviour may be related to the fact that the sodium basis set was 'tuned' for four compounds in which the sodium cation was exclusively coordinated by oxygen, whereas in the case of $NaNO_2$, a nitrogen atom also takes part in the coordination to sodium (see Figure 4.1). It may also be for this reason that the orientation of the ^{23}Na efg tensor is incorrectly determined in the calculation. The second excluded compound is $NaClO_4$. Again, the calculated ^{23}Na quadrupole parameters

are in marked disagreement with those determined experimentally. However, there is no apparent reason for the disagreement is this case. This is particularly so given that the calculated ^{23}Na quadrupole parameters for $NaClO_3$, which contains the same elements, are in reasonably good agreement with experiment. It can only be concluded that the experimental quadrupole parameters are subject to some form of motional averaging, or that the reported crystal structure is in error.

Multiple-site sodium compounds

Calculations using modified 3-21G basis sets for these types of compounds, which can contain large numbers of atoms in unit cells of low symmetry, have the advantage that only modest computer resources are required. The results of the calculations are given in Table 4.12 and a correlation plot, omitting the results for β-$Na_2Si_2O_5$, is shown in Figure 4.8. The overall method of presentation is the same as that already used for the single-site sodium compounds. For all the compounds in Table 4.12, the sodium cations, irrespective of site, are exclusively coordinated to oxygen.

The straight line in Figure 4.8 represents the line of best linear fit to the data ($R^2 = 0.98$); the slope of the line is 0.956 ± 0.033 and the intercept is 0.083 ± 0.073 MHz. Again, there is a very good linear correlation, which is almost 1:1, with very little scatter of the data. Furthermore, as found for the single-site compounds, the presence of hydrogen does not appear to influence the correlation. The slope of the line of best fit is well within the calculated uncertainty for the single-site correlation (0.949 ± 0.031).

Table 4.12 A comparison of experimental and calculated values of ^{23}Na quadrupole parameters for a range of multiple-site sodium compounds

Compound (*site*)	Experimental		Calculated		References	
	C_Q / MHz	η	C_Q / MHz	η	NMR	Struct
β-$Na_2Si_2O_5$ (*1*)	2.50	0.00	-2.24	0.72	59	60
β-$Na_2Si_2O_5$ (*2*)	2.22	0.55	+1.67	0.52		
Na_2SO_3 (*1*)	1.06	0.00	-0.89	0.00	*a*	61
Na_2SO_3 (*2*)	0.33	0.00	-0.28	0.00		
Na_2SO_3 (*3*)	1.14	0.00	+0.99	0.00		
$Na_2S_2O_3 \cdot 5H_2O$ (*1*)	0.83	0.41	+0.85	0.81	62	63
$Na_2S_2O_3 \cdot 5H_2O$ (*2*)	2.26	0.33	+2.43	0.23		
NaH_2PO_4 (*1*)	1.59	0.46	+1.98	0.33	*a*	64
NaH_2PO_4 (*2*)	2.35	0.94	-2.88	0.87		
Na_2HPO_4 (*1*)	2.04	0.70	+2.12	0.84	*a*	65
Na_2HPO_4 (*2*)	1.31	0.20	+0.96	0.86		
Na_2HPO_4 (*3*)	3.84	0.30	+3.97	0.24		
$Na_3P_3O_9$ (*1*)	2.20	0.70	-2.70	0.44	9	66
$Na_3P_3O_9$ (*2*)	1.57	0.55	+1.46	0.72		
$Na_4P_2O_7 \cdot 10H_2O$ (*1*)	1.89	0.21	-1.68	0.64	*a*	67
$Na_4P_2O_7 \cdot 10H_2O$ (*2*)	0.48	0.99	+0.76	0.63		
$Na_5P_3O_{10}$ (II) [b] (*1*)	4.57	0.39	4.03	0.45	*a*	68
$Na_5P_3O_{10}$ (II) (*2*)	2.99	0.19	-3.44	0.21		
$Na_5P_3O_{10}$ (II) (*3*)	1.37	1.00	-1.37	0.86		

[a] This work. [b] Phase II (low temperature) polymorph of anhydrous $Na_5P_3O_{10}$.

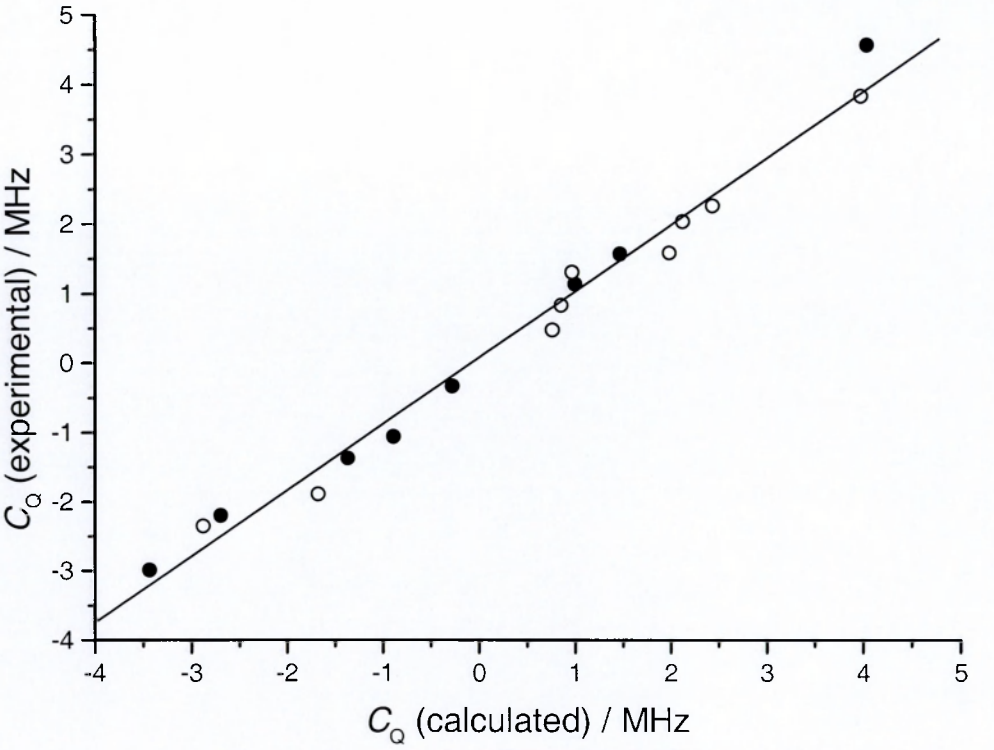

Figure 4.8 A plot of experimental versus calculated values of $C_Q(^{23}Na)$ using data (with the exception of that for β-$Na_2Si_2O_5$) taken from Table 4.12. Compounds involving oxyanions with hydrogen are marked (○) and those without (●).

The correlation plot for $\eta(^{23}Na)$ (Figure 4.9) shows considerable scatter and, in this sense, the behaviour is comparable to that already found for single-site sodium compounds. There is no clear correlation between the calculated values and those determined by experiment.

One compound has been purposefully omitted from the correlation plots for $C_Q(^{23}Na)$ and $\eta(^{23}Na)$. The calculated value for $\eta(^{23}Na)$ for sodium on site (*1*) in β-$Na_2Si_2O_5$ is in marked disagreement with experiment. The experimental value of 0.0 is indicative of a crystallographic site with axial symmetry but this is not the case according to the crystal structure determination. This is an area for further work.

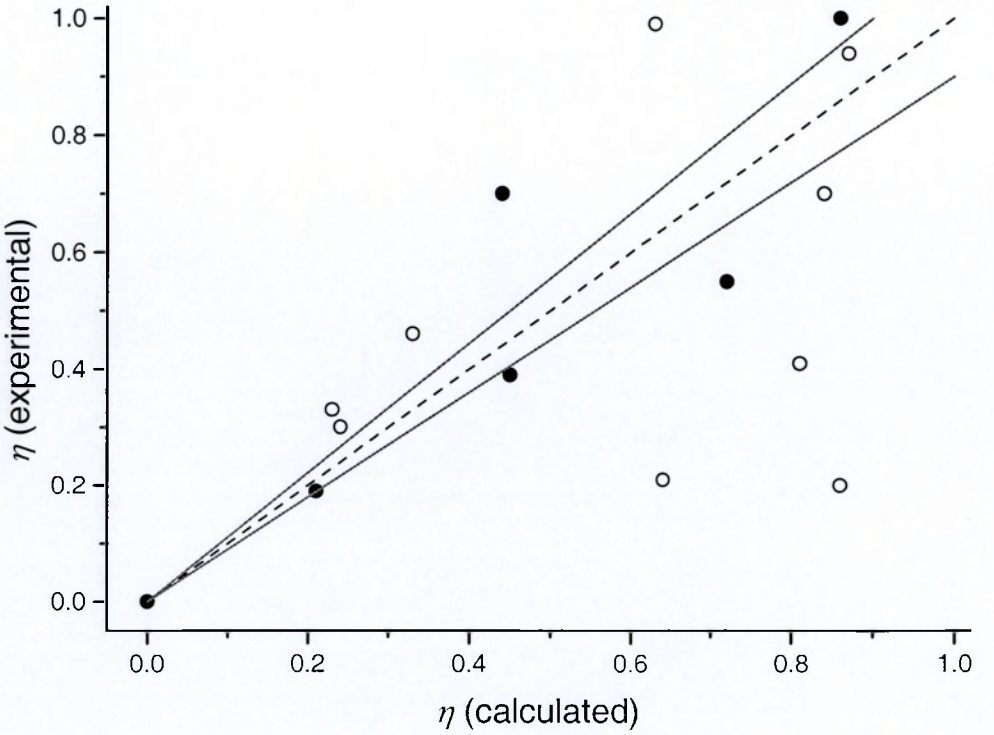

Figure 4.9 A plot of experimental versus calculated values of $\eta(^{23}Na)$ using data (with the exception of that for β-$Na_2Si_2O_5$) taken from Table 4.12. Compounds involving oxyanions with hydrogen are marked (○) and those without (●). The dotted line represents a 1:1 correlation between experimental and calculated values of $\eta(^{23}Na)$. The two solid lines bound a region where the calculated value of $\eta(^{23}Na)$ is within 10% of that determined by experiment.

A summary: single- and multiple- site sodium compounds

A key aim of this section has been to establish whether periodic HF *ab initio* calculations based on the small standard 3-21G basis set can be used in a consistent manner to calculate the ^{23}Na quadrupole parameters for a diverse range of ionic sodium compounds. The results show that this is the case for the calculation of $C_Q(^{23}Na)$ but with the restriction, at least in the present work, that a given sodium cation is exclusively surrounded by coordinating oxygen atoms. The correlations for the single-site (Figure 4.6) and multiple-site (Figure 4.8) sodium compounds are combined into a single plot in

Figure 4.10. The straight line in this figure represents the best linear fit to all the data (R^2 = 0.98); the slope of the line is 0.955 ± 0.023 and the intercept is 0.048 ± 0.048 MHz.

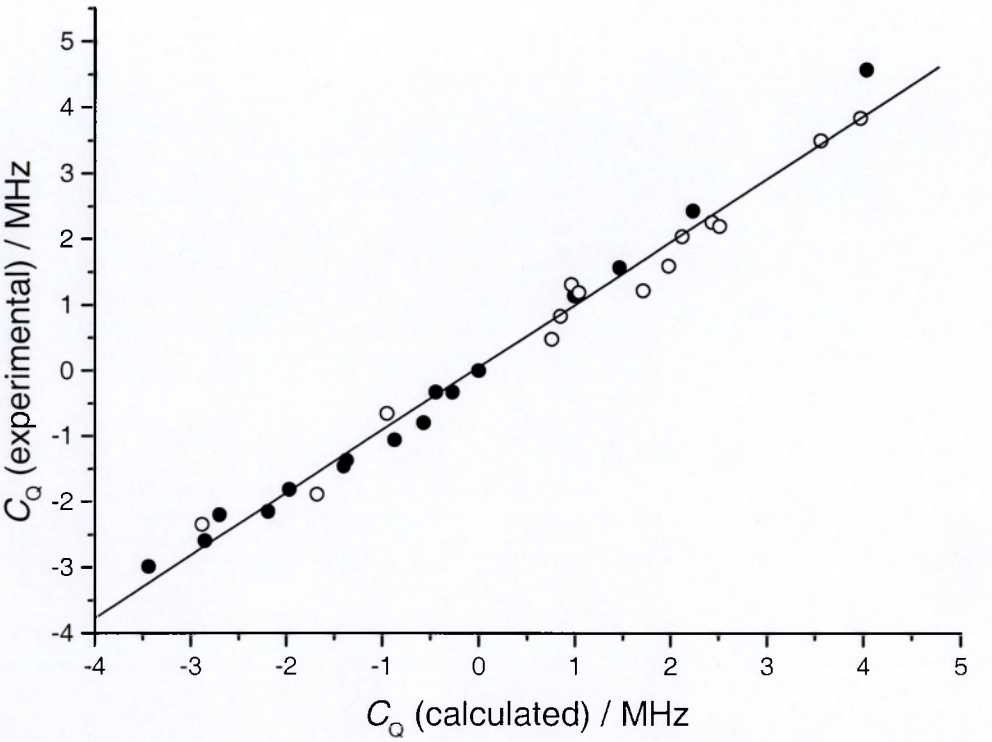

Figure 4.10 A combined plot of experimental versus calculated values of $C_Q(^{23}Na)$ for single- and multiple- site sodium compounds. Compounds involving oxyanions with hydrogen are marked (○) and those without (●).

The correlation between calculation and experiment in Figure 4.10 is very close to 1:1 although it should be emphasised that there is no *a priori* reason why this should be the case given the widely differing structural environments of the compounds studied. Nonetheless, the degree of linear correlation achieved shows that a relatively small basis set, suitably modified, can quite accurately predict the value of $C_Q(^{23}Na)$ from crystal structure information.

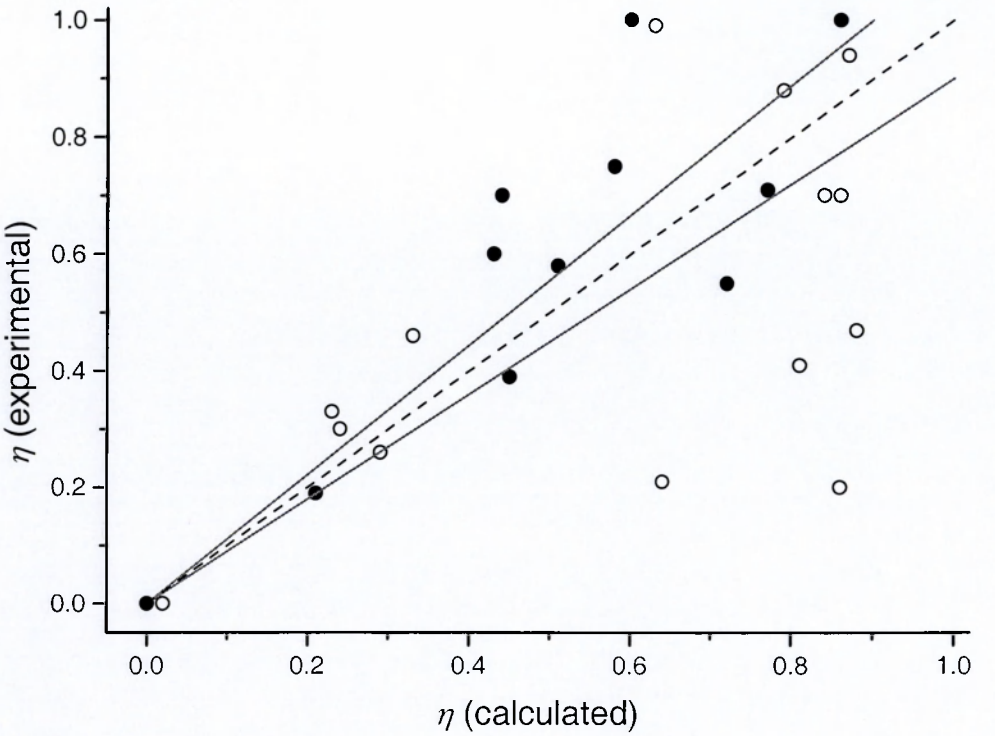

Figure 4.11 A combined plot of experimental versus calculated values of $\eta(^{23}Na)$ for single- and multiple- site sodium compounds. Compounds involving oxyanions with hydrogen are marked (○) and those without (●). The dotted line represents a 1:1 correlation between experiment and calculation. The two solid lines bound a region where the calculated value of $\eta(^{23}Na)$ is within 10% of that determined by experiment.

By contrast, the accuracy of the calculations for $\eta(^{23}Na)$ is markedly variable with the correlation plots (Figures 4.7 and 4.9) showing considerable scatter. The two data sets used for the single- and multiple- sodium site correlations are combined in Figure 4.11. It is only for a few compounds that the calculated values of $\eta(^{23}Na)$ lie within or close to, the 10% boundary lines. It is interesting to note that those compounds that do not contain hydrogen tend to have their calculated values of $\eta(^{23}Na)$ underestimated, whereas those containing hydrogen are overestimated relative to their experimental value.

4.5 Periodic calculations using the 6-21G basis set (with and without d-polarisation functions) and a correlation approach

The standard 3-21G basis set, with appropriate modifications, has produced periodic *ab initio* calculated values for $C_Q(^{23}Na)$ in very good agreement with those determined by experiment. However, the value of $\eta(^{23}Na)$ is not well modelled by this modified basis set. In principle, increasing the size of the basis set should improve the accuracy of the calculation of this parameter. Calculations using the 6-21G basis set were therefore performed. The investigation was carried out in two stages; first using the standard 6-21G basis set and then using this basis set augmented with d-polarisation functions applied to sodium and oxygen.

The atoms represented by the 6-21G basis set had the same modifications to their outermost shells as those already described for the 3-21G basis set. For calculations including d-polarisation functions, the single valence sp exponent on sodium was increased to 0.3 and a d-exponent of 0.2 was applied. It should be noted that this value of the valence exponent was found suitable for calculations for both $NaNO_2$ and $NaNO_3$ in Section 4.3.2 even though the coordination around the sodium cation in $NaNO_2$ is not solely due to oxygen atoms. The oxygen atom had a d-exponent of 0.8 and, in the case of $NaNO_2$, the nitrogen atom also had a d-exponent of 0.8.

4.5.1 Single-site sodium compounds

As in the case of the study of the 3-21G basis set, compounds in which sodium occupies a single crystallographic site were investigated first. This is a useful starting point for testing the transferability of the modified basis sets. The results of the periodic *ab initio* calculations of the ^{23}Na efg tensor are given in Table 4.13.

Table 4.13 A comparison of experimental and calculated (modified 6-21G) values of ^{23}Na quadrupole parameters for a range of compounds in which sodium occupies a single type of crystallographic site

Compound [a]	Experimental		Calculated	
	C_Q / MHz	η	C_Q / MHz	η
Na_2SiO_3	1.46	0.71	+2.12	0.78
α-$Na_2Si_2O_5$	1.82	1.00	+3.01	0.99
Na_2SO_4	2.60	0.58	-4.10	0.58
$NaH_2PO_4{\cdot}H_2O$	1.22	0.26	+2.88	0.38
$NaH_2PO_4{\cdot}2H_2O$	1.19	0.47	+1.55	0.90
Na_2O	0.00	0.00	0.00	0.00
NaOH	3.50	0.00	+5.45	0.02
$NaOH{\cdot}H_2O$	2.20	0.70	+3.49	0.97
$NaNO_2$	-1.10	0.11	-1.04	0.16
$NaNO_3$	-0.34	0.00	-0.57	0.00
$NaHCO_3$	0.66	0.88	-0.98	0.59
$Na_2C_2O_4$	2.43	0.75	+3.54	0.49
$NaAlO_2$	2.15	0.60	-2.84	0.48
$NaClO_3$	0.80	0.00	-1.44	0.00
$NaClO_4$	0.80	0.35	-1.75	0.46

[a] References for the experimental NMR and crystal structure data are the same as given in Table 4.11

A plot of experimental versus calculated values of $C_Q(^{23}Na)$ is shown in Figure 4.12. The straight line in this figure represents the line of best linear fit to the data (R^2 = 0.98); the slope of the line is 0.639 ± 0.025 and the intercept is -0.038 ± 0.069 MHz. There is, again, a high degree of correlation. However, the fit is no longer 1:1 as was found for the 3-21G basis set (Section 4.4.3). The calculations based on the 6-21G basis set overestimate the value of $C_Q(^{23}Na)$ but in a consistent manner. The only difference between the two basis sets, since they use the same valence description, is in the definition of the core shells. It seems likely that the more extended description of these shells is responsible for the observed behaviour and this particular aspect of the calculations is considered in more detail in Chapter 5, Section 5.4.

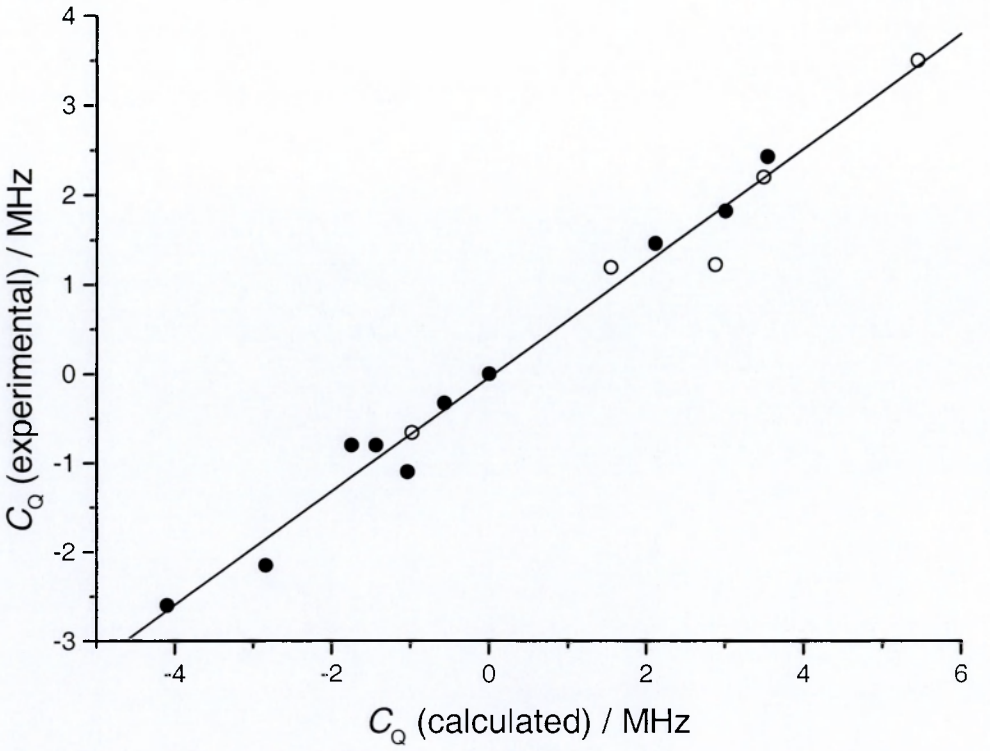

Figure 4.12 A plot of experimental versus calculated values of $C_Q(^{23}Na)$ using data taken from Table 4.13. Compounds involving oxyanions with hydrogen are marked (○) and those without (●).

It is worth noting that the calculated signs of $C_Q(^{23}Na)$ for Na_2SiO_3 and α-$Na_2Si_2O_5$ are opposite to those found using the 3-21G basis set (Table 4.11). Such a change of sign was not found for any of the other compounds investigated. One reason for this behaviour may be that there are errors, although small, in the published crystal structures. Alternatively, the use of different basis sets may have caused a slight change in the calculated electron distributions that, for these particular compounds, have caused a sign change for $C_Q(^{23}Na)$. The latter suggestion seems the more likely.

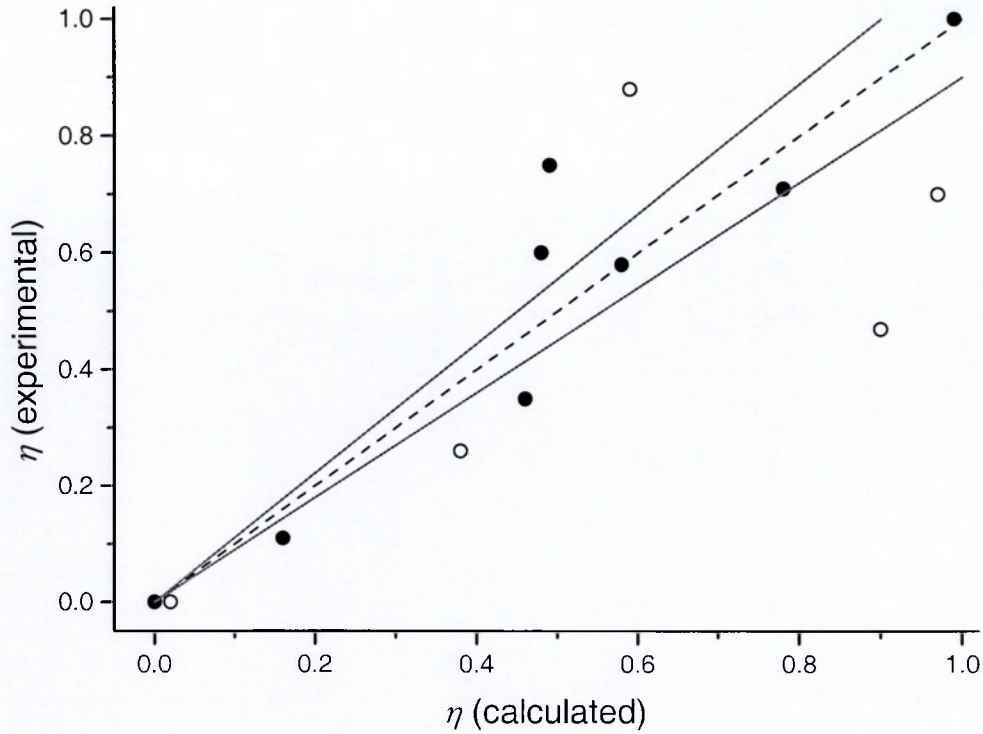

Figure 4.13 A plot of experimental versus calculated values of $\eta(^{23}Na)$ using data taken from Table 4.13. Compounds involving oxyanions with hydrogen are marked (O) and those without (●). The dotted line represents a 1:1 correlation between experimental and calculated values of $\eta(^{23}Na)$. The two solid lines bound a region where the calculated value of $\eta(^{23}Na)$ is within 10% of that determined by experiment.

The correlation plot for $\eta(^{23}Na)$, shown in Figure 4.13, does not indicate any major improvement over that found for the corresponding 3-21G basis set calculations (Figure 4.7). However, there does seem to be some tendency towards more consistent calculations for compounds that do not contain hydrogen.

A separate set of calculations, based on the same selection of single-site compounds was carried out with d-polarisation functions applied to sodium and oxygen and, additionally, on nitrogen in $NaNO_2$; the results are given in Table 4.14.

Table 4.14 A comparison of experimental and calculated (modified 6-21G plus d-polarisation functions as described in the text) values of ^{23}Na quadrupole parameters for a range of compounds in which sodium occupies a single type of crystallographic site

Compound[a]	Experimental		Calculated	
	C_Q / MHz	η	C_Q / MHz	η
Na_2SiO_3	1.46	0.71	+1.91	0.96
α-$Na_2Si_2O_5$	1.82	1.00	+3.01	0.86
Na_2SO_4	2.60	0.58	-3.17	0.70
$NaH_2PO_4{\cdot}H_2O$	1.22	0.26	+2.36	0.31
$NaH_2PO_4{\cdot}2H_2O$	1.19	0.47	+1.51	0.89
Na_2O	0.00	0.00	0.00	0.00
NaOH	3.50	0.00	+5.41	0.01
$NaOH{\cdot}H_2O$	2.20	0.70	+3.33	0.93
$NaNO_2$	-1.10	0.11	-1.12	0.09
$NaNO_3$	-0.34	0.00	-0.33	0.00
$NaHCO_3$	0.66	0.88	-1.11	0.27
$Na_2C_2O_4$	2.43	0.75	+3.56	0.61
$NaAlO_2$	2.15	0.60	-3.14	0.54
$NaClO_3$	0.80	0.00	-1.19	0.00
$NaClO_4$	0.80	0.35	-1.13	0.30

[a] References for the experimental NMR and crystal structure data are the same as those in Table 4.11

A plot of experimental versus calculated values of $C_Q(^{23}Na)$ is shown in Figure 4.14. The straight line in this figure represents the line of best linear fit to the data (R^2 = 0.99); the slope of the line is 0.685 ± 0.020 and the intercept is -0.094 ± 0.052 MHz. There is, again, a high degree of correlation and the fit compares well with that obtained without the addition of d-polarisation functions (Figure 4.12). This suggests that the addition of such functions, at least from the point of view of obtaining a good linear correlation for $C_Q(^{23}Na)$, is not essential using the modified 6-21G basis.

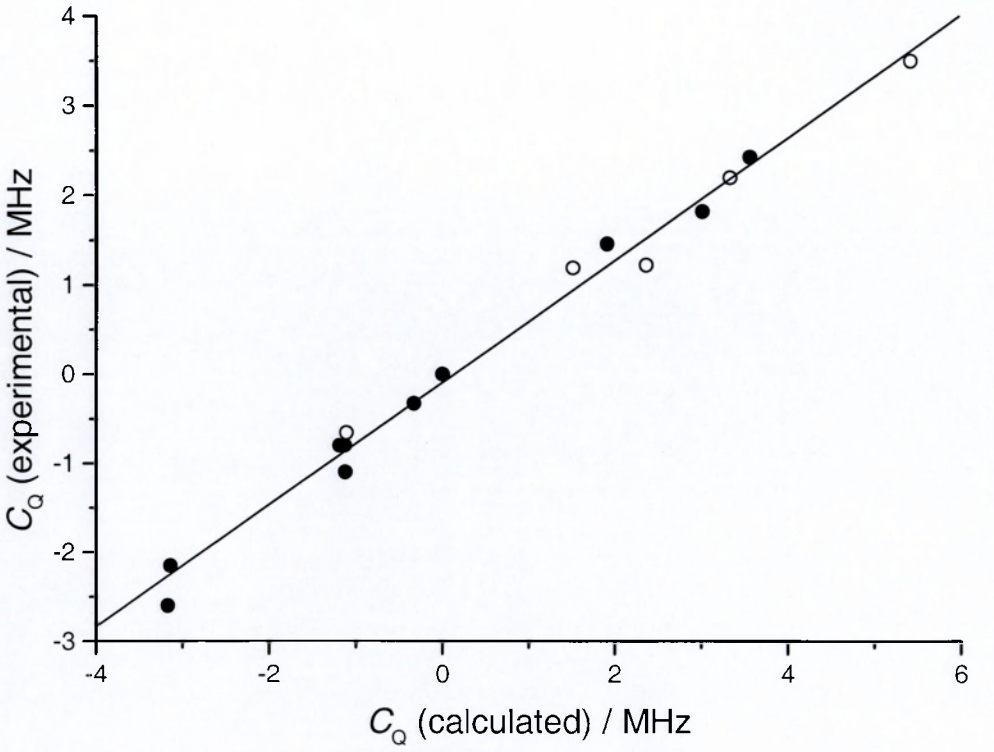

Figure 4.14 A plot of experimental versus calculated values of $C_Q(^{23}Na)$ using data taken from Table 4.14. Compounds involving oxyanions with hydrogen are marked (○) and those without (●).

By contrast, the addition of d-polarisation functions has a noticeable effect on the correlation between calculated and experimental values of $\eta(^{23}Na)$ as shown in Figure 4.15. It can be seen that nearly all of the compounds lie within, or close to, the 10% boundary lines. The two compounds that show the most significant deviation, $NaHCO_3$ (η(experimental) = 0.88, η(calculated) = 0.27) and $NaH_2PO_4{\cdot}2H_2O$ (η(experimental) = 0.47, η(calculated) = 0.89), both contain hydrogen and in both cases the crystal structures were determined by powder X-ray diffraction. It is likely that there are uncertainties in the hydrogen atom positions. It is interesting that if this is the case then the calculated value of $\eta(^{23}Na)$ must be very sensitive to the exact location of the hydrogen atom in these structures. This is an area warranting further study.

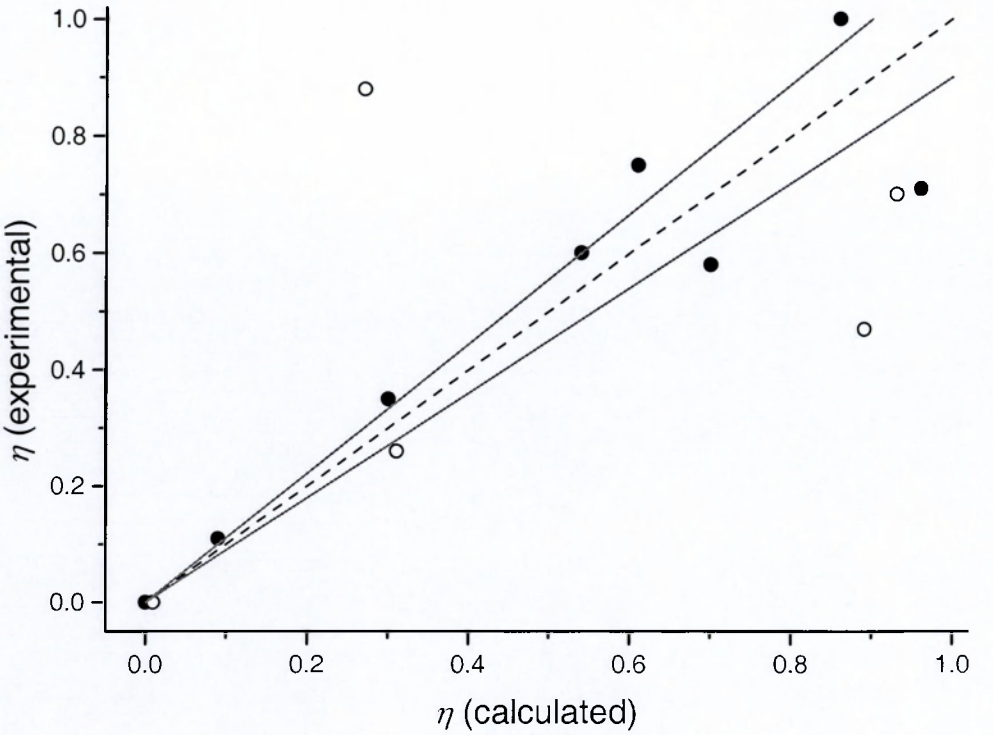

Figure 4.15 A plot of experimental versus calculated values of $\eta(^{23}Na)$ using data taken from Table 4.14. Compounds involving oxyanions with hydrogen are marked (○) and those without (●). The dotted line represents a 1:1 correlation between experimental and calculated values of $\eta(^{23}Na)$. The two solid lines bound a region where the calculated value of $\eta(^{23}Na)$ is within 10% of that determined by experiment.

4.5.2 Multiple-site sodium compounds

For any periodic *ab initio* calculation, computer resources limit the number of basis functions that can be used for a system. In particular, if there are too many atoms per unit cell, due to a low symmetry, the memory requirements can be prohibitive even for a medium-sized basis set. In the present work, due to resource limitations, it was not possible to study all of the multiple-site sodium compounds that were investigated using the smaller 3-21G basis set. Those that could be studied are shown in Table 4.15 for calculations without d-polarisation functions. Corresponding calculations with d-polarisation functions are given later (Table 4.16).

Table 4.15 A comparison of experimental and calculated (modified 6-21G) values for ^{23}Na quadrupole parameters in a range of multiple-site sodium compounds

Compound (*site*)[a]	Experimental		Calculated	
	C_Q / MHz	η	C_Q / MHz	η
β-$Na_2Si_2O_5$ (*1*)	2.50	0.00	-3.24	0.96
β-$Na_2Si_2O_5$ (*2*)	2.22	0.55	+2.91	0.60
Na_2SO_3 (*1*)	1.06	0.00	-1.33	0.00
Na_2SO_3 (*2*)	0.33	0.00	-1.01	0.00
Na_2SO_3 (*3*)	1.14	0.00	+0.90	0.00
Na_2HPO_4 (*1*)	2.04	0.70	-3.34	0.95
Na_2HPO_4 (*2*)	1.31	0.20	+1.90	0.78
Na_2HPO_4 (*3*)	3.84	0.30	+6.30	0.27
$Na_3P_3O_9$ (*1*)	2.20	0.70	-5.21	0.45
$Na_3P_3O_9$ (*2*)	1.57	0.55	+2.41	0.97
$Na_5P_3O_{10}$ (II) [b] (*1*)	4.57	0.39	+6.89	0.45
$Na_5P_3O_{10}$ (II) (*2*)	2.99	0.19	-5.02	0.21
$Na_5P_3O_{10}$ (I (*3*)	1.37	1.00	-2.37	0.72

[a] References for the experimental NMR values and the crystal structure data are the same as those in Table 4.11. [b] Phase II (low temperature) polymorph of anhydrous $Na_5P_3O_{10}$.

The results in Table 4.15 are combined with those for the single-site sodium compounds (Table 4.13, modified 6-21G calculations) and a composite correlation plot for $C_Q(^{23}Na)$ is shown in Figure 4.16. The result for β-$Na_2Si_2O_5$ is omitted from this plot because, as already found in the 3-21G calculations (Section 4.4.3), the calculated value of $\eta(^{23}Na)$ for site (*1*) is in major disagreement with experiment. Indeed, the 6-21G calculations make no improvement to this situation and point further to a discrepancy in the published crystal structure.

The straight line in Figure 4.16 represents the line of best linear fit to the data ($R^2 = 0.98$); the slope of the line is 0.610 ± 0.019 and the intercept is 0.084 ± 0.064 MHz.

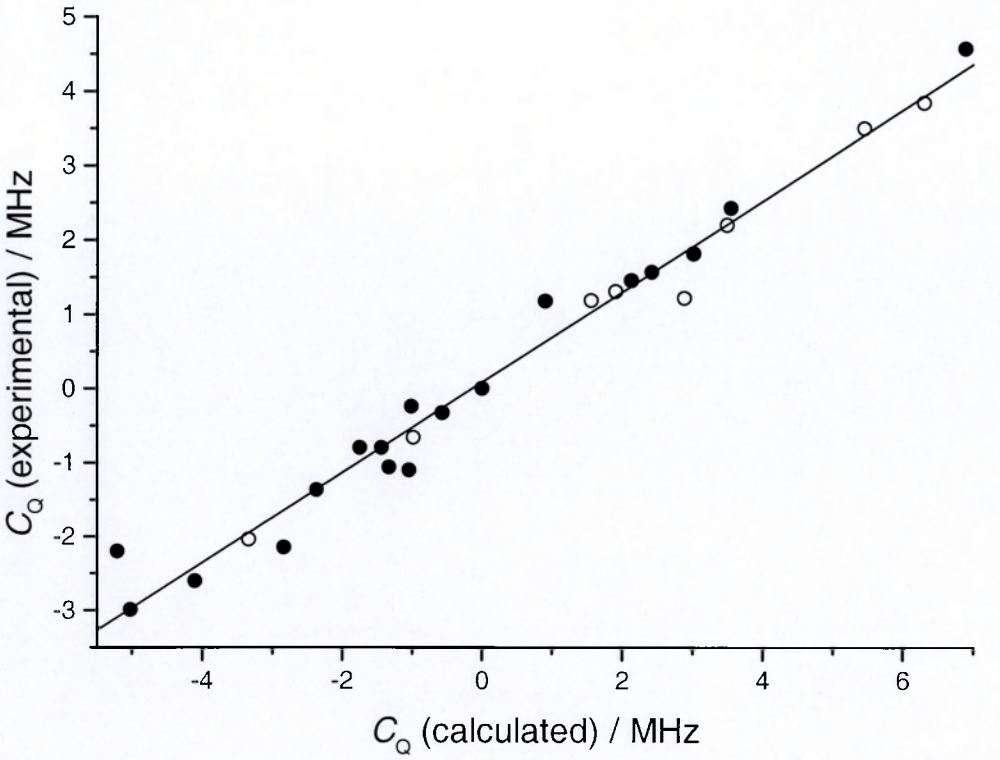

Figure 4.16 A combined plot of experimental versus calculated values of $C_Q(^{23}Na)$ for single- and multiple- site sodium compounds using the modified 6-21G basis set without d-polarisation functions. Compounds involving oxyanions with hydrogen are marked (○) and those without (●).

The addition of the points for the multiple-site compounds reduces the slope slightly but the ranges given by the uncertainties overlap. It can be noted, however, that the calculations for sites (*2*) and (*3*) in Na_2SO_3 are in disagreement with experiment and that the calculations based on the 3-21G basis set performed far better in this case (Table 4.12, $C_Q(^{23}Na)$ for site (*2*) = -0.28 MHz). It would not be possible to assign the ^{23}Na NMR spectrum for Na_2SO_3 using just the information in Table 4.15.

The corresponding combined correlation plot for $\eta(^{23}Na)$ is shown in Figure 4.17. The distribution of points is qualitatively very similar to that obtained for the smaller 3-21G basis set (Figure 4.11). This probably reflects the fact that the two basis sets share the

same valence shell descriptions. If the asymmetry parameter is to be successfully modelled, there appears to be little advantage in using a 6-21G basis set description without d-polarisation functions.

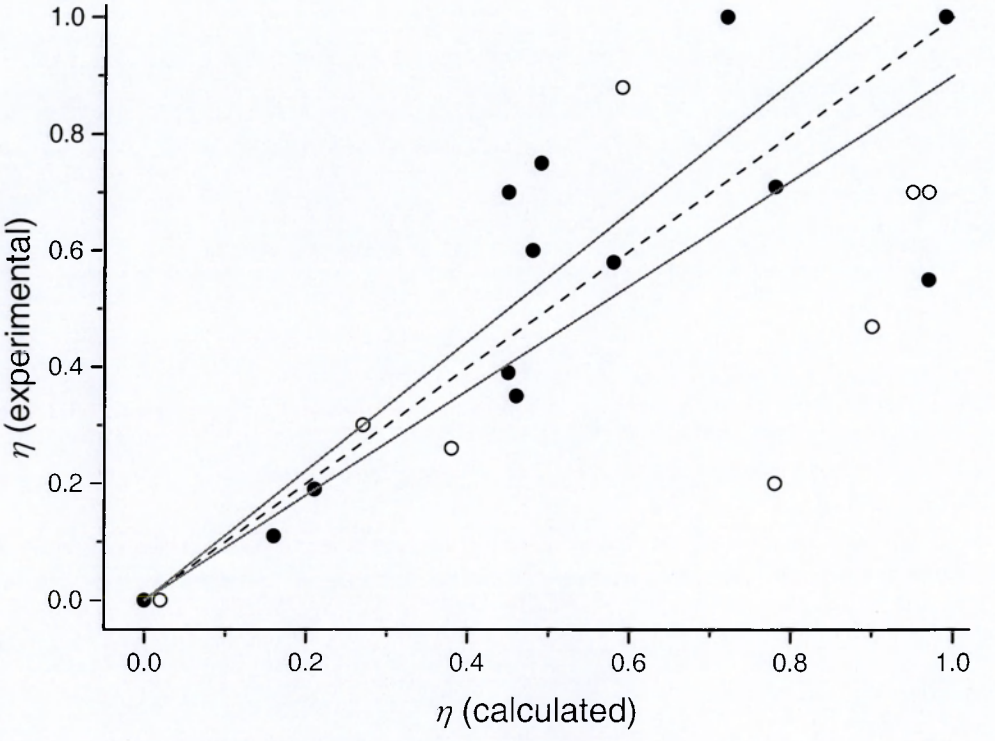

Figure 4.17 A combined plot of experimental versus calculated values of $\eta(^{23}Na)$ for single- and multiple- site sodium compounds using the modified 6-21G basis set without d-polarisation functions. Compounds involving oxyanions with hydrogen are marked (○) and those without (●). The dotted line represents a 1:1 correlation between experimental and calculated values of $\eta(^{23}Na)$. The two solid lines bound a region where the calculated value of $\eta(^{23}Na)$ is within 10% of that determined by experiment.

The final stage of this investigation was to calculate the ^{23}Na quadrupole parameters in the multiple-site sodium compounds using the 6-21G basis set with appropriate d-polarisation functions; that is d-exponents of 0.2, 0.8 and 0.8 for Na, O and N, respectively. The results are given in Table 4.16 for those compounds it was possible to apply d functions.

Table 4.16 A comparison of experimental and calculated (modified 6-21G plus appropriate d-polarisation functions) values for ^{23}Na quadrupole parameters in a range of multiple-site sodium compounds

Compound (*site*) [a]	Experimental		Calculated	
	C_Q / MHz	η	C_Q / MHz	η
β-$Na_2Si_2O_5$ (*1*)	2.50	0.00	-2.92	0.90
β-$Na_2Si_2O_5$ (*2*)	2.22	0.55	+2.42	0.53
Na_2SO_3 (*1*)	1.06	0.00	-0.61	0.00
Na_2SO_3 (*2*)	0.33	0.00	-0.75	0.00
Na_2SO_3 (*3*)	1.14	0.00	+1.03	0.00
Na_2HPO_4 (*1*)	2.04	0.70	+3.11	0.94
Na_2HPO_4 (*2*)	1.31	0.20	+1.47	0.93
Na_2HPO_4 (*3*)	3.84	0.30	+5.92	0.28
$Na_3P_3O_9$ (*1*)	2.20	0.70	-4.26	0.50
$Na_3P_3O_9$ (*2*)	1.57	0.55	+2.27	0.63
$Na_5P_3O_{10}$ (II) (*1*)	4.57	0.39	+6.67	0.45
$Na_5P_3O_{10}$ (II) (*2*)	2.99	0.19	-4.80	0.16
$Na_5P_3O_{10}$ (II) (*3*)	1.37	1.00	-1.98	0.89

[a] References for the experimental NMR values and the crystal structure data are the same as those in Table 4.11. [b] Phase II (low temperature) polymorph of anhydrous $Na_5P_3O_{10}$.

A combined correlation plot of the results in Table 4.16 with those obtained for the single-site sodium compounds (Table 4.14) is shown in Figure 4.18; once again the results for β-$Na_2Si_2O_5$ have been omitted (see earlier discussion).

The straight line shown in the figure ($R^2 = 0.98$) has a slope equal to 0.661 ± 0.019 and an intercept equal to 0.005 ± 0.058 MHz. Again, the degree of correlation is high. However, it should be pointed out that the results for Na_2SO_3 are still anomalous.

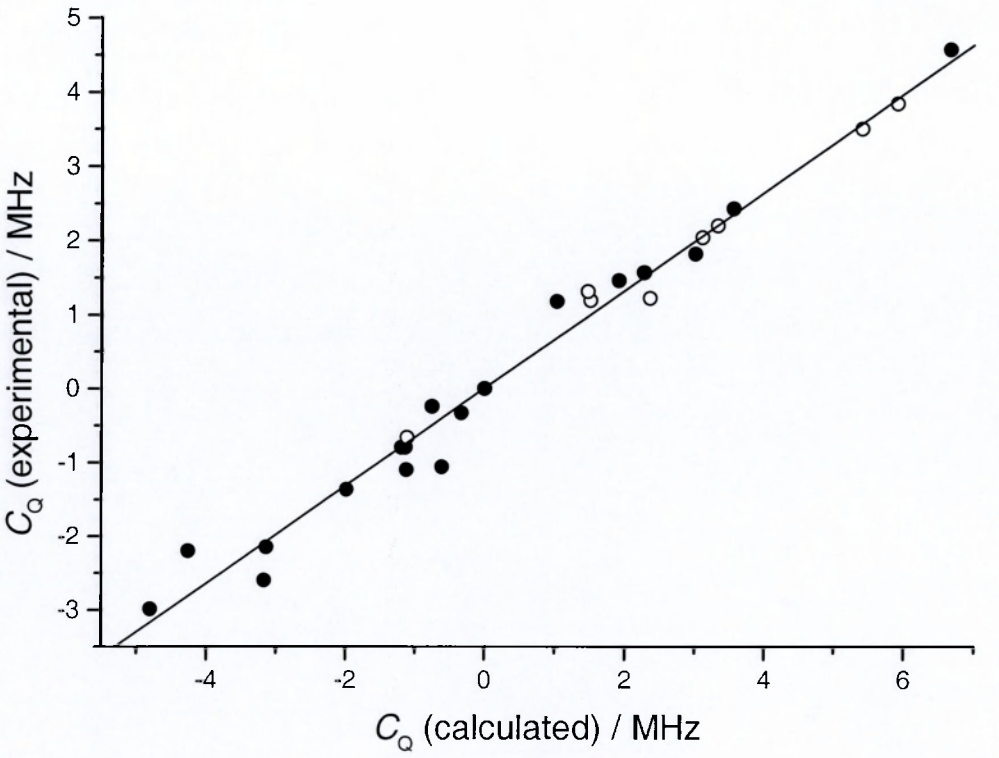

Figure 4.18 A combined plot of experimental versus calculated values of $C_Q(^{23}Na)$ for single- and multiple- site sodium compounds using the modified 6-21G basis set with d-polarisation functions as described in the text. Compounds involving oxyanions with hydrogen are marked (○) and those without (●).

The corresponding combined correlation plot for $\eta(^{23}Na)$ is shown in Figure 4.19. In this case, there is a marked improvement in the overall correlation with nearly all of the compounds investigated located within, or close to, the 10% boundary lines. This strongly suggests that a larger basis set, incorporating appropriate d-polarisation functions, is essential for modelling the sodium asymmetry parameter.

There are three points in Figure 4.19, all associated with hydrogen-containing compounds that do not show the same degree of correlation as the other compounds. These points correspond to the single sodium sites in $NaHCO_3$ and $NaH_2PO_4 \cdot 2H_2O$, and the Na(2) site in Na_2HPO_4.

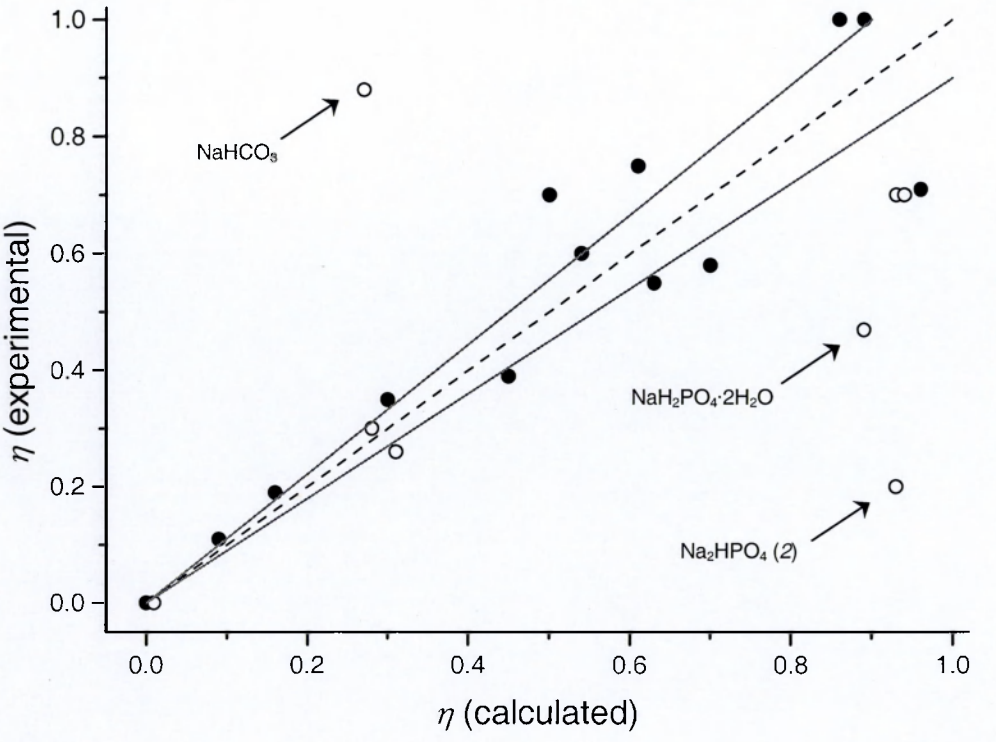

Figure 4.19 A combined plot of experimental versus calculated values of $\eta(^{23}Na)$ for single- and multiple- site sodium compounds using the modified 6-21G basis set with d-polarisation functions as described in the text. Compounds involving oxyanions with hydrogen are marked (○) and those without (●). The dotted line represents a 1:1 correlation between experimental and calculated values of $\eta(^{23}Na)$. The two solid lines bound a region where the calculated value of $\eta(^{23}Na)$ is within 10% of that determined by experiment.

A common feature of these three compounds is that their crystal structures were determined from powder X-ray diffraction studies in which there is a high degree of uncertainty in the hydrogen atom positions. These results add further weight to the suggestion that the periodic *ab initio* calculation of $\eta(^{23}Na)$ can be very sensitive to the position of hydrogen atoms in a crystal structure. It is interesting to note that the Na(*1*) and Na(*3*) sites in Na_2HPO_4 are reasonably well modelled. The discrepancy for the Na(*2*) site is discussed in more detail in Chapter 6.

4.6 A comparison of 3-21G / 6-21G and 3-21G / 6-21G (with d-polarisation) calculations

Useful generalisations concerning the relative effect of basis set size can be found by reviewing the results for those compounds that were investigated using both modified 3-21G and 6-21G basis set descriptions.

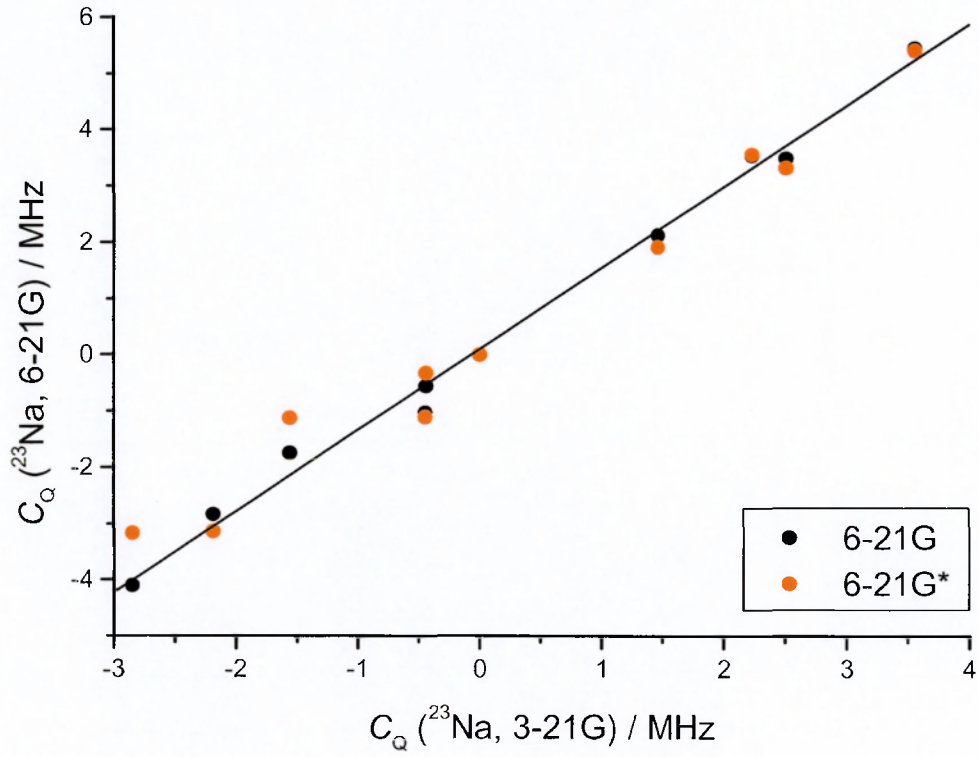

Figure 4.20 Correlations between calculated values of $C_Q(^{23}Na)$ for single-site sodium compounds depending on different basis set descriptions. The straight line represents a fit to the 3-21G / 6-21G data only. 6-21G* represents modified 6-21G basis sets with d-polarisation functions.

Figure 4.20 shows a combined plot which shows how values of $C_Q(^{23}Na)$ for single-site sodium compounds correlate with one another when calculated (i) using modified 3-21G and 6-21G basis set descriptions and (ii) modified 3-21G and 6-21G (with appropriate d-polarisation functions) basis set descriptions.

The 3-21G / 6-21G correlation has a line of best fit ($R^2 = 0.99$) given by the equation

$$C_Q(\text{6-21G}) = 1.441\ C_Q(\text{3-21G}) + 0.1029\ \text{MHz} \qquad (4.1)$$

This indicates that both basis sets are consistent in their calculation of $C_Q(^{23}\text{Na})$ for single-site sodium compounds and this is most probably a reflection of the fact that both basis sets share the same valence shell description. The magnitude of $C_Q(^{23}\text{Na})$ calculated using the modified 6-21G basis set is significantly larger than that predicted using the corresponding 3-21G basis set and, as mentioned previously, this behaviour is most likely linked to the difference in the core shell descriptions. However, the addition of d-polarisation functions to the modified 6-21G basis has a particular effect. It can be seen from Figure 4.20 that the largest deviations are confined to those values where $C_Q(^{23}\text{Na})$ is found to be negative. This behaviour can be rationalised in terms of a redistribution of electron density away from oxygen and onto the sodium cation. This will result in a reduced charge gradient between sodium and the surrounding oxygen atoms and, consequently, the value of $C_Q(^{23}\text{Na})$ will be reduced.

A similar type of plot to that in Figure 4.20 is shown for $\eta(^{23}\text{Na})$ in Figure 4.21. These results show that both basis sets without d-polarisation functions give a reasonable correlation. However, with d-polarisation the correlation shows considerable scatter reflecting the fact that the 6-21G basis incorporating appropriate d-polarisation functions improves the accuracy of the calculation of $\eta(^{23}\text{Na})$.

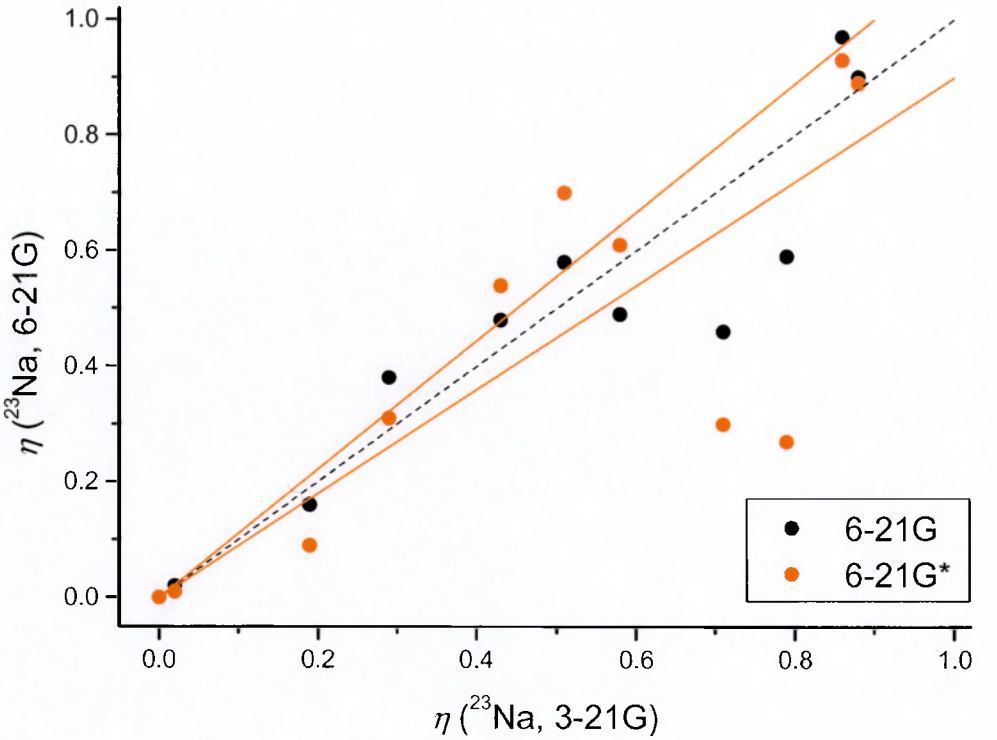

Figure 4.21 Correlation between calculated values of $\eta(^{23}Na)$ for single-site sodium compounds depending on different basis set descriptions. The dotted line represents a 1:1 correlation and the two solid lines are 10% boundary lines. 6-21G* represents modified 6-21G basis sets with d-polarisation functions.

4.7 Density functional theory calculations

When applied to the cluster model for the calculation of the ^{23}Na efg tensor in $NaNO_2$ (Section 4.2), the DFT approach tended to overestimate both $C_Q(^{23}Na)$ and $\eta(^{23}Na)$. The periodic *ab initio* DFT approach for this same compound, using both a relatively large basis set and a smaller standard set, again resulted in significant discrepancies between calculation and experiment (Section 4.3.3). These results, however, relate to a single compound. A further DFT study was undertaken, therefore, for a small range of compounds using the same 3-21G basis set description that had proved successful in the HF calculations (Section 4.4.3). In the LDA calculations, the VWN and LDA parameterisations were selected for the correlation and exchange functionals, respectively.

PWGGA and Becke parameterisations replaced these functionals in the GGA calculations. Overall, the results of the calculations are variable with no significant improvements being achieved with the DFT approach.

The results of the investigation are shown in Table 4.17. It is interesting to note that it was only the hybrid B3LYP method, which was able to reach convergence for all of the compounds selected. However, it is particularly noticeable that the calculated B3LYP results for sites (*1*) and (*3*) for Na_2SO_3 are significantly in disagreement with experiment. (It should be recalled for calculations using a modified 6-21G basis set, see Table 4.15, that the opposite was found: site (*2*) was problematic.) Further investigations, in which the outermost shell exponent on sodium was increased, failed to improve the modelling of the three Na_2SO_3 sites using B3LYP calculations or to bring to convergence the LDA and GGA calculations.

Table 4.17 A comparison of experimental and calculated ^{23}Na quadrupole parameters in a range of sodium compounds using DFT and a modified 3-21G basis set

Compound (*site*)	Experiment		LDA		GGA		B3LYP	
	C_Q / MHz	η	C_Q / MHz	η	C_Q / MHz	η	C_Q / MHz	η
$NaNO_3$	-0.34	0.00	-0.70	0.00	-0.51	0.00	-0.38	0.00
$NaAlO_2$	2.15	0.60	-1.97	0.40	-1.76	0.40	-1.97	0.40
$Na_2C_2O_4$	2.43	0.75	-	-	-	-	2.08	0.61
Na_2SO_4	2.60	0.58	-2.24	0.38	-1.97	0.17	-2.19	0.40
NaOH	3.50	0.00	3.66	0.06	3.20	0.05	4.03	0.01
Na_2SiO_3	1.46	0.71	-	-	-	-	-1.17	0.63
NaH_2PO_4 (*1*)	1.59	0.46	1.45	0.46	0.98	0.76	1.55	0.34
NaH_2PO_4 (*2*)	2.35	0.94	-1.95	0.97	1.52	0.77	-2.15	0.98
Na_2SO_3 (*1*)	1.06	0.00	-	-	0.41	0.00	0.31	0.00
Na_2SO_3 (*2*)	0.33	0.00	-	-	-0.66	0.00	-0.44	0.00
Na_2SO_3 (*3*)	1.14	0.00	-	-	0.17	0.00	0.16	0.00

A more extensive investigation was carried out using the hybrid B3LYP approach for a much wider range of compounds. However, in a few cases, including Na_2HPO_4 and β-$Na_2Si_2O_5$, convergence could not be obtained. In order to overcome this problem the single valence shell exponent on sodium was increased from 0.18 to 0.20 and the results of the subsequent analysis are given in Table 4.18.

The B3LYP results, (except for those for β-$Na_2Si_2O_5$ as explained earlier), are shown in the correlation plot in Figure 4.22. The straight line shown in this figure was obtained by a linear least squares fit to the data ($R^2 = 0.98$); the slope of the line is 0.661 ± 0.019 and the intercept is 0.005 ± 0.058 MHz. There is clearly a reasonable linear correlation, although a qualitative appraisal indicates a greater scatter than compared to the corresponding plot using HF calculations (Figure 4.10). It should be noted that the results for Na_2SO_3 in Table 4.18 remain highly sensitive to the change in basis set description.

Table 4.18 A comparison of experimental and calculated ^{23}Na quadrupole parameters in a range of sodium compounds using the hybrid B3LYP DFT approach and a modified 3-21G basis set

Compound (*site*)	Experimental		Calculated	
	C_Q / MHz	η	C_Q / MHz	η
$NaNO_3$	-0.34	0.00	-0.31	0.00
$NaAlO_2$	2.15	0.60	-2.09	0.43
$Na_2C_2O_4$	2.43	0.75	2.26	0.57
Na_2SO_4	2.60	0.58	-2.25	0.48
NaOH	3.50	0.00	4.43	0.07
Na_2SiO_3	1.46	0.71	-1.14	0.63
NaH_2PO_4 (*1*)	1.59	0.46	1.73	0.30
NaH_2PO_4 (*2*)	2.35	0.94	-2.41	0.93
Na_2SO_3 (*1*)	1.06	0.00	0.29	0.00
Na_2SO_3 (*2*)	0.33	0.00	-0.75	0.00
Na_2SO_3 (*3*)	1.14	0.00	0.03	0.00
$NaH_2PO_4 \cdot H_2O$	1.22	0.26	1.56	0.20
$NaH_2PO_4 \cdot 2H_2O$	1.19	0.47	0.78	0.26
Na_2HPO_4 (*1*)	2.04	0.70	-1.64	1.00
Na_2HPO_4 (*2*)	1.31	0.20	0.92	0.73
Na_2HPO_4 (*3*)	3.84	0.30	3.60	0.26
$Na_3P_3O_9$ (*1*)	2.20	0.70	-2.01	0.44
$Na_3P_3O_9$ (*2*)	1.57	0.55	1.14	0.68
$NaOH \cdot H_2O$	2.20	0.70	2.58	0.62
$NaHCO_3$	0.66	0.88	0.80	0.85
$Na_5P_3O_{10}$ (II) (*1*)	4.57	0.39	3.60	0.49
$Na_5P_3O_{10}$ (II) (*2*)	2.99	0.18	-3.02	0.30
$Na_5P_3O_{10}$ (II) (*3*)	1.37	1.00	-1.27	0.90
β-$Na_2Si_2O_5$ (*1*)	2.50	0.00	-1.92	0.86
β-$Na_2Si_2O_5$ (*2*)	2.22	0.55	1.65	0.43
$NaClO_3$	0.80	0.00	-0.51	0.00
$NaClO_4$	0.80	0.35	1.31	0.76

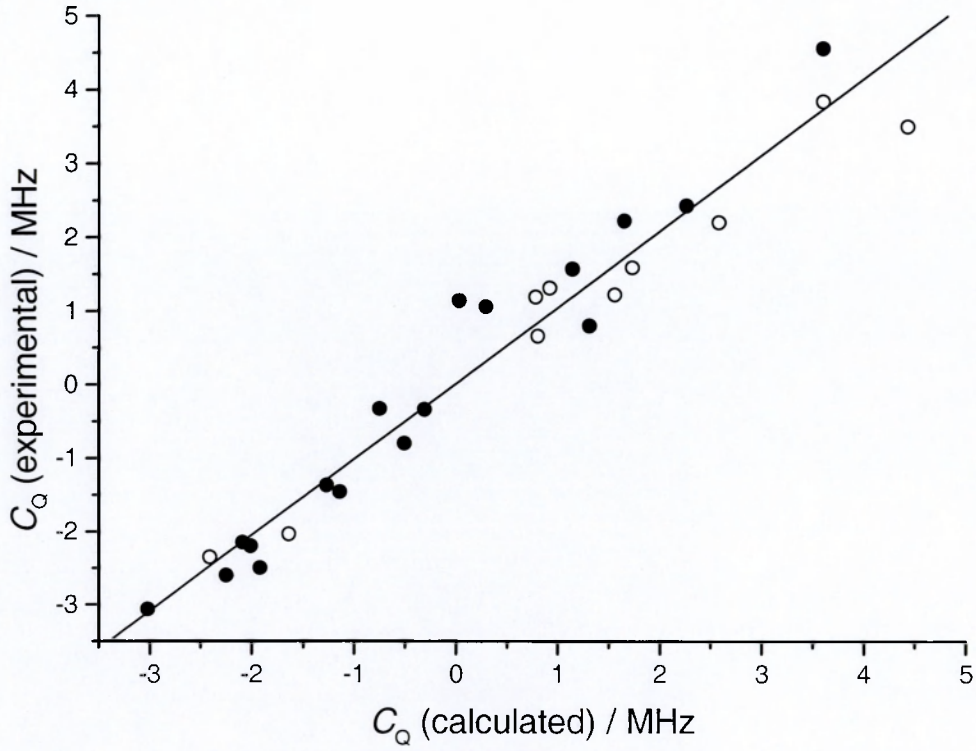

Figure 4.22 A plot of experimental versus calculated values of $C_Q(^{23}Na)$ using the hybrid B3LYP approach for (i) sodium compounds involving oxyanions (●) and (ii) sodium compounds involving oxyanions with hydrogen (○)

The correlation between the calculated and experimental values of $\eta(^{23}Na)$, as shown in Figure 4.23, demonstrates considerable scatter. Although a few compounds lie within or very close to the 10% boundary region, the overall lack of correlation suggests that the B3LYP method is not particularly suited to the calculation of this parameter; at least using relatively simple basis set descriptions.

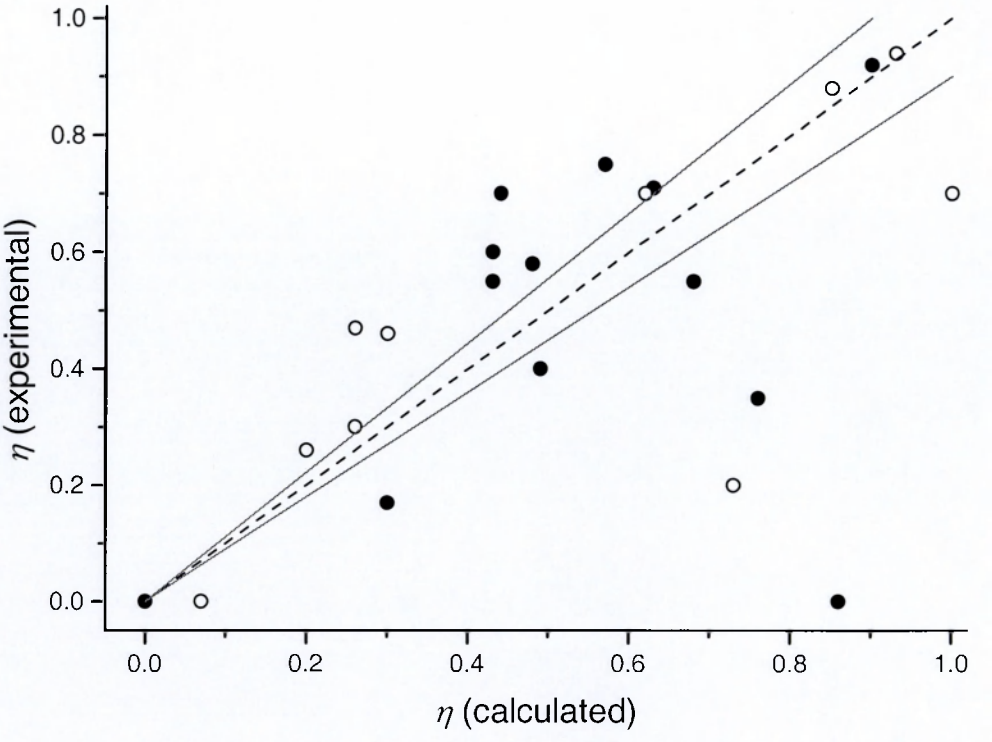

Figure 4.23 A plot of experimental versus calculated values of $\eta(^{23}Na)$ using the hybrid B3LYP approach for (i) sodium compounds involving oxyanions (●) and (ii) sodium compounds involving oxyanions with hydrogen (○). The dotted line represents a 1:1 correlation between experimental and calculated values of $\eta(^{23}Na)$. The two solid lines bound a region where the calculated value of $\eta(^{23}Na)$ is within 10% of that determined by experiment.

4.8 Summary and Conclusions

An important aim of this chapter has been to find a simple, accurate and transferable method, based on a periodic *ab initio* approach, for the calculation of the sodium efg tensor in a wide range of ionic sodium compounds for which crystal structure information is available. Initial embedded cluster calculations of the ^{23}Na quadrupole parameters in $NaNO_2$ found that a relatively large cluster was required but also that the calculated values were highly dependent on the basis set selected. A periodic calculation using a larger [8-511 / 8-41 / 8-411] basis set, for [Na / N / O] respectively, gave improved agreement with experiment but when transferred to $NaNO_3$ the calculation failed to

converge. Subsequent HF calculations using a suitably modified, small, standard 3-21G basis set have been shown to be able to predict the value of $C_Q(^{23}Na)$ with an almost 1:1 degree of correlation between calculation and experiment. The success of this approach is of particular interest for the assignment of ^{23}Na NMR spectra in the solid state. However, the agreement between calculation and experiment for $\eta(^{23}Na)$ was very variable and no consistent correlation was found.

In order to better determine $\eta(^{23}Na)$, calculations using a suitably modified 6-21G basis set were considered. It was found that using this basis set without d-polarisation functions gave no significant improvement on the modified 3-21G based calculations. However, a reasonable linear correlation between calculation and experiment was achieved when d-polarisation functions were used on the coordinating sodium and oxygen atoms along with the modified 6-21G basis set. For several compounds, there was strong evidence that the calculation of $\eta(^{23}Na)$ was particularly sensitive to the location of the hydrogen atoms within the crystal structure. DFT calculations, at least within the context of the present work, offered no distinct advantages.

As already indicated, the ability to predict the magnitude of the ^{23}Na quadrupole parameters is important for assignment purposes and this is particularly so for materials in which sodium is present at a number of different crystallographic sites. This area is investigated more fully in Chapter 6.

References

1. R. J. Bersohn, *J. Chem. Phys.*, **29**, 326, 1958.
2. T.P. Das and R. Bersohn, *Phys. Rev.*, **102**, 360, 1956.
3. L. Pauling, *The Nature of the Chemical Bond*, Cornell University Press, Ithica, 1939.
4. E.R. Andrews, R.G. Eades, J.W. Hehhel and D.G. Hughes, *Proc. Phys. Soc.*, **79**, 954, 1962.
5. J. Skibsted, N.C. Neilsen, H. Bildsøe and H.J. Jakobsen, *J. Magn. Reson.*, **95**, 88, 1991.
6. D.G. Hughes, *J. Chem. Phys.*, **74**, 3236, 1981.
7. J. Itoh and R. Kusaka, *J. Phys, Soc. Japan*, **9**, 434, 1954.
8. W.P. Power, *Magn. Reson. Chem.*, **33**, 220, 1995.
9. H. Koller, G. Engelhardt, A.P.M. Kentgens and J. Sauer, *J. Phys. Chem.*, **98**, 1544, 1994.
10. A. Weiss, *Z. Naturforsch.*, **15a**, 536, 1960.
11. T. Kanashiro, T. Ohno and M. Satoh, *J. Phys. Soc. Jpn.*, **54**, 2720, 1985.
12. D.G. Hughes and L. Pandey, *J. Magn. Reson.*, **75**, 272, 1987.
13. K.T. Han, H.W. Shin, I.W. Park and S.H. Choh, *J. Korean Phys. Soc.*, **25**, 67, 1992.
14. R. Dovesi, V.R. Saunders, C. Roetti, M. Causà, N.M. Harrison, R. Orlando and E. Aprà, *CRYSTAL95 User's Manual*, University of Torino, Torino, 1996.
15. V.R. Saunders, R. Dovesi, C. Roetti, M. Causà, N.M. Harrison, R. Orlando, and C.M. Zicovich-Wilson, *CRYSTAL98 User's Manual*, University of Torino, Torino, 1998.
16. P. Cherin, W.C. Hamilton and B. Post, *Acta Crystallogr.*, **23**, 455, 1967.
17. J. Sauer, *Chem Rev.*, **89**, 199, 1989.

18. A. Weiss and D. Biedenkapp, *Z. Naturforsch.*, **17a**, 794, 1962.

19. W.J. Hehre, R. Ditchfield and J.A. Pople, *J. Chem. Phys.*, **56**, 2257, 1972.

20. M.M. Francl, W.J. Pietro, W.J. Hehre, J.S. Binkley, M.S. Gordon, D.J. DeFrees and J.A. Pople, *J. Chem. Phys.*, **77**, 3654, 1982

21. J.S. Binkley, J.A. Pople, W.J. Hehre, *J. Am. Chem. Soc.*, **102**, 939, 1980.

22. M.S. Gordon, J.S. Binkley, J.A. Pople, W.J. Pietro and W.J. Hehre, *J. Am. Chem. Soc.*, **104**, 2797, 1983.

23. R. Krishnan, J.S. Binkley, R. Seeger and J.A. Pople, *J. Chem. Phys.*, **72**, 650, 1980.

24. A.D. Maclean and G.S. Chandler, *J. Chem. Phys.*, **72**, 5639, 1980.

25. D.B. Chestnut and K.D. Monroe, *J. Comput. Chem.*, **10**, 648, 1989.

26. GAMESS, Version 26 July 1995, M.W. Schmidt, K.K. Baldridge, J.A. Boatz, S.T. Elbert, M.S. Gordon, J.H. Jensen, S. Koseki, N. Matsunaga, K.A. Nguyen, S.J. Su, T.L. Windus, together with M. Dupuis and J.A. Montgomery, *J. Comput. Chem.*, **14**, 1347, 1993.

27. GAUSSIAN 94, Revision E.3, M.J. Frisch, G.W. Trucks, H.B. Schlegel, P.M.W. Gill, B.G. Johnson, M.A. Robb, J.R. Cheeseman, T. Keith, G.A. Petersson, J.A. Montgomery, K. Raghavachari, M.A. Al-Laham, V.G. Zakrzewski, J.V. Ortiz, J.B. Foresman, J. Cioslowski, B.B. Stefanov, A. Nanayakkara, M. Challacombe, C.Y. Peng, P.Y. Ayala, W. Chen, M.W. Wong, J.L. Andres, E.S. Replogle, R. Gomperts, R.L. Martin, D.J. Fox, J.S. Binkley, D.J. Defrees, J. Baker, J.P. Stewart, M. Head-Gordon, C. Gonzalez and J.A. Pople, Gaussian Inc., Pittsburgh PA, 1995.

28. L. Salasco, R. Dovesi, R. Orlando and M. Causà, *Mol. Phys.*, **72**, 267, 1991.

29. R. Dovesi, C. Roetti, C. Freyria-Fava, M. Prencipe and V.R. Saunders, *Chem. Phys.*, **156**, 11, 1991.

30. R. Dovesi, C. Roetti, C. Freyria-Fava, E. Aprà, V.R. Saunders and N.M. Harrison, *Philos. Trans. R. Soc. London, Ser. A*, **341**, 203, 1992.

31. M. Prencipe, A. Zupan, R. Dovesi, E. Aprà and V.R. Saunders, *Phys. Rev. B*, **51**, 3391, 1995.

32. W.J. Hehre, L. Radom, P.V.R. Schleyer and J.A. Pople, *Ab Initio Molecular Orbital Theory*, John Wiley and Sons, New York, 1986.

33. M. Ahtee, M. Nurmela, P. Suortti and M. Jaervinen, *J. Applied Crystallogr.*, **22**, 261, 1989.

34. A.D. Becke, *J. Chem. Phys.*, **98**, 5648, 1993.

35. S.H. Vosko, L. Wilke and M. Nusair, *Can. J. Phys.*, **58**, 1200, 1980.

36. P.A.M. Dirac, *Proc. Cambridge Philos. Soc.*, **26**, 376, 1930.

37. J.P. Perdew and Y. Wang, *Phys. Rev. B*, **33**, 8800, 1986.

38. J.P. Perdew and Y. Wang, *Phys. Rev. B*, **40**, 3399, 1989.

39. J.P. Perdew and Y. Wang, *Phys. Rev. B*, **45**, 13244, 1992.

40. A.D. Becke, *Phys Rev. A*, **38**, 3098, 1988.

41. P. Jönsson, A. Ynnerman, C.F. Fischer, M.R. Gudefroid and J. Olsen, *Phys. Rev. A*, **53**, 4021, 1996.

42. D.A. Fletcher, R.F. McMeeking and D. Parkin, *J. Chem. Inf. Comput. Sci.*, **36**, 746, 1996.

43. S.E. Rasmussen, J.-E. Jorgensen and B. Lundtoft, *J. Appl. Crystallogr.*, **29**, 42, 1996.

44. F. Liu, S.H. Garofalini, R.D. King-Smith and D. Vanderbilt, *Chem. Phys. Letters*, **215**, 401, 1993.

45. W.S. McDonald and D.W.J. Cruickshank, *Acta Crystallogr.*, **22**, 37, 1967.

46. H. Jacobs, J. Köckelkorn and T.Z. Tacke, *Z. Anorg. Allg. Chem.*, **531**, 119, 1985.

47. A.K. Pant and D.W.J. Cruickshank, *Acta Crystallogr. B*, **24**, 13, 1968.

48. M. Catti and G. Ferraris, *Acta Crystallogr. B*, **32**, 359, 1976.

49. H. Bartl, M. Catti and G. Ferraris, *Acta Crystallogr. B*, **32**, 987, 1976.

50. E. Zintl, A. Harder and B. Dauth, *Z. Elektrochemie*, **40**, 588, 1934.

51. H. Jacobs and U.Z. Metzner, *Anorg. Allg. Chem.*, **597**, 97, 1991.

52. M.I. Kay and B.C. Frazer, *Acta Crystallogr.*, **14**, 56, 1961.

53. B.D. Sharma, *Acta Crystallogr. B*, **18**, 818, 1965.

54. D.A. Reed and M.M. Olmstead, *Acta Crystallogr. B*, **37**, 938, 1981.

55. J.A. Kaduk and S.-Y. Pei, *J. Solid State Chem.*, **115**, 126, 1995.

56. H. Sowa, *J. Solid State Chem.*, **118**, 378, 1995.

57. R. Wartchow, H.J. Berthold, *Z. Kristallogr.*, **147**, 307, 1978.

58. P.L. Kuhns and J.S. Waugh, *J. Chem. Phys.*, **93**, 2166, 1992.

59. D. Heidemann, C. Hübert, W. Schwieger, P. Grabner, K.-H. Bergk, P.V. Sarv, *Anorg. Allg. Chem.*, **617**, 169, 1992.

60. A.K. Pant, *Acta Crystallogr. B*, **24**, 1077, 1968.

61. W.H. Zachariasen and H.E. Buckley, *Phys. Rev.*, **37**, 1295, 1931.

62. J. Itoh, R. Kusaka and Yamagata, *J. Phys. Soc. Japan*, **9**, 209, 1954.

63. A.A. Uraz, and N. Armagan, *Acta Crystallogr. B*, **33**, 1396, 1977.

64. R.N.P. Choudray, R.J. Nelmes and K.D. Rouse, *Chem. Phys. Lett.*, **78**, 102, 1981.

65. M. Baldus, B.H. Meier, R.R. Ernst and A.P.M. Kentgens, *J. Am. Chem. Soc.*, **117**, 5141, 1995.

66. H.M. Ondik, *Acta Crystallogr. B*, **18**, 226, 1965.

67. W.S. McDonald and D.W.J. Cruickshank, *Acta Crystallogr.*, **1**, 1948, 1967.

68. D.R. Davies and D.E.C. Corbridge, *Acta Crystallogr.*, **11**, 315, 1958.

Chapter 5

Extensions of the periodic *ab initio* correlation approach to different types of crystalline sodium compounds

5.1 Introduction

The periodic *ab initio* method has been shown to produce reliable correlations between calculation and experiment for $C_Q(^{23}Na)$ for a variety of ionic sodium compounds containing a range of oxyanions in which the central atom is a p-block element. However, the success of this type of correlation method is likely to depend upon:

- the ability of the basis set to accurately reflect the distribution of electron density within the crystalline state, and
- the accuracy of the crystal structure that is used in the calculation.

The purpose of this, and the following chapter, is to explore both of these factors in more detail.

The first section in this chapter sets out to investigate the possibility of extending the modelling method to more complex types of sodium compound. An initial study of compounds containing transition metal oxyanions is followed by an investigation of the use of core pseudopotentials for compounds containing heavy atoms. For this type of compound an all-electron type model would be expected to consume substantial computer resources.

So far, in this work, only compounds in which there are discrete oxyanions coordinating to sodium exclusively through oxygen atoms have been considered. An attempt is made, therefore, to extend the modelling strategy to representative silicates, or aluminosilicates, forming extended three-dimensional structures. Calculations for cryolite and chiolite, in which the coordinating atom is fluorine, are described in their own section.

A recent ^{23}Na MAS NMR study of sodium oxide chloride, Na_3OCl, has revealed the largest ^{23}Na quadrupole coupling constant so far measured ($C_Q(^{23}Na)$ = 11.34 MHz [1]). This compound is unusual in that the sodium cation is present on a non-cubic site in a purely ionic compound and it has been recognised that it can be used as a model system for the evaluation of the Sternheimer factor for the sodium cation [1]. The final section of this chapter considers the application of the periodic *ab initio* method to the calculation of the ^{23}Na quadrupole NMR parameters in this model compound. In addition, the Sternheimer factor is computed by *ab initio* means and is compared with values reported in the literature. Further calculations of the Sternheimer factor are also carried out for a range of relatively simple sodium compounds for comparative purposes. Overall, insight is gained into the nature of the source of the efg at sodium and its connection with the polarisation of sodium 2p core electrons is explored.

5.2 Extensions to different types of sodium compound

5.2.1 Types of compound

Coordination to transition metal oxyanions

The first-row transition metal oxides have been for many years the subject of intense experimental and theoretical interest [2]. *Ab initio* periodic unrestricted-HF methods for crystalline systems containing open-shell ions have been found to be well suited to the study of these materials. However, transition metals forming the central atom in a polyatomic oxyanion tend to be in their highest oxidation state. In such situations, it seems reasonable that the periodic *ab initio* method developed in this thesis for sodium salts containing oxyanions of the lighter p-block elements will still be applicable. To test

this view, three compounds were chosen, α- and β-sodium vanadate (V) and sodium chromate (VI) comprising five different sodium sites between them.

Coordination to heavy atom oxyanions

The treatment of heavy atoms using an all-electron basis set is computationally expensive and, in cases where the crystal symmetry of the compound to be studied is low, this makes calculations impractical due to the large number of basis functions involved. This problem can be overcome by the use of pseudopotentials, which allow the core basis functions to be replaced by a simpler function thereby greatly simplifying the calculation. In order to investigate the appropriateness of pseudopotentials, within the periodic *ab initio* method for the calculation of ^{23}Na quadrupole parameters described in Chapter 4, calculations were performed on a representative group of sodium compounds in which the central atom of the oxyanion was, either selenium, bromine, antimony or tellurium.

Silicates and Aluminosilicates

In Chapter 4, it was demonstrated that the efg tensor at sodium could be reliably calculated in sodium silicates where the silicate anion is present as a discrete entity. However, of more practical interest is the ability to accurately model sodium sites within a three-dimensional silicate or aluminosilicate such as a zeolite. To this end, periodic *ab initio* calculations were made on three structures; the porous sodium trisilicate Mu-11 ($(Na_2Si_3O_7 \cdot H_2O)_4$), natural blue sodalite ($Na_8(AlSiO_4)_6Cl_2$) and sodalite ($Na_6(AlSiO_4)_6$).

5.2.2 Selection of basis sets

The sodium and oxygen atoms, present in all of the compounds studied in this section, were represented on an all-electron basis. The core representation from the Pople 3-21G basis set augmented by a single sp-shell with an exponent set at 0.18 was used for sodium and the Pople 3-21G basis set with the outer valence exponent set to 0.374 was used for oxygen.

Calculations of the ^{23}Na quadrupole parameters for sodium compounds containing transition metal oxyanions used the standard Pople 3-21G basis sets to represent the transition elements chromium and vanadium.

The central heavy atoms (Br, Sb, Se and Te) in their respective oxyanions were modelled using the Hay and Wadt [3] large core pseudopotentials, available as standard within the CRYSTAL code. The pseudopotential core was supplemented by two sp-type (21G) shells, the exponents and coefficients of which were taken from the Pople 3-21G basis set for the same element.

The silicon and aluminium atoms were represented by their unmodified Pople 3-21G basis sets respectively.

5.2.3 Results

The results for the periodic *ab initio* calculation of ^{23}Na NMR quadrupole parameters for all of the sodium compounds considered in this section are summarised in Table 5.1.

Table 5.1 A summary of experimental and calculated values of ^{23}Na NMR quadrupole parameters for selected sodium compounds of transition metal and heavy atom oxyanions, silicates and aluminosilicates

Compound (*site*)	Experimental		Calculated		References	
	C_Q / MHz	η	C_Q / MHz	η	NMR	Struct
Transition metal oxyanions						
α-$NaVO_3$ (*1*)	1.50	0.58	+1.20	0.79	4	5
α-$NaVO_3$ (*2*)	0.77	0.06	+0.76	0.97		
β-$NaVO_3$	1.42	0.27	+1.74	0.93	4	6
Na_2CrO_4 (*1*)	2.78	0.57	-3.41	0.34	7	8
Na_2CrO_4 (*2*)	0.50	-	+0.82	0.43		
Heavy atom oxyanions						
$NaBrO_3$	0.864	0.0	-0.71	0.00	9	10
Na_3SbO_3	3.0	-	+3.22	0.33	11	12
Na_2SeO_4	3.8	-	-3.66	0.46	11	13
Na_2TeO_3 (*1*)	1.36	0.9	-1.37	0.70	14	15
Na_2TeO_3 (*2*)	1.84	0.8	-1.61	0.31		
$Na_2Te_4O_9$ (*1*)	4.4	0.08	-4.10	0.30	14	14
$Na_2Te_4O_9$ (*2*)	3.6	0.12	-2.94	0.87		
Silicates and aluminosilicates						
$(Na_2Si_3O_7{\cdot}H_2O)_4$ (*1*)	2.9	0.7	+2.81	0.76	16	17
$(Na_2Si_3O_7{\cdot}H_2O)_4$ (*2*)	2.7	0.4	-2.65	0.26		
$Na_8(AlSiO_4)_6Cl_2$	0.081	0.35	0.32	0.0	18	19
$Na_6(AlSiO_4)_6$	5.90	0.10	3.38	0.19	7	20

For sodium compounds containing transition metal oxyanions the results demonstrate that, quantitatively, the same *ab initio* method based on the Pople 3-21G basis set, which proved successful for oxyanions of the lighter p-block elements, is an appropriate method for the calculation of $C_Q(^{23}Na)$. It should be noted that the two crystallographically distinct sites in both α-$NaVO_3$ and Na_2CrO_4 are well differentiated. Such a result would allow for an unambiguous site assignment of their respective ^{23}Na MAS NMR spectra.

A similar result is obtained for the ^{23}Na quadrupole parameters in periodic *ab initio* calculations involving sodium compounds of heavy atom oxyanions. It would appear that

simplifying the treatment of the core electrons of the heavy atom by the use of pseudopotentials does not adversely affect the calculation of $C_Q(^{23}Na)$. Once again, the unambiguous assignment of the two distinct sodium sites in both Na_2TeO_3 and $Na_2Te_4O_9$ was possible.

However, for the ionic sodium compounds containing transition metal or heavy atom oxyanions, the calculated values of $\eta(^{23}Na)$ are not in good agreement with experiment. This result is in line with that found for the lighter p-block oxyanions studied in Chapter 4 with the same basis set.

The results of the periodic *ab initio* calculations for the silicates and aluminosilicates are more variable. The porous sodium trisilicate Mu-11 ($(Na_2Si_3O_7 \cdot H_2O)_4$) has a structure consisting of corrugated sheets built from four-, six- and eight-membered ring units forming a three-dimensional framework [17]. The calculation of both $C_Q(^{23}Na)$ and $\eta(^{23}Na)$ for the two distinct sodium sites in this complex compound are in very good agreement with those determined by experiment [16].

However, the results obtained for the two aluminosilicates are at variance with experiment. In the case of natural blue sodalite ($Na_8(AlSiO_4)_6Cl_2$) it would appear that the neutron-diffraction derived crystal structure used in the periodic *ab initio* calculation is inconsistent with that of the mineral sample used in the ^{23}Na MAS NMR study since the experimental value of $\eta(^{23}Na)$ is not that expected for axial symmetry. Other crystal structures available in the literature for natural blue sodalite from deposits in Bolivia [21] and Bancroft Canada [22, 23] also show sodium to occupy a site of axial symmetry. Such an observation would suggest that the ^{23}Na NMR result is not that for sodium in a defect

free sample or, alternatively, that motion is present in the sample on a time scale slow compared with that of the NMR experiment but fast enough to give rise to motional averaging on the diffraction timescale. No attempt was made to model such a situation as the required reduction in symmetry led to the available computational resources being exceeded. It is interesting to note that such a small value of $C_Q(^{23}Na)$, as reported for $Na_8(AlSiO_4)_6Cl_2$, would imply almost perfect symmetry at the sodium site, which is inconsistent with a coordination polyhedron for sodium consisting of three equivalent oxygen atoms (Na–O, 2.354 Å) and one chlorine atom (Na–Cl, 2.734 Å) at the corners of a slightly distorted tetrahedron. Such a value of $C_Q(^{23}Na)$ also contrasts strongly with the relatively large value for the asymmetry factor. As an aside, it can be pointed out that both of these anomalies would be resolved if the two reported values were exchanged; that is $C_Q(^{23}Na) = 0.35$ MHz and $\eta(^{23}Na) = 0.081$. However, there is no comment in the subsequent literature to suggest that the reported values of Ding and McDowell [18] are in error.

In the case of the synthetic sodalite ($Na_6(AlSiO_4)_6$) the discrepancies between calculation and experiment, particularly for $C_Q(^{23}Na)$, may be due to the basis set used for aluminium being unable to adequately reflect the bonding characteristics of the more covalent environment found within the aluminosilicate structure. This problem, of course, may also be present in the calculations for natural blue sodalite. Overall, if there are inadequacies with the aluminium basis set then it must be concluded that the periodic *ab initio* method as developed in the present work is not suitable for the calculation of ^{23}Na quadrupole parameters in complex aluminosilicates. This is an area for further investigation using larger computer resources.

The graph in Figure 5.1 shows a plot of experimental versus calculated values of $C_Q(^{23}Na)$ using data taken from Table 5.1. The dashed line represents the best-fit linear correlation to the data for single- and multi-site sodium compounds as discussed for Figure 4.10 in Chapter 4. Overall, the correlation for the three groups of data, given the relative complexity of the compounds, is very good and would be suitable for assignment purposes.

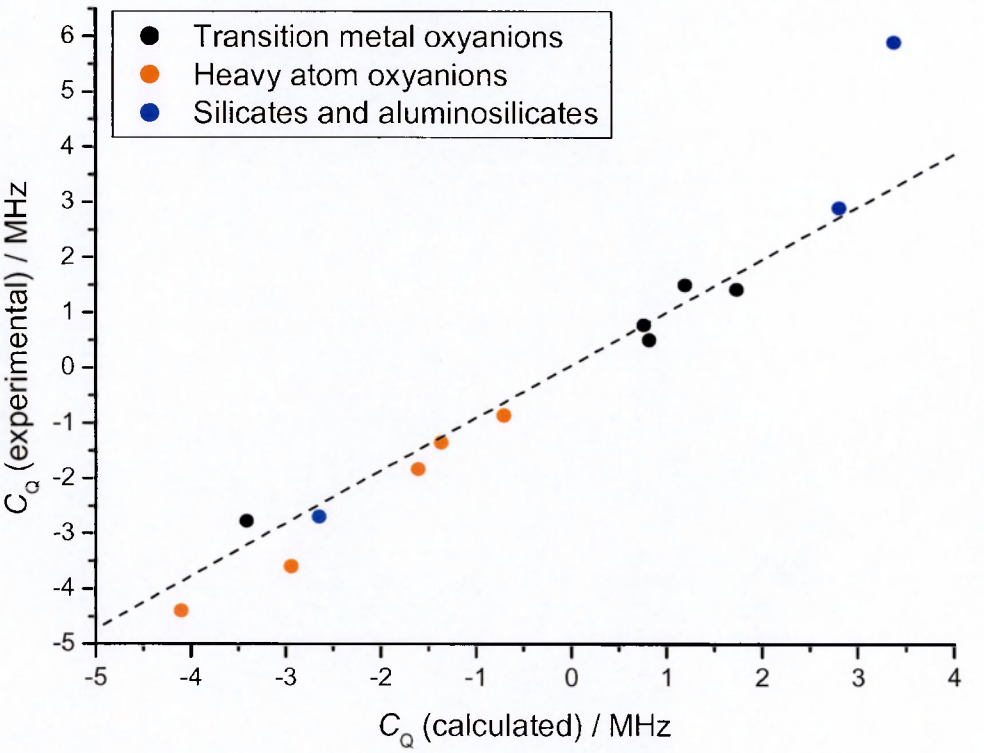

Figure 5.1 A plot of experimental versus calculated values of $C_Q(^{23}Na)$ using data taken from Table 5.1. The dashed line represents the line of best fit found for the general correlation for single- and multi-site sodium compounds as presented in Figure 4.10 in Chapter 4.

5.3 Sodium Fluoroaluminates

Up to this point, the periodic *ab initio* method presented in this thesis has been solely concerned with the calculation of ^{23}Na quadrupole parameters in compounds where sodium is predominantly coordinated to oxygen. For a large range of sodium compounds,

this is typical but there are a few compounds, some of geochemical interest, in which fluorine is the coordinating atom. As examples of these types of material the sodium fluoroaluminates, cryolite and chiolite, were selected.

The basis set used in this investigation was the modified 3-1G set for sodium and an unmodified Pople 3-21G basis set for fluorine. A modification to the standard 3-21G basis set for aluminium with the exponent of the outermost valence sp shell increased to 0.18, to better reflect its ionic character in these compounds, was found to be beneficial.

The compound, cryolite (Na_3AlF_6) contains sodium ions coordinated to fluorine in two different crystallographic environments, a regular octahedral environment and an eightfold environment creating a highly distorted cubic antiprism.

Table 5.2 A summary of experimental and calculated values of ^{23}Na NMR quadrupole parameters for cryolite

Na_3AlF_6	Experimental		Calculated		References	
	C_Q / MHz	η	C_Q / MHz	η	NMR	Struct
Na (6)[a]	0	0.00	-0.90	0.47	24	25
Na (8)[a]	2.3	0.75	-1.31	0.32		
Na (6)[b]	0.9	1.00	-0.91	0.45		26
Na (8)[b]	1.45	0.25	-1.37	0.35		

The ^{23}Na NMR data reported in [24] are [a] by the authors and [b] by J.F. Stebbins and X. Xue.

There have been two crystal structure determinations of cryolite reported in the literature [25, 26] and periodic *ab initio* calculations using both structures gave almost identical ^{23}Na quadrupole parameters as shown in Table 5.2. Such a result indicates that the crystal structure of this material has been consistently determined. However, in a ^{23}Na NMR study of sodium fluoroaluminates, Dirken *et al.* [24] compared their results for the

experimental determination of the ^{23}Na quadrupole parameters in cryolite with those provided as a personal communication by Stebbins and Xue. The periodic *ab initio* calculations of the ^{23}Na quadrupole parameters, based upon either of the literature structure determinations, most closely support the experimental NMR studies of the latter workers.

The ^{23}Na NMR study of a second sodium fluoroaluminate, chiolite ($Na_5Al_3F_{14}$), was also carried out by Dirken *et al.* [24]. This compound, like cryolite, also contains sodium ions coordinated to fluorine in two different structural environments, a highly distorted octahedral environment and an eightfold environment creating a regular rectangular prism.

Table 5.3 A summary of experimental and calculated values of ^{23}Na NMR quadrupole parameters in chiolite

$Na_5Al_3F_{14}$	Experimental		Calculated		References	
	C_Q / MHz	η	C_Q / MHz	η	NMR	Struct
Na (6)	3.2	0.15	3.32	0.16	24	27
Na (8)	1.5	0.00	0.51	0.00		

As shown in Table 5.3, there is good agreement between the calculated and experimental values of the ^{23}Na quadrupole parameters for the distorted octahedral site. This suggests that the crystal structure, determined by Jacoboni and co-workers [27], accurately reflects the structural environment of the octahedrally-coordinated sodium cation in the experimental sample. However, the agreement between the calculated and experimental values of $C_Q(^{23}Na)$ in the case of the 8-coordinate site is not so good. If the experimental NMR study is correct, this suggests some form of inaccuracy with the crystal structure determination for this particular site and its environment.

It is worth noting that the samples of the minerals cryolite and chiolite, used in the ^{23}Na NMR study by Dirken and co-workers, were both obtained from the Ivigtut deposit in Greenland. The crystal structure determinations used in the periodic *ab initio* calculations were also taken from minerals found at Ivigtut. The inconsistencies between the experimental and calculated values of the ^{23}Na quadrupole parameters, therefore, cannot be attributed to the source of the minerals, although it is possible that different samples of these minerals from the same source could contain different levels of defects and impurities that influence either the ^{23}Na NMR results or the crystal structure determination in some distinct way. Ideally, with a naturally-occurring mineral, both the NMR study and the crystal structure refinement should be carried out on the same sample.

Overall, it is remarkable that periodic *ab initio* calculations based upon a small basis set – tuned for sodium with an exclusively oxygen coordination sphere – should be able to give good agreement between calculated ^{23}Na quadrupole parameters and those determined by experiment when the coordinating atom is fluorine.

5.4 Na_3OCl and the Sternheimer factor

Experimental values of $C_Q(^{23}Na) \neq 0$ have almost exclusively been observed in sodium salts containing complex anions (e.g. NO_3^-, SO_4^{2-}, SiO_4^{2-}or PO_4^{3-}) where the charge distribution over the complex anion is difficult to describe by a point-charge model. However, such a method can be applied to the study of sodium salts with monoatomic counteranions like oxides (O^{2-}) or halides (X^-). In most cases, however, these compounds have the sodium cations located exclusively on sites with cubic symmetry. This results in a zero electric field gradient at the sodium nucleus and, consequently, a vanishing quadrupole interaction.

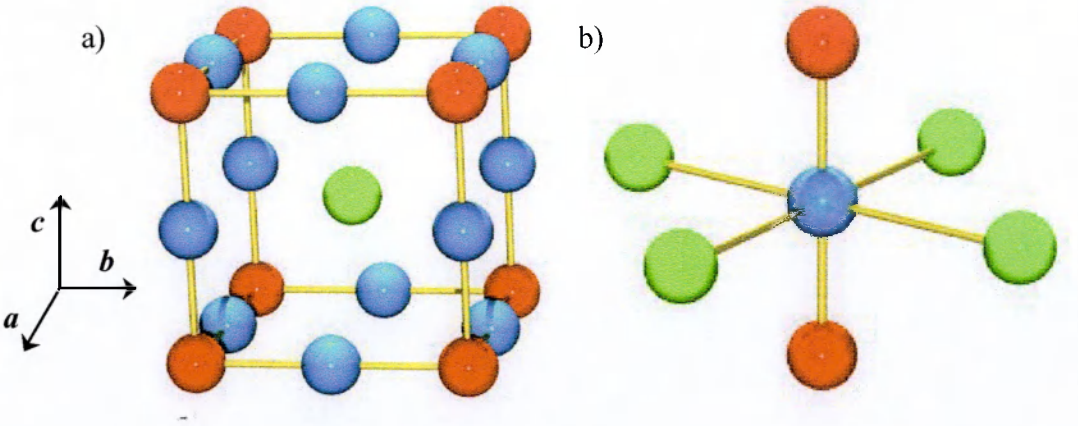

Figure 5.2 The room temperature crystal structure of Na_3OCl. Structure a) shows the anti-perovskite unit cell and b) shows the local environment, within a 3.2 Å sphere, around sodium. In both figures, the sodium atoms are shown in blue, oxygen atoms in red and chlorine atoms in green.

The ternary compound sodium oxide chloride, Na_3OCl, is a rare example of an ionic salt with monoatomic counteranions in which sodium cations occupy non-cubic sites. This compound crystallises in the anti-perovskite structure [28], shown in Figure 5.2(a), in which sodium occupies a rather unusual coordination environment. Figure 5.2(b) shows the local sodium environment; it has two nearest neighbour oxygen ions at a distance of 2.248 Å and four chloride ions at a distance of 3.179 Å.

Sodium oxide chloride is an ideal candidate to test the application of the periodic *ab initio* method, based upon a suitably modified Pople 3-21G basis set, in the case of a purely ionic compound. Calculations were carried out with the Na, O and Cl atoms represented on an all-electron basis: sodium, 3-1G with the single valence exponent set to 0.180; oxygen, 3-21G with the outer valence exponent set to 0.374, and the unmodified Pople 3-21G basis set for chlorine.

The principal component of the ^{23}Na efg tensor was calculated to be:

$$V_{33} = -4.23192 \times 10^{21}\ Vm^{-2}$$

so that $C_Q(^{23}Na)$ = -11.14 MHz. This compares well with results obtained from simulation of the ^{23}Na MAS quadrupolar line shape [1]; that is $C_Q(^{23}Na)$ = 11.34 MHz and $\eta(^{23}Na)$ = 0.0. Such a result demonstrates the ability of the periodic *ab initio* method to calculate $C_Q(^{23}Na)$ in purely ionic compounds even though the basis sets used were 'tuned' for use in compounds containing more covalent polyatomic anions.

5.4.1 A model compound: Na_3OCl

The Sternheimer factor, which for sodium is antishielding, is of fundamental importance in the interpretation of ^{23}Na NMR spectra based upon a point-charge model. However, the value of this factor, which is often taken to be $\gamma_\infty(Na^+)$ = -4.1 [29], has only been poorly determined and it is assumed to be independent of crystal structure. Advanced quantum mechanical calculations have suggested values in the range $-5.0 > \gamma_\infty(Na^+) > -5.6$ [30-33]. Klösters and Jansen [1] used their experimentally-determined value for $C_Q(^{23}Na)$ in Na_3OCl and a point charge model, based on formal charges, to make a determination of $\gamma_\infty(Na^+)$. The appropriateness of their model was justified on the grounds of quantum mechanical calculations on Na_2O [34, 35] and NaCl [36, 37]. These calculations indicated that both compounds were fully ionic and that the Mulliken charges associated with the ions were close to their formal values. Since Na_3OCl is a ternary compound of Na_2O and NaCl it was assumed that it too would be fully ionic. Based upon this model they determined a value of -5.36 for $\gamma_\infty(Na^+)$ which lies within the range of those values determined by quantum mechanical methods. However, it should be noted that the Na–O interatomic distance in Na_3OCl (2.248 Å [28]) is significantly shorter than that in Na_2O (2.403 Å [38]) and may suggest that the interaction between these species is less ionic than has been assumed. Conversely, the Na–Cl interatomic distance in Na_3OCl

(3.179 Å [28]) is significantly larger than the corresponding distance in NaCl (2.820 Å [39]).

Periodic *ab initio* methods do not require the use of the Na^+ Sternheimer factor in order to calculate an electric field gradient tensor. However, such methods can be adapted to calculate a comparable factor as described below. Basically, in a point-charge calculation, the Sternheimer factor is introduced in order to take into account the polarisation of the inner core electron density, on the atom of interest, by the external electric field due to the lattice ions and any quadrupole moment of the nucleus. If, in an *ab initio* calculation, these inner core electrons were to be prevented from becoming polarised then it would be expected that an enhancement, or antishielding, factor would be required to relate calculation to experiment. Such a situation would arise if pseudopotentials were used to represent the core electrons.

For this investigation, both Hay and Wadt (HAYWLC) [3] and Durand and Barthélat (BARTHE) [40] large core pseudopotentials, available within the CRYSTAL code and supplemented by a single sp-type (1G) shell, were chosen to represent sodium. The exponent for this shell was set, as in the all-electron case, at 0.18. The oxygen and chlorine atoms were represented as described in section 5.2.2.

It is important that due consideration be taken of the possible adverse effects on the electronic structure of the model due to the different basis set descriptions, including an all-electron description, of the sodium atom. If these effects are significant then any comparison between the models would be invalid. Therefore, in order to test the proposed modelling strategy, the single lattice parameter $\boldsymbol{a}$ for Na_3OCl, was optimised in all three models by determining the total energy as a function of unit cell volume (a^3).

The results in each case were fitted to an equation of states according to Murnaghan [41] and are shown in Figure 5.3. The equation of state is:

$$E(V) = \frac{B_0 V}{B_0'}\left[\frac{(V_0/V)^{B_0'}}{B_0'} + 1\right] + E_0 \qquad (5.1)$$

where B_0 is the zero pressure bulk modulus, B_0' is the pressure derivative of B at $p = 0$, V_0 is the minimum energy volume and E_0 is the minimum total energy of the system. The fitted parameters are shown in Table 5.4, although literature values are currently not available for the bulk modulus and pressure derivative of Na_3OCl for comparison. However, in most solids the value of B_0' lies between 3 and 5 [42].

Table 5.4 Experimental (at room temperature) and calculated structural parameters of Na_3OCl

	V_0 / Å^3	B_0 / MPa	B_0'
Experiment [a]	90.88	-	-
All-electron	87.14(25)	62.8(3)	3.84(6)
HAYWLC	84.19(39)	71.5(9)	4.13(14)
BARTHE	85.18(13)	65.6(2)	3.86(3)

[a] Experimental volume calculated from experimental lattice parameters in [28].

As can be seen in Table 5.5, the best agreement between experiment and calculation is observed for the calculation based upon the all-electron basis set. However, the pseudopotential results do not differ significantly with the difference in the lattice parameters being at most, -2.5% of the experimentally-determined value.

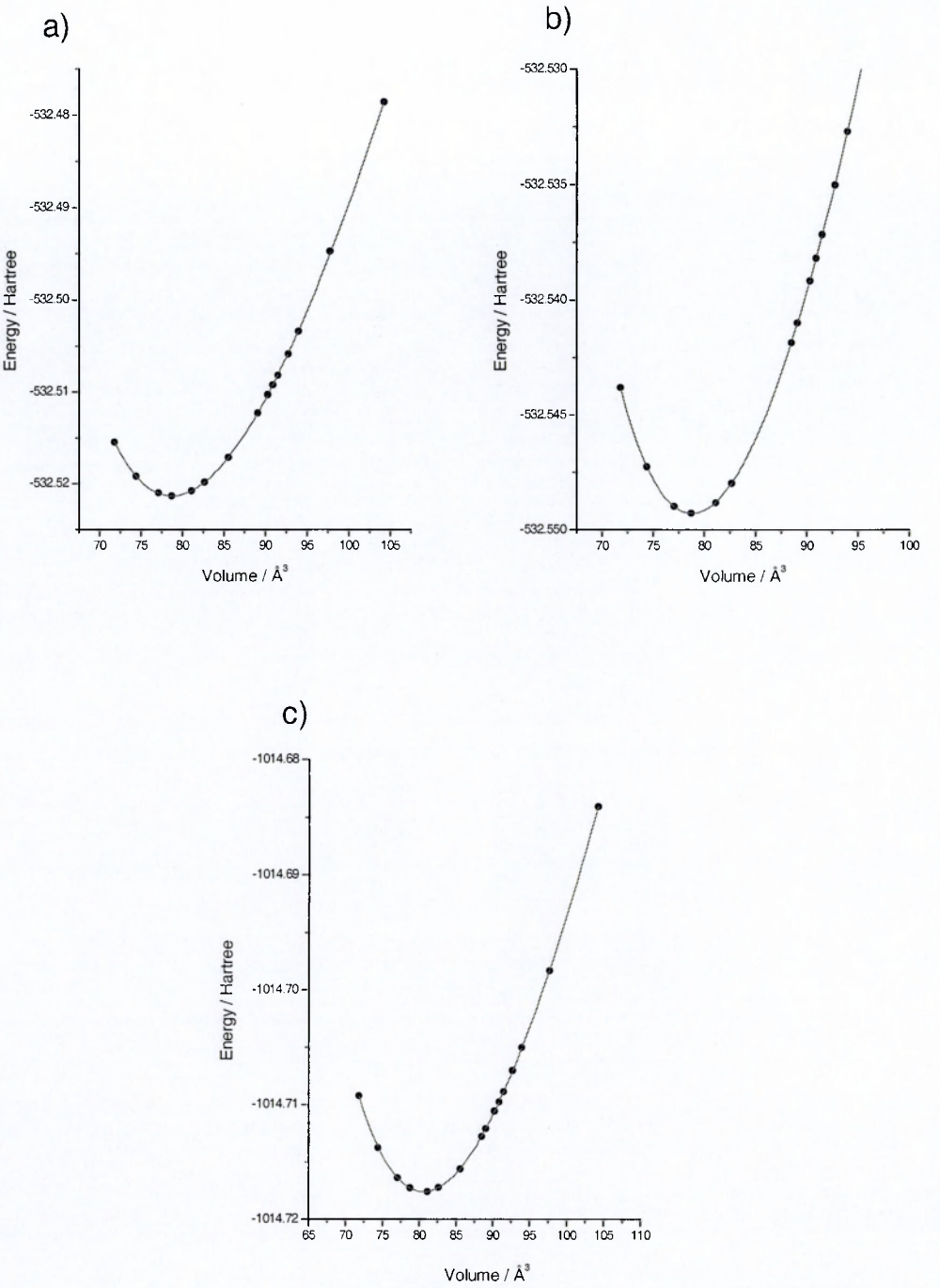

Figure 5.3 Total energy of Na_3OCl versus volume for calculations based on a) an all-electron, b) HAYWLC and c) BARTHE description of the sodium core.

Table 5.5 Experimental (at room temperature) and derived lattice parameters and bond lengths for Na_3OCl

	a / Å	Na–O / Å	Na–Cl / Å	Na–Na / Å
Experiment [a]	4.496(2)	2.248	3.179	3.179
All-electron	4.433	2.163	3.058	3.058
HAYWLC	4.383	2.141	3.029	3.029
BARTHE	4.400	2.145	3.033	3.033

[a] Experimental lattice parameters and bond lengths taken from the crystal structure in [28].

The fitting of the calculated unit cell volume to the Murnaghan equation of states, Figure 5.3, shows that there is little numerical noise affecting the interpolation of the minima. It is reasonable to assume that any residual error is mainly due to basis set incompleteness. The *ab initio* results, more importantly, are within ~1% of each other which would seem to suggest that the three models produce similar electrostatic interactions between the ions and, as a consequence, the same electric field due to the lattice.

Using the results obtained in the two periodic *ab initio* pseudopotential calculations, the principal component of the ^{23}Na efg tensor for Na_3OCl was found to be:

$$V_{33} = -6.30215 \times 10^{20}\ Vm^{-2}\ (BARTHE)$$

$$V_{33} = -6.41506 \times 10^{20}\ Vm^{-2}\ (HAYWLC)$$

These values compare well with those found by Klösters and Jansen [1] using their point-charge model with formal charges:

$$V_{33} = -6.76762 \times 10^{20}\ Vm^{-2}$$

This result strongly suggests that the use of pseudopotentials to represent core electrons produces an efg at the sodium nucleus equivalent to that of a point-charge model. This is an interesting result in its own right.

The enhancement of the efg due to the lattice ions by the polarisation of the inner core electron density, which in this calculation is related to the Sternheimer factor, can be found from the following equation.

$$1 - \gamma_{\infty}^{c}(Na^{+}) = V_{33}\text{ (all electron)} / V_{33}\text{ (pseudopotential)} \qquad (5.2)$$

where $\gamma_{\infty}^{c}(Na^{+})$ is taken to be a factor directly comparable to the Sternheimer factor. This gives a value of -5.60 for $\gamma_{\infty}^{c}(Na^{+})$, based on the HAYWLC pseudopotential and -5.72 using the BARTHE pseudopotential. Both results are in good agreement with the determination of the Sternheimer factor by both Klösters and Jansen [1], and previous quantum mechanical calculations [30-33].

5.4.2 Core polarisation and the Sternheimer factor

The results described above indicate that modelling of the core electrons, especially the 2p orbital, on sodium is essential to the correct simulation of the efg at the nucleus. They also suggest that the all-electron model provides a good description of the electron distribution within the unit cell of Na_3OCl and, in turn, this allows the assumption that this compound is fully ionic to be tested.

The atomic net charges, given by a Mulliken population analysis, indicate that sodium loses about 68% of its valence electron. The electron charge deformation (bulk minus superposition of spherical atomic distribution) map cutting through the Cl–Na–Cl plane is shown in Figure 5.4(a) and is typical for an ionic compound of this symmetry. This interpretation is supported by the atomic net charge on Cl^{-}, which is close to $-1|e|$ ($-0.922|e|$). The Na–Cl bond population (Cl has 12 first neighbour Na ions) is, therefore, very small confirming the fully ionic nature of the bond. However, the calculated

electron charge deformation map in the plane passing through Na–O, Figure 5.4(b), shows clear evidence of the asymmetry that leads to the relatively large efg at the sodium nucleus. The nature of the distortion is in agreement with the anisotropic thermal parameters for sodium [29] in which U_{11} (along the O–Na–O direction) is 0.0125(8) $Å^2$ and U_{22} and U_{33}, perpendicular to it, are 0.0543(9) $Å^2$. A Mulliken population analysis shows the Na–O bond population to be 0.161|*e*| and implies that this bond has some covalent character. This suggests that the use of Na_3OCl as a test compound for the calculation of the Sternheimer factor may not result in the true ionic value.

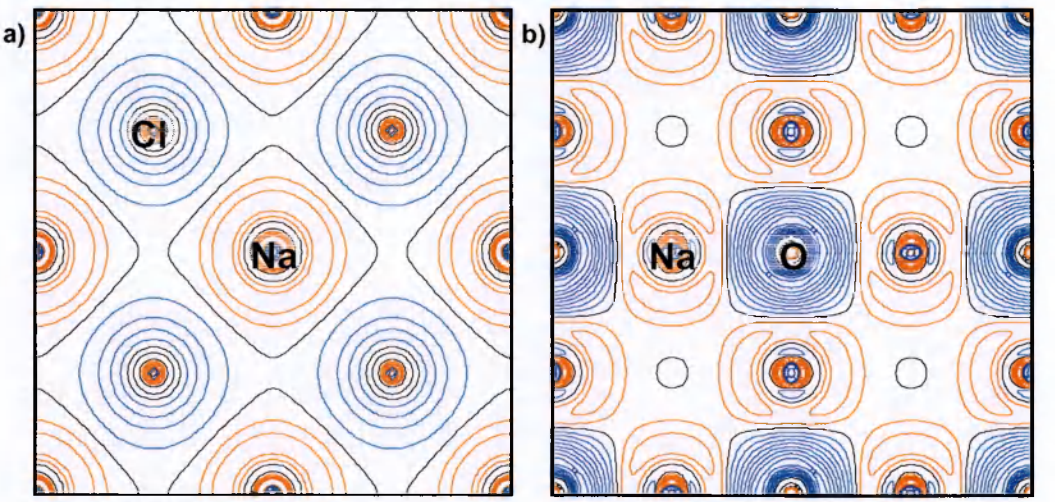

Figure 5.4 Calculated electron charge deformation maps (crystal – isolated atoms) corresponding to (a) cutting the Cl–Na–Cl plane and (b) cutting the O–Na–O plane. Blue and red lines indicate positive and negative values respectively; black lines correspond to the zero-level. Contour intervals correspond to increases of 0.05 electrons $(a.u.)^{-3}$.

A second assumption made when using the Sternheimer factor in point-charge calculations is that its value is independent of the structure of the sodium environment. In order to investigate this assumption a second investigation, using the same method as for Na_3OCl, was carried out on a small group of compounds where sodium occupies a single crystallographic site. Members of this group were chosen because of the accuracy with which the ^{23}Na NMR parameters had been calculated using the periodic *ab initio* method based on modified 3-21G basis sets (Chapter 4).

Although a number of factors influence the calculation of $\gamma_{\infty}^{c}(Na^{+})$, the wide variation in the results, shown in Table 5.6, suggest that the Sternheimer factor itself is highly dependent upon the immediate coordination environment of the sodium nucleus. The closest agreement between calculation and the commonly accepted literature value of $\gamma_{\infty}(Na^{+}) = -4.1$ [29] is found in the case of sodium nitrate. This result may be due to the coordination environment of the sodium cation being the closest to that of a perfect octahedron when compared to those in the other compounds investigated.

Table 5.6 A summary of calculated values of ^{23}Na NMR quadrupole parameters for a range of sodium compounds using all-electron and HAYWLC pseudopotential basis sets. Corresponding values of $\gamma_{\infty}^{c}(Na^{+})$ are given.

Compound	All electron		HAYWLC		$\gamma_{\infty}^{c}(Na^{+})$
	$\lvert C_Q \rvert$ / MHz	η	$\lvert C_Q \rvert$ / MHz	η	
$NaNO_3$	0.42	0.00	0.08	0.00	-4.25
NaC_2O_4	2.23	0.58	0.23	0.63	-8.70
NaOH	3.56	0.02	0.50	0.01	-6.12
$NaClO_3$	0.57	0.00	0.13	0.00	-3.38
Na_2SO_4	2.85	0.51	0.47	0.40	-5.06

5.4.3 Core polarisation: a more detailed investigation

The observation that the all-electron model is able to successfully predict the efg at sodium in Na_3OCl to a significant degree of accuracy allows for a more detailed investigation of the nature of the efg and its relationship to the polarisation of the sodium core 2p electrons. On closer inspection of the electron charge deformation map, Figure 5.4(b), an enhancement of the electron density in a core orbital lying along the direction of the O–Na–O axis is seen. From the periodic *ab initio* calculations, it can be shown that the principal component of the efg tensor in its principal axis frame (V_{33}) also lies along this direction. If it is assumed that this is also the direction of the $2p_z$ orbital, it would

seem appropriate to ascribe the enhancement of the efg at the sodium nucleus to the enhancement of electron density in this orbital.

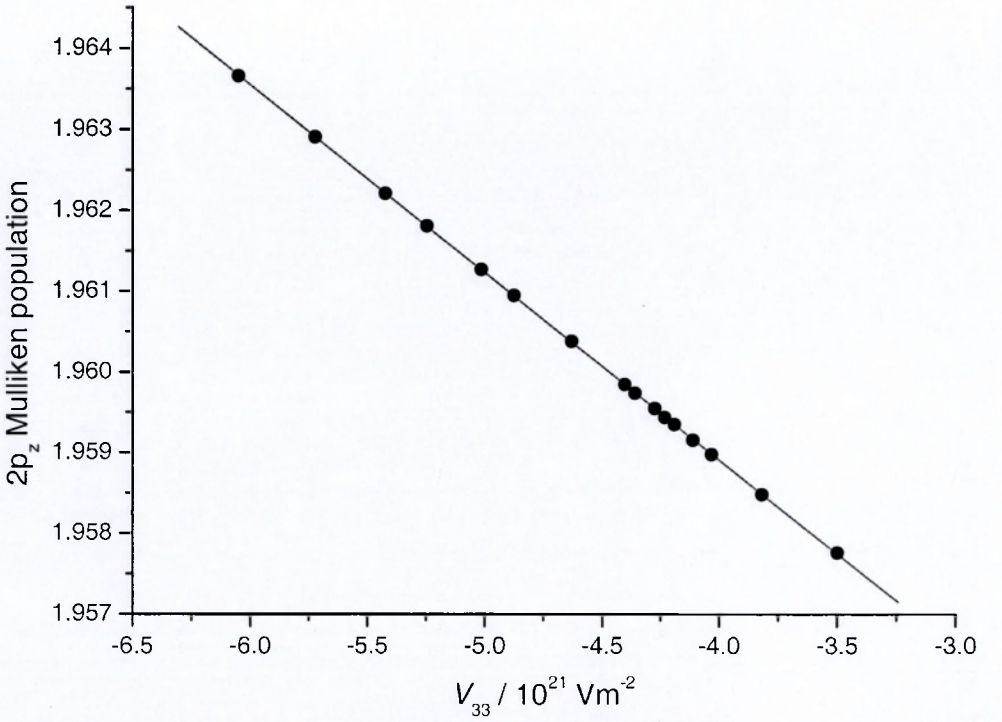

Figure 5.5 A plot of the $2p_z$ Mulliken population versus the principal component of the efg tensor (V_{33}) at sodium calculated for a cubic distortion of the Na_3OCl lattice.

In order to investigate the effect of the polarisation of the $2p_z$ orbital on the efg, the nearest neighbour environment of sodium was varied by simply changing the unit cell parameter. This maintains the symmetry around sodium. Values of this parameter were varied from 4.156 Å to 4.706 Å and the corresponding values of V_{33} and the Mulliken population of the $2p_z$ orbital were calculated at each point. The results of this analysis are shown in Figure 5.5 where the points are fitted to a linear function:

$$2p_z \text{ Mulliken Population} = 1.94963 - 0.00232\ V_{33} \qquad (5.3)$$

It is interesting to note that the principal component of the ^{23}Na efg tensor (V_{33}) is directly proportional to the Mulliken electron population in the $2p_z$ orbital. Unfortunately, a cubic

distortion of the lattice leads to changes in both the Na-O and Na–Cl interatomic distances preventing their individual contributions to the polarisation of the $2p_z$ orbital being investigated. However, a tetragonal distortion of the cubic lattice along ***a***, see Figure 5.6, results in two distinct sodium environments.

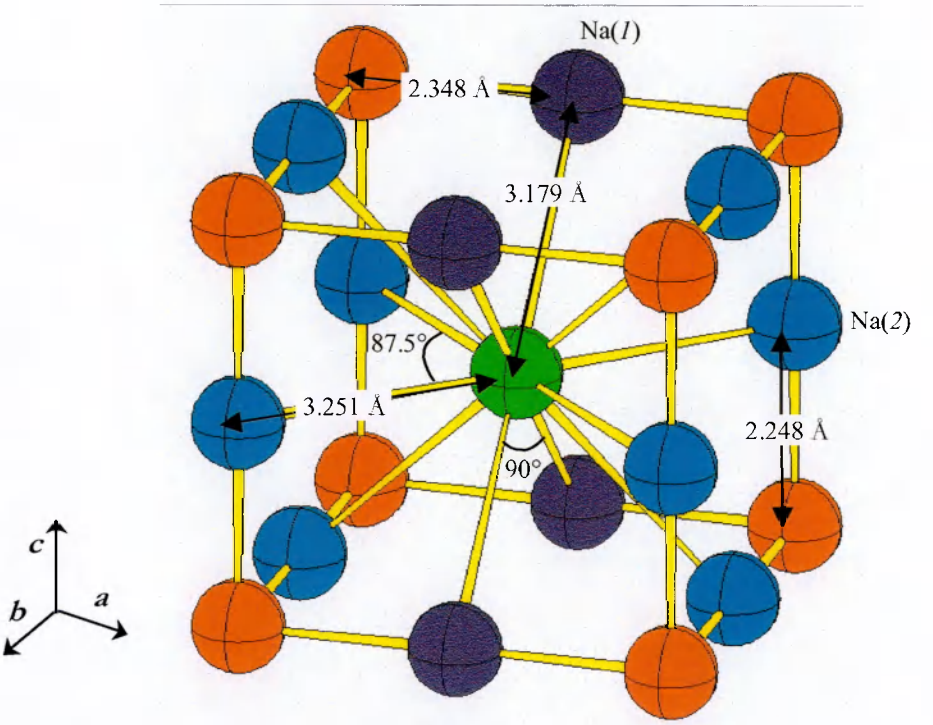

Figure 5.6 The effect of a tetragonal distortion along ***a*** leading to the formation of two distinct sodium environments, Na(*1*) (purple) and Na(*2*) (blue). Oxygen atoms are shown in red and the chlorine atom in green.

Na(*1*) has an environment in which the Na(*1*)–O interatomic distance will change with the distortion but the Na(*1*)–Cl distance and Cl–Na(*1*)–Cl angle remain constant. However, for the Na(*2*) environment it is the Na(*2*)–O distance which remains constant and the distortion leads to changes in both the Na(*2*)–Cl distance and the Cl–Na(*2*)–Cl angle.

In order to investigate the effect of each type of distortion separately, the Na_3OCl unit cell was cast in the P1 space group allowing the magnitudes of the three cell parameters ***a***, ***b*** and ***c*** to be varied independently. The results of such an analysis are shown in Figure 5.7.

The magnitudes of the cell parameter ***a*** were those used in the calculations underlying the plot in Figure 5.5; however, the magnitudes of ***b*** and ***c*** ($b = c$) were fixed at their literature values [28]. In this way, one sodium site (Na(*1*)) had the distortion involving the variation of the Na–O bond only and the other two sites (Na(*2*)) in the unit cell have the Cl–Na–Cl angle distortion with accompanying change in Na–Cl distance.

From the results, it can be seen that the distortion of the sodium environment involving the Na–O interatomic distance has a far larger effect on the efg at the sodium nucleus than distortions of the Cl–Na–Cl angle. This would suggest that the interaction between sodium and oxygen is not a simple electrostatic one.

From the correlation (Equation (5.3)), two interesting observations may be drawn:

- when the efg at the sodium nucleus is zero the Mulliken population of the $2p_z$ orbital and by symmetry those of $2p_x$ and $2p_y$, is equal to ~1.95.
- if the sign of $C_Q(^{23}Na)$ is negative, then the Mulliken population of the $2p_z$ orbital will be >1.95 and, by symmetry since $\eta(^{23}Na) = 0$, that of the $2p_x$ and $2p_y$ orbitals will decrease by half the difference between the polarised value and the zero efg value. The converse argument applies for a positive sign of $C_Q(^{23}Na)$.

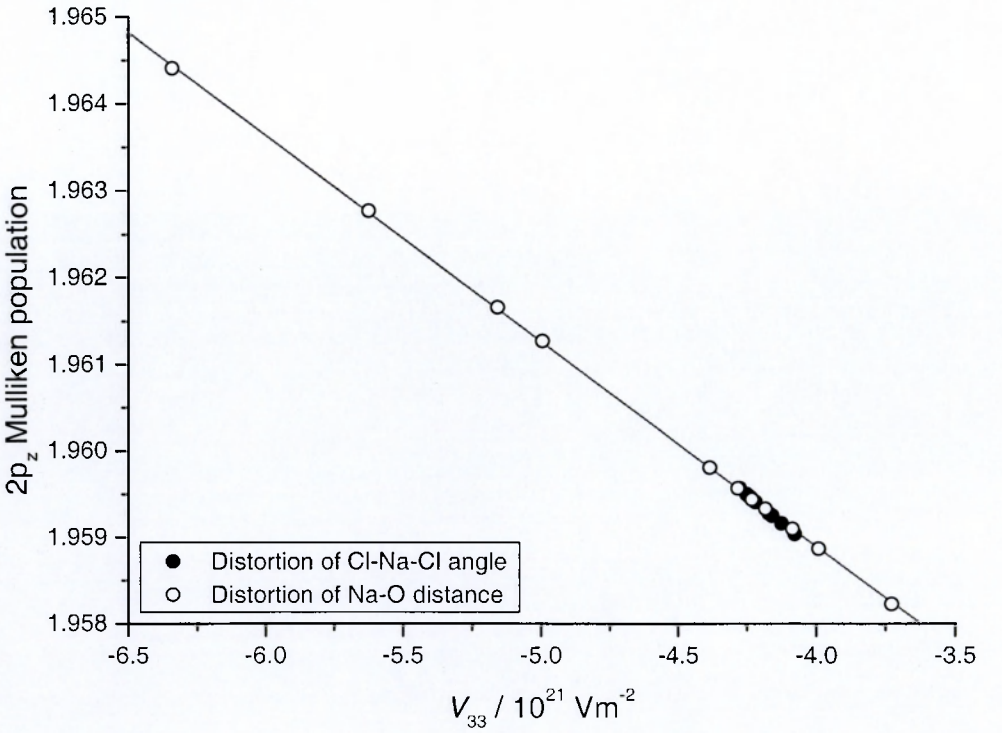

Figure 5.7 A plot of the $2p_z$ Mulliken population versus the principal component of the efg tensor (V_{33}) at the two sodium sites calculated for a tetragonal distortion of the Na_3OCl lattice.

This result would suggest that the correct modelling of the population and polarisability of the 2p orbitals on sodium is the key to any *ab initio* calculation of the efg at sodium. Further to this, it would suggest that the use of the Pople 3-21G basis set, and particularly the gaussians representing the core, provide sufficient flexibility to accommodate this polarisation within a wide range of coordination environments. This conclusion is consistent with the wide range of results discussed in Chapter 4.

In order to investigate a more general link between the $2p_z$ orbital and V_{33}, where z is coincident with direction 3, studies on crystal lattice distortions in both Na_2SO_3 and NaOH were carried out. These compounds were chosen principally because all the sodium sites display axial symmetry along an axis parallel to a lattice vector. This means

that distortion of the crystal along this symmetry axis does not adversely distort the shape of the respective anions and thereby introduce further complications into the analysis. Distortion of the NaOH cell was along the ***b*** lattice vector (11.078 Å to 11.678 Å) and that in Na_2SO_3 was along the ***c*** lattice vector (6.033 Å to 6.433 Å); all other lattice parameters were held fixed at their literature values [43, 44]. The results of the analysis are shown in Figure 5.8 where the points are fitted to a linear function:

$$2p_z \text{ Mulliken Population} = 1.9505 - 0.00248\ V_{33} \qquad (5.4)$$

This correlation is very similar to that found for Na_3OCl and is perhaps surprising given that, apart from axial symmetry, the sodium coordination environments are very different in all three compounds.

This result provides some insight into the reason for the consistent overestimation of the $C_Q(^{23}Na)$ values calculated using modified 6-21G compared to 3-21G basis sets (see Figure 4.16). Such a result may simply be attributable to an increase in the magnitude of the Mulliken population for the 2p orbitals on sodium.

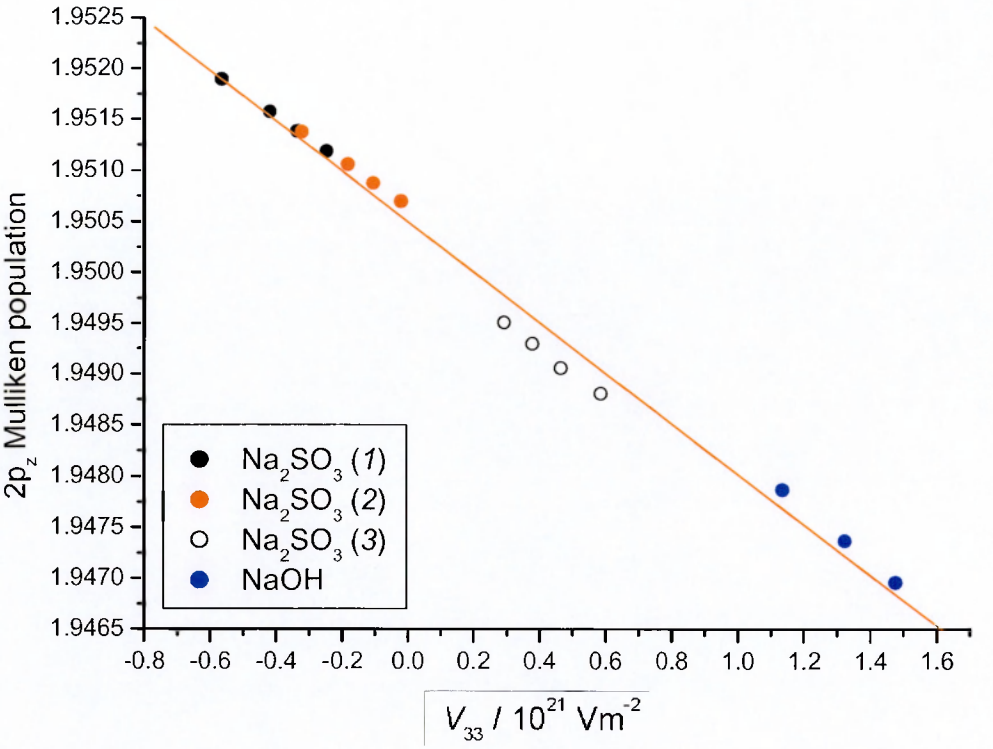

Figure 5.8 A plot of the $2p_z$ Mulliken population versus the principal component of the efg tensor (V_{33}) at the three sodium sites in Na_2SO_3 and the sodium site in NaOH calculated for a tetragonal distortion of their crystal lattices.

5.5 Summary

An important aim of this chapter was to consider the extension of the periodic HF *ab initio* method beyond the discrete oxyanions of the lighter p-block elements studied in Chapter 4. To this end, it has been demonstrated that good correlations can be achieved for the transition metal oxyanions and a reasonable one for the heavy p-block oxyanions. In the later case, the demonstration that the use of core pseudopotentials for the heavy elements is acceptable suggests that the calculations can be extended to many more compounds where symmetry may make the use of all-electron basis sets computationally expensive.

The two sodium sites in the porous sodium trisilicate Mu-11 were very well characterised with both $C_Q(^{23}Na)$ and $\eta(^{23}Na)$ in close agreement with experiment. However, calculations proved more problematic in the case of natural blue sodalite and sodalite where the problem lay with a crystal structure inconsistent with the ^{23}Na NMR data for the former and a suspected problem with the basis set used to model aluminium in the latter. This result suggests that further work is required to successfully apply the periodic *ab initio* method to the calculation of ^{23}Na quadrupole parameters in zeolites.

The periodic *ab initio* method was shown to be applicable to the study of sodium fluoroaluminates; a result that is perhaps somewhat surprising as the sodium basis set was optimised with regard to coordination with oxygen. However, again evidence was found for ^{23}Na NMR data inconsistent with a crystal structure. As in the case of natural blue sodalite, the mineral samples used in these studies were not those for which the structure was obtained. When dealing with natural materials, it is undoubtedly preferable to use the same sample for both NMR studies and crystal structure determination.

Sodium oxide chloride provided a model compound for the extension of the periodic *ab initio* determination of ^{23}Na quadrupole parameters to a fully ionic system. It was possible to calculate an accurate value of $C_Q(^{23}Na)$ and also determine a value for the Sternheimer factor for Na^+ in general agreement with values suggested in the literature. A factor comparable to the Sternheimer factor was also calculated for a range of compounds with different structural environments for sodium. It was found, contrary to assumption, that this factor was highly dependent on structure with the closest fit to the accepted Sternheimer value ($\gamma_\infty(Na^+) = -4.1$) for sodium nitrate in which the sodium environment is the closest to an ideal octahedron.

Specific distortions of the crystal structure of Na_3OCl allowed the origin of the efg at sodium to be investigated and this was found to correlate strongly with the polarisation of the $2p_z$ orbital. Selected distortions of the crystal structures of Na_2SO_3 and NaOH also produced the same result. From such investigations it seems, in general, that the key to the success of the periodic HF *ab initio* method using modified small basis sets is their ability to accurately model the polarisability of 2p orbitals on sodium.

References

1. G. Klösters and M. Jansen, *Solid State Nuclear Magn. Reson.*, **16**, 279, 2000.
2. A. Cox, *The Transition Metal Oxides*, Oxford University Press, Oxford, 1992.
3. P.J. Hay and W.R. Wadt, *J. Chem. Phys.*, **82**, 284, 1985.
4. J. Skibsted, N.C. Neilsen, H. Bildsøe and H.J. Jakobsen, *J. Am. Chem. Soc.*, **115**, 7351, 1993.
5. A.M. Shaikh, *Ferroelectrics*, **107**, 219, 1990.
6. K. Kato and E. Takayama, *Acta Crystallogr. B*, **40**, 102, 1984.
7. H. Koller, G. Engelhardt, A.P.M. Kentgens and J. Sauer, *J. Phys. Chem.*, **98**, 1544, 1994.
8. J.K. Nimmo, *Acta Crystallogr. B*, **37**, 431, 1981.
9. J. Itoh and R. Kusaka, *J. Phys. Soc. Japan*, **9**, 434, 1954.
10. D.H. Templeton and L.K. Templeton, *Acta Crystallogr. A*, **41**, 133, 1985.
11. F.F.F. Vetel, Open University, personal communication.
12. H.D. Stoever and R. Hoppe, *Z. Anorg. Allg. Chem.*, **468**, 137, 1980.
13. B.N. Mehrotra, T. Hahn, W. Eysel, H. Roepke and A. Illguth, *Neues Jahrb. Min., Monatsh.*, **1978**, 408, 1978.
14. S.L. Tagg, J.C. Huffman and J.W. Zwanziger, *Chem. Mater.*, **6**, 1884, 1994.

15. R. Masse, J.C. Guitel and I. Tordjman, *Mater. Res. Bull.*, **15**, 431, 1980.

16. A. Matijasic, A.R. Lewis, C. Marichal, L. Delmotte, J.M. Chezeau and J. Patarin, *Phys. Chem. Chem. Phys.*, **2**, 2807, 2000.

17. A. Matijasic, B. Marler and J. Patarin, *Int. J. Inorg. Mater.*, **2**, 209, 2000.

18. S.W. Ding and C.A. McDowell, *Chem. Phys. Lett.*, **333**, 413, 2001.

19. I. Hassan and H.D. Grundy, *Acta Crystallogr. B*, **40**, 6, 1984.

20. J. Felsche, S. Luger and C. Baerlocher, *Zeolites*, **6**, 367, 1986.

21. J. Loens and H. Schulz, *Acta Crystallogr.*, 23, 434, 1967.

22. T.F.W. Barth, *Z. Kristallog. Kristallg. Kristallp. Kristallch.*, **83**, 405, 1932.

23. L. Pauling, *Z. Kristallog. Kristallg. Kristallp. Kristallch.*, **74**, 213, 1930.

24. P.J. Dirken, J.B.H. Jansen and R.D. Schuiling, *Am. Miner.*, **77**, 718, 1992.

25. H.-X. Yang, S.Ghose and D.M. Hatch, *Phys. Chem. Miner.*, **19**, 528, 1993.

26. F.C. Hawthorne and R.B. Ferguson, *Can. Miner.*, **13,** 377, 1975.

27. C. Jacoboni, A. Leble and J.J. Rousseau, *J. Solid State Chem.*, **36**, 297, 1981.

28. K. Hippler, S. Sitta, P. Vogt and H. Sabrowsky, *Acta Crystallogr. C*, **46**, 736, 1990.

29. R.M. Sternheimer and H.M. Foley, *Phys. Rev.*, **102**, 731, 1956.

30. Y. Michihiro and G.D. Mahan, *Phys. Rev. B*, **56**, 12151, 1997.

31. P.C. Schmidt, K.D. Sen, T.P. Das, and A. Weiss, *Phys. Rev. B*, **22**, 4167, 1980.

32. P. Tripathi and N.C. Mohapatra, *J. Phys B: At. Mol. Opt. Phys.*, **23**, 3241, 1990.

33. A.A. Gusev, I.M. Reznik and V.A. Tsitrin, *J. Phys.: Condens Matter*, **7**, 4855, 1995.

34. R. Dovesi, C. Roetti, C. Freyria-Fava, M. Prencipe and V.R. Saunders, *Chem. Phys.*, **156**, 11, 1991.

35. P. Azavant, A. Lichanot and M. Rerat, *Acta Crystallogr. B*, **50**, 279, 1994.

36. M. Prencipe, A. Zupan, R. Dovesi, E. Apra and V.R. Saunders, *Phys. Rev. B*, **51**, 3391, 1995.

37. M. Causa and A. Zupan, *Int. J. Quantum Chem.*, **28**, 633, 1994.

38. E. Zintl, A. Harder and B. Dauth, *Z. Elektrochem.*, **40,** 588, 1934.

39. W.T. Barrett and W.E. Wallace, *J. Am. Chem. Soc.*, **76**, 366, 1954.

40. P. Durand and J.C. Barthélat, *Theor. Chim. Acta*, **38**, 283, 1975.

41. F. D. Murnaghan, *Proc. Natl. Acad. Sci.* **30**, 244, 1944.

42. R. Gaudoin and W.M.C. Foulkes, *Phys. Rev. B*, **66**, 052104, 2002.

43. H. Jacobs, J. Köckelkorn and T.Z. Tacke, *Z. Anorg. Allg. Chem.*, **531**, 119, 1985.

44. W.H. Zachariasen and H.E. Buckley, *Phys. Rev.*, **37**, 1295, 1931.

Chapter 6

Experimental and periodic *ab initio* investigations of a range of sodium phosphates

6.1 Introduction

Condensed phosphates of sodium, some of which are of commercial importance, provide a range of ionic compounds in which sodium can have multiple site occupancy. It is for this reason that a number of these phosphates have been investigated by a variety of ^{23}Na NMR techniques; for example, the tripolyphosphate, $Na_5P_3O_{10}$, was one of the first compounds to be studied by MQMAS [1]. One aim of the work presented in this chapter is to consider the assignment of sodium resonances in these multi-site sodium compounds; this can be a challenging problem.

Two particular features of the use of periodic *ab initio* methods for the calculation of ^{23}Na quadrupole parameters are demonstrated. Firstly, for specific compounds, it is shown that a comparison between experiment and calculation can reveal inconsistencies in reported crystal structures. In a sense, this links NMR measurements to crystal structure determination and suggests that such measurements could be used, for example, as constraints in the Rietveld refinement of powder diffraction patterns. Secondly, the use of periodic *ab initio* calculations can provide reliable values of quadrupole parameters so that strongly overlapped second-order spectra can be interpreted and so, for example, reveal the values of isotropic chemical shifts for individual resonances.

The final part of this chapter presents an indirect study of hydrogen bonding in anhydrous disodium hydrogenphosphate (Na_2HPO_4). A periodic *ab initio* investigation of the structure and ^{23}Na quadrupole parameters of the three distinct sodium sites in this compound are shown to lead to information about the location of the hydrogen-bonded proton.

It should be noted that all of the calculations of ^{23}Na quadrupole parameters in this chapter, with the exception of $\eta(^{23}\text{Na})$ in Section 6.4, use the periodic *ab initio* method and suitably modified Pople 3-21G basis sets (see Chapter 4, Section 4.4). Furthermore, the calculated values of $C_Q(^{23}\text{Na})$ are taken as directly comparable with experiment since a correlation very close to 1:1 is assumed. In the main, the calculated values of $\eta(^{23}\text{Na})$ are not used for assignment purposes since their values are less reliably calculated using the relatively simple 3-21G basis set. However, this is not the case in the discussion of hydrogen bonding in Na_2HPO_4 in Section 6.4, in which values of $\eta(^{23}\text{Na})$ play a key role and are calculated using a suitably modified 6-21G basis set with d-polarisation functions.

6.2 ^{23}Na MAS NMR study of anhydrous $Na_4P_2O_7$

Tetrasodium pyrophosphate ($Na_4P_2O_7$) crystallises in the $P2_12_12_1$ space group with four formula units per unit cell [2]. The four sodium atoms of each formula unit lie on general positions giving rise to four crystallographically-distinct sodium environments with equal occupation. Consequently, the ^{23}Na NMR spectrum is characterised by four, equal-intensity resonances with distinct quadrupole interaction parameters.

The ^{23}Na MAS NMR spectrum of $Na_4P_2O_7$, measured at 105.8 MHz, is shown in Figure 6.1 and the four second-order resonances are strongly overlapped. The complex spectrum is the reason why $Na_4P_2O_7$ has been used as a model compound in both ^{23}Na MQMAS [3-5] and DOR [4] experiments. In recent work, ^{23}Na MAS, DOR and MQMAS NMR spectra measured at five distinct Larmor frequencies in the range 105.8 MHz to 211.6 MHz have been analysed in order to determine 'best values' of $C_Q(^{23}\text{Na})$, $\eta(^{23}\text{Na})$ and

$\delta_{iso,cs}(^{23}Na)$ for each resonance in the spectrum [6]. The values obtained are summarised in Table 6.1, although no estimates of uncertainties were given in the original work.

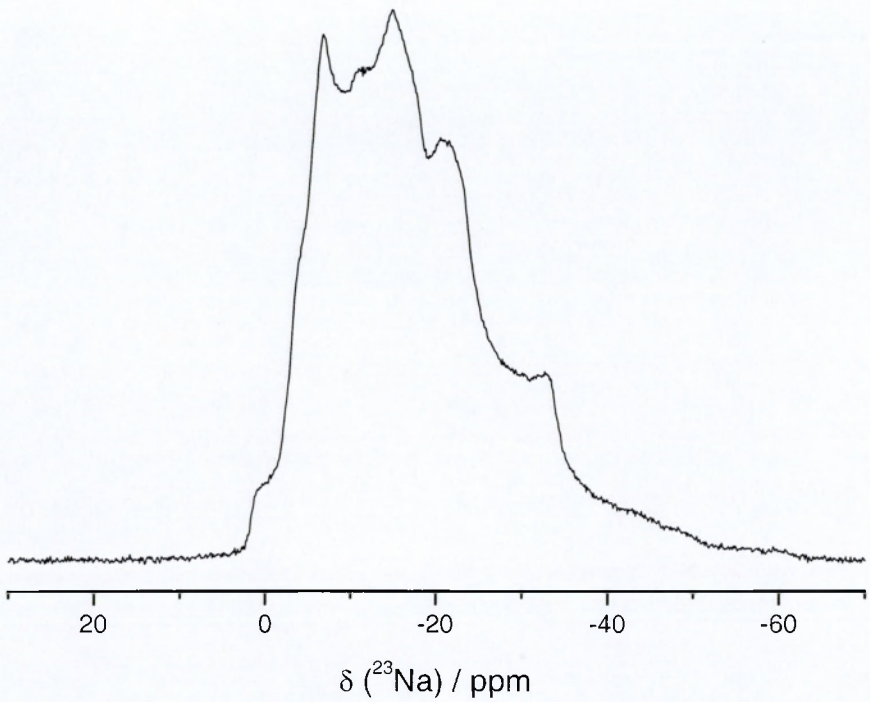

Figure 6.1 Experimental ^{23}Na MAS NMR spectrum of anhydrous $Na_4P_2O_7$.

Table 6.1 A summary of the 'best values' of the experimental ^{23}Na NMR quadrupole parameters for anhydrous $Na_4P_2O_7$ taken from [6]

Resonance [a]	C_Q / MHz	η	$\delta_{iso,cs}(^{23}Na)$ [b] / ppm
I	2.08	0.26	-1.69
II	2.90	0.47	+3.20
III	2.30	0.70	-5.25
IV	3.22	0.56	-0.85

[a] These labels are the Roman equivalents of those used in [6]: they are used to avoid confusion with the crystallographic sodium sites which are labelled 1 to 4: see Table 6.8.
[b] Isotropic chemical shift relative to external solid NaCl.

This compound represents a good test case for the periodic *ab initio* calculation of ^{23}Na quadrupole parameters and the use of the correlation approach for assignment purposes.

The initial calculation of the ^{23}Na quadrupole parameters used the crystal structure of $Na_4P_2O_7$ as refined by Leung and Calvo [2]. The results, shown as 'Calculated (i)' in Table 6.2, demonstrate that this crystal structure gives a calculated $C_Q(^{23}Na)$ value for site (*2*) significantly larger than expected from experiment; indeed the value is unrealistically large. A more detailed inspection of the reported crystal structure [7], however, reveals that for the quoted space group setting an origin shift of (0.25, 0, 0) is required for the standard data. Application of this origin shift results in the calculated values of the ^{23}Na quadrupole parameters labelled as 'Calculated (ii)' in Table 6.2.

Table 6.2 A summary of the calculated values of ^{23}Na NMR quadrupole parameters for anhydrous $Na_4P_2O_7$

Site [a]	Calculated (i)		Calculated (ii)	
	C_Q / MHz	η	C_Q / MHz	η
Na (*1*)	+2.165	0.81	+2.065	0.64
Na (*2*)	+30.839	0.11	+2.465	0.67
Na (*3*)	+4.595	0.24	+3.008	0.51
Na (*4*)	-4.849	0.53	+3.020	0.82

[a] The labels correspond to those used in [2]. Calculated values based on (i) the crystal structure reported in [2] and (ii) after an origin shift (0.25, 0, 0) as described in the text.

Overall, it appears that the original crystal structure is correct once the proper origin is adopted; a suitable remark is now in the ICSD database. Only a partial resonance assignment is possible based upon the calculated values of $C_Q(^{23}Na)$ in Table 6.2. The resonances reported by Engelhardt *et al.* as (I) and (III) can be assigned to sodium on the lattice sites designated (*1*) and (*2*), respectively. Sites (*3*) and (*4*) give almost identical calculated values for $C_Q(^{23}Na)$ and so cannot easily be assigned. It should be noted, however, that the calculated values of the ^{23}Na quadrupole parameters for these two sites are in reasonable agreement with those measured by experiment. The calculated values of $\eta(^{23}Na)$ are not sufficiently reliable for assignment purposes.

The calculated values for the ^{23}Na NMR parameters, along with the knowledge that the resonances must be of equal intensity, provides a powerful starting point for the simulation of the strongly overlapped ^{23}Na MAS NMR spectrum shown in Figure 6.1. The Bruker WINFIT software was used for this simulation with the starting values of the ^{23}Na quadrupole parameters taken as those obtained by periodic *ab initio* calculation. To begin, these values were fixed and only the position and amplitude of each resonance was allowed to vary. When convergence was reached, $\eta(^{23}\text{Na})$ for each resonance was then allowed to vary since this parameter is less well modelled by the periodic *ab initio* method. After convergence, $C_Q(^{23}\text{Na})$ was released. The last step in the fitting process was to allow a small amount of gaussian line broadening for the final fit. The results of the simulation are summarised in Table 6.3 and the simulated MAS NMR spectrum along with its individual components is compared with experiment in Figure 6.2. It should be noted that values of $\delta_{iso,cs}(^{23}\text{Na})$ are also provided by the simulation.

Table 6.3 Values of NMR parameters for the individual resonances in the simulated ^{23}Na MAS NMR spectrum of anhydrous $Na_4P_2O_7$

Resonance [a]	C_Q / MHz	η	$\delta_{iso,cs}(^{23}\text{Na})$ [b] / ppm	Intensity
I	2.06 ± 0.10	0.26 ± 0.05	-1.21 ± 0.5	0.30
II	2.91 ± 0.15	0.46 ± 0.05	+3.63 ± 0.5	0.21
III	2.26 ± 0.11	0.70 ± 0.05	-5.45 ± 0.5	0.24
IV	3.20 ± 0.16	0.56 ± 0.05	-0.74 ± 0.5	0.23

[a] The resonances are labelled in the same way as those in Table 6.1. [b] Isotropic chemical shift relative to external solid NaCl.

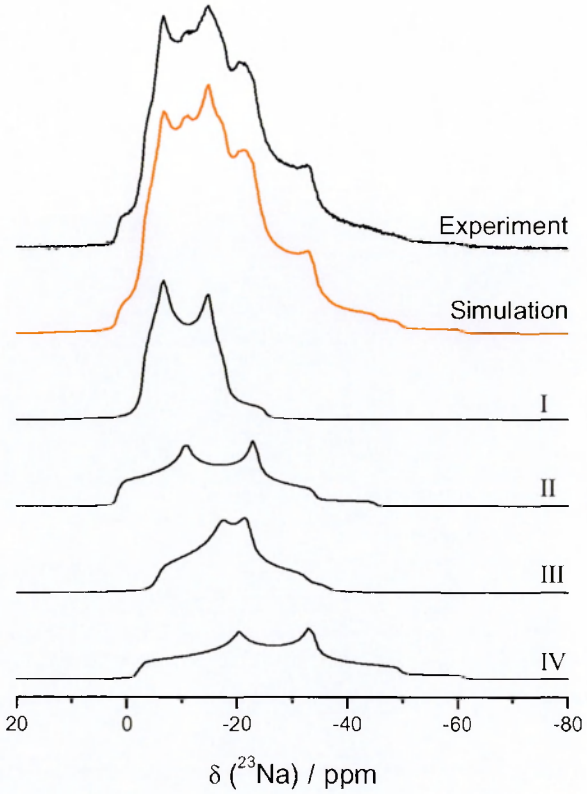

Figure 6.2 Experimental and simulated ^{23}Na MAS NMR spectrum of anhydrous $Na_4P_2O_7$. Individual contributions to the simulated spectrum are shown.

Of the various NMR experiments applied to the study of $Na_4P_2O_7$, Engelhardt *et al.* concluded that the double-frequency-sweep, triple-quantum MAS technique [6] alone was able to derive all the ^{23}Na NMR parameters with sufficient accuracy from a single experiment. They also commented that such a technique is experimentally demanding and not routinely available in all laboratories. However, as demonstrated by a comparison of the results in Tables 6.2 and 6.3, it is equally possible to use relatively straightforward MAS NMR coupled with periodic *ab initio* calculation to extract quadrupole parameters for a material with a known crystal structure. Using the calculated ^{23}Na NMR parameters it is also possible to make some progress towards assigning specific resonances to their respective crystallographic sites.

6.3 Polymorphs of $Na_5P_3O_{10}$

Pentasodium triphosphate, ($Na_5P_3O_{10}$), is one of the main products made from phosphoric acid [8]. It crystallises in two anhydrous polymorphic forms. The low-temperature polymorph, designated phase II, is thermodynamically stable up to about 415°C [9, 10]. At higher temperatures, it is easily converted to the high-temperature polymorph, phase I. The reverse process occurs very slowly with the result that phase I is metastable at room temperature and both polymorphs can exist. Depending upon the thermal history and the technical grade, samples of $Na_5P_3O_{10}$ will be a mixture containing various amounts of both phases. Hydration of anhydrous $Na_5P_3O_{10}$ from the air occurs only slowly and at high relative humidity, but from aqueous solution, $Na_5P_3O_{10}$ crystallises as the hexahydrate: $Na_5P_3O_{10}\cdot 6H_2O$.

The co-existence of three different crystalline forms, at room temperature, presents a further opportunity to test the correlation between calculation and experiment for multi-site sodium ions. Recent work by Fyfe and co-workers [11] has found that the ^{23}Na MQMAS NMR spectrum of the low temperature form (phase II) is consistent with the reported crystallographic data [12]. Assignment of the non-equivalent sites in the crystal structure was by comparison of the relative differences between point-charge derived values of $C_Q(^{23}Na)$ and the corresponding experimental values. A similar investigation of the high temperature form (phase I) indicated three sodium sites but point-charge calculations failed to provide a consistent assignment. It was concluded that there were inaccuracies in the reported crystal structure of this phase. It was also reported that an analysis of the hexahydrate using ^{23}Na MAS and MQMAS NMR spectra recorded at different magnetic fields was in progress but presented a difficult problem.

6.3.1 Anhydrous $Na_5P_3O_{10}$: phase II polymorph

In order to ensure purity of the commercial sample of $Na_5P_3O_{10}$ used in this study, it was heated at 350°C for 72 hours and then allowed to cool slowly. A subsequent XRD analysis confirmed that the phase II polymorph was the only crystalline component present.

The crystal structure of the phase II polymorph indicates that there are three crystallographically distinct sodium sites in the ratio 1:2:2 [12]. The ^{23}Na MAS NMR spectrum, shown in Figure 6.3, indicates three second-order quadrupolar-split resonances, two of which overlap strongly.

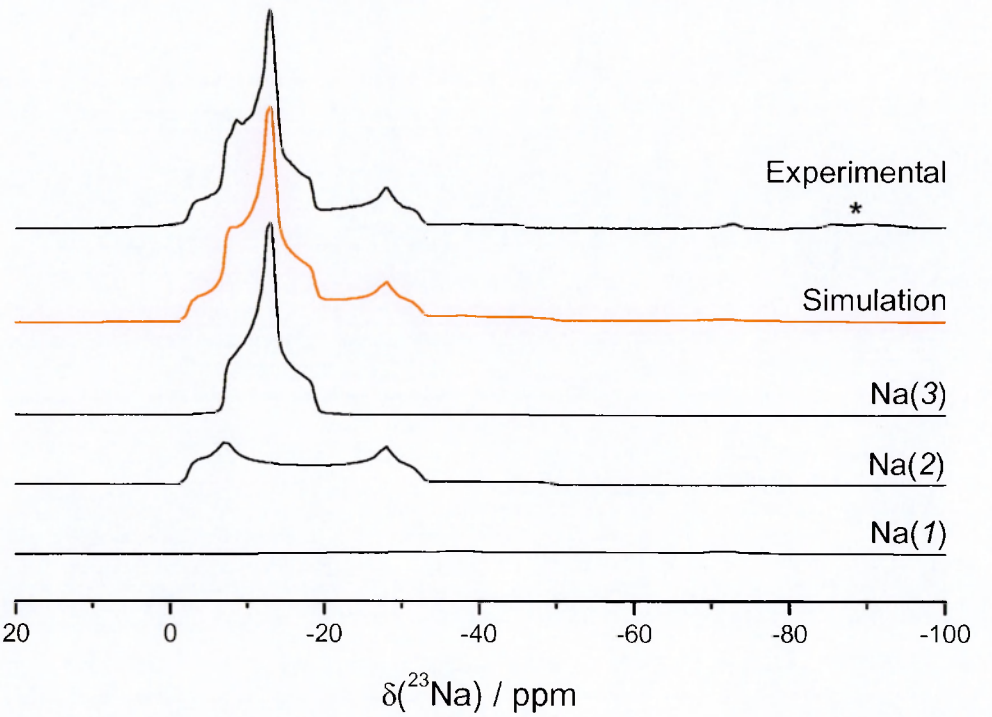

Figure 6.3 Experimental and simulated ^{23}Na MAS NMR spectrum of the anhydrous $Na_5P_3O_{10}$ phase II polymorph. Individual contributions to the simulated spectrum are shown. * represents the position of a spinning sideband.

Direct fitting of this spectrum gave the NMR parameters in Table 6.4 and these are in good agreement with those measured by Fyfe *et al.* [11]. The assignment of the resonances is that proposed by the authors based on point-charge calculations.

Table 6.4 Values of NMR parameters for the individual ^{23}Na resonances for the phase II polymorph of anhydrous $Na_5P_3O_{10}$

Site [a]	C_Q / MHz	η	$\delta_{iso,cs}(^{23}Na)$ [b] / ppm	Ref
Na (*1*)	4.56 ± 0.23	0.40 ± 0.05	-5.2 ± 0.5	*c*
	4.57 ± 0.03	0.39 ± 0.02	-3.7 ± 0.2	11
Na (*2*)	3.06 ± 0.15	0.17 ± 0.05	+2.9 ± 0.5	*c*
	2.99 ± 0.02	0.19 ± 0.02	+2.2 ± 0.4	11
Na (*3*)	1.37 ± 0.07	0.92 ± 0.05	-7.0 ± 0.5	*c*
	1.37 ± 0.02	1.00 ± 0.02	-6.7 ± 0.4	11

[a] The labels correspond to those used in [11]. [b] Isotropic chemical shift relative to external solid NaCl. [c] This work.

The phase II polymorph crystallises in the monoclinic space group *C*2/*c* with four formula units per unit cell [12]. The structure consists of sodium ions surrounding a linear $P_3O_{10}^{5-}$ ion as shown in Figure 6.4.

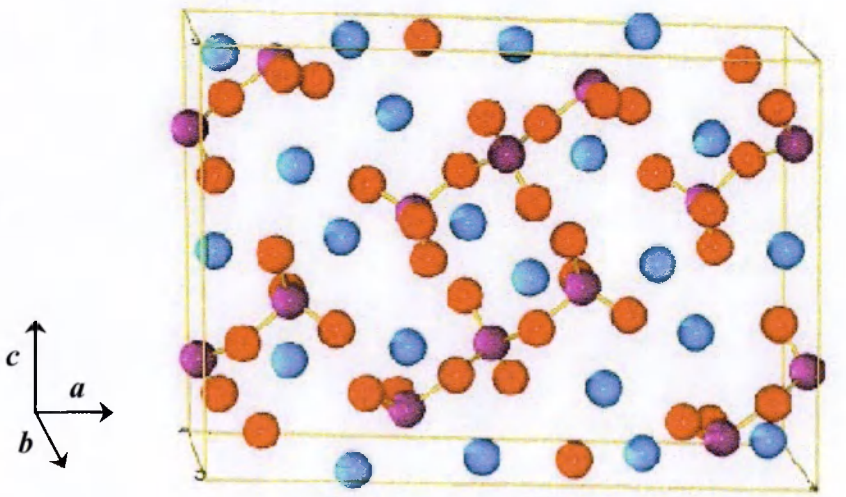

Figure 6.4 The structure of the unit cell of the phase II polymorph of anhydrous $Na_5P_3O_{10}$: sodium atoms (blue), phosphorus atoms (purple) and oxygen atoms (red).

The quadrupole parameters calculated using the periodic *ab initio* method and suitably modified 3-21G basis sets, for the three crystallographically-distinct sodium sites based on this crystal structure are given in Table 6.5. The values of $C_Q(^{23}Na)$ for the three sodium sites agree well with those found from experiment and, in agreement with the conclusions reached by Fyfe *et al.*, provide further evidence for the accuracy of the reported crystal structure.

Table 6.5 A summary of experimental and calculated values of ^{23}Na NMR quadrupole parameters for the phase II polymorph of anhydrous $Na_5P_3O_{10}$

Phase II [a]	Experimental [b]		Calculated	
	C_Q / MHz	η	C_Q / MHz	η
Na (*1*)	4.56	0.40	+4.03	0.45
Na (*2*)	3.06	0.17	-3.44	0.21
Na (*3*)	1.37	0.92	-1.37	0.86

[a] The labels correspond to those used in [12]. [b] This work.

6.3.2 The five sites of $Na_5P_3O_{10}\cdot 6H_2O$

A sample of the hexahydrate was prepared by the slow evaporation of a concentrated aqueous solution of $Na_5P_3O_{10}$. Once the crystals formed, they were filtered from the solution, washed with acetone and allowed to dry in air at room temperature. The hexahydrate crystallises in the triclinic space group $P\bar{1}$ with two formula units per unit cell [13]. The structure, shown in Figure 6.5, comprises sodium cations and $P_3O_{10}^{5-}$ anions along with water molecules, which are distributed in such a way that they partially coordinate the sodium ions and form hydrogen bonds to the triphosphate ions. One terminal PO_4 tetrahedron participates in nine such hydrogen bonds, the other only one, while the central PO_4 unit does not participate in any hydrogen bonds. All atoms lie on general positions within the unit cell, which means there are five independent sodium sites

with equal multiplicities giving rise to five second-order quadrupolar, equal-intensity, resonances in the ^{23}Na MAS NMR spectrum.

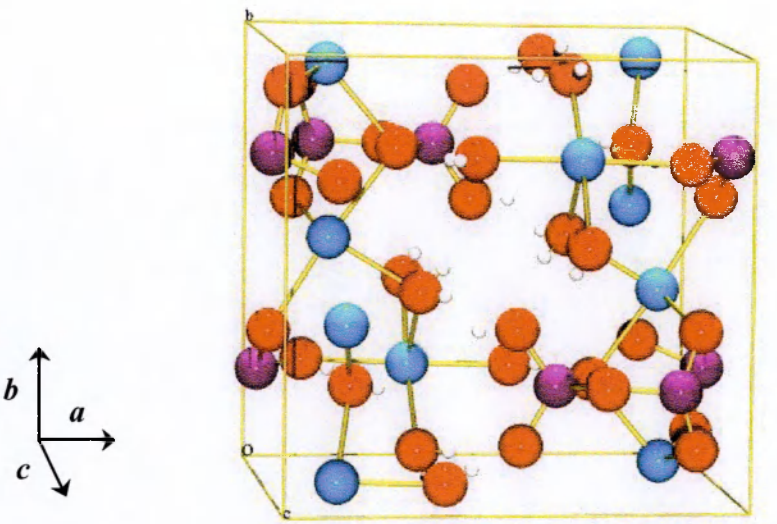

Figure 6.5 The structure of the unit cell of $Na_5P_3O_{10}\cdot 6H_2O$: sodium atoms (blue), phosphorus atoms (purple), oxygen atoms (red) and hydrogen atoms (white).

Figure 6.6 shows that the individual resonances in the spectrum strongly overlap and it is difficult, even with the knowledge that there are five resonances, to identify the individual contributions.

Values for $C_Q(^{23}Na)$ for the five sites of $Na_5P_3O_{10}\cdot 6H_2O$ were calculated using the periodic *ab initio* method and the results are shown in Table 6.6. These values provide a valuable starting point, along with the knowledge that the resonances must be of equal intensity, for the simulation of the experimental ^{23}Na MAS NMR spectrum. The Bruker WINFIT software once again was used for this simulation using an approach based on that already discussed for fitting the ^{23}Na MAS NMR spectrum of $Na_4P_2O_7$ (Section 6.2) but with a different sequence of release of parameters. This was found necessary to achieve a reasonable final fit. The $C_Q(^{23}Na)$ values for all five sites were kept fixed at their calculated values and the $\eta(^{23}Na)$ values were set to zero, leaving only the positions and

amplitudes of the resonances as variables. When convergence was reached, $C_Q(^{23}Na)$ for each resonance was then allowed to vary and after convergence, $\eta(^{23}Na)$ was released. The remaining step was to allow a small amount of gaussian line broadening for a final fit. The results of the simulation are summarised in Table 6.6, which includes values of $\delta_{iso,cs}(^{23}Na)$. The simulated MAS NMR spectrum is compared with experiment in Figure 6.7.

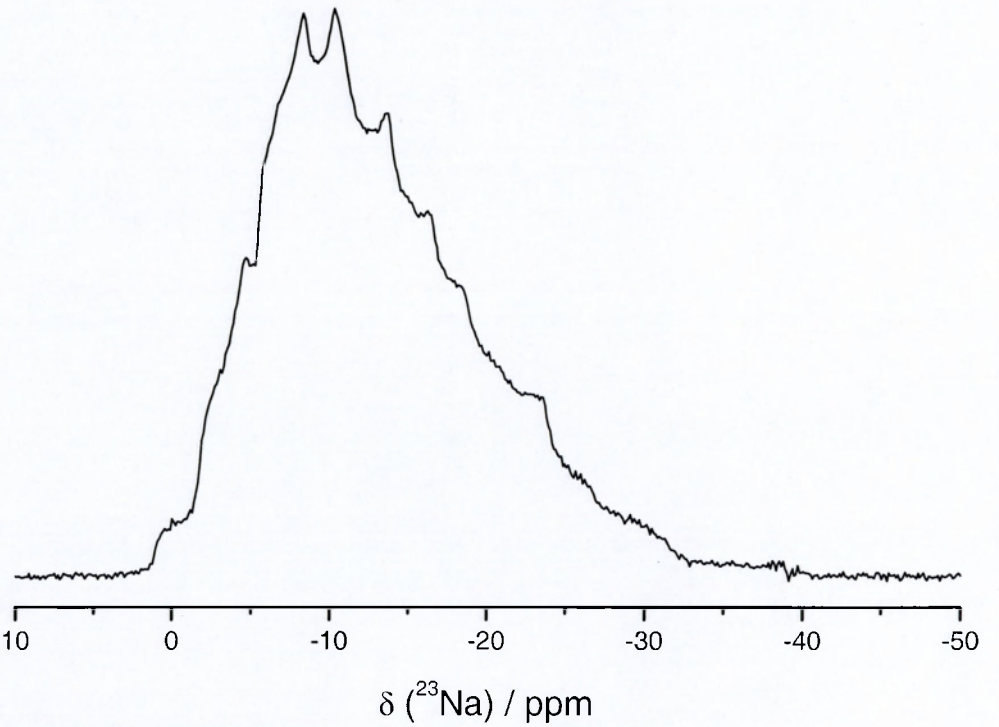

Figure 6.6 Experimental ^{23}Na MAS NMR spectrum of $Na_5P_3O_{10}\cdot 6H_2O$.

Table 6.6 NMR parameters from both periodic *ab initio* calculation and simulation of the experimental ^{23}Na MAS NMR spectrum for the different sodium sites in $Na_5P_3O_{10}.6H_2O$

Site [a]	Calculation	Simulation			
	C_Q / MHz	C_Q / MHz	η	$\delta_{iso,cs}(^{23}Na)$ [b] / ppm	Intensity
Na (*1*)	-1.76	1.74 ± 0.09	0.29 ± 0.05	-0.55 ± 0.5	0.21
Na (*2*)	+2.09	1.97 ± 0.10	0.85 ± 0.05	-5.71 ± 0.5	0.18
Na (*3*)	+2.37	2.09 ± 0.10	0.81 ± 0.05	-9.09 ± 0.5	0.19
Na (*4*)	-2.69	2.40 ± 0.12	0.51 ± 0.05	+2.20 ± 0.5	0.22
Na (*5*)	+1.71	1.69 ± 0.09	0.26 ± 0.05	-4.20 ± 0.5	0.21

[a] The labels correspond to those used in [13]. [b] Isotropic chemical shift relative to external solid NaCl.

The assignment of the individual sodium sites is based upon the assumption of a linear correlation between calculation and experiment, although the relatively small differences between the simulated $C_Q(^{23}Na)$ values does introduce some uncertainty into the assignment. Nonetheless, by using a consistent approach for all five sites, in the absence of any further information, a reasonable interpretation can be made. It is worth noting that the sign of $C_Q(^{23}Na)$, if available experimentally, is an important assignment parameter; for example it would allow the resolution of any ambiguity over the assignment of sites (*1*) and (*5*). Once again the calculated values of $\eta(^{23}Na)$ were not sufficiently reliable for assignment purposes.

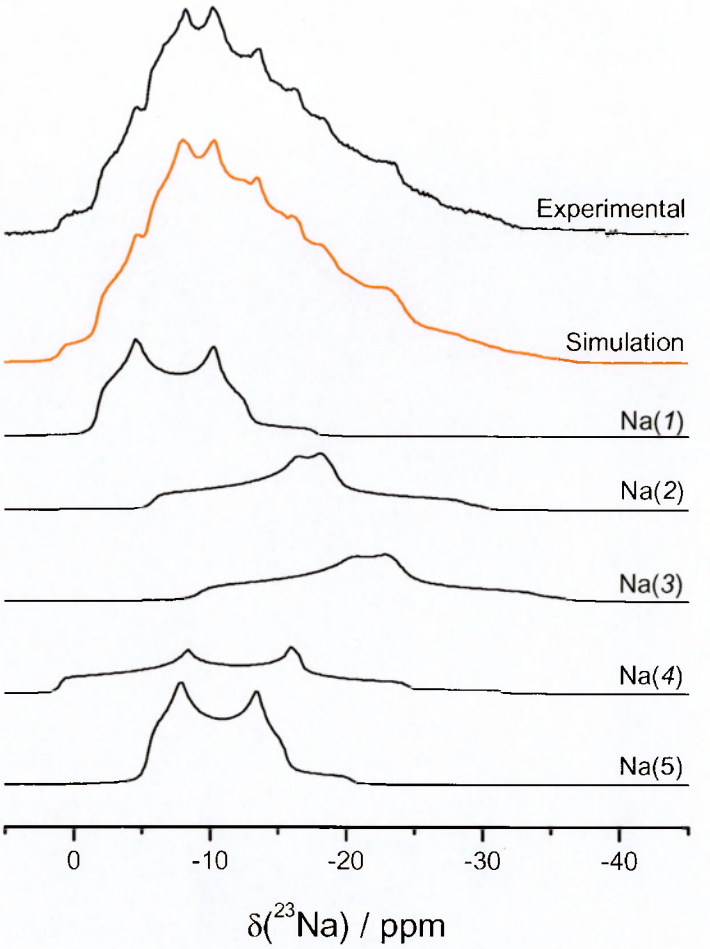

Figure 6.7 Experimental (proton-decoupled) and simulated ^{23}Na MAS NMR spectrum of $Na_5P_3O_{10}{\cdot}6H_2O$. Individual contributions to the simulated spectrum are shown.

6.3.3 Anhydrous $Na_5P_3O_{10}$: phase I polymorph

The high-temperature phase I polymorph of anhydrous $Na_5P_3O_{10}$ was prepared by heating a commercial sample at 550°C for 36 hours, then slowly cooling the solid to 430°C over 12 hours. When the heating cycle was complete, the sample was quenched in liquid nitrogen. A subsequent XRD analysis confirmed that the major product was the phase I polymorph. However, a small component of the phase II was also found. Several attempts were made to form the phase I in pure form, but to no avail. The smallest amount of the phase II

component present was analysed to be ~5% by weight. This was the sample used for the NMR study.

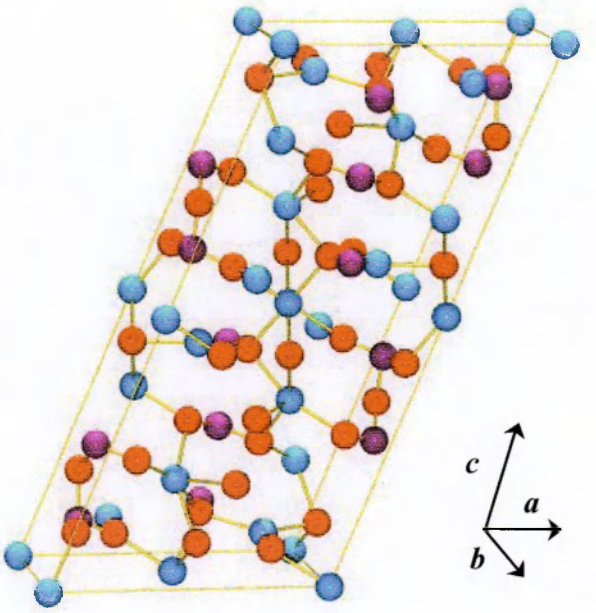

Figure 6.8 The structure of the unit cell of the phase I polymorph of anhydrous $Na_5P_3O_{10}$: sodium atoms (blue), phosphorus atoms (purple) and oxygen atoms (red).

The phase I polymorph, like that of phase II, crystallises in the *C*2*c* space group and the crystal structure, shown in Figure 6.8, indicates that there are three distinct sodium sites in the ratio 1:2:2 [14]. This is consistent with the ^{23}Na MAS NMR spectrum, shown in Figure 6.9, which consists of three second-order quadrupole resonances, two of which are overlapping. Fitting this spectrum, which is of a better quality than that reported by Fyfe et al [11] gave the NMR parameters in Table 6.7. (The improvement in quality of the spectrum may be associated with the purity of the phase I polymorph.) As part of the fitting procedure, account was taken of the ~5% by weight presence of the phase II polymorph.

Table 6.7 Values of NMR parameters for the individual ^{23}Na resonances for the phase I polymorph of anhydrous $Na_5P_3O_{10}$

Site [a]	C_Q / MHz	η	$\delta_{iso,cs}(^{23}Na)$ [b] / ppm	ref
Na (*1*)	1.38 ± 0.05	0.78 ± 0.05	+0.1 ± 0.5	*c*
	1.30 ± 0.03	0.75 ± 0.05	-0.7 ± 0.2	11
Na (*2/3*)	3.83 ± 0.05	0.15 ± 0.05	-5.3 ± 0.5	*c*
	3.72 ± 0.04	0.17 ± 0.05	-5.4 ± 0.2	11
Na (*2/3*)	3.69 ± 0.05	0.29 ± 0.05	-6.2 ± 0.5	*c*
	3.62 ± 0.04	0.29 ± 0.04	-6.3 ± 0.2	11

[a] The labels correspond to those used in [11]. [b] Isotropic chemical shift relative to external solid NaCl. [c] This work.

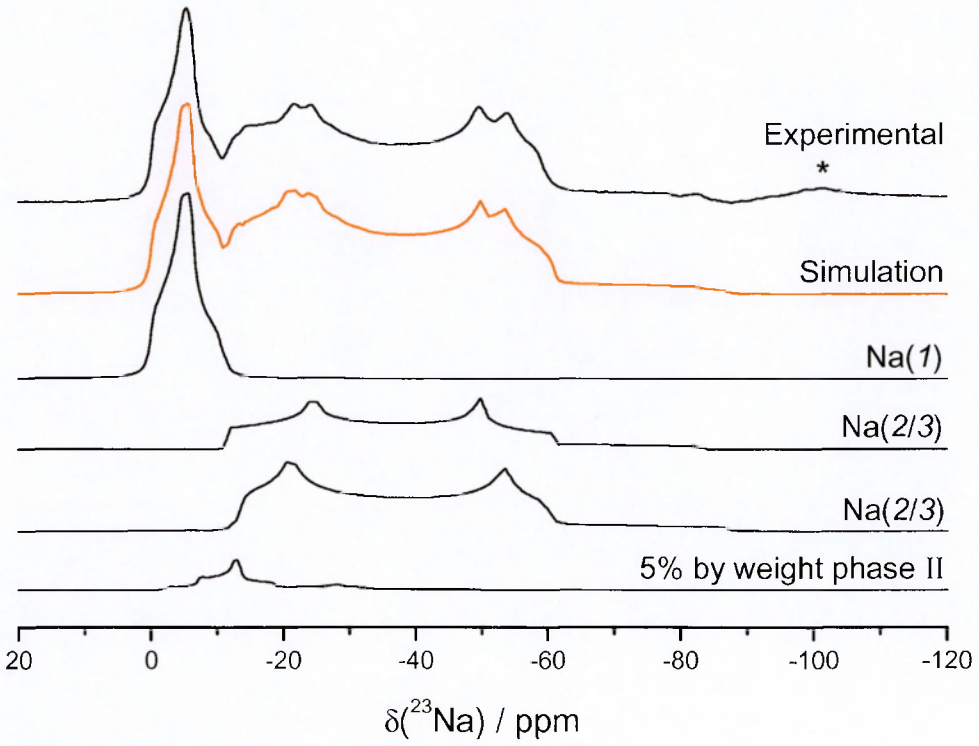

Figure 6.9 Experimental and simulated ^{23}Na MAS NMR spectrum of the anhydrous $Na_5P_3O_{10}$ phase I polymorph. Individual contributions to the simulated spectrum, including that of the phase II polymorph, are shown. * represents the position of a spinning sideband.

Calculation of the values of $C_Q(^{23}Na)$, by Fyfe *et al.*, using point-charge calculations based upon the method outlined by Koller *et al.* [15] deviated significantly from those observed by experiment (2.44 MHz, 3.30 MHz, 2.87 MHz for Na(*1*), Na(*2*) and Na(*3*) respectively). It was suggested that there were possible inaccuracies in the reported single-crystal structure. Assignment of site (*1*) (see Table 6.7) was possible based on the relative intensity of the resonance in the ^{23}Na MAS NMR spectrum.

Corbridge [14], who reported the single-crystal structure of the phase I polymorph, acknowledged in the work that the accuracy of the structure determination was limited by the poor quality of the crystals and, in addition, by experimental problems. The results of periodic *ab initio* calculations based on this structure are given in Table 6.8 under the heading 'Calculated (i)'. The poor correspondence with the experimentally-determined values of the ^{23}Na quadrupole parameters strongly suggests that there are inaccuracies in the reported crystal structure.

Table 6.8 A summary of the calculated values of ^{23}Na NMR quadrupole parameters for the phase I polymorph of anhydrous $Na_5P_3O_{10}$.

Phase I [a]	Calculated (i)		Calculated (ii)	
	C_Q / MHz	η	C_Q / MHz	η
Na (*1*)	+2.39	0.90	+1.44	0.64
Na (*2*)	+5.09	0.18	+4.00	0.19
Na (*3*)	-4.03	0.60	+3.96	0.39

[a] The labels correspond to those used in [14]. Calculated values based on (i) the crystal structure in [14] and (ii) the refined crystal structure of C. Greaves [7].

A critical feature of the results in Table 6.8 is that they indicate that it is the crystallographic positions of the sodium atoms at site (*2*), and to a lesser extent those at site (*1*), which are most likely in error.

Using the *PowderCell* software package [16], the theoretical powder XRD pattern was calculated using the original crystallographic data and compared with the experimental XRD pattern. It can be seen in Figure 6.10(a) that the relative intensities of the diffraction peaks in the region 17° – 21° 2θ for the theoretical pattern are inconsistent with the same region in the experimental pattern. Also, diffraction peaks (*hhh*) with h = 1 to 3 were either missing, or of very low intensity. The *PowderCell* program allows manipulation of individual atoms within the unit cell. By incremental movement of the sodium at site (*2*) it was possible to find better agreement with experiment in the region 17°-21° 2θ. The theoretical powder XRD pattern based upon new coordinates for sodium at site (*2*) is compared with the experimental pattern in Figure 6.10(b). These coordinates were then used, along with other inputs, as a starting point for a re-assessment of the crystal structure using Rietveld refinement [7]. The results of this refinement are given in Appendix B.

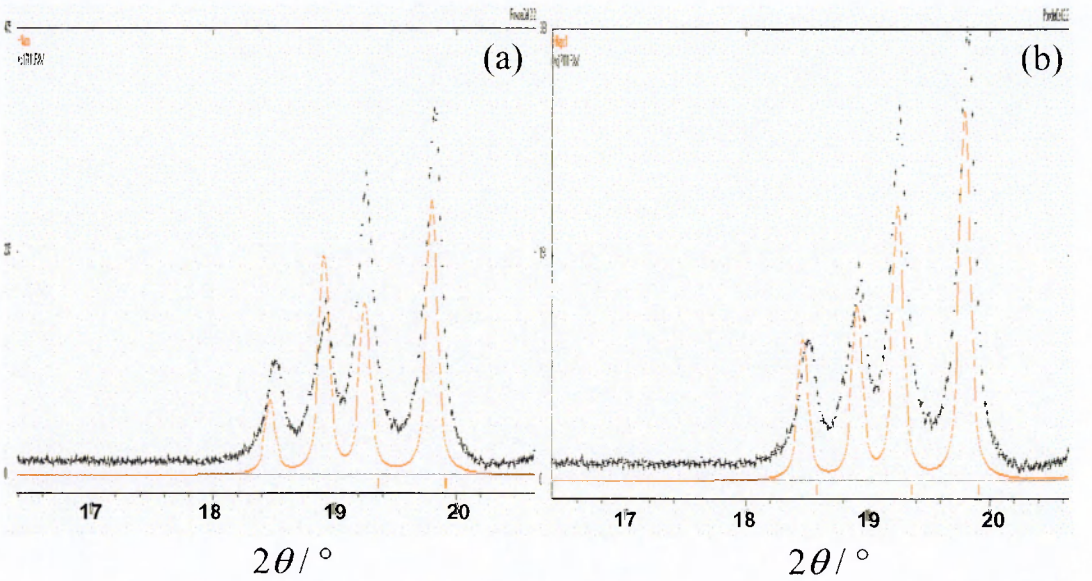

Figure 6.10 A comparison between the experimental (black) and the theoretical (red) powder XRD patterns for (a) the literature crystal structure and (b) the structure found by manipulation of the site (*2*) sodium atom in the *PowderCell* package.

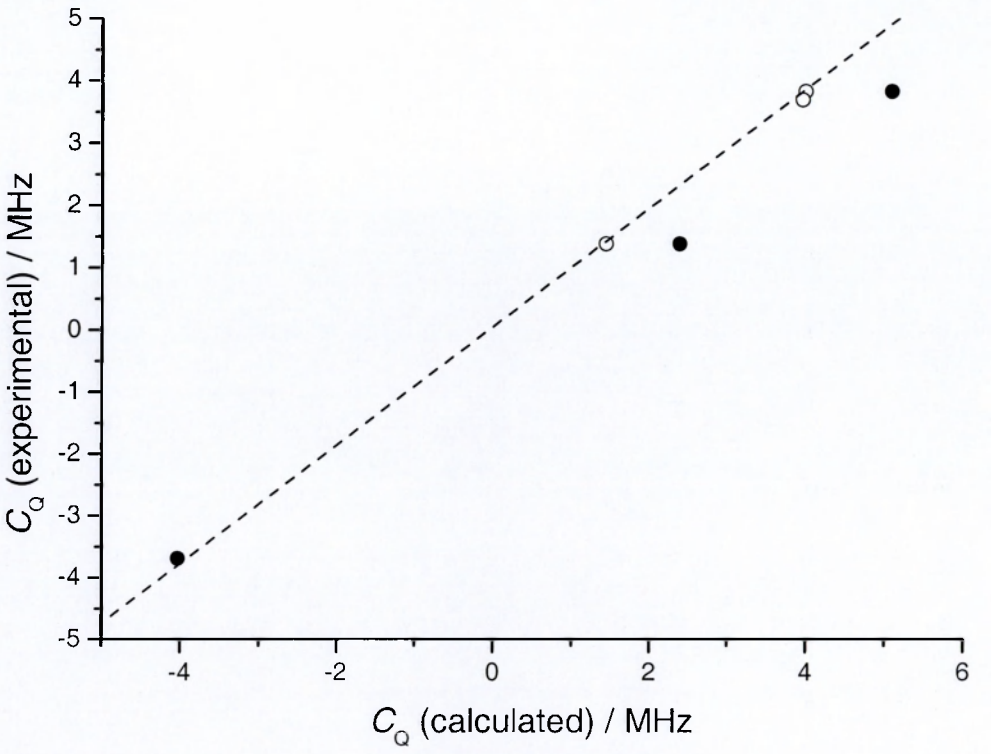

Figure 6.11 A plot of experimental versus calculated values of $C_Q(^{23}Na)$ for the phase I polymorph of anhydrous $Na_5P_3O_{10}$. Filled circles are for calculations based on the crystal structure reported in [14] and open circles are for the refined crystal structure in this work. The dashed line shows the general linear correlation found in Chapter 4, Figure 4.10.

The refined crystal structure was used to calculate the ^{23}Na quadrupole parameters, which were now found to be in better agreement with experiment; see the columns labelled 'Calculated (ii)' in Table 6.8. This conclusion is also supported by the correlation plot in Figure 6.11. There is very good agreement between the calculated values of $C_Q(^{23}Na)$ based on the refined structure and the general linear correlation found in Chapter 4, Figure 4.10. Unfortunately, this result still leaves uncertainties in the assignment of the resonances in the ^{23}Na MAS NMR spectrum to their crystallographic sites. This is because the sodium atoms at sites (*2*) and (*3*), despite having different structural environments, have very similar calculated and experimental values of $C_Q(^{23}Na)$. A tentative assignment based upon a correlation between experimental and calculated values of $\eta(^{23}Na)$ might

suggest that site (*2*) is associated with the resonance at –5.3 ppm and site (*3*) with the resonance at –6.2 ppm. It is interesting to note that for site (*3*), the magnitude of the calculated $C_Q(^{23}Na)$ value does not change markedly depending upon the crystal structure used, however, the sign does. This indicates that the orientation of the efg tensor at sodium on site (3) is different in the two structures with the 3 and 2 axes being interchanged. Knowledge of the sign of the efg tensor, if it were available from experiment, would be a useful test of the validity of the newly proposed structure.

6.4 The position of hydrogen in the hydrogen bond in Na_2HPO_4

The crystal structure of anhydrous disodium hydrogen phosphate was first reported to crystallise in the monoclinic space group $P2_1/m$ [17]. However, a later NMR study by Baldus *et al.* [18] revealed the presence of three sodium resonances, which is one more than would be expected on the basis of the reported space group. Analysis of the powder XRD of Na_2HPO_4 by these workers then placed the crystal structure in the $P2_1/c$ space group. This new assignment strictly meets all reflection conditions and, furthermore, is consistent with the 1:1:2 intensity ratio of the ^{23}Na resonances observed in the MAS NMR spectrum. The unit cell for Na_2HPO_4 is shown in Figure 6.12.

The position of the hydrogen atom within the hydrogen bond in Na_2HPO_4, as refined in [16], was obtained by a least squares fitting procedure based upon a Rietveld refinement of the heavy atom positions. During the fitting, constraints were placed upon the bond length (O(*4*)–H ~1.07 Å), bond angle (P–O(4)–H ~104.5°) and the desire to maximise the distance between the hydrogen atom and the four neighbouring sodium ions. It was placed ~1.0 Å from the oxygen designated O(*4*) and ~1.5 Å from oxygen O(*3*) to which it forms a hydrogen bond.

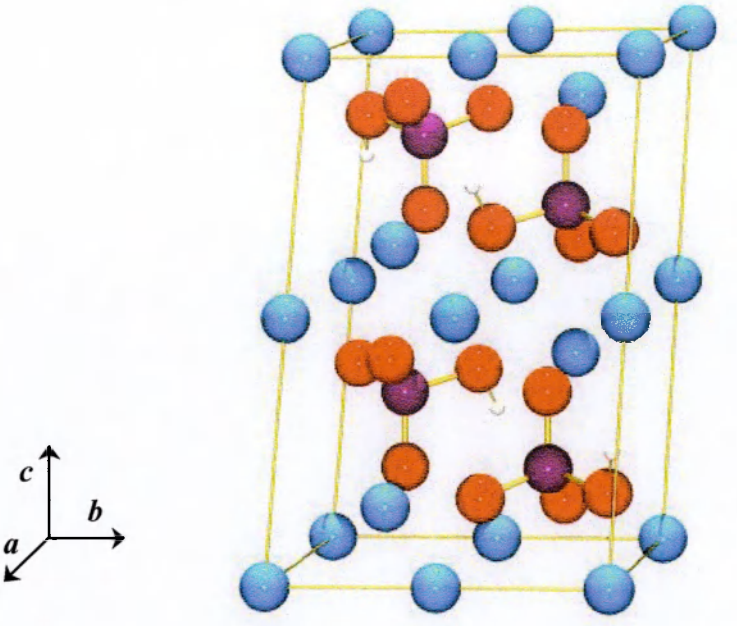

Figure 6.12 The unit cell of Na_2HPO_4: sodium atoms (blue), phosphorus atoms (purple), oxygen atoms (red) and hydrogen atoms (white).

In Chapter 4, with specific reference to Figure 4.19, it was shown that when the position of hydrogen atoms within a unit cell are known (from single crystal neutron diffraction data) then a periodic *ab initio* model, using appropriately modified Pople 6-21G basis sets with d-polarisation functions, can be used to obtain a reasonable linear correlation between experimental and calculated values of both $C_Q(^{23}Na)$ and $\eta(^{23}Na)$. However, the linear correlation for the values of $C_Q(^{23}Na)$ does not correspond to 1:1. It can also be noted that $\eta(^{23}Na)$ values less than 0.5 are particularly well characterised whilst those greater than 0.5 are prone to larger uncertainties (see Figure 4.19). Table 6.9 summarises the results of the periodic *ab initio* calculations using suitably modified Pople 6-21G basis sets with d-polarisation functions for the crystal structure refined by Baldus *et al.* [18].

Table 6.9 A summary of experimental and calculated values of ^{23}Na NMR quadrupole parameters for Na_2HPO_4 using a 6-21G basis set with d-polarisation functions

Na_2HPO_4 [a]	Experimental		Calculated		References	
	C_Q / MHz	η	C_Q / MHz	η	NMR	Struct
Na (*1*)	2.04 ± 0.10	0.70 ± 0.05	+3.11	0.94	*b*	18
Na (*2*)	1.31 ± 0.07	0.20 ± 0.05	+1.47	0.93		
Na (*3*)	3.84 ± 0.19	0.30 ± 0.05	+5.92	0.28		

[a] The labels correspond to those used in [18]. [b] This work.

The calculated values of $C_Q(^{23}Na)$ are, as expected, larger than those determined experimentally. If the correlation equation fitted to the data in Chapter 4, Figure 4.18, that is:

$$C_Q(\text{experimental}) = 0.661\ C_Q(\text{calculated}) + 0.005 \qquad (6.1)$$

is used then the following predicted experimental values of $C_Q(^{23}Na)$ are obtained: Na(*1*) = 2.06 MHz; Na(*2*) = 0.98 MHz; Na(*3*) = 3.92 MHz. The main discrepancy occurs for the Na(*2*) site and this is further brought into focus by a comparison of the experimental and calculated values of $\eta(^{23}Na)$. Overall, it seems that the observed differences may be connected with the location of the hydrogen atom. This was explored in detail.

In order to determine a hydrogen atom position that satisfies a comparison between experiment and calculation for the ^{23}Na quadrupole parameters for all three sodium sites, two possible situations regarding the location of this atom in the hydrogen bond can be considered:

- the hydrogen atom is dynamic; moving between O(*4*) of one phosphate group and the O(*3*) of its nearest neighbour phosphate group. This would give rise to a time-averaged efg at the Na(*2*) site.
- the hydrogen atom is static; at a point between O(*4*) of one phosphate group and O(*3*) of its nearest neighbour.

However, in an earlier study, heat capacity measurements in the range 10 – 320 K gave no indication of residual entropy associated with disorder at low temperature [19]. In addition to the evidence of superstructure peaks found in the XRD pattern of Na_2HPO_4 [18], this would suggest that the hydrogen atoms are ordered and therefore static within the crystal lattice.

The local environment within a 3 Å sphere around the hydrogen atom at the position reported in the crystal structure of Baldus *et al.* [18] is shown in Figure 6.13.

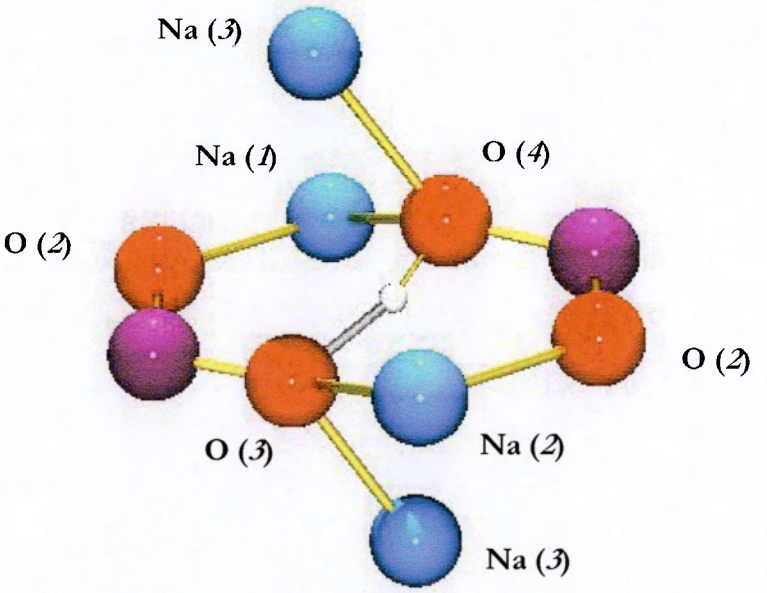

Figure 6.13 The structure of the environment within 3 Å of the hydrogen atom in Na_2HPO_4: sodium atoms (blue), phosphorus atoms (purple), oxygen atoms (red) and hydrogen atom (white). The hydrogen bond is shown in grey.

The hydrogen atom lies in the plane of a puckered 8-membered ring comprising the phosphorous, oxygen O(*2*) and oxygen O(*3*) atoms of one phosphate group, the phosphorous, oxygen O(*2*) and oxygen O(*4*) atoms of a second phosphate group linked together by two sodium atoms occupying sites designated Na(*1*) and Na(*2*) in the crystal structure. Equidistant above and below the plane of the ring are sodium atoms occupying site (*3*). If the forces of repulsion between hydrogen and the four sodium atoms, and

attraction between hydrogen and the four oxygen atoms, were the only constraints placed upon the position of the hydrogen atom then it should be positioned at the midpoint of the line joining the centres of the oxygen atoms O(*4*) and O(*3*).

The periodic *ab initio* method based upon the Pople 6-21G basis set with d-polarisation functions was used to calculate the ^{23}Na quadrupole parameters for ten hydrogen atom positions set at regular intervals along the line between O(*4*) and O(*3*). (The average time for each calculation was ~8 hours using Columbus.) It must be pointed out that no relaxation of the structure was possible using the CRYSTAL code and, consequently, during the calculation the heavy atoms occupy their positions reported in the literature [18].

Figure 6.14 and 6.15 show the effect on the predicted experimental values of $C_Q(^{23}Na)$ and $\eta(^{23}Na)$, respectively, for the three sodium sites as the hydrogen atom is re-located along the line connecting O(*4*) to O(*3*). The horizontal, colour-coded lines represent the experimentally-determined values for the three sodium sites. Overall, the various plots show that as the hydrogen atom changes position all three sites are affected but it is the $\eta(^{23}Na)$ value for the Na(*2*) site that is most dramatically changed in value.

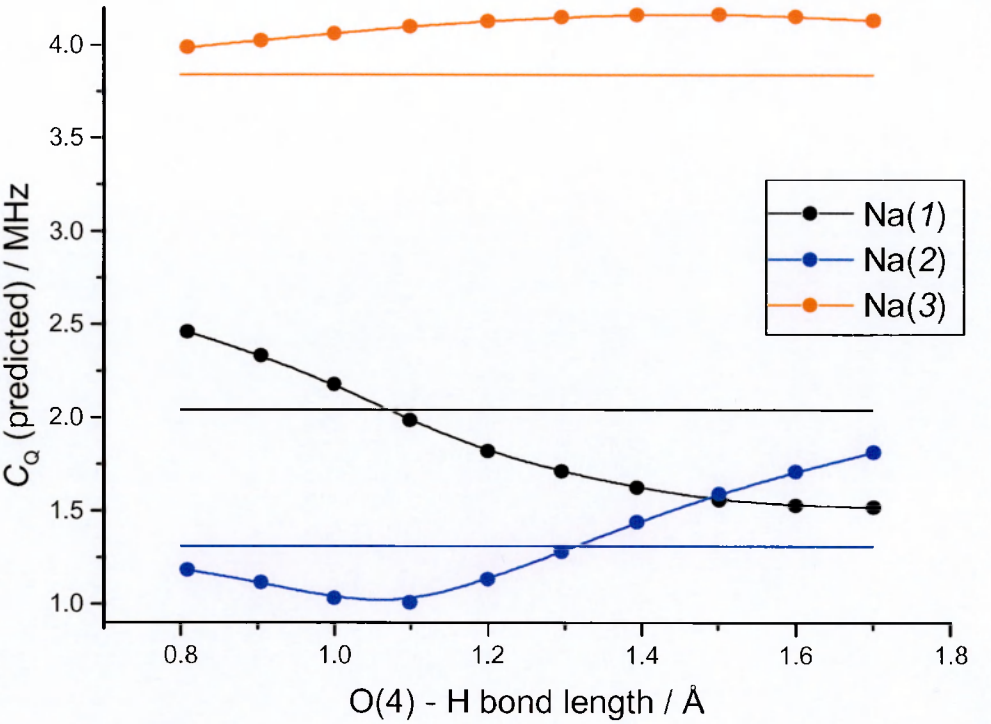

Figure 6.14 Summary of the effect on the predicted experimental value of $C_Q(^{23}Na)$ as a function of the position of the hydrogen atom along a line connecting the centres of oxygens O(*3*) and O(*4*) for the three sodium sites in Na_2HPO_4.

The small change in the predicted experimental value of $C_Q(^{23}Na)$ for Na(*3*) as the hydrogen atom changes position is probably due to the fact that this sodium cation is coordinated to both oxygen atoms involved in the hydrogen bond. For the other two sodium sites, Na(*1*) coordinates to two oxygen O(*4*) atoms and Na(*2*) to two oxygen O(*3*) atoms. Consequently, any change in the position of the hydrogen atom will affect the efg tensors at these sodium sites via a change in electron density on the respective oxygen atoms.

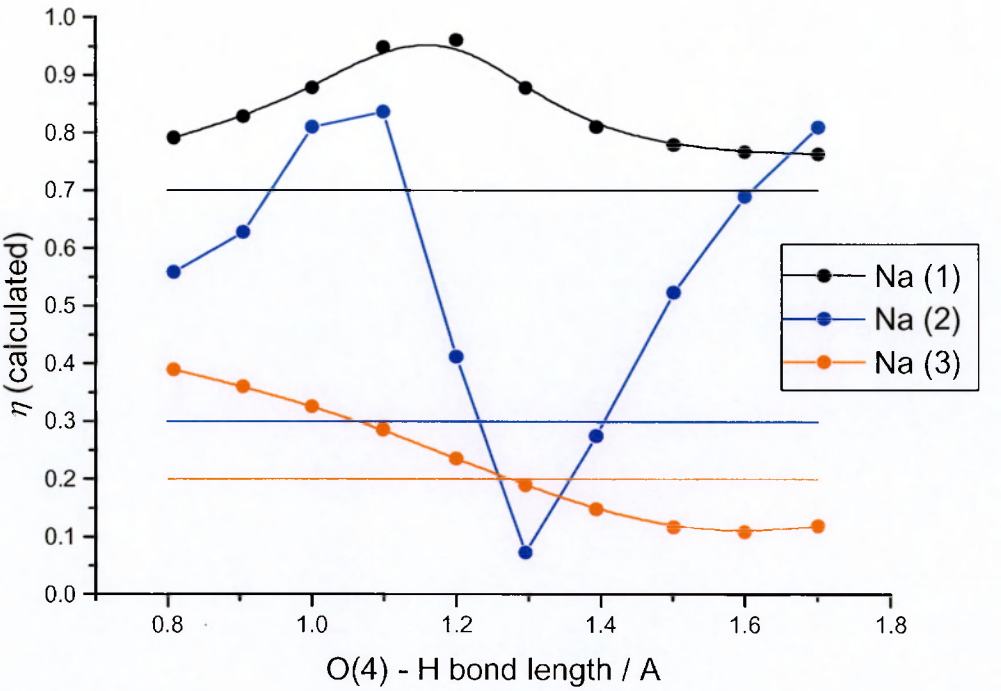

Figure 6.15 Summary of the effect on the calculated values of $\eta(^{23}Na)$ as a function of the position of the hydrogen atom along a line connecting the centres of oxygens O(*3*) and O(*4*) for the three sodium sites in Na_2HPO_4.

The highly sensitive nature of the $\eta(^{23}Na)$ value for the Na(*2*) site with respect to the hydrogen atom position was used as a guide to its position within the crystal lattice. The point at which the asymmetry parameter for Na(*2*), as well as that for Na(*3*), agrees with experiment is in the case of an O(*4*)–H bond length in the region of 1.25 Å. This result puts the hydrogen atom midway between the two oxygen atoms forming the hydrogen bond.

If the hydrogen atom is situated midway between the two oxygen atoms in a hydrogen bond then chemical intuition might suggest that it is highly unlikely that the oxygen atoms on the O(*4*) and O(*3*) sites would be at the positions reported in the literature. This is because this would lead to different P–O bond lengths in what should be a symmetrical

system. In light of the fact that CRYSTAL does not allow for structural relaxation, the two oxygen atoms had their positions manually altered slightly along the P–O directions in order to equalise the bond length (P–O(*4*) = P–O(*3*) = 1.589 Å). Calculations using the periodic *ab initio* method using suitably modified Pople 3-21G basis sets for the new positions of the oxygen and hydrogen atoms gave the results shown in Table 6.10. The use of the smaller basis set in this case is simply to demonstrate its versatility.

Table 6.10 A summary of experimental and calculated values of ^{23}Na NMR quadrupole parameters for Na_2HPO_4 using a modified 3-21G basis set

Na_2HPO_4 [a]	Experimental		Calculated		References	
	C_Q / MHz	η	C_Q / MHz	η	NMR	Struct
Na (*1*)	2.04	0.70	+2.04	0.94	*b*	18
Na (*2*)	1.31	0.20	+1.27	0.21		
Na (*3*)	3.84	0.30	+4.07	0.31		

[a] The labels correspond to those used in [18]. [b] This work.

The agreement between experiment and calculation is surprisingly good at this new hydrogen atom position with 'pseudo-relaxed' oxygen atoms but, of itself, does not provide definitive proof that the structure should be amended in this way. However, it does suggest that the hydrogen atom position reported by Baldus *et al.* is not correct.

A subsequent structure optimisation of the Na_2HPO_4 crystal lattice was undertaken using the planewave DFT code ABINIT [20]. The density functional theory in the local density approximation was used with norm-conserving Troullier-Martins type pseudopotentials generated by Khein and Allan [21]. The energy cut-off for the kinetic energy of the planewaves was set at 30 Ry to ensure good convergence and the optimisation was constrained to have the symmetry and unit cell parameters reported in the literature. The result of the structure optimisation gave an O(*4*)–H bond length of 1.198 Å and a O(4)–H–

O(3) bond angle of 180°. However, the structure was not optimised using the same basis set as used for the periodic *ab initio* determination and, therefore, is not directly comparable; nonetheless, the optimisation does provide further evidence that the position of the hydrogen atom is not as reported in [18].

In a recent NMR study involving Na_2HPO_4, Lupulescu and co-workers [22] analysed the heteronuclear MQMAS spinning-sideband patterns observed for the three-spin H – Na – H system associated with the Na(2) site. Simulations of these patterns also led the authors to question the position suggested by Baldus *et al.* for the location of the hydrogen atom in the hydrogen bond. They proposed two alternative structures whose simulated heteronuclear spinning-sideband patterns were more consistent with the experimental data:

- the H–Na–H bond angle deviated by 10° from linearity,
- the bond angle was linear but the individual Na–H bond lengths were different.

However, neither of these proposed structures takes into account that the Na(2) site occupies a centre of inversion [23] within the $P2_1/c$ crystal lattice which forces both H–Na(2) bond lengths to be equal and the bond angle between them to be 180°. It would appear that confirmation of the true position for the hydrogen atom in the crystal lattice of Na_2HPO_4 must await neutron diffraction analysis although both the periodic *ab initio* calculations and the recent MQMAS study agree that the hydrogen atom position is not at the site proposed in the current literature.

6.5 Summary

A key aim has been to demonstrate that periodic HF *ab initio* calculations of $C_Q(^{23}Na)$, based on the small modified 3-21G basis set, can be used as a predictive tool for the investigation of the crystal structures of a variety of ionic sodium compounds, including

hydrogen bonding, and in the simulation and assignment of strongly overlapping ^{23}Na MAS NMR spectra. This has been illustrated for a range of sodium phosphates. The need for an origin shift to the positional coordinates reported for $Na_4P_2O_7$ and a re-refinement of the crystal structure of the phase I polymorph of anhydrous $Na_5P_3O_{10}$ has been demonstrated. Furthermore, it has been shown that the simulation of the ^{23}Na MAS NMR spectrum of $Na_4P_2O_7$, using periodic *ab initio* calculated values of ^{23}Na quadrupole parameters for the four sodium ions present in the asymmetric unit, gives results consistent with those obtained from the more exacting double-frequency-sweep, triple-quantum MAS technique. A similar simulation approach was used to analyse the strongly-overlapped ^{23}Na MAS NMR spectrum of $Na_5P_3O_{10}\cdot 6H_2O$, which contains five sodium resonances. Finally, the sensitivity of ^{23}Na quadrupole parameters, in particular $\eta(^{23}Na)$, to the location of hydrogen in the hydrogen-bonded compound Na_2HPO_4 was explored. There is strong evidence to suggest that the reported hydrogen-bonded arrangement in the compound requires further refinement.

A linear correlation between experiment and the 'best' $C_Q(^{23}Na)$ values calculated for the sodium phosphates studied in this section is shown in Figure 6.16. There is a very good linear correlation for these compounds and, as shown by the dashed line in the figure, which is taken directly from Figure 4.10, there is good agreement with the results obtained from a wide range of other single- and multiple-site sodium compounds. Such a result highlights the strength of the periodic HF *ab initio* method and the ability of such a small basis set to be used without further tuning in a wide range of compounds.

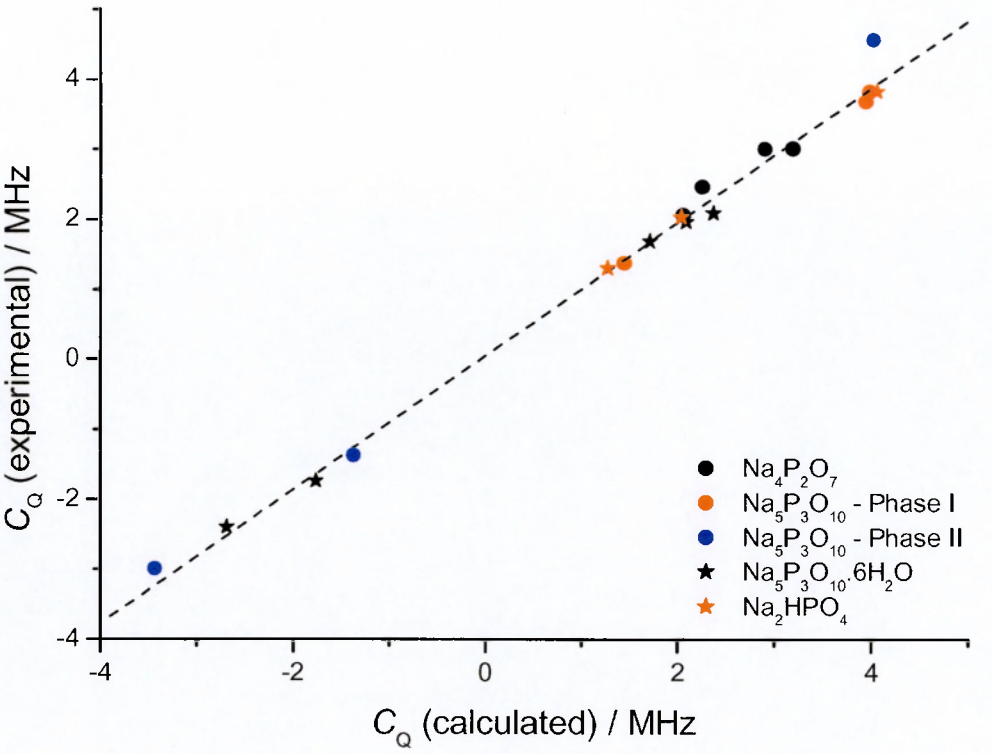

Figure 6.16 A plot of experimental versus calculated 'best' $C_Q(^{23}Na)$ values a range of sodium phosphates. The dashed straight line is taken from Figure 4.18 in Chapter 4.

References

1. A. Medek, J.S. Harwood and L. Frydman, *J. Am. Chem. Soc.*, **117**, 12779, 1995.
2. K.Y. Leung and C. Calvo, *Can. J. Chem.*, **50**, 2519, 1972.
3. S. Steuernagel, H. Forster, F. Engelke, H.-D. Zeiger and E. Naumann, *Bruker Report*, **144**, 30, 1997.
4. T. Anupold, R. Reinhold, P. Sarv and A. Samoson, *Solid State Nucl. Magn. Reson.*, **13**, 87, 1998.
5. A.P.M. Kentgens and R. Verhagen, *Chem. Phys. Lett.*, **300**, 435, 1999.
6. G. Engelhardt, A.P.M. Kentgens, H. Koller and A. Samoson, *Solid State Nucl. Magn. Reson.*, **15**, 171, 1999.

7. C. Greaves, (Birmingham University), personal communication.

8. R.E. Kirk, F. Othmer, H.F. Mark, D.F. Othmer, C.G. Overberger, G.T. Seaborg (editors), *Kirk-Othmer Encyclopedia of Chemical Technology*, 4th ed., John Wiley Sons, New York, **18**, 699, 1996.

9. A. Durif, *Crystal Chemistry of Condensed Phosphates*, Plenum Press, New York, 1995.

10. M–T. Averbuch-Pouchot and A. Durif, *Topics in Phosphate Chemistry*, World Scientific, Singapore, 1996.

11. C. A. Fyfe, H. Meyer zu Altenschildesche and J. Skibsted, *Inorg. Chem.*, **38**, 84, 1999.

12. D.W.J. Cruickshank, *Acta Crystallogr.*, **17**, 674, 1964.

13. D.M. Wiench, M. Jansen and R. Hoppe, *Z. Anorg. Allg. Chem.*, **488**, 80, 1982.

14. D.E.C. Corbridge, *Acta Crystallogr.*, **13**, 263, 1960.

15. H. Koller, G. Engelhardt, A.P.M. Kentgens and J. Saur, *J. Phys. Chem.*, **98**, 1544, 1994.

16. W. Kraus and G. Nolze, *J. Appl. Cryst.* **29**, 301, 1996.

17. D.M. Wiench and M.Z.Z. Jansen, *Anorg. Allg. Chem.* **501**, 95, 1983.

18. M. Baldus, B.H. Meier, R.R. Ernst, A.P.M. Kentgens, H. Meyer zu Altenschildesche and Nesper, *J. Am. Chem. Soc.*, **117**, 5141, 1995.

19. R.J.L. Andon, J.F. Counsell, J.F. Martin and C.J. Marsh, *J. Appl. Chem.*, **17**, 65, 1967.

20. The ABINIT code is a common project of the Universite Catholique de Louvain, Corning Incorporated, and other contributors (http://www.abinit.org, accessed 17-12-02).

21. http://www.abinit.org/ABINIT/Psps/LDA_TM/lda.html, accessed 17-12-02.

22. A. Lupulescu, S.P. Brown and H.W. Spiess, *J. Magn. Reson.*, **154**, 101, 2002.

23. T. Hahn, *International Tables for Crystallography, Vol. A - Space-group symmetry*, Kluver Academic Publishers, Dordrecht/Boston/London, 1995.

Chapter 7

A correlation approach for solid-state ^{17}O NMR spectroscopy

7.1 Introduction

Oxygen is the most abundant element in the Earth's crust and an important constituent of most minerals and many other inorganic compounds making ^{17}O NMR measurements potentially a very important source of structural information. However, the routine use of ^{17}O NMR spectroscopy has been restricted by two main factors:

- isotopic substitution by ^{17}O is usually necessary due to its low natural abundance (0.037%) and this is an expensive process.
- ^{17}O is not a particularly good magnetic nucleus being both quadrupolar (I = 5/2) and having a small magnetic dipole moment. The receptivity relative to ^{13}C is 0.0611.

In silicate minerals, potentially an important application for ^{17}O NMR studies, the efg at oxygen is often large leading to broad, featureless MAS NMR peaks. Modern experimental techniques such as double rotation in high strength magnetic fields and multiple quantum MAS show promise in resolving ^{17}O NMR spectra [1-4].

It has been noted [4] that oxygen is a sensitive structural probe for silicate minerals because it has the largest ionic radius of the framework atoms and is most susceptible to interaction with extra-framework species. In such systems, however, there are generally several oxygen sites with similar but distinct chemical shifts. Assignment of ^{17}O NMR spectra often use the correlation of Townes and Dailey [5] between the average bond angle at oxygen and the efg at the nucleus. Other empirical relationships between ^{17}O NMR parameters and Si–O–Si bond angles have been proposed. Farnan *et al.* [6] analysed the distribution of the ^{17}O NMR parameters in $K_2Si_4O_9$ glass, taking the magnitude of $C_Q(^{17}O)$ to depend upon {cos(Si–O–Si)/[cos(Si–O–Si) – 1]}, while Grandinetti *et al.* [7] fitted

$C_Q(^{17}O)$ values for the five ^{17}O resonances in the silica polymorph, coesite, to an expression that depended upon $\{½ + \cos(Si–O–Si)/[\cos(Si–O–Si) – 1]\}^2$.

Calculated values of ^{17}O chemical shifts and efgs have also been used to assign spectra. Most of these calculations, as in the recent study of siliceous ferrierite [8], have used model clusters to represent the environment of the oxygen. Whilst such an approach has proved successful in the published cases, it is dependent on the right choice of cluster and requires a separate calculation for each site. It is the general aim of this chapter to show that the periodic HF *ab initio* method, based on relatively simple basis sets, can be applied to the calculation of the ^{17}O efg tensor in a range of ionic and covalent compounds. The work described in Chapters 4 to 6 for sodium is thus extended in this chapter.

The chapter begins by demonstrating that a good linear correlation can be found between calculated and experimental values of both $C_Q(^{17}O)$ and $\eta(^{17}O)$ for a selected range of compounds. This is followed by a section that looks in more detail at the application of the periodic HF *ab initio* method to the calculation of ^{17}O efg tensor information in a range of silica polymorphs. These are intended as preliminary studies to provide guidelines for methods aimed at the more demanding task of calculating ^{17}O NMR parameters, for assignment purposes, in zeolites. In particular, the consequences of using fuller basis set descriptions for silicon are explored. These descriptions, however, do lead to the number of basis functions becoming excessive and demand large amounts of computer time. In this context, the use of a core pseudopotential on silicon is demonstrated to give just as good a linear correlation. This 'pseudopotential approach' is then applied to the calculation of the ten distinct ^{17}O efg tensors in the siliceous zeolite – ferrierite. The results demonstrate that the periodic HF *ab initio* method produces results of similar quality, for

the purposes of structure determination, as those obtained by quantum mechanical cluster calculations. In the final section a 3-dimensional correlation between average Si–O bond length, Si–O–Si bond angle and calculated value of $C_Q(^{17}O)$ is shown to be of direct use in predicting the experimental values of $C_Q(^{17}O)$ in siliceous zeolite materials.

The periodic HF ab initio approach can also be applied to other quadrupolar nuclei. A set of preliminary results for the nuclei: ^{27}Al and ^{51}V are summarised in Appendix C.

7.2 A general correlation

Correlations between calculated and experimental values of $C_Q(^{17}O)$ and $\eta(^{17}O)$ respectively, are considered for both single- and multiple-site oxygen compounds. As discussed in Chapter 4, an important feature of the periodic *ab initio* correlation approach is the transferability of elemental basis sets.

For oxygen, the Pople 3-21G basis set with the value of the exponent of the outermost sp shell slightly modified (0.374) was selected. This is the same basis set as used in Chapters 4 to 6. A preliminary attempt to optimise this basis set further failed possibly due to the conflicting requirements imposed by the modelling of compounds in which oxygen bonds purely ionically (oxide), as part of an oxyanion, or as purely covalent. In general, metals had their 3-21G basis sets modified by replacing the valence shells with a single valence sp shell: sodium, lithium and calcium (0.180), magnesium (0.200) and aluminium (0.160), where the value of the exponent is given in brackets. In the specific case of zinc, the full 3-21G basis set with the outer valence sp exponent set to 0.314 was used. In the case of silicon, the outer valence orbital is diffuse and can cause convergence problems. The orbital was therefore removed to leave a 3-2G set.

The results of the calculations of $C_Q(^{17}O)$ for a range of compounds are given in Table 7.1. It should be noted that, to date, no sign of an experimental value of $C_Q(^{17}O)$ for any oxygen site has been determined and, therefore, the experimental values given in Table 7.1 are magnitudes only. The periodic *ab initio* calculations provide a sign for the calculated value of $C_Q(^{17}O)$ and these are shown explicitly. The plot of the experimental versus calculated values of $C_Q(^{17}O)$, Figure 7.1, assumes that the periodic *ab initio* method has correctly determined the sign in all cases.

Table 7.1 A comparison of experimental and calculated values of ^{17}O quadrupole parameters for a range of compounds

Compound (*site*)	Experimental		Calculated		References	
	C_Q / MHz	η	C_Q / MHz	η	NMR	Struct
ZnO	0.13	0.0	0.13	0.0	9	10
Al_2O_3	2.17	0.55	2.89	0.51	11	12
α-$Na_2Si_2O_5$ (*1*)	5.74	0.2	-8.58	0.09	13	14
α-$Na_2Si_2O_5$ (*2*)	4.67	0.3	-7.39	0.41		
α-$Na_2Si_2O_5$ (*3*)	2.40	0.2	-5.36	0.18		
Mg_2SiO_4 (*1*)	2.77	0.28	-4.35	0.50	15	16
Mg_2SiO_4 (*2*)	2.53	0.39	-3.61	0.36		
Mg_2SiO_4 (*3*)	2.42	0.18	-3.85	0.19		
SiO_2 – quartz	5.21	0.19	-8.26	0.20	17	18
SiO_2 – Cristobalite	5.30	0.13	-8.29	0.15	19	20
SiO_2 – Coesite (*1*)	6.05	0.00	-9.47	0.02	7	21
SiO_2 – Coesite (*2*)	5.43	0.17	-8.47	0.24		
SiO_2 – Coesite (*3*)	5.45	0.17	-8.28	0.20		
SiO_2 – Coesite (*4*)	5.52	0.17	-8.53	0.16		
SiO_2 – Coesite (*5*)	5.16	0.29	-7.82	0.30		
NaOH [a]	7.59	0.07	-10.76	0.05	22	23
LiOH	7.01	0.05	-9.149	0	22	24
$Mg(OH)_2$	6.8	0	-8.717	0	25	26
$Ca(OH)_2$	6.5	0	-9.959	0.03	27	29
	6.5	0.3			28	

[a] Measured at 77K.

The straight line in Figure 7.1 represents the line of best linear fit to the data (R^2 = 0.97); the slope of the line is 0.699 ± 0.031 and the intercept is 0.273 ± 0.231 MHz. Overall, there is a good linear correlation although it is not 1:1. It is, perhaps surprising that any linear correlation between experimental and calculated values of $C_Q(^{17}O)$ is found taking into account the different types of bonding environment for oxygen in the compounds studied. Furthermore, the oxygen basis set has not been optimised and is the same as that used in the investigation of ionic sodium compounds in Chapters 4 to 6.

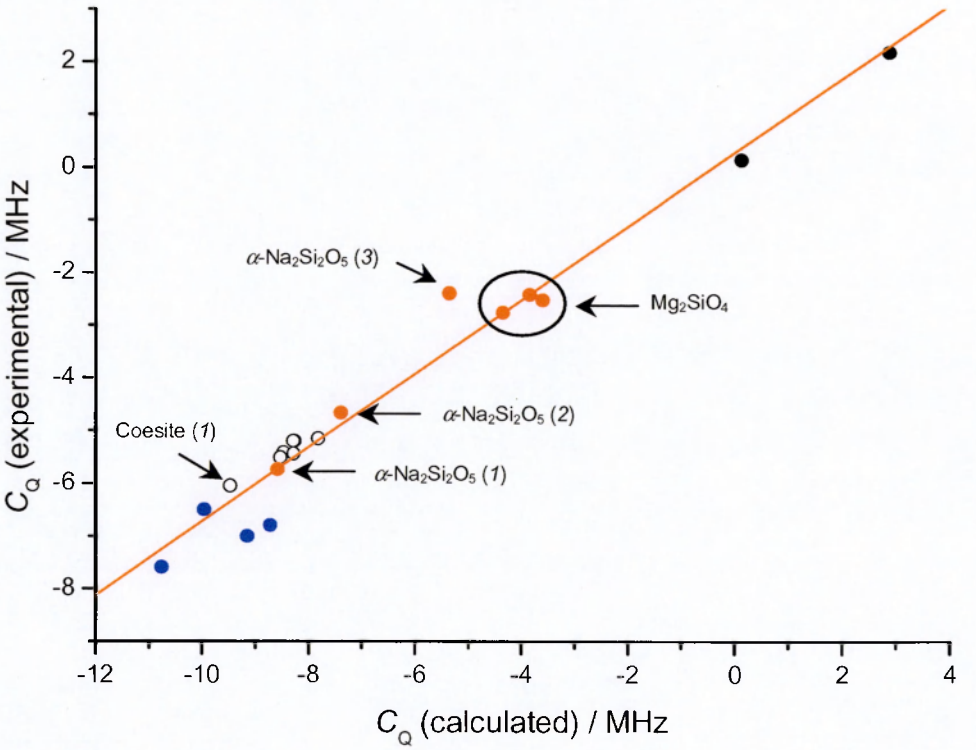

Figure 7.1 A plot of the experimental versus calculated values of $C_Q(^{17}O)$ using data taken from Table 7.1. Compounds involving oxides are shown as black, oxyanions in red, polymorphs of silica in white and hydroxides in blue.

In general, the compounds fall into four groups with the metal oxides being the only ones for which the calculated $C_Q(^{17}O)$ values are positive. Of those for which the calculated value of $C_Q(^{17}O)$ is negative, the silicates, in general, have the smallest magnitude followed

by the polymorphs of silica with the hydroxides displaying the largest magnitude. This result is in agreement with the work of Schramm and Oldfield [30] who observed that $C_Q(^{17}O)$ depends strongly on the ionicity of the bonds. In ionic oxides, small experimental values of $C_Q(^{17}O)$ are found while in the more covalently-bonded silicates these values are significantly larger.

It is interesting to note that there is a degree of overlap between the silicates and the polymorphs of silica, which can be directly attributed to the local environment of the particular oxygen atom. The bridging oxygen, labelled α-$Na_2Si_2O_5$ (*1*), has a coordination shell comprising two silicon atoms with sodium atoms some distance away; the nearest having a Na–O bond distance of 3.794 Å [14]). This isolated environment is very close in nature to that found for bridging oxygen atoms in silica. The α-$Na_2Si_2O_5$ (*2*) oxygen is again bridging but has a single coordinating sodium atom (Na–O = 2.386 Å [14]) along with two silicon atoms. This has the effect of lowering the magnitude of $C_Q(^{17}O)$ so that it lies just above the grouping of silica sites. The local environment of oxygen α-$Na_2Si_2O_5$ (*3*) is the least like that of the oxygen sites in silica. It is a terminal atom having four coordinating sodium atoms at Na–O bond distances ranging from 2.290 Å – 2.600 Å [14] in addition to a single coordinating silicon atom. In Figure 7.1, this site lies close to those of the three oxygen sites in Mg_2SiO_4, which are also terminal with very similar coordination environments in which oxygen is tetrahedrally surrounded by three magnesium atoms and a single silicon atom [16].

The oxygen on site (*1*) in the coesite crystal lattice is separate from the main group of oxygen sites making up the silica polymorphs. Again, the reason is structural in that unlike

all the other coordination shells of silica oxygens, the Si–O–Si bond angle for this site is equal to180°.

The correlation plot for $\eta(^{17}O)$ is shown in Figure 7.2 and, unlike the equivalent plots for $\eta(^{23}Na)$, using the modified 3-21G basis set (see Chapter 4), shows considerably less scatter. The bunching of the points in the lower portion of the plot may reflect the largely similar coordination environment of oxygen in the compounds studied and a tendency towards more axially symmetric environments.

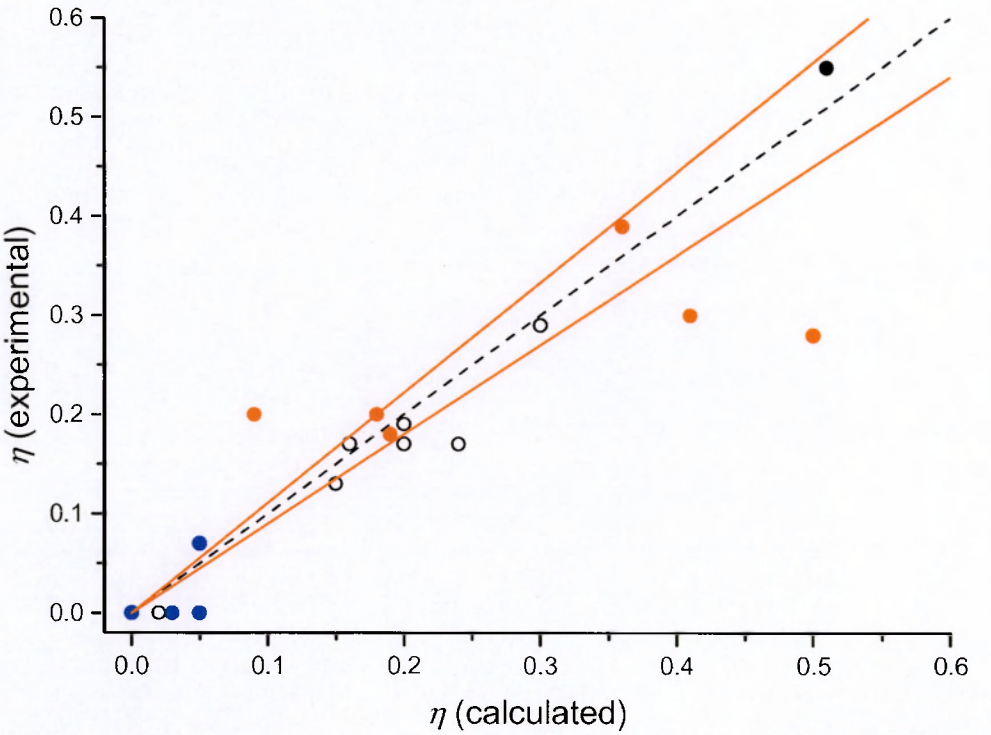

Figure 7.2 A plot of experimental versus calculated values of $\eta(^{17}O)$ using date taken from Table 7.1. Compounds involving oxides are shown as black, oxyanions in red, polymorphs of silica in white and hydroxides in blue. The dotted line represents a 1:1 correlation between experimental and calculated values of $\eta(^{17}O)$. The two red lines bound a region where the calculated value of $\eta(^{17}O)$ is within 10% of that determined by experiment.

7.3 The polymorphs of silica re-investigated

In Figure 7.1, the points representing the polymorphs of silica are clustered together. For this set of solids a more detailed investigation was undertaken to try to find the type of

basis set that would be required to distinguish the different oxygen sites and give a 1:1 correlation between calculation and experiment. The results are shown in Table 7.2. The Pople 3-21G basis set is modified as shown and exponents of 0.50 and 0.96 are used, respectively, for the d-polarisation functions for silicon and oxygen.

Table 7.2 A comparison of experimental calculated values of $C_Q(^{17}O)$ for a range of silica polymorphs using different basis set descriptions on silicon and oxygen

Compound (*site*)	C_Q / MHz [a]				
	Expt	3-2G (Si)	3-21G (Si)	3-21G+d (Si)	3-21G+d (Si + O)
Quartz	5.21	-8.26	-7.26	-5.85	-4.30
Cristobalite	5.30	-8.29	-7.35	-5.91	-4.29
Coesite (*1*)	6.05	-9.47	-8.51	-6.88	-4.92
Coesite (*2*)	5.43	-8.47	-7.44	-6.03	-4.48
Coesite (*3*)	5.45	-8.28	-7.28	-5.93	-4.50
Coesite (*4*)	5.52	-8.53	-7.50	-6.09	-4.60
Coesite (*5*)	5.16	-7.82	-6.89	-5.62	-4.36

[a] A 3-21G basis set for oxygen is used with the exponent of the outermost sp shell equal to 0.374.

A plot of experimental versus calculated values of $C_Q(^{17}O)$ using the data in Table 7.2 is shown in Figure 7.3. The straight lines in this figure represent the lines of best linear fit to the respective data. For the 3-2G basis set for silicon, $R^2 = 0.92$: the slope of the line is 0.567 ± 0.069 and the intercept is -0.661 ± 0.586 MHz. The addition of the extra valence sp shell to give a 3-21G basis set for silicon does not improve the fit, $R^2 = 0.92$: the slope of the line is 0.570 ± 0.070 and the intercept is -1.192 ± 0.525 MHz. However, the addition of d-polarisation functions on just silicon results in the best value for the fitting parameter ($R^2 = 0.96$) and gives the slope of the line as 0.732 ± 0.067 and the intercept as -1.024 ± 0.404 MHz. The use of d-polarisation functions on both silicon and oxygen gives

fitting statistics of $R^2 = 0.94$: the slope of the line is 1.312 ± 0.147 and the intercept is 0.444 $\pm$ 0.662 MHz.

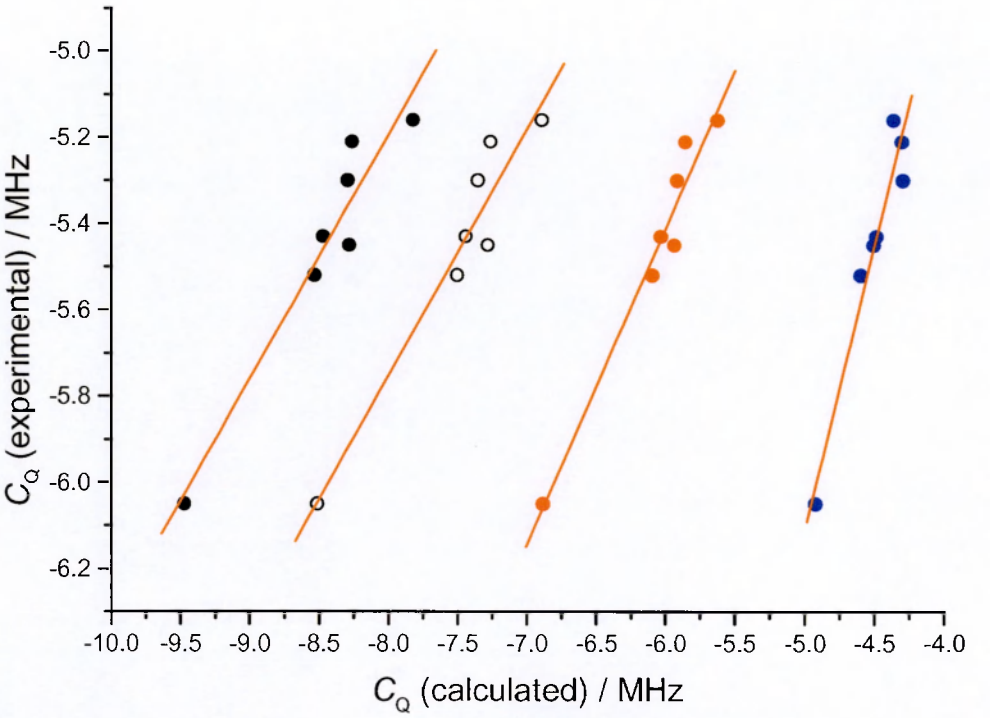

Figure 7.3 A plot of experimental versus calculated values of $C_Q(^{17}O)$ using data taken from Table 7.2. Calculations using a 3-2G basis set for silicon are shown in black, 3-21G in white, 3-21G plus d-polarisation functions on just silicon in red and 3-21G plus d-polarisation on both silicon and oxygen in blue.

It is interesting to note that all four basis set descriptions result in the same relative ordering of the oxygen sites. Although no basis set gives a 1:1 correlation between calculation and experiment, the best linear correlation was found for the 3-21G plus d-polarisation functions on just silicon. Such a result is consistent with the concept of a (d-p) π-bonding model of silicate tetrahedra as proposed by Pauling [31, 32] and Jaffe [33] in the 1950s and discussed more recently, with reference to cristobalite, by Janes and Oldfield [34]. However, the use of d-polarisation functions requires a large overhead in terms of the number of basis functions required to model a particular system and this can become prohibitive in cases where a unit cell contains many hundreds of atoms. For example, even

the relatively simple 3-21G basis set can be restrictive when the unit cell contains 576 atoms as in the case of siliceous faujasite.

In Chapter 5, Section 5.2 it was demonstrated that a pseudopotential core can be used to model a heavy atom in the periodic *ab initio* calculation of an efg tensor. In order to be able to handle siliceous zeolites, therefore, a model in which silicon was represented as a pseudopotential core with the valence shells from the Pople 3-21G basis set (written ps-21G) was tested. The results of using the pseudopotentials of Hay and Wadt (HAYWLC) and Durand and Barthélat (BARTHE) are shown in Table 7.3. Experimental values of $C_Q(^{17}O)$ are also included in this table.

Table 7.3 A comparison of experimental and calculated values of $C_Q(^{17}O)$ for a range of silica polymorphs using different core pseudopotential descriptions on silicon

Compound (*site*)	C_Q / MHz		
	Expt.	HAYWLC	BARTHE
SiO_2 – quartz	5.21	-6.18	-6.98
SiO_2 – Cristobalite	5.30	-6.25	-7.07
SiO_2 – Coesite (*1*)	6.05	-7.22	-8.20
SiO_2 – Coesite (*2*)	5.43	-6.35	-7.14
SiO_2 – Coesite (*3*)	5.45	-6.28	-7.01
SiO_2 – Coesite (*4*)	5.52	-6.48	-7.23
SiO_2 – Coesite (*5*)	5.16	-6.00	-6.63

Plots of experimental versus calculated values of $C_Q(^{17}O)$ using the ps-21G basis set description of silicon for the large-core pseudopotentials BARTHE and HAYWLC are shown in Figure 7.4. The two straight lines shown in this figure represent the lines of best linear fit to the respective data. For the BARTHE core basis set, $R^2 = 0.94$: the slope of the line is 0.588 ± 0.070 and the intercept is -1.221 ± 0.503 MHz and for the HAYWLC core

basis set, R^2 = 0.96: the slope of the line is 0.745 ± 0.058 and the intercept is -0.685 ± 0.374 MHz.

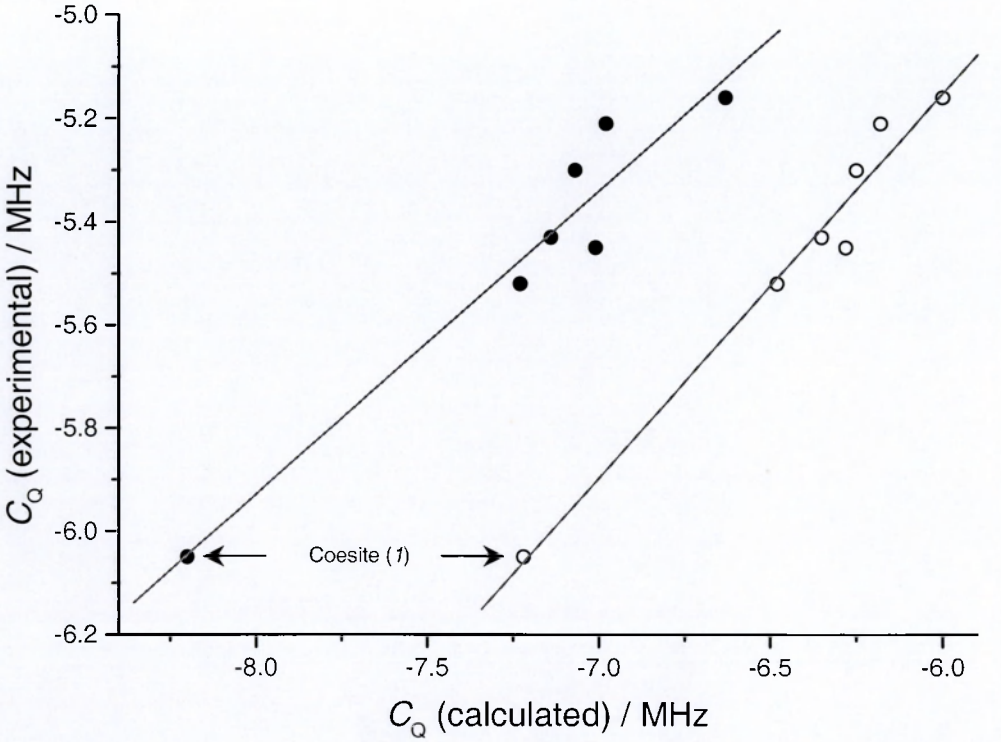

Figure 7.4 A plot of experimental versus calculated values of $C_Q(^{17}O)$ using data taken from Table 7.3. Calculations using a BARTHE core pseudopotential for silicon are shown in black and those using HAYWLC are shown in white.

Again, the oxygen on site (1) for coesite shows a marked separation from the other oxygen sites studied in calculations using both pseudopotential descriptions of silicon. The best correlation between experimental and calculated $C_Q(^{17}O)$ values is found for the ps-21G basis set description of silicon based on HAYWLC.

7.4 A comparison of two siliceous ferrierite structures

All-silica ferrierite has been reported to crystalise in the *Pnnm* space group with five silicon sites and ten distinct oxygen sites [35]. Since the first report of this structure, two

detailed crystal structure determinations have been made in the *Pnnm* space group, one by Morris *et al.* [36] and the other by Lewis *et al.* [37]. In this section, the two respective structures will be referred to simply as Morris and Lewis.

In a recent high resolution NMR study of ferrierite, Bull and co-workers [8] obtained the ^{17}O quadrupole parameters from all ten distinct oxygen sites in the crystal lattice. These workers then went on to demonstrate, by *ab initio* cluster calculations, that the structure of Lewis was more consistent with the experimental data than that of Morris.

The twenty clusters required to model the local environments around each of the oxygen sites in the two crystal structures, in the work of Bull *et al.*, were relatively large, requiring inclusion of the fourth shell of nearest neighbour atoms for convergence of the ^{17}O quadrupole parameters. Here we demonstrate that a periodic *ab initio* method can use the refined crystal structures directly, eliminating the need to consider the cluster size, and requiring only two calculations to obtain all twenty sets of ^{17}O quadrupole parameters.

Table 7.4 shows the quadrupole product, P_Q, defined as:

$$P_Q = C_Q(1+\frac{\eta^2}{3})^{0.5} \tag{7.1}$$

obtained from periodic *ab initio* calculations, using the [HAYWLC]-21G basis set for silicon, for the crystal structures of Lewis and Morris. The value of C_Q in this equation is the predicted value obtained from the correlation equation:

$$C_Q(\text{predicted}) = 0.745\ C_Q(\text{calculated}) - 0.685 \tag{7.2}$$

obtained by the linear fit to the [HAYWLC]-21G data set plotted in Figure 7.4. The results for the same structures taken from [8] are also shown for comparison along with the experimental values, which were numerically ordered and matched to the results of the periodic *ab initio* method for the Lewis structure. It should be noted that this is not

intended as a site assignment but rather as a convenient method for comparing the calculated and experimental data. The oxygen sites are labelled following the scheme used in [8] such that O12 refers to the oxygen atom bridging Si(*1*) and Si(*2*) of the Lewis structure and the equivalent site in Morris (although a different numbering scheme is used in this particular work).

Table 7.4 Comparison of the experimental and calculated values of the ^{17}O quadrupole product for the ten oxygen sites in siliceous ferrierite

Site	$\lvert P_Q \rvert$ / MHz				
	Experiment [a]	Lewis [b]	Morris [b]	Lewis [c]	Morris [c]
O12	5.32	5.34	5.18	5.26	5.14
O15	5.46	5.46	5.45	5.36	5.31
O22	5.29	5.33	5.41	5.23	5.32
O23	5.22	5.31	5.46	5.16	5.35
O24	5.38	5.36	5.28	5.28	5.17
O34	5.57	5.46	5.38	5.42	5.31
O35	5.27	5.31	4.45	5.19	4.48
O43	5.35	5.39	5.54	5.25	5.39
O45	5.62	5.67	6.05	5.43	5.83
O55	5.64	5.67	5.75	5.54	5.62

[a] Values taken from [8] and their relationship to individual oxygen sites is explained in the text. [b] From [8]. [c] This work.

Figure 7.5 shows that the calculated values of $P_Q(^{17}O)$ for the 10 oxygen sites in siliceous ferrierite are extremely sensitive to the structural model used and, therefore, can be used to judge the accuracy of the crystal structure. In general, the periodic *ab initio* method has produced, in a single calculation for each structure, results in good agreement with those of the cluster models presented in [8].

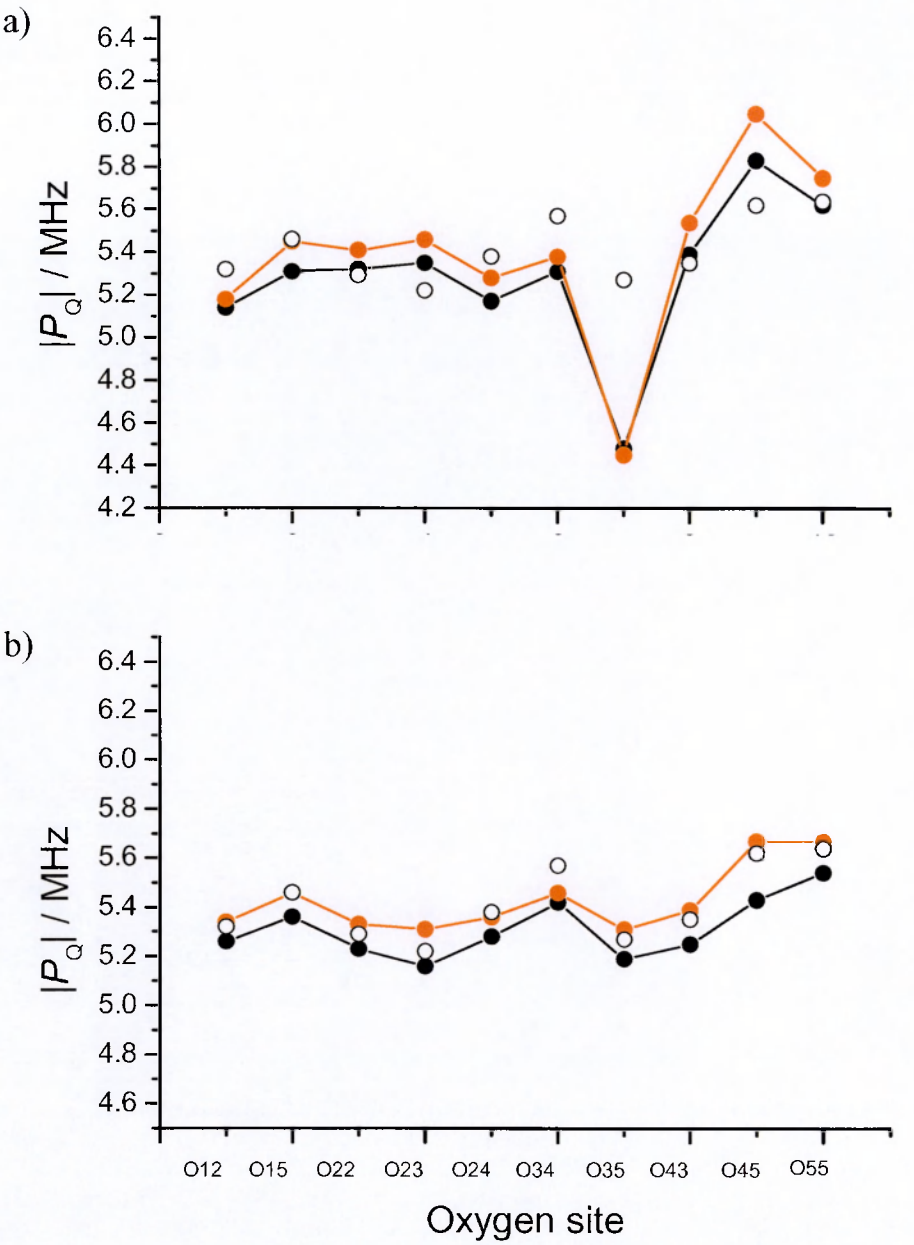

Figure 7.5 Plots of calculated values of $|P_Q(^{17}O)|$ versus oxygen site for (a) Morris and (b) Lewis crystal structures of siliceous ferrierite. Values obtained from periodic *ab initio* calculations are shown in black while those in red are taken from [8]. The experimental values (open circles) are shown as an aid to structure comparison and their relationship to individual oxygen sites is explained in the text. The lines joining the points are an aid to the eye only.

Comparison of the experimental data suggests that the crystal structure of ferrierite proposed by Lewis is in better agreement with experiment than that by Morris, especially for the O35 site. This result is in agreement with the conclusion of Bull *et al.* An

unambiguous site assignment based on the calculated values of $C_Q(^{17}O)$ is not possible because of the relatively small range, covering just 0.4 MHz, of the experimental $C_Q(^{17}O)$ values.

Although the experimental ^{17}O NMR results of Bull *et al.* support the structure of Lewis, it is possible that both structures are correct in so far as they accurately represent the crystal structure of the particular sample each group studied. An X-ray diffraction pattern of the siliceous ferrierite sample prepared by Bull *et al.* was taken but only in order to determine the presence of the correct phase and its crystallinity. If correlations between quadrupole parameters and the local structure of oxygen sites are to be made it would seem prudent that they are based on NMR and structural data obtained from the same sample. Unfortunately, in the case of ^{17}O, the need for expensive isotopic enrichment in most cases precludes the making of the multi-gram quantities required for a neutron diffraction structure determination.

7.5 Approximation of $C_Q(^{17}O)$ values in all-siliceous zeolites

Zeolites are crystalline aluminosilicates with an open framework structure containing extraframework charge-balancing cations. The microporous nature of zeolites is exploited in their use as 'molecular sieves' and the extraframework active centres are sites for selective catalysis [38]. The mineral faujasite, and its structural analogues zeolites X and Y, have a wide variety of industrial applications [39] due to their large pore size. Understanding the nature of the catalytic processes and the sites within the zeolite at which these occur is an important objective in many investigations.

Table 7.5 The Si–O–Si angle, O–Si and average <O–Si> distances for a range of siliceous compounds

Compound (*site*)	∠Si–O–Si / °	O–Si(1) / Å	O–Si(2) / Å	<O–Si> / Å
SiO_2 – quartz	143.72	1.605	1.611	1.608
SiO_2 – Cristobalite	146.71	1.598	1.606	1.602
SiO_2 – Coesite (*1*)	180.00	1.596	1.596	1.596
SiO_2 – Coesite (*2*)	141.97	1.613	1.613	1.613
SiO_2 – Coesite (*3*)	144.10	1.615	1.618	1.6165
SiO_2 – Coesite (*4*)	149.66	1.609	1.615	1.612
SiO_2 – Coesite (*5*)	136.54	1.623	1.626	1.6245
Ferrierite (Morris)				
O12	153.70	1.609	1.585	1.597
O15	156.80	1.581	1.594	1.588
O22	144.70	1.632	1.632	1.632
O23	142.20	1.652	1.625	1.639
O24	152.40	1.572	1.593	1.583
O34	170.70	1.586	1.573	1.580
O35	138.30	1.584	1.563	1.574
O43	149.50	1.559	1.643	1.601
O45	161.30	1.625	1.637	1.631
O55	159.50	1.593	1.593	1.593
Ferrierite (Lewis)				
O12	156.66	1.595	1.593	1.594
O15	155.35	1.586	1.596	1.591
O22	149.13	1.596	1.596	1.596
O23	144.91	1.597	1.605	1.601
O24	152.98	1.591	1.601	1.596
O34	167.37	1.601	1.596	1.596
O35	143.74	1.595	1.602	1.598
O43	148.07	1.600	1.599	1.599
O45	164.50	1.582	1.592	1.587
O55	158.22	1.591	1.591	1.591

Siliceous faujasite crystalises in the $Fd\bar{3}m$ space group with 576 atoms in the conventional unit cell, only five of which belong to the asymmetric unit [40]. A periodic *ab initio* study of this material has been carried out by Zicovich-Wilson and Dovesi [41] requiring a total of 200 hours on a DEC-Alpha 200 4/233 workstation for a full structure optimisation.

Unfortunately, such computational resources were not available for this work. However, recent work by Larin and co-workers [42, 43] have suggested correlations between the periodic *ab initio* calculated oxygen charge, Si–O–Si bond angle and the average O–Si bond length fitted to a wide selection of zeolites. It was decided to investigate the possibility of a similar correlation existing for $C_Q(^{17}O)$ rather than the oxygen charge and in this way to provide a non-computationally intense method of interpreting ^{17}O NMR spectra for siliceous zeolite materials. The structural parameters used in the analysis are summarised in Table 7.5.

A surface, shown in Figure 7.6, was fitted to the uncorrected $|C_Q(^{17}O)|$ values obtained using the silicon [HAYWLC]-21G basis set for all the oxygen sites in the three silica polymorphs and the Lewis and Morris structures of siliceous ferrierite. A satisfactory estimate of the value of $|C_Q(^{17}O)$ / MHz| was obtained with respect to the internal geometric parameters characterising the local oxygen environment as a function of just two coordinates R and θ:

$$|C_Q(\text{est}) / \text{MHz}| = a_1 R^n + a_2(R + R_0)^m \cos(\theta + \theta_0) \qquad (7.3)$$

θ being the Si–O–Si bond angle (in radians) and $R = (R_{O\text{–}Si(1)} + R_{O\text{–}Si(2)}) / 2$ (Å) is the average O–Si bond distance with $a_1 = 0.077$, $n = 9.895$, $a_2 = 356.2$, $R_0 = -1.442$, $m = 2.699$ and $\theta_0 = 1.221$ being obtained by non-linear least squares fitting to the data. The fit was sufficient to give an average uncertainty of 1.64 %.

It is interesting to note that the points in Figure 7.6 are not distributed over the whole surface but rather form an arc along the lower slope of the fitted surface which suggests that only certain bond angles and lengths are favoured within these structures.

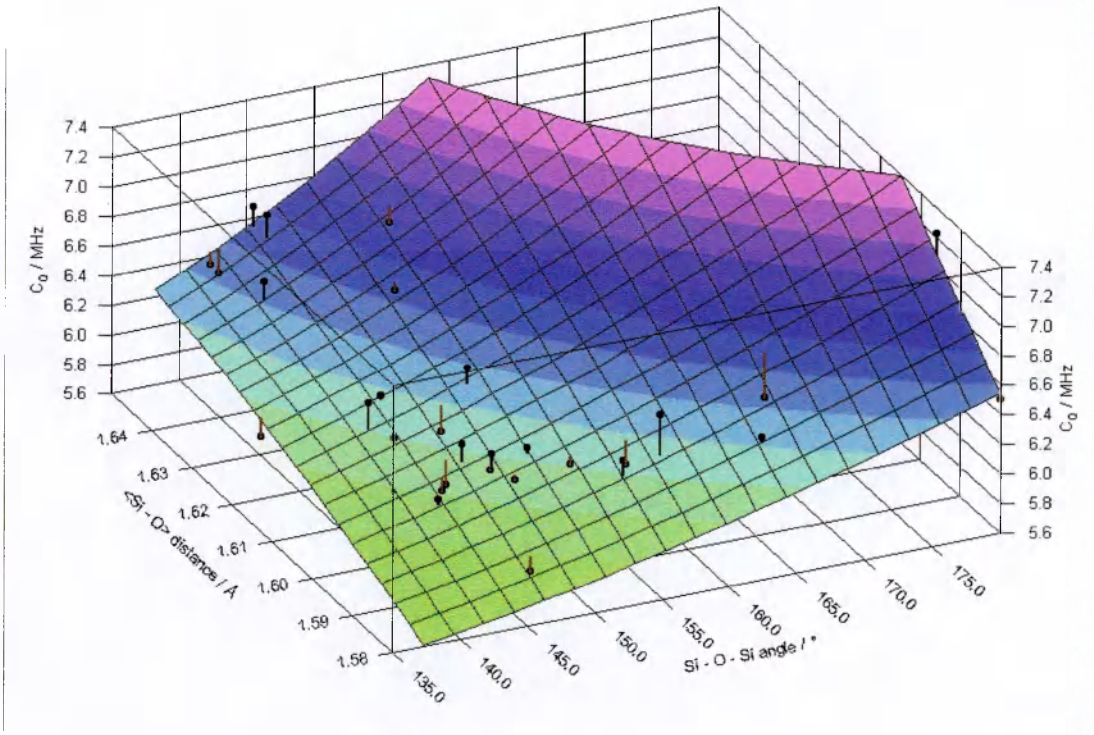

Figure 7.6 Plot of the fitted $|C_Q(\text{est}) / \text{MHz}|$ surface relative to the $|C_Q(\text{calc}) / \text{MHz}|$ values given by periodic *ab initio* calculation using the [HAYWLC]-21G basis set for silicon versus the average Si–O distance (Å) and Si–O–Si angle (°) for the compounds given in Table 7.6.

Although the periodic nature of the *ab initio* calculation takes into account the entire crystal environment, the plot in Figure 7.6 indicates that the immediate environment is the determining factor for the value of $C_Q(^{17}O)$. Thus oxygens in different siliceous structures with similar Si-O-Si bond angles and average Si-O bond distances have similar values of $C_Q(^{17}O)$. The plot, therefore, could be used to estimate $C_Q(^{17}O)$ values in siliceous systems.

The usefulness of this approach is demonstrated in Table 7.6, which gives estimated values of $|C_Q(^{17}O)|$ for the four distinct oxygen sites in faujasite obtained using Equation 7.3 and the structural parameters given in reference [40]. The same material has also been studied experimentally by Bull *et al.* [44] and the experimental $C_Q(^{17}O)$ values for the four sites

have been assigned using quantum mechanical cluster calculations as follows: O(*1*), 5.10 MHz; O(*2*), 5.39 MHz; O(*3*), 5.14 MHz; O(*4*), 5.28 MHz.

Table 7.6 The Si–O–Si angle, average <O–Si> distances and estimated values of $C_Q(^{17}O)$ for siliceous faujasite

Faujasite [a] (*site*)	∠Si–O–Si / °	<O–Si> [b] / Å	$\|C_Q(est)\|$ / MHz
O(*1*)	138.44	1.607	6.00
O(*2*)	149.35	1.597	6.12
O(*3*)	145.84	1.604	6.14
O(*4*)	141.40	1.614	6.16

[a] Structural parameters are taken from [40]. [b] Average O–Si bond length.

These experimental values are in reasonably good agreement with the corrected values of C_Q(est) (using Equation 7.2): O(*1*), 5.15 MHz; O(*2*), 5.24 MHz; O(*3*), 5.26 MHz; O(*4*), 5.27 MHz. However, the small spread of values makes unambiguous assignment difficult. Indeed, the site assignment made by Bull and co-workers [44] was based on the calculated ^{17}O chemical shifts for the four sites as their calculated $C_Q(^{17}O)$ values were significantly larger than those obtained by experiment (O(*1*), 6.61 MHz; O(*2*), 6.73 MHz; O(*3*), 6.54 MHz; O(*4*), 6.74 MHz).

7.6 Summary

The main aim of this chapter has been to demonstrate that the periodic HF *ab initio* method, based upon relatively small basis sets can be transferred from sodium and used to calculate $C_Q(^{17}O)$ and $\eta(^{17}O)$ values in reasonable agreement with experiment. The results show that this is the case for a range of compounds with the oxygen sites falling into distinct groups depending upon the ionicity of the oxygen bond.

The three polymorphs of silica were used as model systems in order to find a basis set that could be used to calculate ^{17}O quadrupole parameters for large siliceous systems. A basis set in which the Hay and Wadt large core pseudopotential was used on silicon provided a good, although not 1:1, correlation between experimental and calculated $C_Q(^{17}O)$ values. This basis set was used to calculate the $C_Q(^{17}O)$ values for the oxygen sites in the two experimental determinations of the structure of siliceous ferrierite; the Lewis structure was identified as being most in keeping with experiment. This result supports the similar conclusion of Bull *et al.* [8] but only two separate calculations were required using the periodic HF *ab initio* method in contrast to their twenty separate cluster calculations.

Finally, a correlation between the periodic *ab initio* calculated $C_Q(^{17}O)$ value, Si–O–Si bond angle and the average O–Si bond length was proposed and fitted to a surface of the functional form:

$$|C_Q(\text{est}) / \text{HMz}| = a_1 R^n + a_2(R + R_0)^m \cos(\theta + \theta_0) \qquad (7.3)$$

θ being the Si–O–Si bond angle (in radians) and $R = (R_{O\text{–}Si(1)} + R_{O\text{–}Si(2)}) / 2$ (Å) is the average O–Si bond distance. With the appropriate fitting parameters, the experimentally-determined $C_Q(^{17}O)$ values for the four sites in siliceous faujasite were modelled but the total range of values is too small to make unambiguous assignments.

References

1. E. Oldfield, C. Coretsopoulos, S. Yang, L. Reven, H. C. Lee, J. Shore, O. H. Han, E. Ramli and D. Hinks, *Phys. Rev. B*, **40**, 6852, 1989.
2. M. H. Cohen and F. Reif, *Solid State Phys.*, **5**, 321, 1957.
3. M. E. Smith, *Appl. Magn. Reson.*, **4**, 1, 1993.

4. R. Dupree, Z. P. Han, A.P. Howes, D. M. Paul and M. E. Smith, *Physica C*, **175**, 269, 1991.

5. C.H. Townes and B.P. Dailey, *J. Chem. Phys.*, **17**, 782, 1949.

6. I. Farnan, P. J. Grandinetti, J. H. Baltisberger, J. F. Stebbins, U. Werner, M.A. Eastman and A. Pines, *Nature*, **358**, 31, 1992.

7. P. J. Grandinetti, J. H. Baltisberger, I. Farnan, J. F. Stebbins, U. Werner and A. Pines, *J. Phys. Chem.*, **99**, 12341, 1995.

8. L.M. Bull, B. Bussemer, T. Anupold, A. Reinhold, A. Samoson, J. Sauer, A.K. Cheetham and R. Dupree, *J. Am. Chem. Soc.*, **122**, 4948, 2000.

9. T.H. Walter and E. Oldfield, *J. Phys. Chem.* **93**, 6744, 1989.

10. O. Garcia-Martinez, R.M. Rojas, E. Vila and J.L. Martin de Vidales, *Solid State Ionics*, **63**, 442, 1993.

11. T.H. Walter and E. Oldfield, *J. Phys. Chem.* **93**, 6744, 1989.

12. H. Sawada, *Mater. Res. Bull.*, **29**, 127, 1994.

13. H. Maekawa, P. Florian, D. Massiot, H. Kiyono and M. Nakamura, *J. Phys. Chem.*, **100**, 5525, 1996.

14. A.K. Pant and D.W.J. Cruickshank, *Acta Crystallogr. B*, **24**, 13, 1968.

15. R. Fritsch, D. Brinkmann, S.S. Hafner, S. Hosoya, J. Lorberth and J. Roos, *Phys. Lett. A*, **118**, 98, 1986.

16. K. Fujino, S. Sasaki, Y. Takeuchi, R. Sadanaga, *Acta Crystallogr. B*, **37**, 513, 1981.

17. L.H. Flemming and I. Farnan, *Chem. Phys. Lett.*, **357**, 403, 2002.

18. G. Will, M. Bellotto, W. Parrish and M. Hart, *J. App. Crystallogr.*, **21**, 182, 1988.

19. D.R. Spearing, I. Farnan and J.F. Stebbins, *Phys. Chem. Miner.*, **19**, 307, 1992.

20. J.J. Pluth, J.V. Smith and J. Faber, *J. App. Phys.*, **57**, 1045, 1985.

21. J.R. Smyth, J.V. Smith, G. Artioli and A. Kvick, *J. Phys. Chem.*, **91**, 988, 1987.

22. I.J.F. Poplett, *J. Magn. Reson.*, **50**, 382, 1982.

23. H. Jacobs, J. Köckelkorn and T.Z. Tacke, *Z. Anorg. Allg. Chem.*, **531**, 119, 1985.

24. S.L. Mair, *Acta Crystallogr. A*, **34**, 542, 1978.

25. F. Babonneau, J. Maquet and J. Livage, *Ceram. Trans.* **55**, 53, 1995.

26. F. Zigan and R. Rothbauer, Neues Jahrbuch fuer Mineralogie. Monatshefte, 1967, 137, 1967.

27. G. Wu, D. Rovnyak, P.C. Huang and R.G. Griffin, *Chem. Phys. Lett.*, **277**, 79, 1997.

28. X. Cong and R.J. Kirkpatrick, J. Am. Ceram. Soc., 79, 1585, 1996.

29. L. Desgranges, D. Grebille, G. Calvarin, G. Chevrier, N. Floquet and J.-C. Niepce, *Acta Crystallogr.*, **49**, 812, 1993.

30. S. Schramm and E. Oldfield, *J. Am. Chem. Soc.*, **106**, 2502, 1984.

31. L. Pauling, *J. Phys. Chem.*, **56**, 361, 1952.

32. L. Pauling, *The Nature of the Chemical Bond*, Cornell University Press, Ithaca, New York, 1960.

33. H.H. Jaffe, *J. Phys. Chem.*, **58**, 185, 1954.

34. N. Janes and E. Oldfield, *J. Am. Chem. Soc.*, **108**, 5743, 1986.

35. A. Kuperman, S. Nadimi, S. Oliver, G.A. Ozin, J.M. Garces and M.M. Olken, *Nature*, **97**, 239, 1993.

36. R.E. Morris, S.J. Weigel, N.J. Henson, L.M. Bull, M.T. Janicke, B.F. Chmelka and A.K. Cheetham, *J. Am. Chem. Soc.*, **116**, 11849, 1994.

37. J.E. Lewis, C.C. Freyhardt and M.E. Davis, *J. Phys. Chem.*, **100**, 5039, 1996.

38. D.W. Breck, *Zeolite Molecular Sieves. Structure, Chemistry and Use*, Wiley-Interscience, New York, 1974.

39. A. Corma, *Chem. Rev.*, **95**, 559, 1995.

40. J.A. Hriljac, M.M. Eddy, A.K. Cheetham, J.A. Donohue and G.J. Ray, *J. Solid State Chem.*, **106**, 66, 1993.

41. C.M. Zicovich-Wilson and R. Dovesi, *Chem. Phys. Lett.*, **277**, 227, 1997.

42. A.V. Larin, L. Leherte and D.P. Vercauteren, *Chem. Phys. Lett.*, **287**, 169, 1998.

43. A.V. Larin and D.P. Vercauteren, *Int. J. Quantum Chem.*, **70**, 993, 1998.

44. L.M. Bull, A.K. Cheetham, T. Anupold, A. Reinhold, A. Samoson, J. Sauer B. Bussemer, Y. Lee, S. Gann, J. Shore, A. Pines and R. Dupree, *J. Am. Chem. Soc.*, **120**, 3510, 1998.

Appendices

A : 8-411G basis set for nitrogen

Table A.1 The 8-411G basis set derived for nitrogen in $NaNO_2$. Exponents and coefficients of the gaussian-type functions are given.

		Coefficient	
Shell type	Exponent	s	p
1s	5.570×10^{3}	1.080×10^{-3}	
	8.776×10^{2}	8.040×10^{-3}	
	1.797×10^{2}	5.324×10^{-2}	
	5.157×10^{1}	1.681×10^{-1}	
	1.807×10^{1}	3.581×10^{-1}	
	6.771	3.855×10^{-1}	
	2.613	1.468×10^{-1}	
	8.850×10^{-1}	7.280×10^{-2}	
2sp	1.673×10^{1}	-6.979×10^{-3}	1.869×10^{-2}
	4.020	-1.698×10^{-1}	1.078×10^{-1}
	1.266	-8.108×10^{-2}	3.169×10^{-1}
	7.622×10^{-1}	-3.205×10^{-1}	3.746×10^{-1}
3sp	3.806×10^{-1}	1.0	1.0
4sp	7.000×10^{-2}	1.0	1.0

B : Rietveld refined structure of the phase I polymorph of anhydrous $Na_5P_3O_{10}$

Space group: *C2/c*

Cell parameters:

a	9.64510(2)	α	90
b	5.36297(1)	β	111.92605(11)
c	19.85486(4)	γ	90

Atom parameters:

Atom	*x*	*y*	*z*	B_{iso} / Å^2	Multi
Na (*1*)	0.00000	0.00000	0.00000	1.39(8)	4
Na (*2*)	0.35930(35)	0.56615(44)	0.32571(14)	2.17(7)	8
Na (*3*)	0.26358(30)	1.02040(49)	0.42958(14)	2.96(8)	8
P (*1*)	0.00000	0.65387(46)	0.25000	1.49(7)	4
P (*2*)	0.07384(21)	0.52231(32)	0.39976(8)	1.10(4)	8
O (*1*)	0.14345(42)	0.79759(71)	0.26787(18)	1.20(10)	8
O (*2*)	0.01968(42)	0.45384(70)	0.31282(18)	1.30(9)	8
O (*3*)	0.97927(40)	0.34904(62)	0.42577(19)	1.35(10)	8
O (*4*)	0.04274(39)	0.79711(68)	0.40466(19)	1.28(10)	8
O (*5*)	0.23863(43)	0.45868(66)	0.43205(20)	2.29(11)	8

C : Experimental and calculated C_Q correlations for other quadrupolar nuclei

Although not reported in detail in this thesis, the periodic HF *ab initio* method has been applied to the study of the ^{27}Al and ^{51}V efg tensors in a range of compounds.

C.1 Aluminium

Attempts to model the efg at aluminium in a range of compounds using a single transferable basis set met with limited success. The compounds studied divided into two overlapping groups and may be indicative of the nature of the bonding in these compounds. The 3-2G basis set was used where aluminium might be expected to have covalent character to its bonding. A modified Pople 3-21G basis with the outer exponent increased to 0.160 was used for more ionic compounds. For the other elements, the metals had their valence sp shells replaced by a single sp shell; the single valence exponent for lithium, sodium and potassium was set equal to 0.180. In the specific case of scandium, the valence exponent of the single sp shell and the d shell were both set to 0.200. For the non-metal elements H, Si and O present in the compounds studied, their basis sets were as reported elsewhere in this thesis. The results of the calculations are shown in Table C.1

Table C.1 A comparison of experimental and calculated values of ^{27}Al quadrupole parameters for a range of compounds

Compound (*site*)	Experimental		Calculated		References	
	C_Q / MHz	η	C_Q / MHz	η	NMR	Structure
3-2G Basis						
$LiAlH_4$	3.9	0.3	+3.54	0.75	1	2
$LiAlO_2$	1.8	0.56	+0.77	0.62	3	4
$NaAlO_2$	1.4	0.5	-1.45	0.40	5	6
$MgAl_2O_4$	3.68	0	+2.48	0.00	7	8
Sillimanite [a] (*1*)	8.93	0.46	-8.73	0.26	9	10
Sillimanite (*2*)	6.77	0.53	-5.65	0.24		
3-21G Basis						
α-Al_2O_3	2.403	0.009	+2.23	0.00	11	12
AlN	2.2	0	+1.09	0.00	13	14
Andalusite [a] (*1*)	15.59	0.08	+10.81	0.10	9	15
Andalusite (*2*)	5.90	0.70	+3.56	0.93		
Kyanite [a] (*1*)	10.01	0.26	+6.23	0.18	9	16
Kyanite (*2*)	3.70	0.86	-3.02	0.91		
Kyanite (*3*)	6.51	0.59	-4.05	0.97		
Kyanite (*4*)	9.43	0.36	-6.37	0.43		

[a] Polymorphs of Al_2SiO_5.

The straight line in Figure C.1 represents the line of best linear fit to the data obtained using the 3-2G basis set for aluminium (R^2 = 0.99: the slope of the line is 1.480 ± 0.048 and the intercept is 0.120 ± 0.261 MHz).

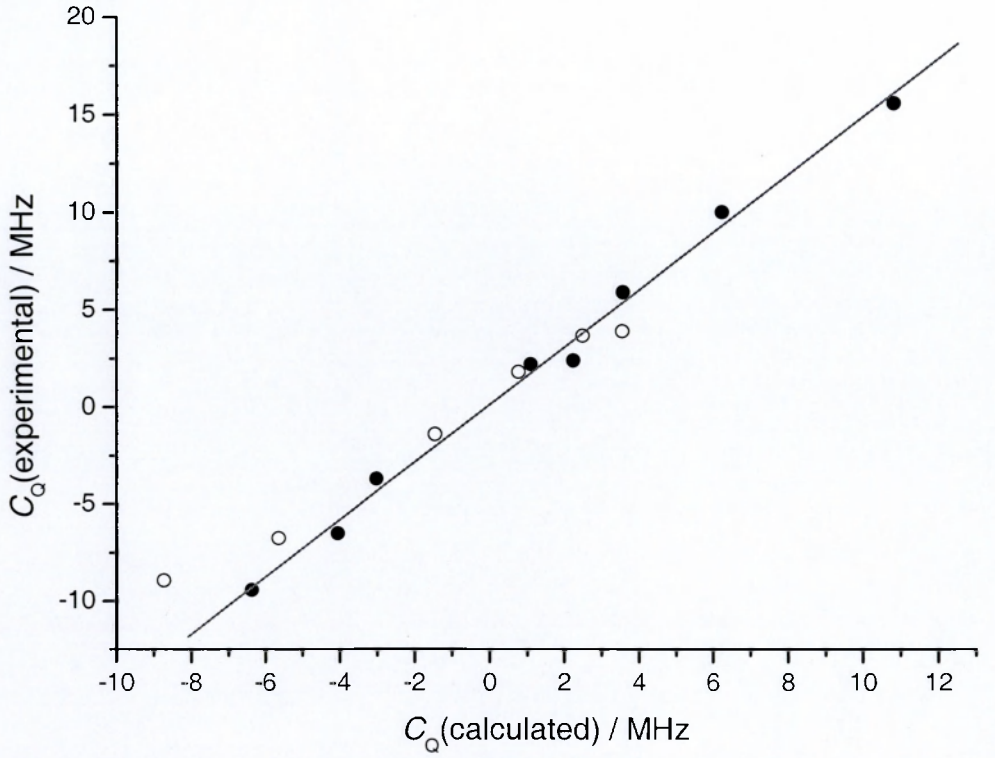

Figure C.1 A plot of experimental versus calculated values of $C_Q(^{27}Al)$ using data taken from Table C.2. The results of calculations performed using the 3-2G (black) and the modified 3-21G (white) aluminium basis set are shown.

C.2 Vanadium

For the all-electron calculations of the ^{51}V quadrupole parameters, the standard Pople 3-21G basis set was selected for vanadium and nitrogen along with the same slightly modified hydrogen and oxygen basis sets used in Chapters 4 to 7. In general, the metals had their valence sp shells replaced by a single sp shell: lithium (0.200), sodium and potassium (0.180), where the value of the exponent is given in brackets. In the specific case of scandium, the valence exponent of the single sp shell and the d shell were both set to 0.200. For the non-metal elements H, N and O present in the compounds studied, their basis sets were as reported elsewhere in this thesis. The results for the calculations are shown in Table C.2

Table C.2 A comparison of experimental and calculated values of ^{51}V quadrupole parameters for a range of compounds

Compound	Experimental		Calculated		References	
	C_Q / MHz	η	C_Q / MHz	η	NMR	Struct
all-electron						
α-$NaVO_3$	3.80	0.46	+2.41	0.38	17	18
NH_4VO_3	2.95	0.30	+2.04	0.04	17	19
$LiVO_3$	3.18	0.87	-2.01	0.52	17	20
Li_3VO_4	1.52	ND	-1.26	0.12	21	22
$ScVO_4$	3.81	0.00	+2.36	0.00	23	24
KVO_3	4.20	0.80	-4.98	0.03	17	25
V_2O_5	0.81	0.04	+0.98	0.62	26	27
pseudopotential						
$ScVO_4$	3.81	0.00	+3.20	0.00	23	24
YVO_4	4.75	0.00	+4.06	0.00	23	28
$LaVO_4$	5.21	0.69	+4.39	0.71	21	29
$BiVO_4$ (533 K)	5.03	0.00	+4.14	0.00	30	31
$BiVO_4$ (300 K)	4.86	0.38	+4.07	0.29	30	31

ND - not determined.

HAYWLC large core pseudopotential potentials along with a single sp and d shell were used to model the heavy atoms scandium (0.200, 0.200), yttrium (0.200, 0.200) and lanthanum (0.5917, 0.2537), where the values in brackets are the exponents of the single sp and d shells, respectively. The basis set for bismuth was generated specifically for this study and was based on the large core pseudopotential potential of Barthélat and Durand [32, 33] with a -21G valence description detailed in Table C.3. The results of the pseudopotential study are shown in Table C.2.

Table C.3 The valence description of the ps-21 basis set derived for bismuth in $BiVO_4$. Exponents and coefficients of the gaussian-type functions are given.

		Coefficient	
Shell type	Exponent	s	p
6sp	9.7583×10^{-1}	-7.1582×10^{-1}	1.9587×10^{-2}
	1.7033×10^{-1}	1.26561	9.9182×10^{-1}
7sp	1.0000×10^{-1}	1.0	1.0

The straight lines in Figure C.2 represent the lines of best linear fit to the data for the all electron basis set (R^2 = 0.99: the slope of the line is1.908 ± 0.098 and the intercept is – 0.849 ± 0.201 MHz) and the pseudopotential basis set (R^2 = 0.99: the slope of the line is1.199 ± 0.041 and the intercept is –0.032 ± 0.154 MHz), respectively.

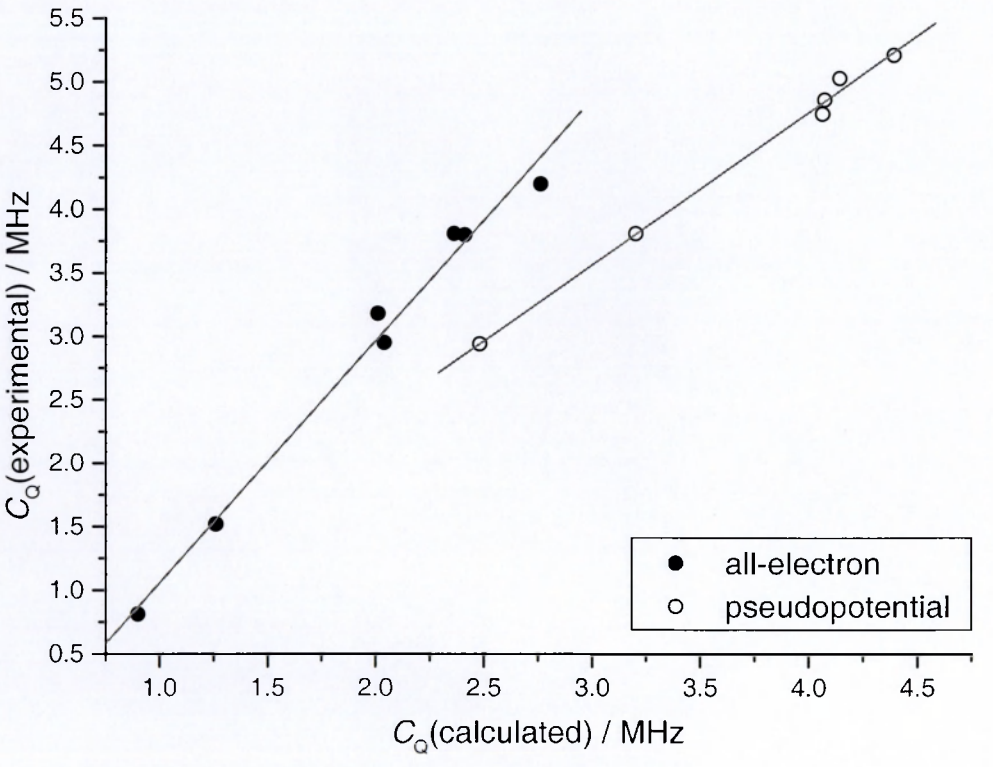

Figure C.2 A plot of experimental versus calculated values of $C_Q(^{51}V)$ using data taken from Table C.3.

References

1. P.A. Casabella and N.C. Miller, *J. Chem. Phys.*, **40**, 1362, 1964.
2. N. Sklar and B. Post, *Inorg. Chem.*, **6**, 669, 1967.
3. D. Muller, W. Gessner and G. Scheler, *Polyhedron*, **2**, 1195, 1983.
4. M. Marezio, *Acta Crystallogr.*, **19**, 396, 1965.
5. D. Muller, W. Gessner, A, Samoson, E. Lippmaa and G. Scheler, *J. Chem. Soc. Dalton Trans.* 1277, 1986.
6. J.A. Kaduk and S.-Y. Pei, *J. Solid State Chem.*, **115**, 126, 1995.
7. M.E. Smith, *Appl. Magn. Reson.*, **4**, 1, 1993.
8. T. Yamanaka, Y. Takeuchi and M. Tokonami, *Acta Crystallogr. B*, **40**, 96, 1984.
9. M. Raymond, *Phys. Rev. B*, **3**, 3692, 1971
10. H. Yang, R.M. Hazen, L.W. Finger, C.T. Prewitt and R.T. Downs, *Phys. Chem. Miner. (Germany)*, **25**, 39, 1997.
11. T. Vosegaard and H.J. Jakobsen, *J. Magn. Reson.*, **128**, 135, 1997.
12. H. Sawada, *Mater. Res. Bull.*, **29**, 127, 1994.
13. M.E. Smith, *Appl. Magn. Reson.*, **4**, 1, 1993.
14. K. Karch, G. Portisch, F. Bechstedt, P. Pavone and D. Strauch, *Institute of Physics Conference Series (1985),* **142**, 967, 1996.
15. C.W. Burnham and M.J. Buerger, *Z. Kristallog., Kristallg., Kristallp., Kristallch.*, **115**, 269, 1961.
16. H. Yang, R.T. Downs, L.W. Finger, R.M. Hazen, and C.T. Prewitt, *Am. Miner.*, **82**, 467, 1997.
17. J. Skibsted, N.C. Nielsen, H. Bildsøe and H.J. Jakobsen, *J. Am. Chem. Soc.*, **115**, 7351, 1993.
18. A.M. Shaikh, *Ferroelectrics*, **107**, 219, 1990.

19. F.C. Hawthorne and C. Calvo, *J. Solid State Chem.*, **22**, 157, 1977.

20. R.D. Shannon R D and C. Calvo, *Can. J. Chem.*, **51**, 265, 1973.

21. O.B. Lapina, V.M. Mastikhin, A.A. Shubin, V.N. Krasilnikov and K.I. Zamaraev, *Prog. Nucl. Magn. Reson. Spectrosc.*, **24**, 457, 1992.

22. R.D. Shannon and C. Calvo, *J. Solid State Chem.* **6**, 538, 1973.

23. F.F.F. Vetel, Open University, personal communication.

24. B.C. Chakoumakos, M.M. Abraham and L.A. Boatner, *J. Solid State Chem.*, **109**, 197, 1994.

25. F.C. Hawthorne and C. Calvo, *J. Solid State Chem.* **22**, 170, 1977.

26. C. Fernandez, P.Bodart and J.P. Amoureux, *Solid State Nucl. Magn. Reson.*, **3**, 79, 1994.

27. R. Enjalbert and J. Galy, *Acta Crystallogr. C*, 42, 1467, 1986.

28. B.C. Chakoumakos, M.M. Abraham and L.A. Boatner, *J. Solid State Chem.* **109**, 197, 1994.

29. C.E. Rice and W.R. Robinson, *Acta Crystallogr. B*, **32**, 2232, 1976.

30. S.H. Choh, *Z. Naturforsch*, **51a**, 591, 1996.

31. A.W. Sleight, H.Y. Chen, A. Ferretti and D.E. Cox, *Mater. Res. Bull.*, **14**, 1571, 1979.

32. J.C. Barthelat and P. Durand, *Gazz. Chim. Ital.*, **108**, 225, 1978.

33. J.C. Barthelat, P. Durand and A. Serafini, *Mol. Phys.*, **33**, 159, 1977.